INNATE IMMUNE EVASION AND INTERFERON ANTAGONISM BY PORCINE EPIDEMIC DIARRHEA VIRUS

BY

QINGZHAN ZHANG

DISSERTATION

Submitted in partial fulfillment of the requirements
for the degree of Doctor of Philosophy in VMS-Pathobiology
in the Graduate College of the
University of Illinois at Urbana-Champaign, 2017

Urbana, Illinois

Doctoral Committee:

Professor Dongwan Yoo, Chair, Director of Research
Professor Lin-Feng Chen
Professor Daniel Rock
Professor Federico Zuckermann

ABSTRACT

Porcine epidemic diarrhea (PED) is a highly contagious and acute enteric disease of swine featured by vomiting, watery diarrhea, and severe dehydration causing high mortality in piglets. In the U.S., PED emerged for the first time in 2013 and severely affected most pig-producing states. The causative agent is PED virus (PEDV), which is an enveloped, positive-sense, single-strand RNA virus in the genus *Alphacoronavirus* of the family *Coronaviridae* in the order *Nidovirales*. The innate immune system is the first line of host defense in response to viral infections. Type I interferons (IFN-α/β) are the major components of the innate immune system, and in turn many viruses have evolved to modulate the host interferon responses.

In the present study, the PEDV IFN antagonism was investigated. We found that IFN-β production was significantly suppressed during PEDV infection, and of 16 PEDV nonstructural proteins (nsps), nsp1, nsp3, nsp7, nsp14, nsp15, and nsp16 were found to inhibit the IFN-β and IRF3 promoter activities. The sole accessory protein ORF3 and the envelope (E), membrane (M), and nucleocapsid (N) proteins were also determined to inhibit such activities. Since nsp1 is the first viral protein synthesized during PEDV infection and appears to be the most potent IFN antagonist, nsp1 was further investigated for its action. PEDV nsp1 did not interfere the IRF3 phosphorylation and nuclear translocation upon stimulation but interrupted the enhanceosome assembly of IRF3 and CREB-binding protein (CBP) by degrading CBP. The CBP degradation by nsp1 was proteasome-dependent.

We further showed that PEDV inhibited both NF-κB and proinflammatory cytokine production in porcine epithelial cells. PEDV blocked the p65 activation in infected cells and suppressed the PRD II-mediated NF-κB activity. Nine proteins were identified as NF-κB antagonists, and nsp1 was the most potent suppressor of proinflammatory cytokines. Nsp1

interfered the phosphorylation and degradation of IκBα, and thus blocked the p65 activation. Mutational studies demonstrated the essential requirements of the conserved residues of nsp1 for NF-κB suppression.

Recent reports showed that type III interferons (IFN-λs) play a vital role to maintain the antiviral state of the mucosal epithelial surface in the gut. The intestinal epithelial cells selectively produce and respond to type III IFNs. To study the type III IFN response to PEDV, a line of porcine intestinal epithelial cells was developed as a cell model for PEDV replication. Recombinant proteins IFN-λ1 and IFN-λ3 inhibited PEDV replication, indicating the anti-PEDV activity of type III IFNs. Of the total of 21 PEDV proteins, nsp1, nsp3, nsp5, nsp8, nsp14, nsp15, nsp16, ORF3, E, M, and N were found to suppress the type III IFN response. PEDV specifically inhibited IRF1 nuclear translocation. Peroxisomes are the innate antiviral signaling platforms for activation of IRF1-mediated IFN-λ production, and they were found to decrease in number in PEDV-infected cells. PEDV nsp1 blocked the nuclear translocation of IRF1 and reduces the number of the peroxisomes to suppress the IRF1-mediated type III IFN production. The conserved residues of nsp1 were crucial for IRF1-mediated IFN-λ suppression. Taken together, these studies provide the evidence that PEDV and its nsp1 protein, a potent multifunctional IFN antagonist, evade both type I and type III IFN responses and the molecular basis for this antagonism.

ACKNOWLEDGMENTS

First and foremost, I would like to express my deep gratitude to my advisor Dr. Dongwan Yoo for his continuous guidance of my Ph.D. research, for his patience, encouragements, motivation, gracious supports, unique perspectives, and broad knowledge throughout the course of my work! I appreciate his great ideas, precious time, and funding that makes my research possible, enjoyable, and productive. It has been a great honor to be a student of his, and his expertise as a virologist and the enthusiasm in scientific research will continue to motivate me in the next chapter of my career.

My sincere thanks to my Ph.D. committee members, Dr. Daniel Rock, Dr. Federico Zuckermann, and Dr. Lin-Feng Chen, for their continuous supports, encouragements, and insightful comments, which lead me to widen my research from various perspectives. Also, thanks to Ms. Karen Nichols, Dr. Mariangela Segre, and Ms. Paula Moxley, who have given me endless help during my graduate studies.

I would like to express my special thanks to my previous and current labmates Dr. Mingyuan Han, Dr. Kaichuang Shi, Dr. Jinyou Ma, and Hanzhong Ke for the stimulating discussions, encouragements, and all the fun we have had in the past several years. Also, sincere thanks to my friends Weiyu Chen, Jinjun Lin, Xuejin Zhang, and Chiyong Kim for your discussions, friendship, and encouragements. I also wish to thank all the faculty members, staff, and students in the Department of Pathobiology, University of Illinois at Urbana-Champaign.

Last but not the least, my deepest thanks to my family, for their selfless love, endless support, inspiring encouragements, and enormous patience to me. To my parents Xinmin Zhang and Xuerong Teng, my brother Qingju Zhang, and his four beautiful kids. Words cannot describe how thankful I am to have you in my life. The love and support that you have given me over the

years are unbelievable. I would not be where I am today and who I am today without everything you have done for me. Thank you for letting me explore my passions!

TABLE OF CONTENTS

CHAPTER 1: LITERATURE REVIEW

1. 1 INTRODUCTION

1.1.1 Coronavirus enteritis in pigs

Coronavirus enteritis is a highly contagious viral disease in pigs characterized by severe diarrhea, vomiting, and dehydration accompanied with a high mortality, especially in neonatal piglets less than 2 weeks of age. Transmissible gastroenteritis virus (TGEV) is a frequent cause for endemic and epidemic viral enteritis in neonates and older pigs (Kim et al., 2000; Laude et al., 1993), and recently porcine epidemic diarrhea virus (PEDV) has become a major concern in the swine industry in the US since its emergence in April 2013. As with TGEV, PEDV causes severe enteritis in newborn piglets but the mortality can be much higher reaching up to 100% during epidemics (Debouck and Pensaert, 1980; Song and Park, 2012). PED is first described in the UK in the early 1970s and has since become endemic in some parts of Europe. Highly virulent PEDV has recently emerged in Asia and subsequently in the U.S. (Chen et al., 2014; Marthaler et al., 2013; Mole, 2013; Stevenson et al., 2013). PEDV has quickly spread to most states, and as of November 2017, 39 states have become endemic for PEDV, raising a significant economic concern (www.aphis.usda.gov/animal-health/secd). Porine delta-coronavirus (PDCoV) is a newly identified swine enteric coronavirus first described in Hong Kong, China, in a surveillance study in 2012 (Woo et al., 2012). PDCoV is an additional enteric virus emerged in the US in February 2014 (Wang et al., 2014). PDCoV has been identified in the feces and intestinal samples of pigs experiencing severe diarrhea without PEDV and TGEV (Wang et al., 2014). Retrospective studies show that PDCoV has been present in the US at least since August 2013

This chapter has appeared as an article in Virus Research. The original citation is: Zhang, Q., Yoo, D., 2016. Immune evasion of porcine enteric coronaviruses and viral modulation of antiviral innate signaling. Virus Res. 226, 128-141. The copyright owner, Elsevier B.V., permits that author can include the article, in full or in part, in a thesis, or dissertation, for a wide range of scholarly, non-commercial purposes.

(McCluskey et al., 2016; Sinha et al., 2015). PDCoV has also spread to at least 20 states of the US (www.aphis.usda.gov/animal-health/secd), Korea, and China (Dong et al., 2015; Lee and Lee, 2014). PDCoV infection seems clinically milder with a lower death rate of 30%-40% in neonates than typical PEDV infection (Wang et al., 2014), but co-infection with PEDV, TGEV, or porcine rotavirus is common and results in a severe form of disease (Marthaler et al., 2014; Wang et al., 2014). Clinical symptoms by PDCoV are reproducible in both gnotobiotic pigs and conventional pigs, and present diarrhea accompanied by severe histopathological lesions such as villi atrophy in the absence of other pathogens (Chen et al., 2015; Jung et al., 2015c; Ma et al., 2015). Although the clinical signs and pathological lesions are indistinguishable among PEDV, TGEV, and PDCoV (Jung et al., 2014), these coronaviruses are antigenically distinct, and thus cross-protection is absent (Lin et al., 2015). Pathogenesis of these coronaviruses may include destruction of enterocytes and villous atrophy of the intestinal mucosa in the jejunum and ileum (Debouck and Pensaert, 1980; Jung et al., 2014).

Coronaviruses are enveloped viruses containing the genome of single-stranded positive-sense RNA. The coronavirus genome ranges of 28-30 Kb in length and is currently the largest known viral RNA genome. Coronaviruses are grouped in the *Coronavirinae* subfamily of the family *Coronaviridae*, comprising of 4 genera; *Alpha*-, *Beta*-, *Gamma*- and *Delta*-coronaviruses (http://www.ictvonline.org/virustaxonomy.asp [ICTV, 2017]). Evolutionary studies suggest that *Alphacoronavirus* and *Betacoronavirus* are originated from bats while *Gammacoronavirus* and *Deltacoronavirus* are likely from birds (Woo et al., 2012). In humans, coronaviruses infect the respiratory tract and cause symptoms ranging from common colds to severe pneumonia and acute respiratory distress. Severe acute respiratory syndrome coronavirus (SARS-CoV) and Middle East respiratory syndrome coronavirus (MERS-CoV) belong to *Betacoronavirus* and

cause lower respiratory tract infections of significant public concerns (Gralinski and Baric, 2015). Among swine enteric coronaviruses, TGEV and PEDV belong to *Alphacoronavirus* and share a similar genome organization, whereas PDCoV belongs to *Deltacoronavirus* (http://www.ictvonline.org/virustaxonomy.asp).

The PEDV genome is approximately 28 Kb in length with the 5'-cap and 3'-polyadenylated tail. The genome is arranged with ORF1a-ORF1b-S-ORF3-E-M-N in order with both termini flanked with untranslated regions (UTRs) (Duarte et al., 1993). ORF1a codes for a large polyprotein pp1a, while ORF1b is expressed as the pp1ab fusion protein via the ribosomal frameshifting. These polyproteins are proteolytically cleaved to 16 nonstructural proteins, nsp1 through nsp16, by the proteinase activity of nsp3 and nsp5. The TGEV genome is similar to that of PEDV and arranged as ORF1a-ORF1b-S-ORF3a-ORF3b-E-M-N-ORF7 in order (Alonso et al., 2002). For PEDV, ORF3 encodes the sole accessory protein, whereas for TGEV, three accessory proteins are encoded by ORF3a, ORF3b, and ORF7 (Brian and Baric, 2005). The PDCoV genome is the smallest of the three coronaviruses with 26 Kb in length, and includes two accessory genes of NS6 and NS7 with the gene order of ORF1a-ORF1b-S-E-M-NS6-N-NS7 (Woo et al., 2012). Notably, PDCoV lacks the nsp1 gene and thus codes for only 15 nsps in total. Genomic similarities and dissimilarities for coronaviruses are illustrated in Fig. 1.1.

1.1.2 Early response to viral infection

Upon virus infection, a host reacts quickly to an invading virus by producing type I interferons (IFN-α/β) and elicits an antiviral state in infected cells and uninfected neighbor cells. Three different types of IFNs are known: type I IFNs (IFN-α/β), type II IFN (IFN-γ), and type III IFNs (IFN-λ) (Table 1.1). For humans, type I IFNs contain 13 subtypes of IFN-α and a single

subtype for IFN-β, IFN-ε, IFN-κ, and IFN-ω. For pigs, IFN-α is produced from as many as 17 functional genes. For type II IFN, only a single subtype of IFN-γ is reported for pigs, which is mainly produced in immune cells. Type III IFNs include IFN-λ1 (interleukin 29 [IL-29]), IFN-λ2 (IL-28A), IFN-λ3 (IL-28B), and IFN-λ4 (Kotenko et al., 2003; Prokunina-Olsson et al., 2013; Sheppard et al., 2003).

Different types of IFNs signal through different receptors. IFN-α/β signal through a heterodimeric complex composed of a single chain of IFN-α receptors 1 (IFNAR1) and 2 (IFNAR2), which is believed to be expressed on the surface of all nucleated cells (Gibbert et al., 2013; Pestka et al., 2004). IFN-γ forms a homodimer for signaling through the IFN-γ receptor (IFNGR) complex, which is composed of a dimer of two transmembrane-spanning receptors [IFN-γ receptors 1 (IFNGR1) and 2 (IFNGR2)] with broad tissue distributions. IFN-λ signals through heterodimers of interleukin-10 receptor 2 (IL10R2) and IFN-λ receptor 1 (IFNLR1). While IL-10R2 is widely distributed in different cell types, IFNLR1 is largely restricted to epithelial cells (Sommereyns et al., 2008), and thus subtypes of IFN-λ limit their antiviral functions to epithelial cells. All IFNs activate the Janus kinase (JAK)-signal transducer and activator of transcription (STAT) signaling pathway to establish an antiviral state. Since IFNGR1/2 are widely distributed, most cell types are capable of responding to IFN-γ (Valente et al., 1992). While the IFN-γ has pleiotropic effects on immune cells, a direct antiviral activity is rather limited. In contrast, both IFN-α/β and IFN-λ induce a potent antiviral state by regulating the expression of hundreds of interferon stimulating genes (ISGs). Even though IFN-α/β and IFN-λ utilize different receptors for downstream signaling, their induction and antiviral mechanism are similar, and *in vivo* studies for IFN-λ show a high degree of redundancy of these two IFN systems in lung epithelial cells (Ank et al., 2008; Mordstein et al., 2008; Mordstein et

al., 2010), raising a question why two seemingly redundant antiviral systems exist. The IFN signaling cascades are summarized in Fig. 1.2.

Swine enteric viruses are mostly transmitted via the fecal-oral route and a possible aerosol transmission, and some of them are highly infectious. TGEV infects and replicates primarily in small intestinal enterocytes and to a lesser extent in the respiratory tract (Kim et al., 2000). PEDV and PDCoV also infect the small intestinal enterocytes (Jung et al., 2015c; Jung and Saif, 2015), and thus intestinal epithelial surface is the first line of host defense to prevent enteric viral infections. Due to the distinctive features of the intestinal epithelial mucosal surface, induction and signaling of IFNs are unique. Coronaviruses have a large genome and have evolved to carry redundant mechanisms to counteract the host innate immune response. For SARS-CoV, at least 11 viral proteins have been identified as type I IFN antagonists (Kindler and Thiel, 2014; Shi et al., 2014a; Totura and Baric, 2012). By contrast, acute infection of TGEV induces a high level of IFN-α in newborn pigs (La Bonnardiere and Laude, 1981). Despite the variation of genome organization, swine enteric coronaviruses seem to utilize similar but distinct mechanisms for activation and evasion of host innate immunity on the intestinal epithelial surface.

1.2 PRODUCTION OF TYPE I IFNS AND THE IFN SIGNALING

The host innate immune system utilizes PRRs (pattern-recognition receptors) to sense and respond to PAMPs (pathogen-associated molecular patterns) of invading viruses (Kawai and Akira, 2011). This recognition of the membrane-bound PRRs triggers the activation of IFN induction pathway. Toll-like receptors (TLRs) are among the best-characterized groups of PRRs (Kawai and Akira, 2011). TLRs constitutes a family of single transmembrane proteins with

ectodomains containing the leucine-rich repeats for recognition of PAMPs and a cytosolic TIR (toll/IL-1 receptor) domain as a key domain transducing signals to downstream adaptors including TRIF (TIR-containing adaptor protein inducing IFN-β) and MyD88 (myeloid differentiation primary response gene 88) (Kawai and Akira, 2010). Among TLRs, TLRs 3, 7, 8, 9, and 13 are involved in endosomal nucleic acid sensing. TLR3 is the dsRNA sensor and responds to poly(I:C), a synthetic RNA analog (Kariko et al., 2004; Okahira et al., 2005). TLR7 and TLR8 recognize ssRNA derived from RNA viruses (Diebold et al., 2004; Heil et al., 2004), whereas TLR9 senses CpG DNA motifs in the genome of DNA viruses (Vollmer et al., 2004). TLR13 has recently been identified as the sensor for bacterial 23S ribosomal RNA (Oldenburg et al., 2012). The RLR (RIG-I-like receptor) family is responsible for the sensing of cytosolic RNA. The RLR members include RIG-I (activated retinoic acid-inducible gene I), MDA5 (melanoma differentiation gene 5), and LPG2 (laboratory of genetics and physiology 2). RIG-I and MDA5 respond to poly(I:C) with their specificities based on the length of dsRNA. RIG-I senses shorter dsRNA (~300 bp) containing a 5'-triphosphate panhandle structure, whereas MDA5 recognizes long dsRNA (>4 kb) fragments (Kato et al., 2008; Schlee et al., 2009; Schmidt et al., 2009). Cytoplasmic DNA sensors have been addressed including STING (stimulator of IFN genes) and cGAS (cyclic GMP-AMP synthase) for cytosolic DNA sensing (Ishikawa and Barber, 2008; Sun et al., 2013; Wu et al., 2013). For type I IFNs production, activated RIG-I or MDA5 binds to the mitochondrial adaptor protein MAVS/IPS-1 and recruits TRAF3 (TNF receptor-associated factor 3) and TRAF6. TRAF3 activates downstream IKK (IκB kinase)-related kinases such as TBK1 (TANK-binding kinase 1) and IKKε for induction of IRF3/IRF7-dependent type I IFN production (Fitzgerald et al., 2003; Sharma et al., 2003). TRAF6 leads to TAK1 activation, followed by NF-κB activation for type I IFN and other cytokine productions (Rajsbaum and

Garcia-Sastre, 2013). Within the IFN-β promoter, there are four regulatory cis elements, namely, positive regulatory domains (PRDs) I, II, III, and IV. PRD I/III, PRD II, and PRD IV are binding sites for IRFs, NF-κB, and ATF-2/c-Jun (AP-1), respectively (Honda et al., 2006). The expression of IFN-β requires the assembly of these regulatory factors on PRDs to form an enhanceosome complex which recruits CBP for IFN production (Randall and Goodbourn, 2008). Following production and secretion, IFNs bind to the cell surface receptors to trigger the activation of JAK-STAT pathway for the IFN-signaling cascade. The three different IFN systems signal through distinct IFN receptors. Type I IFNs and type III IFNs trigger the formation of ISGF3 complex for production of hundreds of ISGs. In contrast, type II IFN triggers the phosphorylation of STAT1 and subsequent formation of IFN-γ activation factor (GAF) for antiviral genes expression (Schneider et al., 2014).

Expression of the membrane-bound PRRs is cell type-dependent. Specific molecular features of the PRRs and the cell type that recognizes them are two main factors for the specificity in IFN subtype production (Hoffmann et al., 2015). Nearly all nucleated cells are capable of producing IFN-β through activation of IRF3 and NF-κB, but IFN-α subtypes are primarily produced by leukocytes (Cantell et al., 1981). Plasmacytoid dendritic cells (pDCs) are the most potent type I IFN producers with up to a hundred to a thousand times more IFN-α than other cell types (Siegal et al., 1999). Activated pDCs migrate to the lymph nodes and potentially influence various cell types through the secreted IFNs. How IFN responses vary during virus infection is still unclear. A recent study shows that different IFN responses depend on the activation of pDCs by interactions with infected cells or virus alone (Frenz et al., 2014). Levels of total IFN-α production in pDCs vary greatly with invading virus, time, and amount of inoculum (Thomas et al., 2014). Another study shows that pDCs produce a highly uniformed

IFN-α profile regardless of the PAMP (Szubin et al., 2008). Similar to IFNs-α/β, IFN-λ can be induced in different cell types by various viruses. IFN-λ can be expressed in a variety of cell types of the hematopoietic lineage, which also produces IFNs-α/β in abundance. Among the nonhematopoietic cells, epithelial cells are potent producers for IFN-λ. The IFN-λ response is largely restricted to the epithelium such that lung epithelial cells respond to IFNs-α/β and IFN-λ whereas intestinal epithelial cells respond exclusively to IFN-λ (Mordstein et al., 2010; Pott et al., 2011; Sommereyns et al., 2008).

1.3 ROLE OF IFNS ON THE INTESTINAL EPITHELIAL SURFACE

1.3.1 Intestinal epithelial barrier

Small intestinal epithelial cells (IECs) form a physical barrier to segregate the mucosal immune system and commensal microbial communities in the lumen. The Paneth and goblet cells secrete mucus and antimicrobial proteins to exclude invading bacteria and viruses from the epithelial surface, and renewal of the epithelial cell layer is controlled by the intestinal stem cells in the crypts. Secreted IgA (sIgA) also contributes to the barrier function. The lamina propria is made of stromal cells, B cells, T cells, dendritic cells, and macrophages. Intraepithelial lymphocytes (IELs) are localized between IECs, and these cells constitute a large and highly conserved T cell compartment, which serves through cytolysis of dysregulated IECs and renewal of IECs. Microfold (M) cells are found in the gut-associated lymphoid tissues (GALT) of the Peyer's patches and the mucosa-associated lymphoid tissue (MALT) of other parts of the gastrointestinal tract, and they are specialized for antigen sampling and initiation for mucosal immune responses (Peterson and Artis, 2014). Unlike the lung epithelium, the intestinal epithelium has to maintain the tolerance to the symbiotic gastrointestinal microflora while

mounting an effective immune response during infection. The intestinal epithelial barrier is depicted in Fig. 1.3.

1.3.2 Roles of IFN-α/β and IFN-λ in the intestine

Type I IFNs (IFNs-α/β) are major cytokines to restrict viral infections. Recent studies however shed a new light on the importance of IFN-λ for restricting viral infection in the intestinal epithelium. In the rotavirus model, IFNs-α/β rather play a minor role for restricting viral infections, and instead, IFN-λ plays a major role to inhibit viral replication in the intestinal epithelium (Angel et al., 1999; Pott et al., 2011). IECs strongly respond to IFN-λ but only marginally respond to IFNs-α/β *in vivo*. The effects of IFNs-α/β and IFN-λ are compartmentalized with the major effect of IFNs-α/β on the intestinal lymphocytes and IFN-λ on the epithelial cells (Pott et al., 2011). Distinct roles of IFNs-α/β and IFN-λ for controlling systemic and local dissemination of rotavirus, respectively, have been suggested. IFNs-α/β produced by mucosal pDCs can enhance B cell response to promote viral clearance and protection against re-infection (Deal et al., 2013). For rotavirus, significance of IFNs-α/β seems to vary depending on the viral strains, host, and synergy with other types of IFNs, but IFN-λ determines localized intestinal epithelial antiviral defense. A recent finding shows that activated IELs upregulate the IFNs-α/β and IFN-λ expression to mount a rapid antiviral state for protection of IECs (Swamy et al., 2015). Activation of IELs *in vivo* rapidly provokes ISGs expression through the IFN-α and IFN-λ receptors. Thus, activation of IELs offers an overt means to promote an innate antiviral potential of the intestinal epithelium.

Resistance of invading viruses in the gut epithelium relies mainly on IFN-λ, not IFNs-α/β, which raises a question on the ubiquitous expression of receptors for IFNs-α/β. A recent study

shows that mouse IECs minimally express functional type I IFN receptors and thus do not respond to type I IFNs, explaining why the IFNs-α/β system is unable to compensate the IFN-λ deficiency during enteric epitheliotropic viral infections (Mahlakoiv et al., 2015). This study shows that virus-infected IECs are potent producers of IFN-λ, suggesting that the gut mucosa possesses a compartmentalized IFN system in which epithelial cells respond predominantly to IFN-λ, whereas other cells of the gut rely on IFNs-α/β for antiviral defense. Timely production of IFN-λ in IECs drives rapid clearance of intestinal viral infections and limits viral shedding in the feces. The intestinal epithelium responds exclusively to IFN-λ in a non-redundant fashion to control epitheliotropic viruses (Pott et al., 2011). For reovirus, IFN-λ restricts initial viral replication and reduces viral shedding in the feces, whereas IFNs-α/β are critical for the prevention of systemic infection. Similarly, norovirus infection also requires IFN-λ to control persistent enteric infection, although IFNs-α/β restrict the systemic spread (Nice et al., 2015).

In the gut, the protective effect of the innate immunity, in particular IFN-λ, is counteracted by intestinal commensal bacteria (Baldridge et al., 2015). PEDV infection causes the decrease of commensal bacteria present in the healthy gastrointestinal tract and induces an unbalanced shift of gut microbiota (Koh et al., 2015; Liu et al., 2015b), suggesting a possible modulation of IFN-λ response by PEDV. The border surface of the intestinal epithelium is the major entry site for enteric viruses, and specific mechanisms are needed for the fail-safe protection of such multi-layered surfaces. Although IFN-λ production by IECs is required, it is not sufficient for protection of the epithelium from rotavirus-induced cell damages. The production and release of IL-1α by IECs following rotavirus infection enhances IL-22 production. A recent study identifies a cooperation of IFN-λ and IL-22 to synergistically curtail mucosal viral infection (Hernandez et al., 2015). The receptors for IL-22 and IFN-λ are restricted to

epithelial cells, and simultaneous engagement of both receptors on IECs is required for restriction of rotavirus infection, suggesting a second layer control is necessary (Hernandez et al., 2015). Downregulation of IFNLR1 and interference of the STAT1 signaling may be an important strategy for viral evasion (Sen et al., 2014).

After stimulation with poly(I:C) and infection with reovirus, both IECs and hematopoietic cells in the intestinal epithelium express IFN-λ strongly and quickly, but do not express IFNs-α/β genes (Mahlakoiv et al., 2015). Thus, mechanisms seem to have evolved to produce IFN-λ specifically and potently in the intestinal epithelium. Since common pathways are believed to be utilized for induction of both IFNs-α/β and IFN-λ (Onoguchi et al., 2007), the IFNs-α/β pathway is specifically blocked in IECs by an unknown mechanism. Another study shows that peroxisome-bound MAVS may preferentially activate IFN-λ expression (Odendall et al., 2014). Nlrp6 (nucleotide-binding oligomerization domain-like receptor 6) is an intracellular protein specific for tissues and cell-types with the highest expression in IECs (Elinav et al., 2011). Nlrp6 binds to viral RNA via the RNA helicase Dhx15 as a RNA sensor and triggers MAVS-dependent expression of IFN-α/β and IFN-λ plus ISGs, and thus plays an important role for intestinal antiviral response (Wang et al., 2015b).

Using gene-knockout mice for specific IFN receptors, IFN-λ has been identified to play an important role in the defense against SARS-CoV and other respiratory viral infections (Mordstein et al., 2010). Fecal shedding of SARS-CoV can be detected from mice lacking both receptors for IFN-α/β and IFN-λ but not from mice lacking single receptors, suggesting that IFN-λ controls viral infections in epithelial cells of both respiratory and gastrointestinal tracts. Relative contributions of the various IFN subtypes for restricting enteric coronavirus infections remain elusive. Both TGEV and PEDV can infect and replicate in PAMs in the respiratory tract

in vivo (Park and Shin, 2014). PEDV has also been shown to infect macrophages infiltrated in the lamina propria and modulates immune responses after infection of monocyte-derived DCs (MoDCs) and intestinal DCs (Gao et al., 2015; Lee et al., 2000). In summary, IFN-λ seems to be critical to efficiently restrict enteric coronavirus infections in the intestinal epithelial surface, including PEDV, TGEV, and possibly PDCoV infections, and in turn, these viruses may modulate the host IFN-λ response. It is of great interest to investigate how such enteric coronaviruses regulate the IFN-λ response in pigs. A full-length infectious cDNA clone is available for PEDV, and it will be useful to study individual gene functions using replicating mutants *in vivo*. As such, we will be able to better understand the pathogenic mechanisms of porcine enteric coronaviruses and host responses to such infections (Beall et al., 2016; Jengarn et al., 2015).

1.4 MODULATION OF IFN RESPONSE BY PORCINE ENTERIC CORONAVIRUSES

1.4.1 Aminopeptidase N (CD13) as the cellular receptor and viral tissue tropism

For coronaviruses, S protein and its interaction with a receptor on susceptible cells determine the host range and viral tropism (Bosch et al., 2003; Gallagher and Buchmeier, 2001). Unlike many other coronaviruses, cell culture adaptation of PEDV triggers mutations in the S protein sequence (Lawrence et al., 2014) and requires the supplement of an exogenous protease, typically trypsin, to activate the S protein to induce membrane fusion after binding to the cellular receptor (Hofmann and Wyler, 1988; Park et al., 2011; Wicht et al., 2014). The trypsin dependency of PEDV *in vitro* is consistent with the tissue tropism of trypsin-rich small intestine in pigs. Some of cell-adapted PEDV strains lose the trypsin-dependency (Nam and Lee, 2010; Wicht et al., 2014). PEDV-infected cells produce distinct cytopathic effects including cell fusion,

multinucleated syncytia formation, vacuolation, and detachment due to apoptotic cell death (Kim and Lee, 2014). A recent study shows that heparan sulfate on the cell-surface may function as an attachment factor for PEDV (Huan et al., 2015). As with TGEV, PEDV also utilizes aminopeptidase N (APN; CD13) as a functional receptor. APN is a heavily glycosylated transmembrane protein and is expressed by most cells of myeloid origin including monocytes, macrophages, granulocytes, and their hematopoietic precursors (Chen et al., 1996; Mina-Osorio, 2008; Riemann et al., 1999). It is also abundantly expressed in the brush border of epithelial cells from the small intestine and renal proximal tubules and some other cell membranes. In the small intestine, it plays a role in the final digestion of peptides generated from hydrolysis of proteins by gastric and pancreatic proteases (Kruse et al., 1988). TGEV utilizes APN as receptor for entry into swine testis (ST) cells, which however cannot render efficient propagation of PEDV (Delmas et al., 1992). This differentiation may be due to the relatively low level expression of APN on ST cells (Li et al., 2007). Over-expression of APN enhances PEDV infection, and an increased APN density enhances the PEDV susceptibility in cultured ST cells (Li et al., 2007; Nam and Lee, 2010; Oh et al., 2003). Porcine intestinal tissues are more sensitive for high-titer virus production for PEDV natural infection, which may due to the abundant expression of APN in porcine intestinal brush border membrane (Li et al., 2007). Collectively, the high-level expression of APN at the intestinal barrier correlates with the efficient replication of both TGEV and PEDV, and infectivity of PEDV is dependent on APN density. Additionally, PEDV also infects cultured cells of pigs, humans, monkeys, and bats (Liu et al., 2015a; Zhang et al., 2016), which suggests that PEDV may utilize APN of other species origin. Yet, Vero cells lack of APN mRNA transcripts (Li et al., 2016), and do not express detectable APN protein even by mass spectrometry analyses (Guo et al., 2014; Li et al., 2007; Shirato et al., 2011a,b; Zeng et al., 2015).

A Recent study showed that genetic ablation of APN expression had no effect on their susceptibility to PEDV, demonstrating that APN is not required for PEDV cell entry (Li et al., 2017b). This suggests that PEDV may utilize other unidentified receptors or co-receptors for efficient entry. Both PEDV and TGEV infect alveolar macrophages besides small intestinal epithelial cells (Laude et al., 1984; Park and Shin, 2014) . PEDV also infect infiltrated macrophages in the lamina propria *in vivo* (Lee et al., 2000). Even though the clinical signs of epidemic PEDV and TGEV infections are indistinguishable, it is of great interest to investigate whether the cell and tissue tropism contributes to the differential pathogenesis *in vivo*.

1.4.2 Activation of IFNs-α/β by TGEV

Porcine enteric coronaviruses replicate in IECs and are transmitted via a fecal-oral route. The viral entry and release for TGEV are restricted to the apical surface of polarized epithelial cells (Rossen et al., 1994). Experimental infection of newborn piglets with TGEV induces a strong and early IFN-α production in serum and intestinal secretions (La Bonnardiere and Laude, 1981). The blocking of the viral receptor still induces IFN-α response, indicating that the entry is not needed for IFN induction in leukocytes (Riffault et al., 1997). Early and strong IFN-α production can also be induced in nonimmune cells after exposure to TGEV-infected epithelial cells (Charley and Laude, 1988). The rapid and massive release of IFN-α in serum is mediated by M and E proteins of TGEV (Charley and Laude, 1988; Laude et al., 1992; Riffault et al., 1997). A specific point mutation in the M protein results in lower IFN-α induction as compared to wild-type virus (Splichal et al., 1997), and the virus-like particles made of M and E proteins induce IFN-α production in porcine leukocytes as almost efficiently as fully infectious TGEV (Baudoux et al., 1998). However, reconstituted virosomes lose the ability to induce IFN-α

production, indicating that the native envelope structure is essential (Riffault et al., 1997). Immunohistochemistry analysis of the tissues from TGEV-infected piglets show that IFN-α-producing cells (IPCs) are almost exclusively detected in the intestinal tissues and mesenteric lymph nodes (MLNs) at an early time of infection such as 6 h and disappeared by 24 h (Riffault et al., 2001). The majority of IPCs are localized between enterocytes in the epithelial layer, the lamina propria, around the Peyer's patches, and are accumulated in the MLNs (Riffault et al., 2001). The number of IPCs in spleen or peripheral lymph nodes is limited, and thus circulating IFN-α is likely originated from the gut and MLNs triggered by virus (Riffault et al., 2001). IPCs in pigs are identified as pDCs (Calzada-Nova et al., 2010). Interestingly, gut-associated IPCs express swine leucocyte antigen II (SLA II) and are distinct from TGEV-positive cells, suggesting that these cells may be the mucosal counterparts of the intestinal pDCs (Riffault et al., 2001). Contrary to pDCs that produce high levels of IFN-α and TNF-α after infection, porcine monocyte-derived DCs do not respond to TGEV (Guzylack-Piriou et al., 2006). The frequency of intestinal pDCs, however, is low comparing to other DCs, and thus the limited populations of intestinal pDCs may not be a major subset of antigen-presenting DCs. The production of IFN-α by intestinal pDCs in MLNs may flood the T cell area to influence the immune outcome (Charley et al., 2006). In addition to the production of IFN-α/β, TGEV induces phosphorylation and nuclear translocation of STAT1 in virus-infected cells and enhances the expression of ISGs (An et al., 2014). TGEV infection also promotes the p53 signaling to regulate apoptosis, and the viral nucleocapsid protein is responsible for this action and the cell cycle arrest (Ding et al., 2014a; Huang et al., 2013a).

IFN-α has been shown to inhibit TGEV protein expression without reducing viral RNA in TGEV-infected cells (Jordan and Derbyshire, 1995). Infection of TGEV upregulates the

expression of 2'-5'-oligoadenylate (2'-5'A) synthetase for inhibition of viral replication (Bosworth et al., 1989; Jordan and Derbyshire, 1995). Swine IFN-α has been shown to enhance the protection from TGEV and alleviate clinical signs in piglets when orally co-administered with *Salmonella enterica* serovar Typhimurium expressing swine IFN-α with or without cytokine IL-18 (Kim et al., 2010; Lee et al., 2011). The viral load is significantly reduced in intestinal segments of piglets when treated with an IFN inducer before challenge, but no reduction in viral yields is seen when simultaneously inoculated with TGEV and IFN-α, suggesting that IFN may be more useful prophylactically (Jordan and Derbyshire, 1994).

1.4.3 PEDV pathogenesis and innate signaling

PEDV is cytolytic with an acute necrosis in IECs, leading to villous atrophy in the small intestine (Jung et al., 2014). The high mortality of PEDV in piglets is associated with extensive dehydration resulting from severe villous atrophy. The severe dehydration may be due to the extensive structural destruction and disorganization of tight junctions and adherens junctions during infection in nursing piglets (Jung et al., 2015b). The slower turnover of the enterocytes, which is mediated by the regeneration of crypt stem cells in nursing piglets compared to weaned piglets, is probably responsible for the age-dependent resistance to PED (Jung et al., 2015a). PEDV antigens are mainly observed in villous enterocytes of the small and large intestines. PEDV also infect macrophages infiltrated in the lamina propria *in vivo* (Lee et al., 2000). Experimental infection of TGEV shows that the lung is the tract sustaining viral replication and IFN synthesis (La Bonnardiere and Laude, 1983). TGEV can replicate in porcine alveolar macrophages (PAMs) *in vitro* and induces a marked synthesis of type I IFNs (Laude et al., 1984). Similarly, PEDV can also infect and replicate in PAMs *in vivo* (Park and Shin, 2014), suggesting

an extra-intestinal replication of PEDV. Additionally, PEDV has been shown to induce apoptotic cell death *in vitro* and *in vivo* through the caspase-independent mitochondrial apoptosis-inducing factor (AIF) pathway (Kim and Lee, 2014). Another study claims that PEDV may not induce the death of enterocytes in the small intestine through apoptosis pathway in infected pigs (Jung and Saif, 2015).

After binding to APN, PEDV is internalized into target cells by direct membrane fusion, and the genomic RNA is released into the cytosol for replication. The sensing of viral nucleic acids by PRRs in the endosome or cytosol initiates the innate immune signaling. Like other coronaviruses, PEDV likely replicates in the double membrane vesicles to hide the viral RNA from sensing by PRRs and to attenuate the innate immune response (Angelini et al., 2013; Snijder et al., 2006). A recent study shows that TLR2, TLR3, and TLR9 may contribute to NF-κB activation in response to PEDV infection in IECs *in vitro* but does not cause RIG-I activation (Cao et al., 2015b). TLR2 on the plasma membrane responds to viral glycoproteins on the envelope to induce production of IFNs and inflammatory cytokines, while TLR3 and TLR9 are localized largely in the endosome to sense dsRNA and CpG DNA, respectively (Boehme and Compton, 2004). This suggests that PEDV may initiate the innate immune response through its surface glycoprotein and viral nucleic acids in the endosomes. PEDV activates the ERK (extracellular signal-regulated kinase) pathway early during infection independently from viral RNA replication (Kim and Lee, 2015). Knockdown or inhibition of ERK suppresses viral transcription, protein expression, and progeny production, which suggests that the activation of ERK pathway is beneficial and required for PEDV replication (Kim and Lee, 2015). Proteomics analysis of PEDV-infected cells shows differential expression of proteins involved in apoptosis, signal transduction, and stress responses (Zeng et al., 2015), and ERK1 is significantly

downregulated during PEDV infection. Thus, the ERK pathway modulation by PEDV is of further interest to study. In one study, six different signaling pathways have been shown to be differentially regulated by PEDV, which includes the RLR, Rap1, PI3K-Akt, MAPK, JAK-STAT, and TLR signaling pathways (Sun et al., 2015), suggesting the modulation of host innate immunity by PEDV.

For PDCoV, little is known about the viral modulation of host immunity. The PDCoV N protein forms non-covalently linked oligomers localized in the nucleolus (Lee and Lee, 2015). The N protein alters the expression of cellular proteins relevant to cell division, metabolism, stress response, protein biosynthesis and transport, cytoskeleton networks, and cell communication (Lee and Lee, 2015). Notably, PDCoV N protein upregulates two members of the heat shock protein 70 (HSP70) family. In two lines of swine cells (LLC-PK1 and ST), which are used to isolate and propagate PDCoV (Jung et al., 2016), apoptosis is induced *in vitro*, but no apoptosis is observed *in vivo* in PDCoV-infected intestinal enterocytes (Jung et al., 2016). This suggests that a better cell system is needed to mimic *in vivo* conditions for PDCoV infections, and for this purpose IECs, intestinal enteroids, or organoids may be useful (Finkbeiner et al., 2012; Jung et al., 2016).

PEDV infection in suckling pigs does not alter the natural killer (NK) cell activity compared to weaned pigs that show significantly higher NK cell activities in the blood and ileum (Annamalai et al., 2015). Interestingly, PEDV infection seems to stimulate a marked induction of serum IFN-α in suckling pigs at 1-day postinfection which then declines to the basal level by 5-day post-infection (Annamalai et al., 2015). In weaned pigs however, PEDV infection causes a slight induction of serum IFN-α at 3-day postinfection and a decrease to the basal level at 5-day postinfection. The peak production of serum IFN-α coincides with the peak of viral RNA

shedding in the feces and serum of suckling pigs or serum in weaned pigs and the onset of diarrhea. PEDV infection differentially modulates inflammatory cytokines in both suckling and weaned pigs and induces a similar level of TNF-α and IFN-α (Annamalai et al., 2015). According to this study, PEDV is capable of modulating IFN-α production especially in weaned pigs. Since PEDV infection occurs in the small intestine as with TGEV, it is of interest to examine IFN-α in the intestinal secretions and how PEDV modulates type I IFN induction in the intestinal pDCs. Intestinal DCs are highly effective antigen-presenting cells distributed beneath the epithelial lining. Unlike TGEV, PEDV infects MoDCs and produces high levels of IL-12 and INF-γ without alteration of the IL-10 expression (Gao et al., 2015). Interaction between PEDV and MoDCs affects the stimulation of T cell response *in vitro*. PEDV may also enhance the ability of porcine intestinal DCs to sample antigens and activate T-cell proliferation *in vivo* (Gao et al., 2015). How the intestinal pDCs respond to PEDV infection and modulate innate immune signaling remains to be determined.

1.4.4 Evasion of IFN response by PEDV

IFNs-α/β play an important role in restricting viral infections, and enteric coronaviruses have evolved redundant mechanisms to counteract the host innate immunity for optimal viral adaptation and replication. Even though TGEV activates IFNs-α/β production, its accessory protein 7 modulates IFNs-α/β expression by interacting with PP1 and prolongs viral dissemination for increased survival (Cruz et al., 2011). Accumulating evidence shows that PEDV also has an ability to evade host IFN response. PEDV does not activate IFN-β expression even after poly(I:C) stimulation in virus-infected cells (Xing et al., 2013). It appears that PEDV infection inhibits IRF3 nuclear translocation and thus blocks IRF3-mediated IFN induction. IECs

are major target cells of PEDV in pigs, and in these cells, PEDV blocks the activation of MAVS/IPS-1 and IRF3 nuclear translocation in the RIG-I-mediated pathway and do not induce IFN-β expression (Cao et al., 2015a). IPEC-J2 cells are epithelial cells derived from the jejunum of a colostrum-deprived neonatal pig of 12 h of age (Zhao et al., 2014; Dr. A. Blikslager, North Carolina State University). These cells however appear to be non-permissive for PEDV infection (unpublished data), and thus they are less useful than the initial anticipation for the study of PEDV innate immune evasion.

PEDV dramatically decreases the level of ubiquitin (Ub)-conjugated proteins in the cytoplasm. Papain-like proteinase 2 (PLP2) in nsp3 of PEDV contains a deubiquitinase (DUB) activity to process the cytosolic K48- and K63-linked polyubiquitin chains (Xing et al., 2013). PLP2 in nsp3 of both α-CoV and β-CoV could process both lysine-48- and lysine-63-linked polyubiquitin chains of the cytosolic proteins (Chen et al., 2014; Clementz et al., 2010). SARS-CoV PLP2 reduces the levels of ubiquitinated forms of RIG-I, STING, TRAF3, TBK1, and IRF3 in the STING-TRAF3-TBK1 complex for inhibition of the type I interferon signaling pathway (Chen et al., 2014). Similarly, PEDV PLP2 interacts with deubiquitinated RIG-I and STING to antagonize IFN response. PLP2 of SARS-CoV specifically deubiquitinates MDM2 (mouse double minute 2 homolog) and degrades p53 to suppress IFN signaling (Yuan et al., 2015). Similarly, PEDV upregulates MDM2 expression, degrades p53, and significantly inhibits IRF7 expression, suggesting that PEDV PLP2 may also target the p53 pathway for innate immune evasion and inhibit p53-dependent apoptosis (Yuan et al., 2015). Collectively, PEDV differentially modulates ubiquitination levels in the cytoplasm and the nucleus for modulation of innate immune responses.

PEDV infection leads to activation of the NF-κB pathway in IECs (Cao et al., 2015b). In another study, PEDV normally induces activation of NF-κB and AP-1 following poly(I:C) stimulation at 24 h postinfection (Xing et al., 2013). These studies represent a relatively late stage for PEDV infection. PEDV may inhibit NF-κB activation at an early stage for optimal survival and then activates it for inflammation at the late stage. For porcine reproductive and respiratory syndrome virus (PRRSV), which is an arterivirus of the *Nidovirales* order, NF-κB is activated 30 min after infection (Fu et al., 2012). Thus, how PEDV inhibits NF-κB during an early time of infection is of question and needs to be explored. For SARS-CoV, the N protein activates NF-κB (Liao et al., 2005) whereas the M protein suppresses NF-κB probably through a direct interaction with IKKβ (Fang et al., 2007). For PEDV, the E and N proteins cause ER stress leading to activation of the NF-κB pathway for up-regulation of IL-8 and Bcl-2 (Xu et al., 2013a; Xu et al., 2013b), and the M protein of PEDV is reported to induce a cell cycle arrest at the S phase via the cyclin A pathway (Xu et al., 2015). In other study, the N protein blocks the IFN-β production and ISGs expression, leading to suppression of the IRF3 and NF-κB activities (Ding et al., 2014b). The N protein is an RNA-binding protein and shuttles between the cytoplasm and nucleus (Shi et al., 2014b). Furthermore, N interacts with TBK1 and sequesters its association with IRF3 to block the phosphorylation and nuclear translocation of IRF3 leading to inhibition of IRF3-mediated IFN production (Ding et al., 2014b). The nsp5 protein of PEDV is a 3C-like proteinase and has been shown as an IFN antagonist. The cysteine proteinase activity of nsp5 cleaves NEMO which is an essential NF-κB modulator and disrupts the RIG-I/MDA5 signaling (Wang et al., 2015a). Modulation of innate immune response and signaling by PEDV infection is summarized in Table 1.2.

For betacoronavirus SARS-CoV, nsp14 is an exoribonuclease and nsp15 is an endoribonuclease, and both function through a specific digestion of dsRNA and subsequent removal of RNA-PAMPs, leading to suppression of IFN responses (Kindler and Thiel, 2014). SARS-CoV nsp16 is a 2'-*O*-methlytransferase that modifies the 5' cap structure of viral RNA and functions to avoid detection by the host immune system (Totura and Baric, 2012). PEDV nsp14, nsp15, and nsp16 correspond to nsp14, nsp15, and nsp16 of SARS-CoV and the innate immune evasion functions remain to be examined. The M protein plays an important role in viral assembly and induction of PEDV neutralizing antibodies, and ORF3 is the sole accessory protein of PEDV and its role for pathogenesis remains enigmatic. Some strains of cell-adapted PEDV display internal deletions in the ORF3 gene (Park et al., 2008), suggesting that ORF3 relates to adaptation and pathogenicity. ORF3 has also been shown to function as an ion channel protein and thus the suppression of ORF3 expression inhibits viral production (Wang et al., 2012). Additionally, ORF3 delays the S phase in dividing cell and suppresses the cell cycle progression (Ye et al., 2015). A contradictory data exists that ORF3 causes an inability to recover progeny virus from a full-length infectious clone, suggesting that ORF3 negatively modulates PEDV replication *in vitro* (Jengarn et al., 2015). However, the deletion of entire ORF3 by targeted RNA recombination has been possible and ORF3 appears nonessential for PEDV replication *in vitro* (Li et al., 2013). ORF3 facilitates the vesicle formation in ORF3-expressing cells (Ye et al., 2015), implicating an important role of ORF3 for innate immune evasion. The viral antagonists may target different signaling pathways to modulate the host innate immunity synergistically and efficiently during infection. The modulation of type I IFN responses by PEDV and the IFN antagonism by PEDV proteins is shown in Fig. 1.2.

1.4.5 Coronavirus nsp1 as a multifunctional IFN antagonist

Coronavirus nsp1 is the N-terminal cleavage product of polyproteins pp1a and pp1a/b processed by the papain-like proteinase 1 (PLP1) activity of nsp3 (Ziebuhr, 2005). The nsp1 gene is one of the most divergent genes among four different genera. Only the genome of α-CoV and β-CoV codes for nsp1, whereas the genome of γ-CoV and δ-CoV lacks the nsp1 gene (Woo et al., 2010; Woo et al., 2012; Ziebuhr, 2005; Ziebuhr et al., 2007). The nsp1 gene of α-CoV is much smaller than that of β-CoV and the sequence homology is also limited. The PEDV nsp1 gene encodes for 110 amino acids with the predicted molecular migration of 12 kD. The protein sequence of nsp1 does not harbor any known cellular functional motifs (Connor and Roper, 2007) and thus is a genus-specific genetic marker (Snijder et al., 2003). However, nsp1 of α-CoV and β-CoV shares similar functions. Coronavirus nsp1, especially β-CoV nsp1, regulates host cell and viral gene expression (Narayanan et al., 2014). The nsp1 protein of α-CoV and β-CoV is a potent IFN antagonist, and among all coronaviruses, SARS-CoV nsp1 is best characterized. SARS-CoV nsp1 inhibits the reporter gene expression under the constitutive promoters as well as the IFN-β promoter (Kamitani et al., 2006). As with SARS-CoV nsp1, murine hepatitis coronavirus (MHV) nsp1 and HCoV-229E nsp1 affect the cellular gene expression by suppressing IFN-β, IFN-stimulated response element (ISRE), and SV40 promoter (Zust et al., 2007). MHV nsp1 facilitates viral replication in mice by suppressing IFN-α/β through an unknown mechanism. MHV nsp1 and SARS-CoV nsp1 are distributed in the cytoplasm of virus-infected cells (Brockway et al., 2004; Kamitani et al., 2006), and SARS-CoV nsp1 suppresses IFN mRNA accumulation without altering the IRF3 dimerization (Kamitani et al., 2006). SARS-CoV nsp1 blocks the NF-κB, IRF3, and IRF7 activities. SARS-CoV nsp1 also inhibits IFN-dependent signaling by interfering STAT1 phosphorylation (Wathelet et al., 2007). Bat-CoV

nsp1 inhibits type I IFNs and ISGs production (Tohya et al., 2009), HCoV-229E nsp1 and HCoV-NL63 nsp1 also inhibits the IFN-β, ISRE, ISG15 activities as well as the SV40, HSV-TK and CMV promoters (Wang et al., 2010; Zust et al., 2007).

The emerging enteric coronaviruses PEDV has caused epidemic and endemic infections in pig populations in many countries and have become a major economic threat to the pork industry. The intestinal epithelial surface is the first line of defense to restrict the enteric viral infections, and both IFN-α/β and IFN-λ are important antiviral cytokines that viruses have evolved to counteract. Since enteric coronaviruses infect intestinal epithelial surface, several questions remain to be answered (Fig. 1.3). Firstly, the type I IFN antagonists of PEDV need to be identified. Secondly, whether PEDV and PDCoV selectively activate and/or modulate IFN-λ production and whether IFN-λ plays a protective role on the intestinal surface. Thirdly, how different cell types such as IECs, pDCs, and IELs in the intestinal barrier induce different types of IFNs and function for mucosal defense. Additionally, the intestinal epithelium constantly interacts with commensal bacteria and opportunistic viral infections, and thus IFN systems must be able to deal with these organisms without severe inflammation and tissue damages. Thus, better research models for cells and animals are needed to truly reflect viral evasions from innate immune defense. Lastly, specific cytokine mediators are produced in IECs, and how they respond to porcine enteric viral infections is of an additional interest.

1.5 HYPOTHESIS AND OBJECTIVES OF THE THESIS

Viruses infect and replicate in the host cells to complete their life cycle. The virus-host interactions provide valuable information on the understanding of viral pathogenesis. The immune response, especially the early innate immune response is essential to protect host cells

against invading viruses. In turn, viruses have developed sophisticated mechanisms to counteract host innate immunity and to establish productive infection. Especially, RNA viruses with a relative small coding capacity have evolved to arm with multifunctional innate immune antagonists.

Both type I and type III interferons (IFNs) are important innate immune components against viral infections. Suppression of type I IFNs have been observed for both arteriviruses and coronaviruses in the order *Nidovirales*. For PRRSV, an arterivirus, six viral proteins have been identified as IFN antagonists, whereas for SARS-CoV, a betacoronavirus, eleven proteins have been identified as IFN antagonists. For PEDV, an alphacoronavirus, the current understanding on the modulation of innate immune signaling is rather limited. Modulation of innate immune response by PEDV at the intestinal surface needs to be investigated.

In the present study, PEDV modulation of host innate immune responses will be studied and the molecular basis for this modulation will be investigated. A suitable cell system to study the innate modulation by PEDV will be identified. The IFN viral antagonists will be identified. Important functional motifs and residues in the IFN antagonist will be determined, and PEDV modulation of cytokine expressions will be addressed. Interactions between viral IFN antagonist and host cells will be determined for a better understanding for evasion mechanisms. This study will form the basis for pathogenic mechanisms of PEDV and may facilitate the design of an effective control measure for PED.

1.5.1 Principle hypothesis

PEDV has the capacity to suppress the induction of both type I and type III IFNs. It is anticipated that PEDV encodes multiple IFN antagonists. The most potent IFN antagonist will be

further studied for its molecular action and structural requirements. Due to the unique features of intestinal mucosal surface and the crucial role of type III IFN for the intestinal antiviral defense, PEDV will modulate the type III IFN response during infection.

1.5.2 Specific aims

Specific aim 1: Suppression of type I IFN induction by PEDV and identification of IFN antagonists. Type I IFN antagonists will be identified and the molecular basis for evasion strategy will be examined.

Specific aim 2: Examination of cytokine expression profile by PEDV and the molecular basis for temporal modulation of NF-κB activity. Viral proteins regulating the NF-κB activity will be identified and the mechanism of action will be explored.

Specific aim 3: Modulation of type III IFN induction by PEDV in intestinal epithelial cells. A porcine intestinal epithelial cell model for PEDV will be developed and how PEDV modulates the induction and signaling of IRF1-mediated type III IFNs in the porcine intestinal epithelial cells will be examined.

1.6 FIGURES AND TABLES

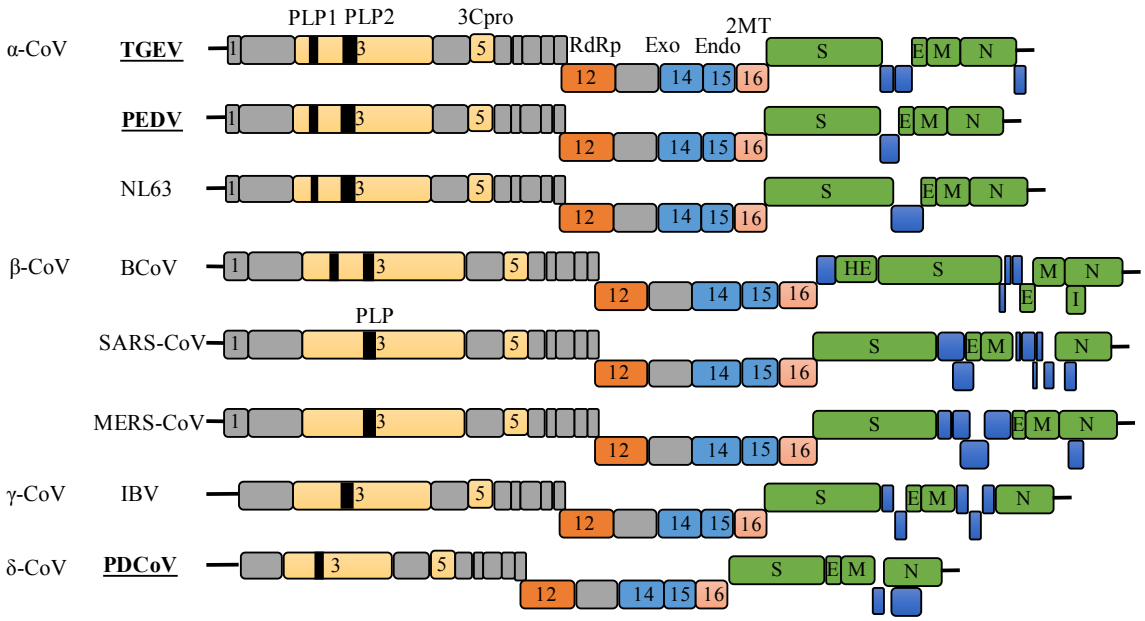

Fig. 1.1: Comparative genome organization of the representative coronaviruses from each genus in the family Coronaviridae. Swine enteric coronaviruses (TGEV, PEDV, and PDCoV) are indicated in bold underlined. Structural proteins are presented in green. Putative accessory proteins are shown in blue. Nonstructural proteins in ORF1a/b are presented in grey or other colors. Papain-like proteinases (PLP1 and PLP2), coronavirus 3C-like proteinase (3Cpro), RNA-dependent RNA polymerase (RdRp), two viral nucleases (nsp14 as exonuclease and nsp15 as endonuclease), and 2'-*O*-methytransferase (2MT; nsp16) are indicated by respective nsp numbers. The genome for *Alaphacoronavirus* and *Betacoronavirus* contains the nsp1 gene in different lengths, whereas the genome for *Gammacoronavirus* and *Deltacoronavirus* lacks the nsp1 gene. TGEV, transmissible gastroenteritis coronavirus; PEDV, porcine epidemic diarrhea virus; NL63, human coronavirus NL63; BCoV, bovine coronavirus; SARS-CoV, severe acute respiratory syndrome coronavirus; MERS-CoV, middle east respiratory syndrome coronavirus; IBV, avian infectious bronchitis virus; PDCoV, porcine deltacoronavirus; HE, hemagglutinin-esterase; S, spike; E, envelope; M, membrane; N, nucleocapsid; I, internal open reading frame.

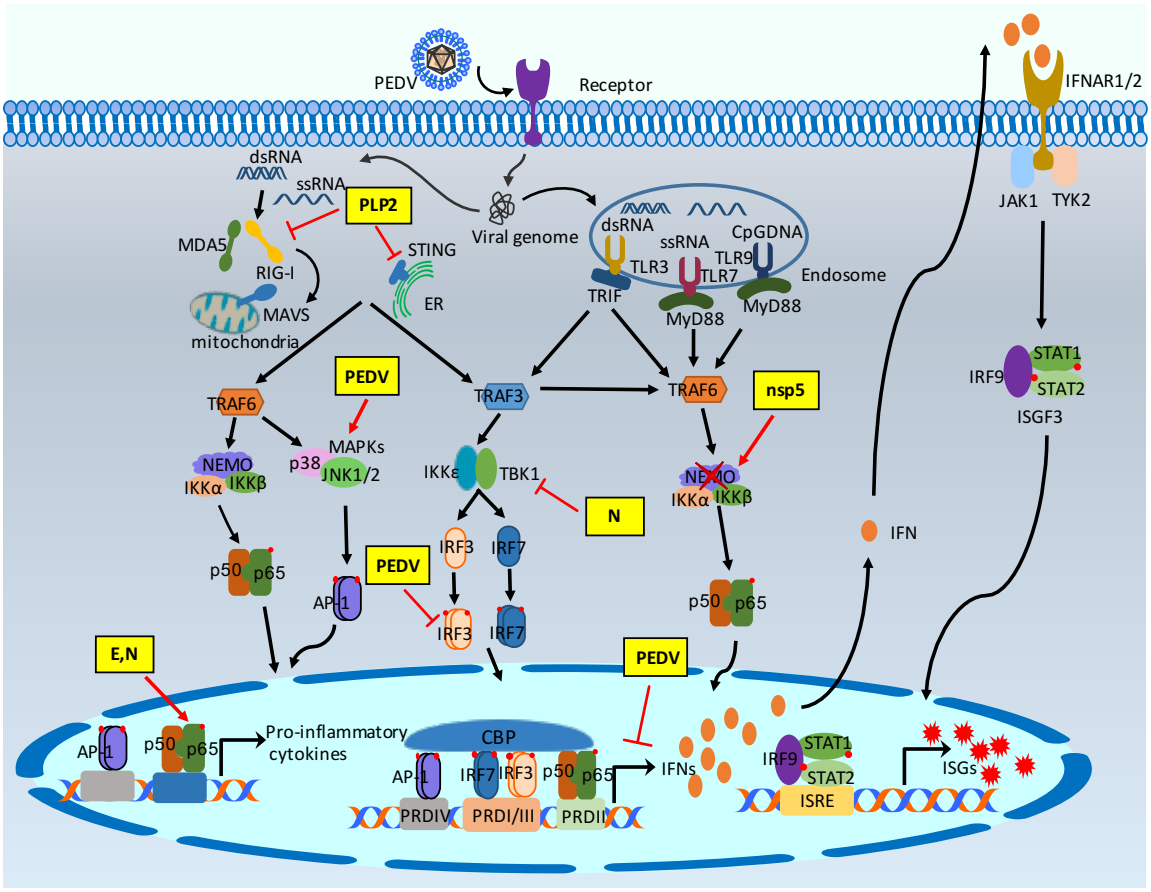

Fig. 1.2: Modulation of type I IFN response by PEDV proteins. After binding to the celluar receptor APN, PEDV is internalized into target cells by direct fusion of viral-cellular membranes, and the viral genomic RNA is released into the cytosol for replication. The single-stranded viral RNA as well as dsRNA as a replicative intermediate are sensed by host innate nucleic acids sensors in the cytoplasm and the endosome. The activation of innate immune sensors further initiates the production of type I interferons or pro-inflammatory cytokines after binding of activated NF-κB, AP-1, IRF3, and IRF7 to the respective PRD regions. Type I IFNs are secreted and bind to the cell surface receptors of both virus-infected and non-infected neighbor cells to induce the nuclear localization of ISGF3 complex. Activation of JAK-STAT pathway induces the production of hundreds of interferon stimulating genes (ISGs) for establishment of the antiviral state. The PEDV IFN antagonists intervene the IFN signaling pathway at different stages. The modulation of the type I IFN response by PEDV and PEDV proteins are shown in yellow boxes.

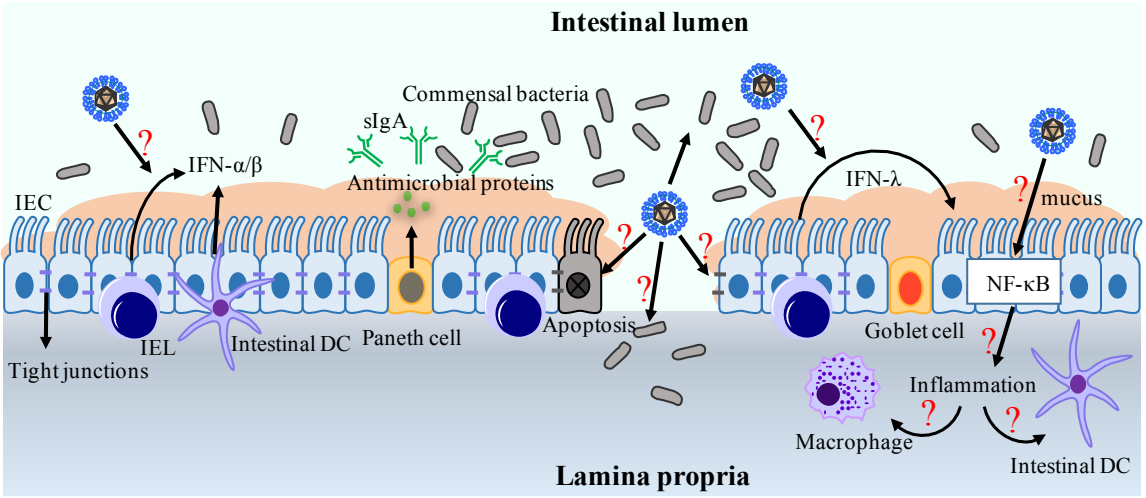

Fig. 1.3: Infection of porcine enteric coronaviruses and innate immune defense at the intestinal epithelial barrier. PEDV suppresses IFN-α/β production and PEDV-specific viral antagonists have been identified (see text). Some questions need to be explored for host-PEDV/PDCoV interactions and their pathogenic mechanisms. Question marks (red) indicate unknown mechanisms that remain to be studied as described in the text. IEC, intestinal epithelial cells; IEL, intraepithelial lymphocytes; DC, dendritic cells.

Table 1.1: Types of interferons, antiviral functions, and their cellular receptors.

IFN	Subtype	Celluar source	Antiviral function	IFN receptor	Receptor distribution
Type I IFN	IFN-α (17 for pig, and 13 for human), IFN-β (1), IFN-ε (1), IFN-κ (1), IFN-ω (1)	Nearly all nucleated cells produce IFN-β. IFN-α subtypes are primarily produced by leukocytes. pDCs are the most potent type I IFN producers. IFN-κ and IFN-ε produced in a tissue-specific manner.	Potent antiviral activities.	IFNAR1 and IFNAR2	Nearly all nucleated cells, except intestinal epithelial cells (IECs).
Type II IFN	IFN-γ (1)	Made primarily by immune cells such as CD4 and CD8 T cells, NK and NKT cells, DCs, and macrophages.	More of an interleukin than an interferon. Modest antiviral activity.	IFNGR1 and IFNGR2	Broad tissue distribution.
Type III IFN	IFN-λ (4)	A variety of human primary cell types of hematopoietic lineage. Epithelial cells are the potent producers for type III IFNs among the nonhematopoietic cells.	Largelyrestricted to epithelium. lung epithelium responds to both type I and III IFNs. IECs respond exclusively to type III IFNs.	IFNLR1 and IL-10R2	IL-10R2 is widely distributed across cell types. IFNLR1 is mainly restricted to epithelial cells.

Table 1.2: Modulation of innate immune response and signaling by PEDV.

Modulation of innate immune responses by PEDV	Model	References
Suppression of IFN-β induction upon poly(I:C) stimulation and inhibits IRF3 nuclear translocation.	Vero E6 cells	Xing et al., 2013
Lack of poly(I:C)-mediated IFN-β induction and blocking activation of IPS-1 in RIG-I-mediated pathway.	Intestinal epithelial cells (IECs)	Cao et al., 2015a
Ativation of NF-κB pathway through TLR2, TLR3, and TLR9.	IECs	Cao et al., 2015b
Activation of extracellular signal-regulated kinase (ERK) pathway early during infection.	Vero cells	Kim and Lee, 2015
PEDV infection causes undetectable natural killer (NK) cell activity in suckling piglets compared to weaned pigs.	Pigs	Annamalai et al., 2015
A marked induction of serum IFN-α in suckling pigs at 1 day post infection, but it is declined significantly to the base level at 5 days post-infection.	Pigs	Annamalai et al., 2015

CHAPTER 2: SUPPRESSION OF TYPE I INTERFERON PRODUCTION BY PORCINE EPIDEMIC DIARRHEA VIRUS AND DEGRADATION OF CREB-BINDING PROTEIN BY NSP1

2.1 ABSTRACT

Type I interferons (IFN-α/β) are the major components of the innate immune response of hosts, and in turn many viruses have evolved to modulate the host response during infection. We found that the IFN-β production was significantly suppressed during PEDV infection in cells. To identify viral IFN antagonists and to study their suppressive function, viral coding sequences for the entire structural and nonstructural proteins were cloned and expressed. Of 16 PEDV nonstructural proteins (nsps), nsp1, nsp3, nsp7, nsp14, nsp15 and nsp16 were found to inhibit the IFN-β and IRF3 promoter activities. The sole accessory protein ORF3, structure protein envelope (E), membrane (M), and nucleocapsid (N) protein were also shown to inhibit such activities. PEDV nsp1 did not interfere the IRF3 phosphorylation and nuclear translocation but interrupted the enhanceosome assembly of IRF3 and CREB-binding protein (CBP) by degrading CBP. A further study showed that the CBP degradation by nsp1 was proteasome-dependent. Our data demonstrate that PEDV modulates the host innate immune responses by degrading CBP and suppressing ISGs expression.

2.2 INTRODUCTION

Porcine epidemic diarrhea (PED) is a highly contagious acute enteric disease characterized by vomiting, watery diarrhea, and severe dehydration of up to 80-100% mortality in suckling piglets (Song and Park, 2012; Sun et al., 2012a; Debouck and Pensaert, 1980; Junwei

This chapter has appeared as an article in Virology. The original citation is: Zhang, Q., Shi, K., Yoo, D., 2016. Suppression of type I interferon production by porcine epidemic diarrhea virus and degradation of CREB-binding protein by nsp1. Virology 489, 252-268.

et al., 2006). PED was first reported in England in feeder and fattening pigs during 1970s (Wood, 1977), and reemerged in Asia since 2010 with greater virulence and economic losses (Chen et al., 2013; Li et al., 2012; Puranaveja et al., 2009; Yang et al., 2013). In the US, PEDV appeared for the first time in 2013 and severely affected most pig-producing states (Chen et al., 2014; Marthaler et al., 2013; Mole, 2013; Stevenson et al., 2013). The causative agent is porcine epidemic diarrhea virus (PEDV), which belongs to the *Alphacoronavirus* genus in the family *Coronaviridae* (http://ictvonline.org/virustaxonomy.asp). PEDV is an enveloped virus with a single-stranded positive-sense RNA genome of approximately 28 kb in length with the 5'-cap and the 3'-polyadenylated tail. The PEDV genome is arranged with ORF1a, ORF1b, S, ORF3, E, M, N, in order with both termini flanking with the 5'- and 3'-untranslated regions (UTRs) (Duarte et al., 1993). ORF1a codes for the large polyprotein PP1a, while ORF1b is always expressed as a fusion protein PP1a/b with PP1a through a ribosomal frameshifting. PP1a and PP1a/b are further processed to 16 nonstructural proteins, nsp1 through nsp16. ORF3 codes for an accessory protein which is likely an additional nonstructural protein, whereas S, E, M and N genes code for four structural proteins (Song and Park, 2012).

During viral infection, the sensing of foreign nucleic acids in the cytosol leads to the activation of an innate immune response to produce type I interferons (IFN-α/β) and establishes an antiviral state. The type I IFNs and IFN-mediated response provide a first line of defense against viral infection. The host innate immune system deploys the pattern-recognition receptors (PRRs) to sense and respond to the pathogen-associated molecular patterns (PAMPs) of virus (Kawai and Akira, 2011). This recognition triggers the activation of retinoic acid-inducible gene I (RIG-I) or melanoma differentiation gene 5 (MDA5), which further binds to the mitochondrial adaptor protein MAVS/IPS-1 and recruits TNF receptor-associated factor 3/6 (TRAF3 and

TRAF6). TRAF3 activates IκB kinase (IKK)-related kinases such as TANK-binding kinase 1 (TBK1) and IKKε for phosphorylation of interferon regulatory factors 3 and 7 (IRF3/IRF7) and type I IFN production (Fitzgerald et al., 2003; Sharma et al., 2003). TRAF6 leads to TANK1 activation, followed by NF-kB activation and cytokine production (Rajsbaum and Garcia-Sastre, 2013). Upon TBK1 activation, phosphorylated IRF3 undergoes homodimerization and unveils the nuclear localization signal leading to the nuclear translocation, where it forms a complex with the transcription co-activator CREB (cAMP responsive element binding)-binding protein (CBP)/p300 (Dragan et al., 2007; Lin et al., 1998; Panne et al., 2007). The IRF3-CBP/p300 complex further binds to the positive regulatory domain (PRD) I–IV regions of the IFN-β promoter to assemble the enhanceosome together with NF-κB and other factors to turn on the transcription of type I IFN genes (Honda and Taniguchi, 2006). The IRF3-CBP/p300 interaction is crucial for IFN transcription. Following production and secretion, IFN molecules bind to the cell surface receptors and trigger the activation of Janus kinase-signal transducers and activators of transcription (JAK-STAT) signaling cascade. Phosphorylated STAT1 and STAT2 associate to form a heterodimer, which in turn recruits the IFN-regulatory factor 9 (IRF9) to form the IFN-stimulated gene factor 3 (ISGF3). ISGF3 translocates to the nucleus and induces genes regulated by IFN-stimulated response elements (ISRE), resulting in expression of hundreds of antiviral genes and establishment of an antiviral state (Stark and Darnell, 2012).

In turn, many viruses have evolved to counteract the host innate immune defense and such viral functions are often redundant. For *nidoviruses*, eleven and six viral proteins have been described as IFN antagonists for severe acute respiratory syndrome coronavirus (SARS-CoV) and porcine reproductive and respiratory syndrome virus (PRRSV), respectively (Huang et al., 2014; Kindler and Thiel, 2014; Shi et al., 2014; Sun et al., 2012b; Totura and Baric, 2012). For

Betacoronaviruses, nsp1 has been reported as a multifunctional viral antagonist for innate immune response (Huang et al., 2011b; Narayanan et al., 2008; Wang et al., 2010). For PEDV, the viral modulation of innate immune signaling is poorly understood. PEDV infects Vero cells, but these cells are type I IFN-deficient due to a chromosomal deletion (Desmyter et al., 1968). In the present study, we identified MARC-145 cells as a suitable line of cells for PEDV infection and for study of innate immune modulation. We showed that PEDV suppressed the type I interferon production and ISGs expression in these cells, and identified nsp1, nsp3, nsp7, nsp14, nsp15, nsp16, E, M, N and ORF3 as the viral IFN antagonists. We showed that PEDV nsp1 caused the CBP degradation by the proteasome-dependent pathway. The CBP degradation is a novel mechanism of coronavirus nsp1 for IFN suppression and our study provides a new insight into the immune modulation and evasion strategy of PEDV.

2.3 MATERIALS AND METHODS

2.3.1 Cells, viruses, antibodies and chemicals

HeLa cells (NIH AIDS Research and Reference Reagent Program, Germantown, MD) and MARC-145 cells (Kim et al., 1993) were maintained in minimum essential medium (MEM) and Dulbecco's modified Eagle's medium (DMEM) (Mediatech, Manassas, VA), respectively, supplemented with 10% heat inactivated fetal bovine serum (FBS) (Hyclone, Logan, UT). Vero cells (ATCC® CCL-81™) were grown in DMEM supplemented with 10% FBS. The IPEC-J2 cell line is a continuous line of epithelial cells derived from the jejunum of a 12 hours old, unsuckled mixed breed piglet and was obtained from Dr. Anthony Blikslager (North Carolina State University). IPEC-J2 was maintained in DMEM/F12 with 5% FBS supplemented with 5 μg/ml of insulin/selenium/transferrin (Life Technologies), and 5 ng/ml of epidermal growth

factor (Life Technologies). PEDV (USA/Colorado/2013; GenBank: KF272920) was obtained from Agricultural Research Service US Department of Agriculture (Ames, IA). PEDV was propagated in MARC-145 cells with DMEM or Vero cells with MEM supplemented with 0.3% tryptose phosphate broth (Sigma, St. Louis, MO), 0.02% yeast extract (Teknova, Hollister, CA), and trypsin 250 (Sigma-Aldrich, St. Louis, MO). The trypsin concentration was 2 μg/ml for MARC-145 cells and 5 μg/ml in Vero cells. The recombinant vesicular stomatitis virus expressing green fluorescent protein (VSV-GFP) was kindly provided by Dr. A. Garcia-Sastre (Mount Sinai Hospital, New York, NY).

Polyinosinic: polycytidylic acid [(poly (I:C)], DAPI (4', 6-diamidino-2-phenylindole), and cycloheximide (CHX), rat anti-FLAG mAb were purchased from Sigma (St. Louis, MO). Human recombinant IFN-β and MG132 were purchased from Calbiochem (San Diego, CA). Anti-β-actin mAb (sc-47778), anti-CBP mAb (sc-7300), anti-hsp90 mAb (sc-69703), anti-PARP pAb (sc-7150), and anti-IRF3 pAb (sc-9082) were purchased from Santa Cruz Biotechnologies Inc. (Santa Cruz, CA). Anti-phospho-IRF3 PAb (Ser396) were purchased from Cell Signaling (Danvers, MA). Rabbit anti-PEDV M pAb was kindly provided by Dr. Y. Fang (Kansas State University, Manhattan, KS). Mouse anti-PEDV N mAb was purchased from Medgene (Brookings, SD). Lipofectamine 2000 Transfection Reagent was purchased from Invitrogen (Carlsbad, CA). QIAamp Viral RNA mini kit and RNeasy mini kit were purchased from QIAGEN (Venlo, Limburg). Power SYBR Green PCR master mix was purchased from Life Technologies (Carlsbad, CA). Alexa Fluor 594-conjugated (goat anti-rabbit, red) and 488-conjugated (goat anti-mouse, green) secondary antibodies and Pierce™ ECL Western blotting substrate were purchased from Thermo Scientific (Waltham, MA).

2.3.2 Plasmids and gene cloning

The firefly luciferase genes were used as reporters with its expression under the control of various promoters as indicated below. The plasmid pIFN-β-Luc contains the entire IFN-β enhancer-promoter. The plasmid p4×IRF3-Luc contains four copies of IRF3 binding region PRD I-III of the IFN-β promoter. pIFN-β-Luc and p4×IRF3-Luc were obtained from Dr. Stephan Ludwig at Heinrich-Heine-Universität, Düsseldorf, Germany (Ehrhardt et al., 2004). The Renilla luciferase plasmid pRL-TK (Promega) contains the herpes simplex virus thymidine kinase (HSV-tk) promoter and was included in all experiments to serve as an internal control. Active stimulator pMAVS/IPS-1 was obtained from Dr. J. Shisler (University of Illinois, Urbana, IL). pIRF3 was kindly provided by Dr. B. Gotoh (University of Fukui, Fukui, Japan). pDsRed2-ER and pDsRed2-Mito were purchased from Clontech.

Plasmids with the FLAG tag for expression of nsp1 through nsp16, and the S, S1, S2, ORF3, E, M and N genes were cloned from the viral genomic RNA by standard reverse transcription and PCR techniques using indicated primers (Table 2.1). Twenty-three viral genes were amplified and cloned into the eukaryotic expression vector pXJ41 using indicated restriction enzymes. The nsp1 to nsp16, ORF3, and N genes were expressed as fusion proteins with the N-terminal FLAG tag, and the S, S1, S2, E, and M genes were expressed as fusion proteins with the C-terminal FLAG tag to avoid the functional disruption of the signal sequence. The constructs were confirmed by sequencing, immunofluorescence, and western blot. PRRSV nsp1α and its cystine mutant P-nsp1α(m) (C28S) are described elsewhere (Han et al., 2013; Song et al., 2010).

2.3.3 DNA transfection and luciferase reporter assay

HeLa cells were seeded in 12-well plates and grown to 80% confluency prior to transfection. Individual viral protein genes, luciferase reporters, and pRL-TK as an internal control were transfected at a ratio of 10:10:1 in a total of 1.05 μg/well using Lipofectamine 2000 according to the manufacturer's instruction (Invitrogen). At 24 h post-transfection, cells were stimulated by transfection with 0.5 μg/well of poly(I:C) for 12 h. Cells were then lysed and luciferase assays were performed using the Dual Luciferease assay system according to the manufacturer's instructions (Promega). Values were normalized using the Renilla luciferase activity as the internal control and presented in fold-changes. Three independent assays were performed with each assay in triplicate.

2.3.4 Relative quantitative real-time RT-PCR

Total RNA was extracted from HeLa or MARC-145 cells using RNeasy mini kit according to the manufacturer's instructions (QIAGEN). The RNA was treated with DNase I to remove contaminating genomic DNA. Reverse transcription (RT) reaction was performed with 1 μg of total RNA using random primers and M-MLV reverse transcriptase (Invitrogen). SYBR Green real-time PCR was conducted in the ABI 7500 real-time PCR system according to the manufacturer's instructions (Life Technologies). The real-time PCR primers for IFN-β, ISG15, ISG56 and β-actin were listed in Table 2.2. For each sample, the β-actin gene was amplified and used as an internal control. Specific amplification was confirmed by sequencing PCR products. The threshold cycle for target genes and the difference between their C_t values (ΔC_t) were determined. The relative transcript levels of target gene are equal to $2^{-\Delta\Delta Ct}$ threshold method

(Livak and Schmittgen, 2001) and are shown as fold changes relative to the respective untreated control samples.

2.3.5 VSV-GFP interferon bioassay

HeLa cells were seeded in 6-well plates and transfected with 2 μg of plasmid. At 24 h post-transfection, cells were stimulated by transfection with 1 μg of poly(I:C) for 12 h. Supernatants were harvested for bioassay. For PEDV, MARC-145 cells were infected with PEDV at an MOI of 1 for 12 h prior to poly(I:C) stimulation. Supernatants from virus-infected cells were UV-irradiated for 30 min to remove infectivity prior to bioassay. The supernatants were then serially diluted by 2-fold. MARC-145 cells were freshly grown in 96-well plates and incubated with 100 μl of each dilution for 24 h. Cells were then infected in 100 μl of VSV-GFP at 10^4 PFU/ml for 16 h and GFP expression was examined by inverted fluorescence microscopy (Nikon Eclipse TS100, 10x10). Each dilution was examined twice in triplicate each.

2.3.6 Indirect immunofluorescence assay (IFA) and confocal microscopy

Cells were seeded on coverslips and transfected with plasmids or infected with PEDV. For transfection of HeLa cells, total 2 μg of individual plasmids were transfected for 24 h using Lipofectamine 2000 according to the manufacturer's instructions (Invitrogen). Cells were then either treated with poly(I:C) for 12 h or IFN-β for 40 min. Cells were fixed with 4% paraformaldehyde in PBS overnight at 4 ℃ and permeabilized using 0.1% Triton X-100 for 15 min at room temperature (RT). After blocking with 1% BSA in PBS at RT for 30 min, cells were incubated with a primary antibody in PBS for 1-3 h. Cells were then washed three times with PBS and incubated with Alexa Fluor 488-labeled anti-mouse or anti-rabbit secondary antibody,

or Alexa Fluor 594-labeled anti-rabbit secondary antibody (Thermo Scientific) for 1 h at RT in the dark. Cells were incubated with DAPI for 5 min at RT for nuclear staining. After washing with PBS, cover slips were mounted on microscope slides using Fluoromount-G mounting medium (Southern Biotech, Birmingham, AL), and visualized by fluorescence microscopy (Nikon Eclipse TS100). Confocal microscopy was conducted as described elsewhere (Kannan et al., 2009).

2.3.7 Cell fractionation

HeLa cells were seeded in 6-well plates to 80% confluency and transfected with 2 μg/well of nsp1 plasmid for 24 h. Cells were stimulated with 1 μg of poly(I:C) for 12 h and fractionated using the Nuclear/Cytosol Fractionation kit (BioVision, Milpitas, CA) with minor modifications. Briefly, cells were washed with cold PBS and collected using cell scrapers in 1 ml of cold PBS. Cell pellets were resuspended in 200 μl CEB-A buffer and incubated on ice for 10 min. After addition of CEB-B, tubes were vortexed and incubated on ice for 1 min. The cell lysates were then centrifuged at 4°C 5 min at 16,000xg and supernatants were collected as the cytosolic fraction. The cell pellets were suspended in NEB buffer and vortexed for 30 s and repeated 5 times every 10 min. The nuclear pellets were finally centrifuged for 10 min at 4°C 16,000xg and kept the supernatants as the nuclear fraction.

2.3.8 Western blot

Cells were harvested in RIPA buffer [20 mM Tris (pH 7.5), 150 mM NaCl, 1 mM EDTA, 1 mM phenylmethanesulphonyl fluoride (PMSF), 0.1% SDS, 0.5% sodium deoxycholate, 1% NP-40] containing the proteinase inhibitors cocktail (Promega). Cells were frozen-thawed,

collected in the pre-cold tubes, and centrifuged to remove insoluble components. Total protein concentration was determined using Pierce BCA protein assay kit (Thermo Scientific). Equal amounts of proteins were resolved by SDS-PAGE and blotted to PVDF membranes (Millipore). After blocking with 5% nonfat dry milk in TBST (0.05% Tween-20) for 1 h, membranes were incubated with a primary antibody in TBST containing 5% nonfat dry milk overnight at 4°C, followed by washing and incubation with horseradish peroxidase (HRP)-conjugated secondary antibody for 1 h at RT. The membrane was visualized using Pierce ECL Western Blotting Substrate (Thermo Scientific) and images were taken by FluorChem™ R System according to the manufacturer's instructions (ProteinSimple).

2.3.9 Co-immunoprecipitation

Co-immunoprecipitation (co-IP) was performed as described previously with modifications (Kim et al., 2010). Gene-transfected cells were lysed in lysis buffer [50mM Tris (pH 8.0), 150 mM NaCl, 5mM Na_3VO_4, 1mM PMSF, 100 mg/ml leupetin, 1% NP-40, 10% glycerol] supplemented proteinase inhibitors cocktail (Promega). Cell lysates were clarified by centrifugation at 4°C for 10 min at 16,000xg. Supernatants were transferred to fresh tubes and incubated with either FLAG- or IRF3-antibody at 4°C overnight, followed by incubation with protein G Agarose beads (Fast Flow, Millipore) at 4°C for 4 h. Pellets were collected by centrifugation and washed for five times. The final pellets were eluted with Laemmli sample buffer (Bio-Rad) and were subjected to western blot.

2.3.10 Statistical analysis

Student's *t*-test was used for all statistical analyses. Asterisks indicate the statistical significance. *, $P<0.05$, **, $P<0.01$ and ***, $P<0.001$.

2.4 RESULTS

2.4.1 Infection of PEDV in Vero and MARC-145 cells

PEDV replicates in the cytoplasm of villous epithelial cells of the small and large intestines (Debouck and Pensaert, 1980; Sueyoshi et al., 1995). The viral antigen is also detectable in the macrophages that infiltrated the lamina propria (Lee et al., 2000). Histological studies showed that PEDV replicates the porcine respiratory tract in vivo and transformed alveolar macrophages (3D4) in vitro (Park and Shin, 2014). Vero cells are widely used for PEDV for diagnosis, virus isolation, and research, but these cells are type I IFN-deficient due to the chromosomal deletion (Desmyter et al., 1968). To study a possible regulation of innate immune signaling by PEDV, various cell lines were examined for susceptibility. Cells were infected with PEDV at an MOI of 0.1 in various trypsin concentrations and CPE was examined daily for up to 5 days. In Vero and MARC-145 cells, apparent CPE of multinucleation was observed by 24 h post-infection (Fig. 2.1A, 2.1B, left panel). Trypsin activates the cleavage of S protein and induces membrane fusion to trigger infection (Park et al., 2011; Wicht et al., 2014). PEDV infection was characterized by syncytia formation (Hofmann and Wyler, 1988) and infection foci were visualized by anti-PEDV M and N antibodies, indicating the susceptibility of both cell types for PEDV infection (Fig. 2.1A, 2.1B, middle and right panel). The viral proteins were detected using specific antibodies by western blot and the specific bands were corresponding to the M and N proteins, further confirming the productive infection of these cells by PEDV (Fig.

2.1C). The optimal trypsin concentration for PEDV propagation was 5 μg/ml and 2 μg/ml for Vero and MARC-145 cells, respectively. MARC-145 cells have been used to study type I IFN signaling of porcine arterivirus (Kim et al., 2010; Overend et al., 2007; Patel et al., 2010), and thus infection of these cells by PEDV allowed us to study IFN modulation and signaling cascade.

2.4.2 Suppression of IFN-β production in PEDV-infected cells

To determine whether PEDV infection antagonized the type I IFN response, IFN-β mRNA was determined in virus-infected cells. MARC-145 cells were infected with PEDV and stimulated with poly(I:C) followed by qRT-PCR for IFN-β mRNA using total RNA. As shown in Fig. 2.2A, PEDV infection did not induce the level of IFN-β mRNA expression whereas poly(I:C) alone induced the IFN-β gene expression effectively, indicating the suppression of IFN-β response by PEDV. To further evaluate the IFN-β response in PEDV-infected cells, a dual luciferase assay was performed. The results showed the suppression of IFN-β promoter activity in PEDV-infected cells upon poly(I:C) stimulation (Fig. 2.2B), demonstrating the modulation of IFN production by PEDV infection. IRF3 was additionally examined for its role for PEDV-mediated IFN-β suppression. The IRF3 promoter activity was found to be inhibited (Fig. 2.2C). The suppression of IFN-β production was confirmed by bioassay using VSV-GFP. VSV is sensitive to type I IFN treatment and thus commonly used for IFN bioassays. Culture supernatants were collected from PEDV-infected cells and were UV-irradiated, followed by incubation with MARC-145 cells and infection with VSV-GFP. VSV grew normally (Fig. 2.2D), whereas it did not grow with supernatants collected from poly(I:C)-treated cells for up to 1:8 dilution. VSV-GFP also grew normally with supernatants from both PEDV-infected cells with or without poly (I:C) stimulation, confirming the suppression of type I IFN production by PEDV.

2.4.3 Identification of viral IFN antagonists

The viral IFN antagonism is often redundant, and at least 11 viral proteins have been identified as IFN antagonists for SARS-CoV (Kindler and Thiel, 2014; Shi et al., 2014; Totura and Baric, 2012). To identify such proteins for PEDV, we cloned PEDV genes representing nsps 1 through 16, and structural genes for S, E, M, and N including the ORF3 accessory protein gene (Fig. 2.3A). Among these, nsp11 is a small oligopeptide generated from PP1a when ribosomal frameshifting does not occur and so was not included in this study. Each gene was inserted into the pXJ41 expression vector with the FLAG tag at either N- or C-terminus, and examined for IFN suppression. The protein expression of cloned genes was examined by immunofluorescence (Fig. 2.3B) and western blot (Fig. 2.3C) using anti-FLAG antibody. All genes were expressed as anticipated. HeLa cells were then co-transfected with an individual gene along with pIFN-β-Luc and pRL-TK, and reporter assays were conducted. PRRSV nsp1α (P-nsp1α) is known as an IFN-β suppressor, and its cystine mutant P-nsp1α(m) (C28S) is an IFN suppression revertant (Han et al., 2013; Song et al., 2010), and so they were included as positive and negative controls, respectively. Poly(I:C) upregulated the IFN-β transcription in cells expressing pXJ41, GST, and P-nsp1α(m), while P-nsp1α suppressed the IFN-β promoter activity as expected (Fig. 2.3D, 3E). Of the nsps, nsp1, nsp3, nsp7, nsp14, nsp15 and nsp16 were shown to down-regulate the IFN-β activity (Fig. 2.3D). For structural proteins, E, M, and N were found to suppress the IFN induction (Fig. 2.3E), and ORF3 was additionally identified as an IFN suppressive protein (Fig. 2.3E). The findings from the reporter assays were validated by VSV-GFP bioassays. The dilution corresponding to 50% of cells exhibiting GFP expression was determined as the end-point inhibition. For pXJ41, GST, and nsp9, GFP expression was evident and their end-point

inhibitions were determined as 1:64 (Fig. 2.3F). In contrast, the viral proteins identified as the luciferase suppressors showed an apparent inhibition of VSV-GFP replication and their end-points were determined to 1:4 to 1:16 (Fig. 2.3F). These titers represent 4- to 16-fold lower than that of control. Taken together, these data demonstrate that PEDV has the ability for IFN suppression, and nsp1, nsp3, nsp7, nsp14, nsp15, nsp16, ORF3, E, M and N are the viral IFN antagonists.

To determine the target for IFN inhibition, the IRF3 pathway was examined for individual viral proteins using the IRF3 luciferase reporter constructs. Upon stimulation, the IRF3-dependent luciferase expression was reduced by nsp1, nsp3, nsp7, nsp14, nsp15, nsp16, ORF3, E, M, and N, comparing to those of pXJ41 and GST (Fig. 2.3G). This suggests that the IRF3 signaling pathway was interfered by these viral proteins for the suppression of the IFN-β production.

2.4.4 PEDV nsp1 antagonism is a nuclear event

SARS-CoV is a *betacoronavirus* and its nsp1 triggers inhibition of type I IFN induction and downstream signaling, host mRNA decay and cleavage, and inhibition of protein translation (Huang et al., 2011b; Lokugamage et al., 2012; Narayanan et al., 2008; Tanaka et al., 2012). Transmissible gastroenteritis virus (TGEV) is an *alphacoronavirus* and its nsp1 inhibits host protein expression (Huang et al., 2011a). Nsp1 of *alphacoronavirus* and *betacoronavirus* lacks the overall sequence similarity (Narayanan et al., 2014), and thus *alphacoronavirus* nsp1 may have a distinct basis for its biological function. Since nsp1 appeared the most potent suppressor in our study on PEDV, nsp1 was chosen to study the molecular basis for the IFN suppression. The subcellular localization was first examined by confocal microscopy in transiently expressing

cells. The nsp1 distribution was evident in the both nucleus and cytoplasm (Fig. 2.4A), which is consistent with TGEV nsp1 (Narayanan et al., 2014). Co-expression of nsp1 with either the endoplasmic reticulum or mitochondrial marker showed the site for cytoplasmic nsp1 in the endoplasmic reticulum (Fig. 2.4B). Quantitative RT-PCR was conducted to evaluate IFN-β suppression in nsp1-gene transfected cells. The expression of nsp1 significantly suppressed the IFN-β mRNA transcription (Fig. 2.5A), further validating the nsp1 antagonism against IFN-β production. Subsequently, the IFN-mediated antiviral gene expression was examined for ISG15 and ISG56 by qRT-PCR. PEDV nsp1 reduced the poly(I:C)-stimulated mRNA levels of both ISG15 (Fig. 2.5B) and ISG56 (Fig. 2.5C), indicating the suppression of IFN signaling by nsp1. The suppression of IFN-β, IRF3, and NF-κB activations raises a possibility that nsp1 may target a component of the RIG-I like receptor (RLR) signaling pathway. To examine this premise, nsp1 was co-expressed with one of the main components in the RLR signaling pathway, and IFN luciferase activities were determined at 24 h post-transfection. The over-expression of IPS-1, or IRF3 led to the robust activation of the IFN-β promoter as anticipated, whereas the activation was significantly inhibited by nsp1 (Fig. 2.6A, 2.6B). Collectively, it suggests that nsp1 targets the RLR pathway downstream of the IRF3 activation.

IRF3 is a resident protein in the cytoplasm. When stimulated, it is phosphorylated and homodimerized, leading to the translocation to the nucleus (Dragan et al., 2007). To determine whether PEDV nsp1 targeted the IRF3-dependent pathway, the IRF3 phosphorylation was first examined. nsp1-gene transfected cells were stimulated with poly(I:C), and the IRF3 phosphorylation was examined by western blot. As anticipated, the poly(I:C) stimulation led to IRF3 phosphorylation in pXJ41-transfected cells, and similarly, in nsp1-expressing cells, the IRF3 phosphorylation was evident and comparable to that of control (Fig. 2.7A, top panel, lane

4), suggesting that PEDV nsp1 exerts its suppression downstream of the IRF3 phosphorylation. Thus, the nuclear translocation of IRF3 was next examined. PRRSV nsp1α is known not to block the IRF3 nuclear localization, and so was used as a control in this study. Endogenous IRF3 was normally diffused and distributed in the cytoplasm, but translocated to the nucleus when stimulated by poly(I:C) (Fig. 2.7B, second panel). Similar to PRRSV nsp1α-expressing cells (Fig. 2.7B, fourth panel), IRF3 also localized normally in the nucleus after stimulation in PEDV nsp1-expressing cells (Fig. 2.7B, bottom panel), suggesting that the IFN suppression by PEDV nsp1 may be a nuclear event. The IRF3 nuclear translocation in nsp1-expressing cells was further confirmed by cell fractionation and western blot analyses. While IRF3 was phosphorylated and localized in the nucleus after stimulation, PEDV nsp1 did not inhibit the IRF3 phosphorylation and nuclear translocation (Fig. 2.7C), further indicating that the nsp1-mediated IFN suppression was a nuclear event.

2.4.5 Interruption of IRF3 and CBP association by nsp1

After nuclear translocation, an IRF3 dimer associates with the CREB-binding protein (CBP). This complex then binds to the PRD I–III regions of the IFN-β promoter to assemble the basal transcription machinery complex together with NF-κB and other transcription factors to turn on the transcription of type I IFN genes (Honda and Taniguchi, 2006). Thus, the IRF3-CBP/p300 interaction for the assembly of enhanceosome is crucial for IFN expression. Since PEDV nsp1 did not block the IRF3 phosphorylation and nuclear translocation in our study, it was hypothesized that nsp1 might disrupt the formation of enhanceosome in the nucleus. To address this, the IRF3/CBP association was first examined in nsp1-expressing cells. Cells were transfected with the nsp1 gene and stimulated with poly(I:C) followed by co-

immunoprecipitation using anti-IRF3 antibody and immunoblot with anti-CBP antibody. In unstimulated cells, CBP was undetectable due to the absence of IRF3/CBP association (Fig. 2.8A, left lane), but IRF3/CBP association became evident upon stimulation (Fig. 2.8A, middle lane). In nsp1-expressing cells however, the association of IRF3 and CBP disappeared even upon stimulation (Fig. 2.8A, right lane) and the detectable level of IRF3 remained unchanged (Fig. 2.8A, second panel). Absence of the association of CBP/IRF3 may occur when nsp1 binds to either IRF3 or CBP, or when IRF3 is unstable in the presence of nsp1. Since PEDV nsp1 was found to be a nuclear protein (Fig. 2.4A, 2.4B, 2.7B, 2.7C), nsp1 in the nucleus might interact with either IRF3 or CBP. However, neither the interaction between IRF3 and nsp1, nor between CBP and nsp1 was observed by co-immunoprecipitation in our study. IRF3 was also stable in the presence of nsp1 (Fig. 2.7A, 2.7C), indicating that the absence of IRF3/CBP association was not due to the instability of IRF3. Interestingly, the level of CBP was found to decrease in nsp1-expressing cells (Fig. 2.8A), leading us to investigate the degradation of CBP by nsp1.

2.4.6 Degradation of CBP by nsp1 is proteasome-dependent

Some viruses including HTLV, adenovirus, and an orthormyxovirus Thogoto interact with CBP to modulate type I IFN induction, suppress protein expression, or promote virus infection (Ferrari et al., 2014; Jain et al., 2015; Jennings et al., 2005; Wurm et al., 2012; Zhang et al., 2008). Degradation of CBP has been described for the porcine arterivirus PRRSV as a strategy for IFN antagonism (Han and Yoo, 2014). Since the level of CBP was found to decrease in PEDV nsp1-expressing cells (Fig. 2.8A), CBP expression was validated in PEDV-infected cells by co-staining using anti-CBP antibody and anti-PEDV M pAb. In uninfected cells, CBP was predominately localized in the nucleus in MARC-145 and Vero cells (Fig. 2.8B, yellow

arrows). In contrast, CBP was depleted in virus-infected cells (Fig. 2.8B, white arrows), demonstrating that the CBP was degraded by PEDV. We further sought to study whether the CBP degradation by PEDV was mediated by nsp1 protein. CBP was exclusively nuclear in control cells, whereas it was depleted in nsp1-expressing cells (Fig. 2.9A). PRRSV nsp1α is known to degrade CBP in the nucleus (Han and Yoo, 2014), and in PRRSV nsp1α-expressing cells, CBP was significantly depleted (Fig. 2.9A). The CBP degradation was quantified by examining the ratio of nsp1-expressing cells showing CBP degradation out of the chosen number of nsp1-expressing cells (Fig. 2.9B). Approximately 92% of PRRSV nsp1α-expressing cells showed more than 80% reduction of CBP, which is in consistent with the previous report (Han et al., 2013). For PEDV nsp1-expressing cells, approximately 90% cells showed more than 80% reduction of CBP, while no CBP reduction was observed in control cells. This finding was confirmed by western blot. In PEDV nsp1-expressing cells, CBP degradation was evident compared to that of control cells (Fig. 2.9C, top panel, lane 3). To eliminate a possibility that the reduction of CBP might be due to the short half-life of CBP, cyclohexamide (CHX) treatment was conducted (Fig. 2.9D). At 24 h post-transfection, cells were treated with CHX to shut down the new protein synthesis for indicated times followed by western blot. In nsp1-expressing cells, CBP reduction was evident at the beginning of CHX treatment, and further decreased by 2 h post-treatment. The CBP degradation was complete by 4 h post-treatment, whereas nsp1 and β-actin remained stable (Fig. 2.9D). Together, our data show that PEDV nsp1 was the viral protein contributing to the CBP degradation. Unlike PRRSV nsp1α, PEDV nsp1 does not contain a proteinase activity, and no direct interaction between CBP and nsp1 was identified in our study. It is thus unlikely that CBP would be a direct substrate of PEDV nsp1. Therefore, it was of interest to examine whether the CBP degradation was a proteasome-dependent process. The

treatment with MG132 blocked the CBP degradation by nsp1. As little as 5 μM of MG132 was sufficient to inhibit the CBP degradation, and 10 μM was able to restore the CBP level back to the control level (Fig. 2.9E). To eliminate the CBP degradation by nsp1 was cell-type specific, we further tested the CBP degradation by nsp1 in pig intestinal epithelial cell line (IPEC-J2 cells), which reported to be susceptible to PEDV (Zhao et al., 2014). CBP degradation in nsp1-expressing cells was evident comparing to control cells (Fig. 2.9F, top panel). Additionally, The CBP degradation by nsp1 was also blocked by MG132 treatment in IPEC-J2 cells (Fig. 2.9F, bottom panel). This study indicates that the CBP degradation by PEDV nsp1 was proteasome-dependent in the nucleus.

2.5 DISCUSSION

The innate immune system is the first line of host defense in response to viral infection. It initiates the production of type I IFNs and proinflammatory cytokines through the recognition of PAMPs by PRRs and establishes antiviral states, which are highly effective on resisting and controlling infections. In turn, many viruses have developed strategies to counteract the host innate immune response to establish productive infection. Previous studies have shown that PEDV infection fail to induce the IFN-β promoter activation and that PLP2 (papain-like proteinase 2) of PEDV antagonizes the IFN response by deubiquitinating RIG-I and STING (Xing et al., 2013b). The PEDV N protein suppresses the IRF3 and NF-κB activities and antagonizes the IFN-β production by disrupting the interaction between IRF3 and TBK1 (Ding et al., 2014). On the contrary, a recent study shows that PEDV infection induces NF-κB activation in intestinal epithelial cells with the N protein as the activator (Cao et al., 2015b). In the present study, we have identified MARC-145 as PEDV permissive cells, and used these cells as a model

to study the innate immune modulation for PEDV. We have shown the suppression of type I IFN production by PEDV, which is consistent to the recent finding in IECs (Cao et al., 2015a). We also have identified multiple viral proteins responsible for this suppression. We have further determined PEDV nsp1 as the viral component promoting CBP degradation in the nucleus via the proteasome-dependent pathway.

Many viruses in the order *Nidovirales* are able to modulate the host innate response, which plays an important role for their pathogenesis. In the family *Arteriviridae*, equine arteritis virus suppresses type I IFN production in equine endothelial cells (Go et al., 2014), and PRRSV also suppresses IFN production (Albina et al., 1998). PRRSV is susceptible to type I IFNs in cells and the suppression of type I IFN varies for different isolates (Albina et al., 1998; Lee et al., 2004; Overend et al., 2007). Mouse hepatitis virus (MHV), which is a *betacoronavirus,* induces a high level of IFN-α secretion by plasmacytoid dendritic cells (pDCs) during infection (Cervantes-Barragan et al., 2007). However, other cell types infected by MHV such as macrophages, microglia, and oligodendrocytes produce extremely low levels of type I IFNs (Li et al., 2010; Roth-Cross et al., 2008; Zhou and Perlman, 2007). The MHV ns2 protein is dispensable for virus replication in cells but is required for induction of hepatitis in mouse (Schwarz et al., 1990). The 2′,5′-phosphodiesterase (PDE) activity of ns2 mediates the cleavage of 2′,5′-oligoadenylate and prevents the activation of RNase L, while enhancing viral growth and pathogenesis, thus ns2 is a viral IFN antagonist (Zhao et al., 2012). SARS-CoV, which is another member virus in the genus *betacoronavirus,* impairs the IFN response in virus-infected cells, and an IFN therapy has been suggested to be efficacious for SARS patients (Cinatl et al., 2004; Spiegel et al., 2005). MERS-CoV is also a *betacoronavirus,* and both MERS-CoV and SARS-CoV do not induce a pronounced IFN-response in polarized airway epithelial cells (Calu-3),

alveolar adenocarcinoma cells (A549) and human monocyte-derived macrophages (Lau et al., 2013; Zhou et al., 2014; Zielecki et al., 2013). Even though the acute infection of TGEV induces a high level of IFN-α in newborn pigs (La Bonnardiere and Laude, 1981), protein 7 counteracts the host antiviral response and influences viral pathogenesis (Cruz et al., 2013; Cruz et al., 2011). The 7a protein of an *alphacoronavirus* feline infectious peritonitis virus is a type I IFN antagonist (Dedeurwaerder et al., 2014). Type I IFNs of chickens inhibits viral replication and respiratory illness of the *gammacoronavirus* infectious bronchitis coronavirus (IBV) (Pei et al., 2001). IBV delays the IFN response and the 3a and 3b accessory proteins have been identified as the IFN antagonists (Kint et al., 2015). Thus, modulation of type I IFN response seems to be a common evasion strategy of viruses in the order *Nidovirales*.

We have shown in the present study the direct evidence that PEDV indeed downregulates type I IFNs production during infection. PEDV suppresses the IFN-β and IRF3 activities. Since IRF3 is a key element in the production of type I IFNs, our finding leads to a hypothesis that PEDV modulation of type I IFNs production targets the IRF3 signaling pathway. Interestingly, PEDV normally activates the NF-κB activity in Vero E6 cells (Xing et al., 2013b). A recent study confirms that PEDV infection in intestinal epithelial cells induces NF-κB activation (Cao et al., 2015b). In that study, nuclear localization of p65 increases by PEDV after 12 h through 48 h. However, activation of NF-κB during viral infection is generally an early event. For PRRSV, NF-κB is activated 30 min after infection (Fu et al., 2012). Thus, how PEDV modulates NF-κB activation during early time of infection needs to be further investigated. We have identified at least ten viral IFN antagonists and all ten proteins inhibit the IRF3 activity. Whether these IFN antagonists modulate the NF-κB activity needs to be further investigated. The PEDV N protein suppresses Sendai virus-induced NF-κB activity in a dose-dependent manner (Ding et al., 2014).

In other study, N protein activates NF-κB in intestinal epithelial cells (Cao et al., 2015b). A possible explanation is that the NF-κB activation may be time-dependent and cell type-dependent. Together, the IRF3 signaling is likely the target by PEDV for type I IFNs modulation.

At least eleven viral proteins have been identified as IFN antagonists for SARS-CoV (Kindler and Thiel, 2014; Shi et al., 2014; Totura and Baric, 2012), whereas ten proteins have been identified for PEDV in our study. Thus, coronaviruses seem to arm with multiple antagonists. A possible explanation for such a functional redundancy is that coronavirus genomes are the largest RNA known to biology and undergo continuous genetic evolution. When a functional mutation occurs in a major antagonist, other antagonists may complement the function to ensure efficient replication and adaptation in hosts. For SARS-CoV, nsp1 is a multifunctional protein with the suppressive activity for IFN and blocks the phosphorylation of STAT1 and degrades host cell mRNA (Totura and Baric, 2012). SARS-CoV nsp14 and nsp15 works as exoribonuclease and endoribonuclease, respectively, thus specific digestion of dsRNAs and the consequent removal of RNA-PAMPs may lead to an inadequate activation of IFN response (Kindler and Thiel, 2014). SARS-CoV nsp16 contains 2'-O-methlytransferase activity and modifies the cap of viral RNAs in order to evade the detection by the host immune system (Totura and Baric, 2012). The SARS-CoV M protein impedes the formation of TRAF3·TANK·TBK1/IKKϵ complex for suppression of type I IFN production (Siu et al., 2014; Siu et al., 2009). The PLP2 domain of SARS-CoV nsp3 negatively modulates type I IFN pathway and functions as a viral deubiquitinase. In our study, the full length PEDV nsp3 indeed inhibit the IFN activity. All ten antagonists identified for PEDV correspond to the respected antagonists of SARS-CoV. The corresponding proteins of PEDV may share the similar motifs and functions with those of SARS-CoV. Additionally, SARS-CoV encodes several accessory

proteins. They are nonessential for viral replication but function as innate immune antagonists. For PEDV, ORF3 is the sole accessory protein, and a previous report shows that ORF3 functions as an ion channel protein and is relevant to infectivity and pathogenicity (Wang et al., 2012). ORF3 is nonessential for viral replication *in vitro* as shown by targeted RNA recombination (Li et al., 2013). In our study, ORF3 is a potent IFN antagonist. The viral antagonists may target different pathways of the host innate immune signaling and their synergistic effects may shut down the host innate immune response more efficiently during the course of infection.

CBP is a histone acetyltransferase and plays a key role in transcription regulation. The CBP/p300 coactivators interact with hundreds of transcription factors including STATs, c-Myc, PIAS1, p53, NF-κB, and IRF family (Bedford and Brindle, 2012; Goodman and Smolik, 2000; Long et al., 2004). For IFN expression, the assembly of an enhanceosome consisting of NF-κB, IRFs, ATF2/c-Jun, and the architectural protein HMG I(Y) is required in response to virus infection. The IFN enhanceosome recruits CBP/p300 for synergistic activation of transcription (Merika et al., 1998). Some viruses modulate the CBP activity for viral evasion. Two distinct regions in the simian virus 40 T antigen can independently alter the levels and loading of CBP/p300 transcripts onto polysomes for cell immortalization and transformation (Saenz Robles et al., 2013). African swine fever virus nuclear protein A238L inhibits the expression of TNF-α by displacing the CBP/p300 coactivators (Granja et al., 2006), and herpes simplex virus 1 (HSV-1) ICP0 protein recruits activated IRF3 and CBP/p300 to the nuclear foci, which may result in reduced transcription of IFN-β and inhibition of the host response (Melroe et al., 2007). HSV-1 VP16 protein inhibits NF-κB activation and interferes the recruitment of IRF3 to CBP to block the IFN-β production (Xing et al., 2013a). The ML protein of Thogoto virus interferes with IRF3 function without blocking its nuclear translocation but interrupts the association of IRF3

with CBP (Jennings et al., 2005), which is similar to the function of PEDV nsp1. The ML protein was later found to interact with the RNA polymerase II transcription factor IIB (TFIIB), however, this interaction hardly interferes the host general gene expression but strongly suppresses both the IRF3- and NF-κB-regulated promoter activities (Vogt et al., 2008). Thus, it is hypothesized that the virus-mediated CBP degradation may play a specific and key role for IFN modulation with a little impact on general cellular gene transcriptions. The degradation of CBP is a novel strategy for IFN modulation and has been extensively studied in the family of *Arteriviridae*, especially for PRRSV (Han and Yoo, 2014). For PRRSV nsp1α, CBP degradation is associated with the zinc-finger motif and is likely the key mechanism for IFN suppression (Han et al., 2013). For PEDV, nsp1 is the most potent IFN suppressor among all viral antagonists without affecting the IRF3 phosphorylation and nuclear localization. In line with this, PEDV infection depletes the endogenous CBP. Furthermore, PEDV nsp1 disrupts the association of CBP-IRF3 and degrades CBP in a proteasome–dependent manner. SARS-CoV nsp1 inhibits type I IFN production, induces host mRNA degradation, and suppresses host protein translation (Narayanan et al., 2008). However, the domains of SARS-CoV nsp1 responsible for suppression of host gene expression and type I IFN production are absent in PEDV nsp1 (Huang et al., 2011b; Narayanan et al., 2008). Even though nsp1s of *alphacoronavirus* and *betacoronavirus* share similar functions, they lack an overall sequence similarity and neither conserved motifs nor domains exist in viruses of *alphacoronaviruses*. Thus, it is plausible that nsp1 of *alphacoronaviruses* may have a distinct function regulating host innate immune responses and gene expression. TGEV nsp1 suppresses protein translation in cells and cell-free extracts. However, the suppression of protein translation by PEDV nsp1 may not be a general event since the β-actin shows the similar level of expression after infection and transfection. The lack of association of CBP-nsp1 and IRF3-nsp1 suggests

that the CBP degradation by nsp1 is an indirect event that needs to be further determined. Similar to TGEV nsp1, the subcellular localization of PEDV nsp1 is nuclear-cytoplasmic. The sequence of PEDV nsp1 does not harbor any known nuclear localization signal, and thus nsp1 may piggy-bag a nuclear protein to enter the nucleus. The proteasome-dependent CBP degradation seems a unique viral tactic utilized to inhibit IFN-β production. It is of interest to study whether this is a common evasion strategy for coronaviruses.

CBP localizes in the PML nuclear bodies, which are discrete nuclear foci that are disrupted in acute promyelocytic leukemia (Boisvert et al., 2001; Doucas et al., 1999; LaMorte et al., 1998). The PML nuclear bodies dynamically colocalize with numerous proteins including CBP, PML, p53, Rb, sp100, DAXX, eIF4E, and SUMO (Jensen et al., 2001). Upon inhibition of proteasome activity, PML, sp100, EBNA-5, SUMO-1, and the 20S proteasome subunit move to the nucleolus, suggesting that proteasomal degradation occurs at the nuclear loci (Boddy et al., 1996). HAUSP, the ubiquitin-specific hydrolase in the PML nuclear bodies, removes ubiquitin moieties from proteins prior to proteasomal degradation (Everett et al., 1998). Thus, PML nuclear bodies may represent the sites where ubiquitinated proteins are processed by enzymes such as HAUSP prior to degradation in the nucleolus (St-Germain et al., 2008). Valproic acid, a histone deacetylase inhibitor, could induce CBP degradation through the ubiquitin-proteasome pathway, while increasing the colocalization of CBP with ubiquitin nuclear speckles and with PML nuclear bodies (St-Germain et al., 2008), suggesting that PML nuclear bodies may be the sites for the ubiquitin-dependent degradation of CBP. It is of interest to examine whether PEDV nsp1 promotes ubiquitination of CBP for degradation in the nucleus and whether this degradation associates with PML nuclear bodies.

PEDV infects Vero cells and MARC-145 cells. Porcine amino peptidase N (pAPN) has been identified as the major cell entry receptor for PEDV (Li et al., 2007; Nam and Lee, 2010). Transient expression of pAPN confers PEDV non-permissive canine kidney cells (MDCK) to be permissive for PEDV infection. pAPN also increases the PEDV infectivity in porcine small intestine epithelial cells (IECs) (Cong et al., 2015). The respiratory tract may support PEDV infection in pigs and the virus infects and replicates in transformed alveolar macrophages (3D4) *in vitro* (Park and Shin, 2014). Primate APN or receptor-independent pathways in Vero and MARC-145 cells may complement the function of pAPN for PEDV infection (Taguchi and Matsuyama, 2002).

In summary, we have shown the suppression of type I IFN production by PEDV and have identified specific viral IFN antagonists. Among these antagonists, nsp1 is the most potent protein and functions to degrade CBP in the nucleus. Our data provides a novel insight into the understanding of the immune evasion strategy of PEDV.

2.6 FIGURES AND TABLES

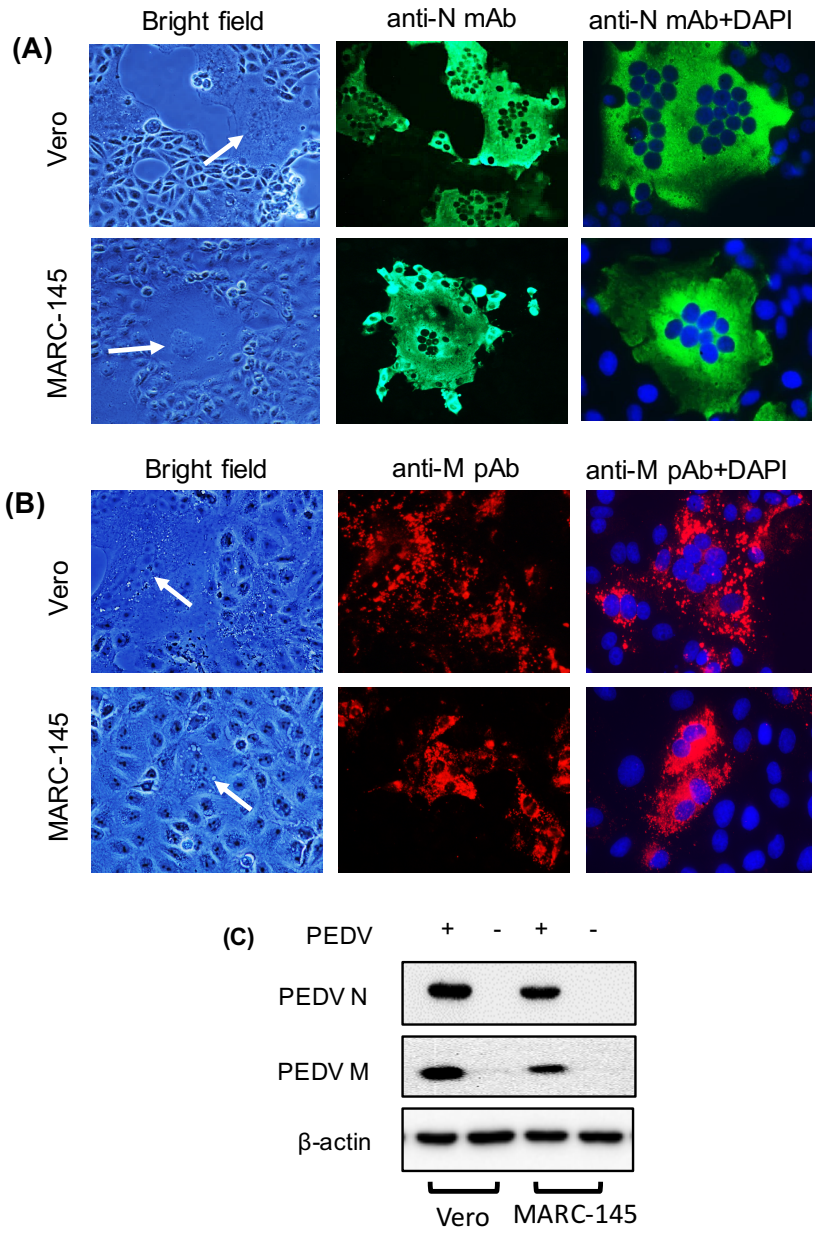

Fig. 2.1: PEDV infection in Vero and MARC-145 cells. (A) and (B), Immunofluorescence showing the expression of nucleocapsid (N, green) and membrane (M, red) proteins in PEDV-infected cells. Vero and MARC-145 cells were infected with PEDV at an MOI of 0.1. Cells were fixed with 4% paraformaldehyde in PBS and stained with mouse anti-N monoclonal antibody (mAb) or rabbit anti-M polyclonal antibody (pAb). Arrows show multi-nucleated cells by fusion. (C), Detection of the N and M proteins in PEDV-infected cells. Cell lysates were prepared at 24 h post-infection, and Western blots were conducted using antibodies against N and M proteins.

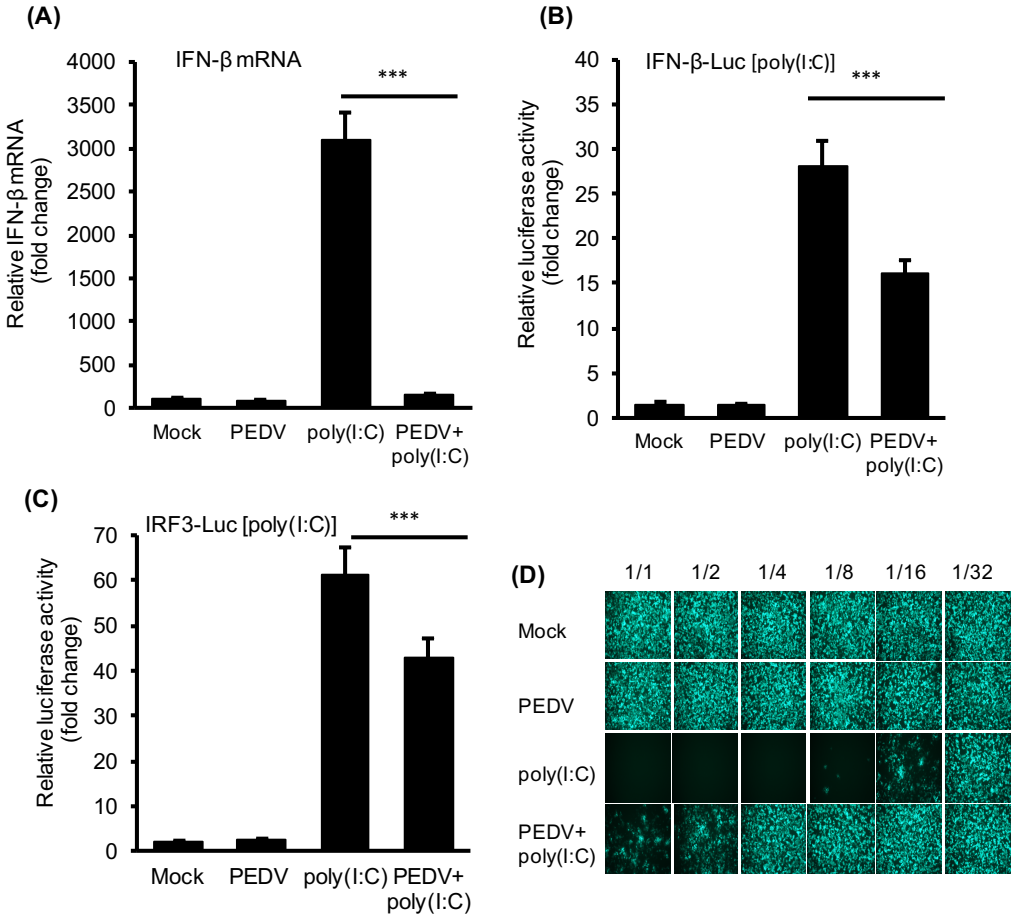

Fig. 2.2: Suppression of IFN-β production by PEDV. (A), Inhibition of IFN-β gene transcription in virus-infected cells. MARC-145 cells were infected with PEDV at an MOI of 1 for 12 h in 12-well plates. Cells were transfected with poly(I:C) (0.5 μg/well) for 12 h, and qRT-PCR was conducted for IFN-β mRNA. Relative quantitation values for IFN-β mRNA are presented. (B, C), Regulation of IFN-β and IRF3 activities by PEDV. MARC-145 cells were co-transfected with pIFN-β-Luc (B), or pIRF3-Luc (C) along with pRL-TK in 12-well plates for 6 h followed by PEDV infection at an MOI of 1 for 12 h. Cells were then stimulated with poly(I:C) for 12 h, and cell lysates were prepared for dual-luciferase reporter assay. Results from three independent experiments were expressed as mean relative luciferase with standard deviation. Each experiment was carried out in triplicate. Asterisks indicate statistical significance calculated by the Student's *t* test. *, $P<0.05$; **, $P<0.01$; ***, $P<0.001$. (D), VSV-GFP bioassay for IFN production. MARC-145 cells were infected with PEDV in 6-well plates at an MOI of 1 for 12 h and stimulated with poly(I:C) for 12 h. Cell culture supernatants were collected and UV-irradiated for 30 min. Fresh MARC-145 cells were grown in 96-well plates and incubated with supernatants of 2-fold serial dilutions of up to 1:32. After 24 h of incubation, cells were infected with VSV-GFP at an MOI of 0.1 for 16 h. GFP expression was assessed by fluorescent microscopy. Each dilution was tested in triplicate.

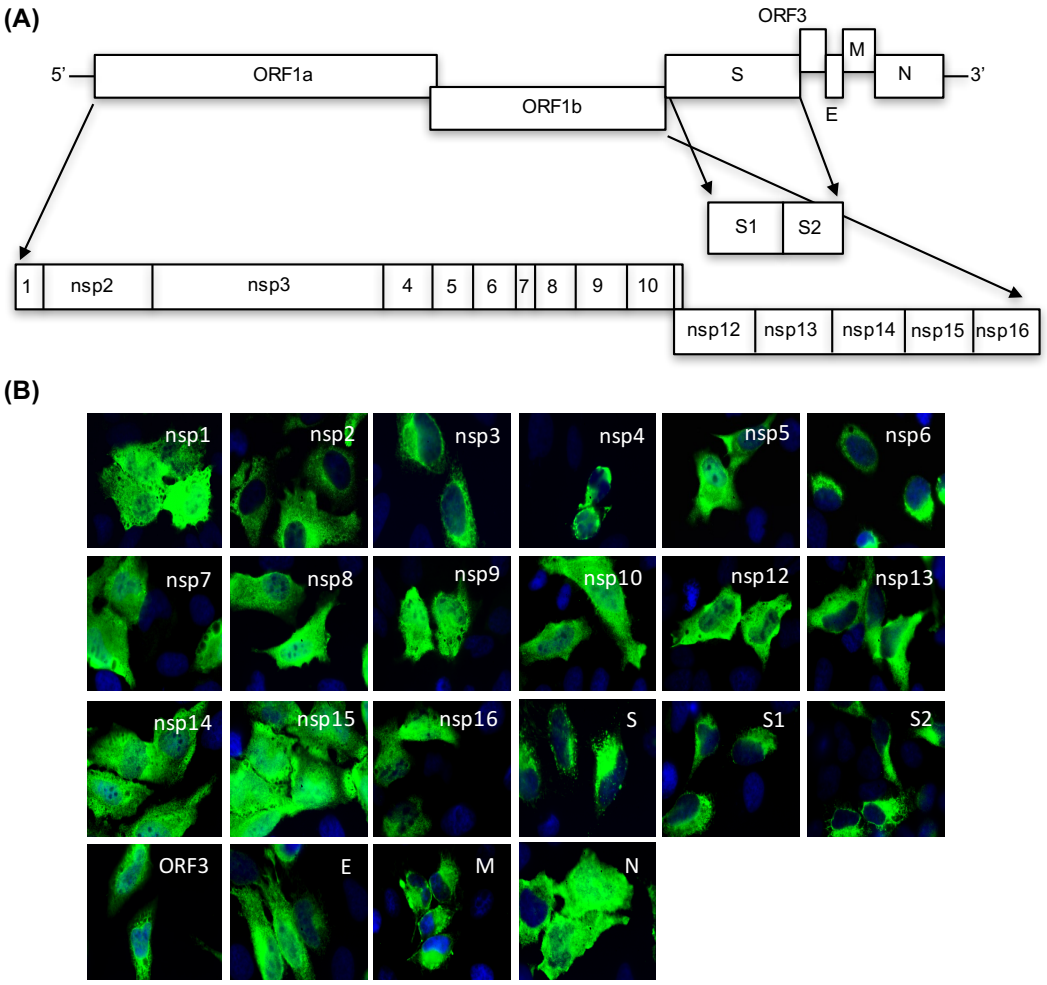

Fig. 2.3: Cloning of PEDV genes and identification of viral proteins antagonizing type I IFN cascade. (A), Genome organization of PEDV. The PEDV genome is organized as 5' UTR-ORF1a-ORF1b-S(S1+S2)-ORF3-E-M-N-3'UTR in order. Sixteen nonstructural proteins encoded in ORF1a and ORF1b are depicted. (B) and (C), Confirmation of cloned gene expression. One μg of each of the cloned genes was transfected to HeLa cells and protein expression was determined by immunofluorescence and Western blot. (D) and (E), Regulation of poly(I:C)-induced IFN-β promoter activity by individual PEDV proteins. HeLa cells were seeded in 12-well plates and co-transfected with pIFN-β-Luc along with individual PEDV genes and pRL-TK at a ratio of 1:1:0.1. PRRSV nsp1α (P-nsp1α) is a known type I IFN suppressor, and the IFN-suppression of its mutant P-nsp1α(m) was lost. At 24 h post-transfection, cells were stimulated with poly(I:C) (0.5μg/ml) for 12 h and the luciferase activities were measured. The reporter experiments were repeated three times, each time in triplicate. Asterisks indicate the statistical significance. Statistical analysis was performed by Student's *t* test using GST as a control. *, $P<0.05$, **, $P<0.01$ and ***, $P<0.001$. (F), VSV-GFP bioassay. The cell culture supernatants for IFN-β promoter luciferase assays were collected and diluted serially by 2-folds up to 1:64. Fresh MARC-145 cells were grown in 96-well plates and incubated with each dilution of supernatants for 24 h, and then infected with VSV-GFP at an MOI of 0.1 for 16 h. VSV replication was measured by monitoring the fluorescence by GFP expression using fluorescent microscopy. Data were presented as $\log_2$ sample dilution folds. (G), Inhibition of IRF3 promoter activation by PEDV proteins. The IFN antagonists were further examined for IRF3 activities by luciferase reporter assays.

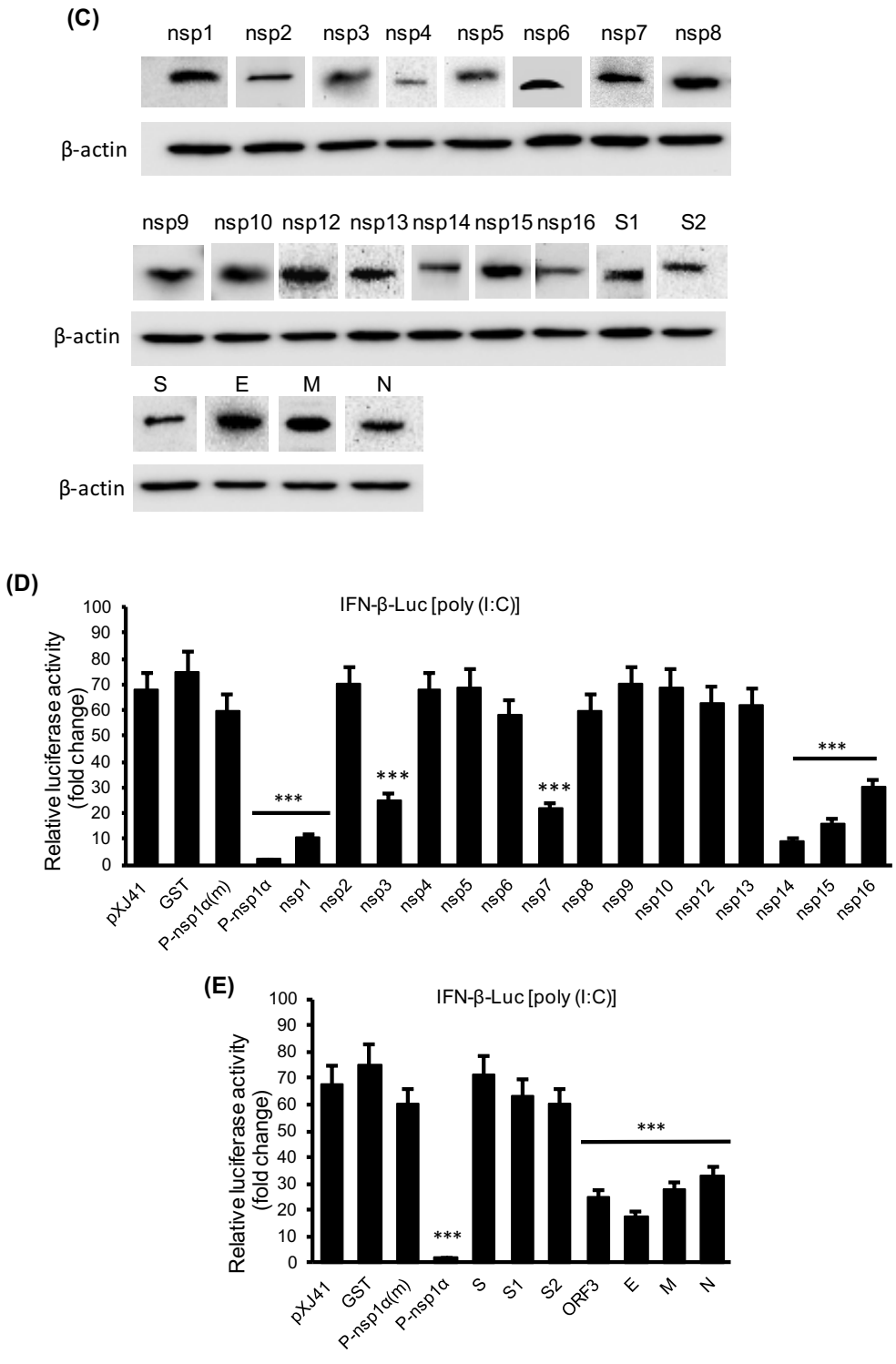
(C)
nsp1
nsp2
nsp3
nsp4
nsp5
nsp6
nsp7
nsp8
β-actin
nsp9
nsp10
nsp12
nsp13
nsp14
nsp15
nsp16
S1
S2
β-actin
S
E
M
N
β-actin
(D)
IFN-β-Luc [poly (I:C)]
Relative luciferase activity (fold change)
100
90
80
70
60
50
40
30
20
10
0
***
***
***
***
pXJ41
GST
P-nsp1α(m)
P-nsp1α
nsp1
nsp2
nsp3
nsp4
nsp5
nsp6
nsp7
nsp8
nsp9
nsp10
nsp12
nsp13
nsp14
nsp15
nsp16
(E)
IFN-β-Luc [poly (I:C)]
Relative luciferase activity (fold change)
100
90
80
70
60
50
40
30
20
10
0
***
***
pXJ41
GST
P-nsp1α(m)
P-nsp1α
S
S1
S2
ORF3
E
M
N

Fig. 2.3 (cont.)

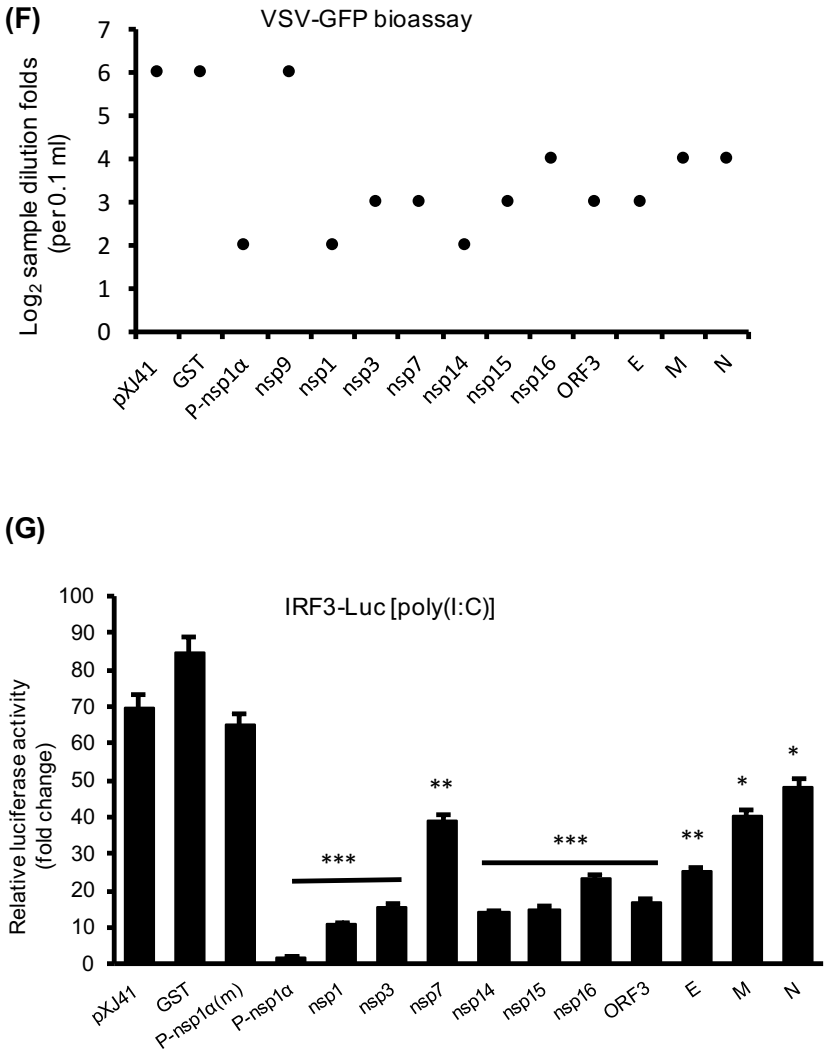
(F)
VSV-GFP bioassay
Log2 sample dilution folds (per 0.1 ml)
0
1
2
3
4
5
6
7
pXJ41
GST
P-nsp1α
nsp9
nsp1
nsp3
nsp7
nsp14
nsp15
nsp16
ORF3
E
M
N
(G)
IRF3-Luc [poly(I:C)]
Relative luciferase activity (fold change)
0
10
20
30
40
50
60
70
80
90
100
***
**
***
**
*
*
pXJ41
GST
P-nsp1α(m)
P-nsp1α
nsp1
nsp3
nsp7
nsp14
nsp15
nsp16
ORF3
E
M
N

Fig. 2.3 (cont.)

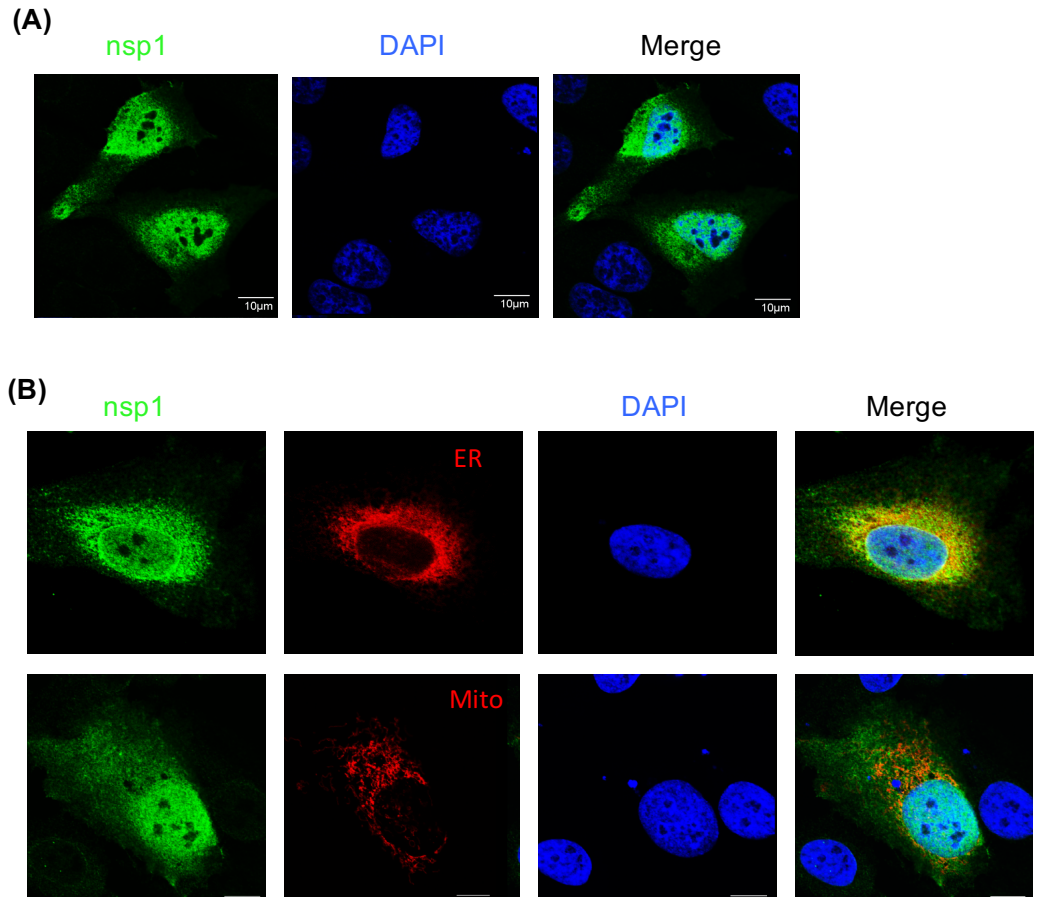

Fig. 2.4: Subcellular localization of PEDV nsp1. HeLa cells were seeded on slides in 6-well plates and transfected with PEDV nsp1 gene (A), or co-transfected with nsp1 and pDsRed2-ER or pDsRed2-Mito (B). At 24 h post-transfection, cells were fixed and permeabilized with Triton X-100. Cells were then incubated with mouse anti-FLAG mAb for 1 h, followed by Alexa Fluor 488-conjugated goat anti-mouse (green) secondary antibody to visualize nsp1. The ER and mitochondrial proteins were fused with the ER and mitochondria targeting sequence (Clontech) and so directly visualized (red). Nuclei (blue) were stained with DAPI. Images were collected using a Zeiss LSM-510 META confocal laser-scanning microscope and processed with the LSM image browser (Zeiss).

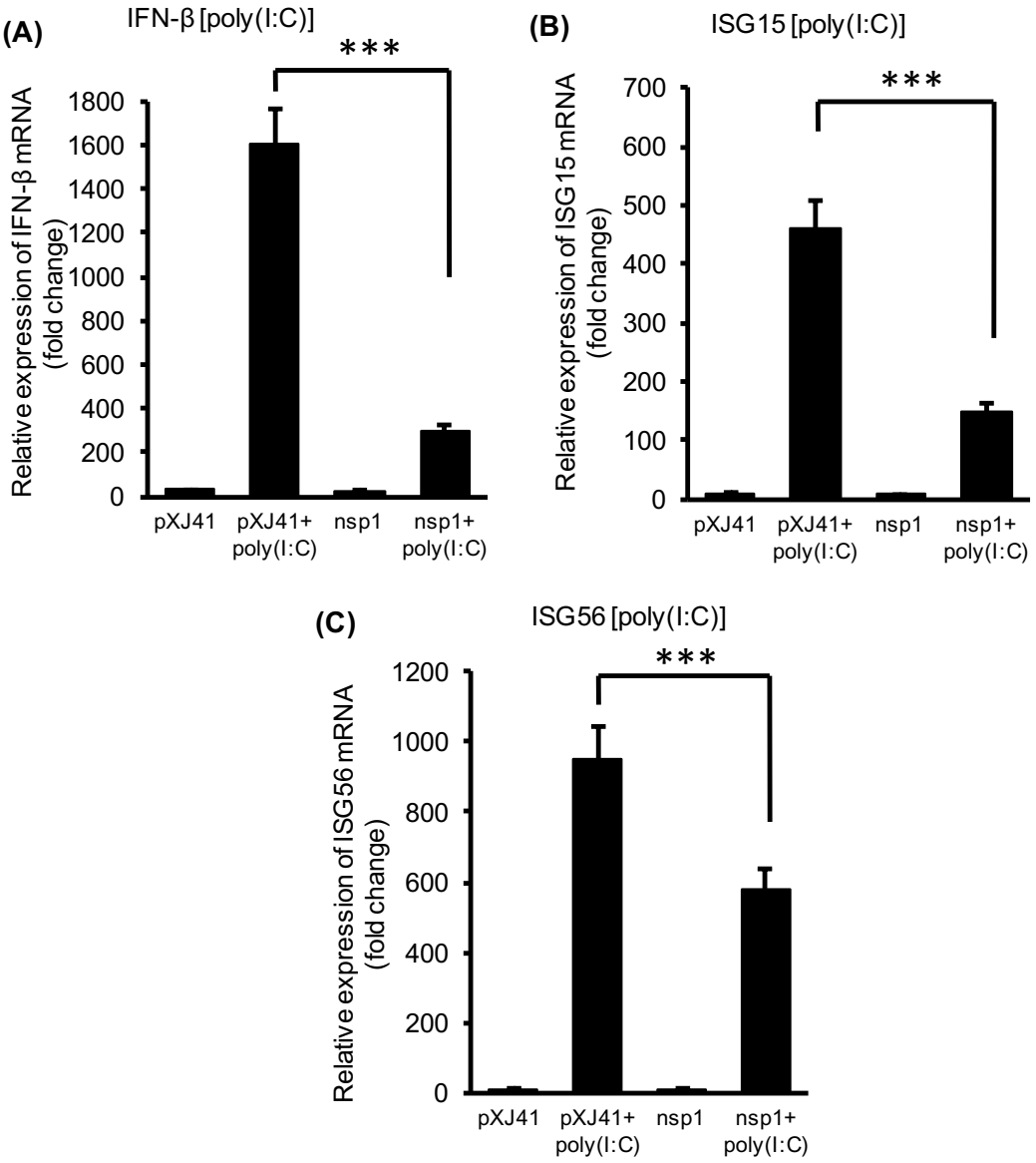

Fig. 2.5: Inhibition of IFN-β and ISG expression by nsp1. HeLa cells were seeded in 12-well plates and transfected with the nsp1 gene for 24 h, and stimulated with poly(I:C) for 12 h. Total RNA was extracted and mRNA expression was evaluated by qRT-PCR for IFN-β (A), ISG15 (B), and ISG56 (C). Results were normalized using β-actin mRNA and expressed as relative changes in mRNA levels with respect to those in cells without stimulation. Data are presented from three independent experiments, each in triplicate. Statistical analysis was performed by Student's *t* test. *, $P<0.05$; **, $P<0.01$; ***, $P<0.001$.

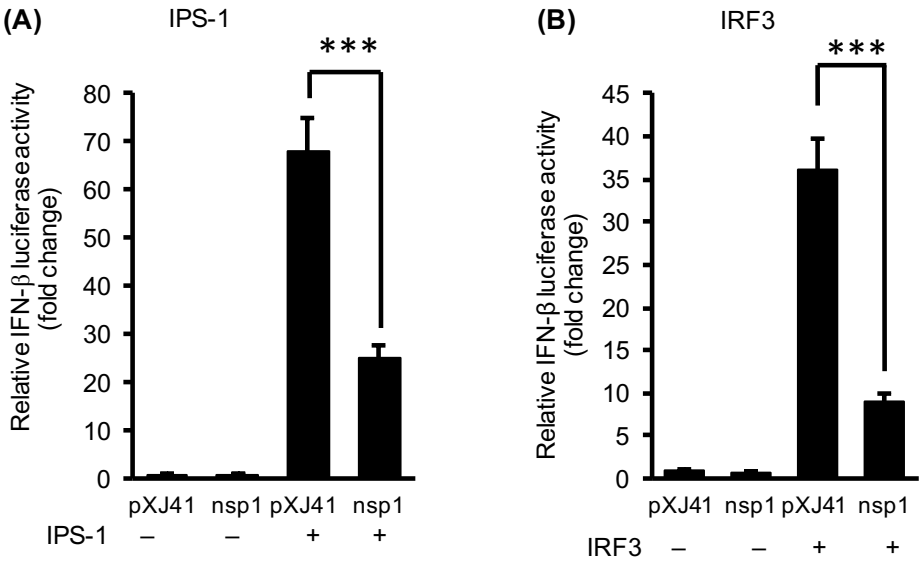

Fig. 2.6: Disruption of IRF3-mediated IFN signaling by nsp1. HeLa cells were seeded in 12-well plates and co-transfected with pMAVS/IPS-1 (A) or pIRF3 (B) along with the nsp1 gene, pRL-TK, and IFN-β-Luc reporter for 24 h. Cells were harvested to measure the firefly and renilla luciferase activities. Relative luciferase activity was defined as a ratio of the firefly luciferase to renilla luciferase activities. Data are presented as mean value ± standard deviation from three independent experiments. Statistical analysis was performed by Student's *t* test. *, $P<0.05$; **, $P<0.01$; ***, $P<0.001$.

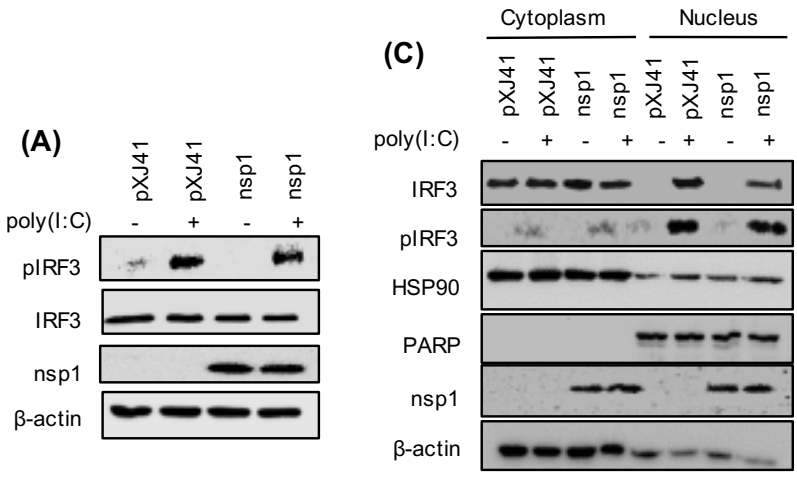

Fig. 2.7: IRF3 phosphorylation and nuclear translocation by nsp1. (A), HeLa cells were transfected with the nsp1-epressing plasmid for 24 h, followed by poly(I:C) stimulation for 8 h. Cells were lysed and subjected to Western blot to determine phosphorylated (p) IRF3. (B), Immunofluorescence staining for IRF3 nuclear translocation by nsp1. HeLa cells were transfected with the nsp1-expressing plasmid (2 μg/well) in 6-well plates for 24 h and stimulated by poly(I:C) for 8 h. Cells were fixed and incubated with rabbit anti-IRF3 pAb and mouse anti-FLAG mAb for 1 h. PRRSV nsp1α does not inhibit the IRF3 nuclear localization and was used as a control. Alexa Fluor 594-conjugated goat anti-rabbit and 488-conjugated goat anti-mouse secondary antibodies were used to visualize IRF3 (red) and viral nsp1 (green), respectively. Nuclei (blue) were stained with DAPI. Yellow arrows indicate IRF3 localization in the nucleus in the absence of nsp1 expression. White arrows indicate IRF3 localization in the nucleus in nsp1-expressing cells. (C) Phosphorylation and nuclear localization of IRF3 by nsp1. HeLa cells were transfected with the PEDV nsp1 gene for 24 h, then stimulated with poly(I:C) for 8 h. Cells were lysed for nuclear-cytoplasmic fractionations and subcellular distribution of IRF3 and pIRF3. Hsp90 was used as a cytosolic protein marker and PARP was used as a nuclear protein marker.

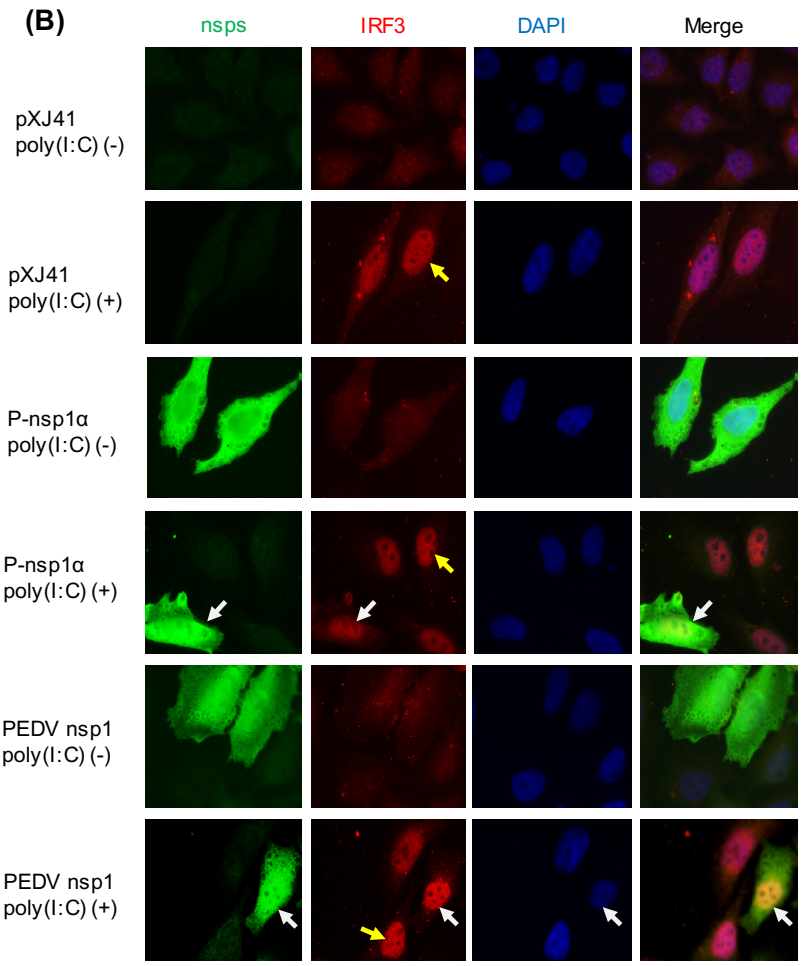
(B)
nsps
IRF3
DAPI
Merge
pXJ41
poly(I:C) (-)
pXJ41
poly(I:C) (+)
P-nsp1α
poly(I:C) (-)
P-nsp1α
poly(I:C) (+)
PEDV nsp1
poly(I:C) (-)
PEDV nsp1
poly(I:C) (+)

Fig. 2.7 (cont.)

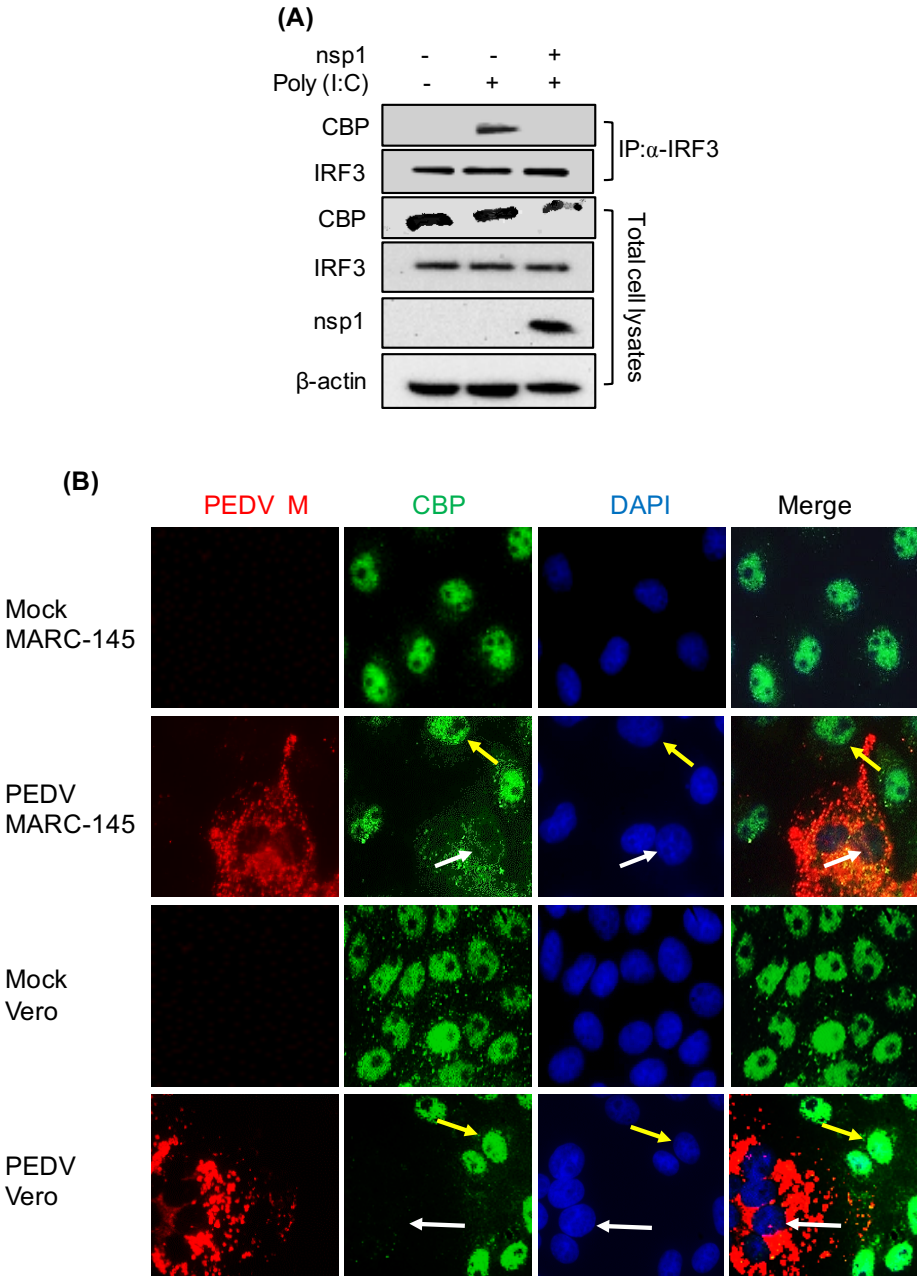

Fig. 2.8: Degradation of CBP in PEDV-infected cells. (A), Interruption of the IRF3 and CBP association by nsp1. HeLa cells were transfected with 2 μg/well of pXJ41-FLAG-nsp1 for 24 h and stimulated with poly(I:C) for 6 h. Cells were lysed and co-IP was carried out using rabbit anti-IRF3 and protein G-Agarose fast-flow beads (Millipore), followed by Western blot analysis using CBP antibody (panel 1, numbered from top) and IRF3 antibody (panel 2). Total cell lysates were probed for expression of CBP (panel 3), IRF3 (panel 4), nsp1 (panel 5), and β-actin as a loading control (panel 6). (B), Degradation of CBP in PEDV-infected cells. MARC-145 and Vero cells were seeded on coverslips placed on 6-well plates and grew to 80% confluency. Cells were infected with PEDV at an MOI of 0.1 for 24 h. Cells were then fixed and co-stained with rabbit anti-M pAb and mouse anti-CBP mAb. Alexa Fluor 594-conjugated goat anti-rabbit (red) and 488-conjugated goat anti-mouse (green) secondary antibodies were used to visualize protein expression. Nuclei (blue) were stained with DAPI. Yellow arrows indicate CBP in PEDV-uninfected cells. White arrows indicate CBP in PEDV-infected cells.

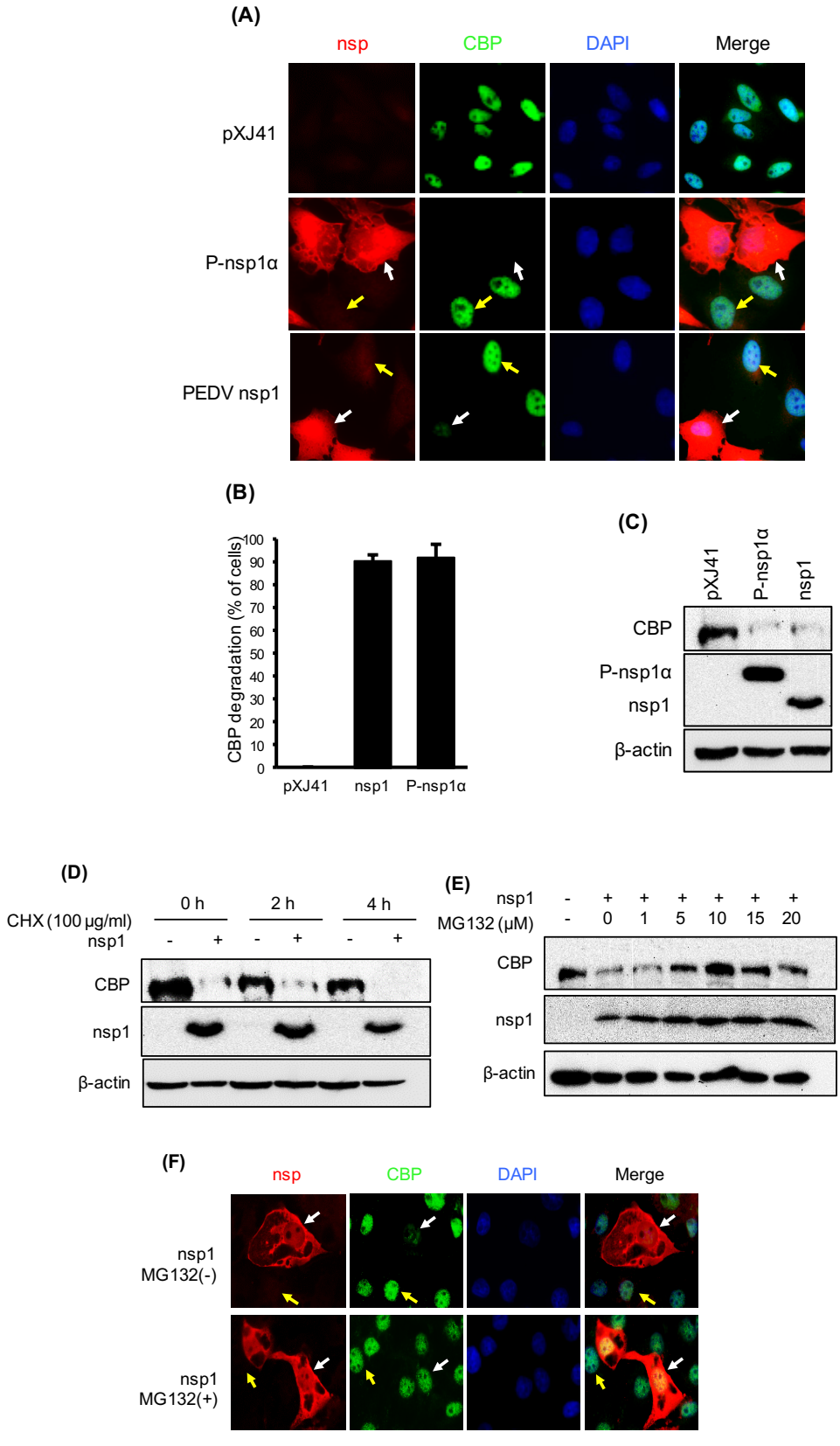
(A)
nsp
CBP
DAPI
Merge
pXJ41
P-nsp1α
PEDV nsp1
(B)
CBP degradation (% of cells)
100
90
80
70
60
50
40
30
20
10
0
pXJ41
nsp1
P-nsp1α
(C)
pXJ41
P-nsp1α
nsp1
CBP
P-nsp1α
nsp1
β-actin
(D)
0 h
2 h
4 h
CHX (100 μg/ml)
nsp1
- + - + - +
CBP
nsp1
β-actin
(E)
nsp1 - + + + + + +
MG132 (μM) - 0 1 5 10 15 20
CBP
nsp1
β-actin
(F)
nsp
CBP
DAPI
Merge
nsp1
MG132(-)
nsp1
MG132(+)

Fig. 2.9 (cont.)

Fig. 2.9 (cont.): CBP degradation in the nucleus is mediated by nsp1. (A), CBP degradation by nsp1 as determined by immunofluorescence assay. HeLa cells were transfected with PRRSV nsp1α which is known to degrade CBP in the nucleus, or PEDV nsp1. At 24 h post-transfection, cells were fixed and co-stained with rabbit anti-FLAG pAb and mouse anti-CBP mAb. Alexa Fluor 594-conjugated goat anti-rabbit and 488-conjugated goat anti-mouse (green) secondary antibodies were used to visualize nsp1 (red) and CBP (green). Nuclei (blue) were stained with DAPI. Yellow arrows indicate CBP in the absence of nsp1 expression, and white arrows indicate CBP in cells expressing viral nsp1. (B), Percent number of cells in which CBP was degraded by PEDV nsp1 and PRRSV nsp1α (P-nsp1α). Data are presented by % calculation of transfected cells showing more than 80% reduction of CBP fluorescent intensity compared to the control CBP staining out of 150 randomly chosen nsp1-expressing cells. (C), CBP degradation by nsp1 determined by Western blot. At 24 h transfection, cells lysates were prepared for Western blot using mouse anti-CBP mAb to examine the level of endogenous CBP. (D), PEDV nsp1-mediated degradation of CBP after cycloheximide (CHX) treatment. After 24 h transfection with the nsp1 gene, cells were treated with 100 μg/ml of CHX for indicated times, followed by Western blot using mouse anti-CBP mAb (top panel) and mouse anti-FLAG mAb for nsp1 detection (middle panel). (E), Inhibition of nsp1-mediated CBP degradation by MG132. After 24 h transfection with the nsp1 gene, HeLa cells were treated with MG132 at indicated concentrations for 16 h. Cells lysates were prepared and western blot was conducted using mouse anti-CBP mAb (top panel) or mouse anti-FLAG mAb (middle panel). (F), The CBP degradation by PEDV nsp1 in porcine intestinal epithelial cells IPEC-J2. IPEC-J2 cells were maintained as described in the Material and Methods, and transfected with the PEDV nsp1 gene. At 24 h post-transfection, cells were treated with or without 10μM MG132 for 16h, and then fixed for IFA. Yellow arrows indicate CBP in the absence of nsp1 expression, and white arrows indicate CBP in cells expressing viral nsp1.

Table 2.1: Primers used for the cloning of PEDV nonstructural and structural genes.
(Restriction enzyme recognition sequences are underlined. The FLAG tag is italicized and underlined.)

Primer	Sequence (5'-3')
nsp1-F	GCCGAATTCACCATG*GATTACAAGGATGACGACGATAAG*ATGGCTAGCAACCATG
nsp1-R	GCCCTCGAGCTAACCACCACGACG
nsp2-F	GCCGGATCCACCATG*GATTACAAGGATGACGACGATAAG*AACATCGTGCCAG
nsp2-R	GCCGGTACCCTAACCACCTTTCTTC
nsp3-F	AGTCTCGAGACCATG*GATTACAAGGATGACGACGATAAG*GGTGATGTCAAATTC
nsp3-R	GCCAGATCTCTATGCACCCTTCTTATTTG
nsp4-F	GCCGGATCCACCATG*GATTACAAGGATGACGACGATAAG*GGTCTTCCTAGTTTTTC
nsp4-R	GCCCTCGAGCTACTGTAGAGTTGAATTG
nsp5-F	GCCGAATTCACCATG*GATTACAAGGATGACGACGATAAG*GCTGGCTTGCGTAAG
nsp5-R	GCCCTCGAGCTACTGAAGATTAACGCC
nsp6-F	GCCGAATTCACCATG*GATTACAAGGATGACGACGATAAG*AGTGGTTATGTTTC
nsp6-R	GCCCTCGAGCTACTGAACGGAAG
nsp7-F	GCCGAATTCACCATG*GATTACAAGGATGACGACGATAAG*TCTAAACTGACTG
nsp7-R	GCCCTCGAGCTACTGCAACATAC
nsp8-F	GCCGAATTCACCATG*GATTACAAGGATGACGACGATAAG*AGTGTTGCATCTAC
nsp8-R	GCCCTCGAGCTACTGGAGCTTGAC
nsp9-F	GCCGAATTCACCATG*GATTACAAGGATGACGACGATAAG*AATAATGAAATTATTCC
nsp9-R	GCCCTCGAGCTACTGCAAGCGTAC
nsp10-F	GCCGAATTCACCATG*GATTACAAGGATGACGACGATAAG*GCTGGTAAACAAACAG
nsp10-R	GCCCTCGAGCTATTGCATAATGGATC
nsp12-F	GCCGGATCCACCATG*GATTACAAGGATGACGACGATAAG*AGCACTGATATGGC
nsp12-R	GCCCTCGAGCTATTGTAAAACTGCAG
nsp13-F	GCCGAATTCACCATG*GATTACAAGGATGACGACGATAAG*TCTGCAGGGCTTTGTG
nsp13-R	GCCCTCGAGCTACTGCAAATCAG
nsp14-F	GCCGAATTCACCATG*GATTACAAGGATGACGACGATAAG*GCTAATGAGGGTTGTG
nsp14-R	GCCCTCGAGCTATTGCAAATTGTTAC
nsp15F	GCCGAATTCACCATG*GATTACAAGGATGACGACGATAAG*GGTCTTGAGAACATTGC
nsp15R	GCCCTCGAGCTACTGAAGTTGCGGAT
nsp16F	GCCGAATTCACCATG*GATTACAAGGATGACGACGATAAG*GCCAGTGAATGGAAG
nsp16R	GCCCTCGAGTCATTTGTTTACGTTG
S-F	GCCGAATTCACCATGAAGTCTTTAACCTAC
S-R	GCCCTCGAGTCA*CTTATCGTCGTCATCCTTGTAATC*CTGCACGTGGACCTTTTC
S1-F	GCCGAATTCACCATGATGAAGTCTTTAACCTAC
S1-R	GCCCTCGAGTCA*CTTATCGTCGTCATCCTTGTAATC*AATACTCATACTAAAG
S2-F	GCCGAATTCACCATGAGGACAGAATATTTACAG
S2-R	GCCCTCGAGTCA*CTTATCGTCGTCATCCTTGTAATC*CTGCACGTGGACCTTTTC
ORF3-F	GCCGAATTCACCATG*GATTACAAGGATGACGACGATAAG*ATGTTTCTTGGAC
ORF3-R	GCCCTCGAGTCATTCACTAATTGTAG
E-F	GCCGAATTCACCATGCTACAATTAGTG
E-R	GCCCTCGAGTCA*CTTATCGTCGTCATCCTTGTAATC*TACGTCAATAACAGTAC
M-F	GCCGAATTCACCATGTCTAACGGTTCTATTC
M-R	GCCCTCGAGTCA*CTTATCGTCGTCATCCTTGTAATC*GACTAAATGAAGCAC
N-F	GCCGGATCCACCATG*GATTACAAGGATGACGACGATAAG*ATGGCTTCTGTCAG
N-R	GCCCTCGAGTCAATTTCCTGTGTCGAAG

Table 2.2: Primers used for relative quantitative real-time PCR.

Primer	Sequence (5'-3')
IFN-β-F	GATTTATCTAGCACTGGCTGG
IFN-β-R	CTTCAGGTAATGCAGAATCC
ISG15-F	CACCGTGTTCATGAATCTGC
ISG15-R	CTTTATTTCCGGCCCTTGAT
ISG56-F	CCTCCTTGGGTTCGTCTACA
ISG56-R	GGCTGATATCTGGGTGCCTA
β-actin-F	ATCGTGCGTGACATTAAG
β-actin-R	ATTGCCAATGGTGATGAC

CHAPTER 3: INHIBITION OF NF-KB ACTIVITY BY THE PORCINE EPIDEMIC DIARRHEA VIRUS NONSTRUCTURAL PROTEIN 1 FOR INNATE IMMUNE EVASION

3.1 ABSTRACT

Porcine epidemic diarrhea virus emerged in the US is known to suppress the type I interferons response during infection. In the present study using porcine epithelial cells, we showed that PEDV inhibited both NF-κB and proinflammatory cytokines. PEDV blocked the p65 activation in infected cells and suppressed the PRD II-mediated NF-κB activity. Of the total of 22 viral proteins, nine proteins were identified as NF-κB antagonists, and nsp1 was the most potent suppressor of proinflammatory cytokines. Nsp1 interfered the phosphorylation and degradation of IκBα, and thus blocked the p65 activation. Mutational studies demonstrated the essential requirements of the conserved residues of nsp1 for NF-κB suppression. Our study showed that PEDV inhibited NF-κB activity and nsp1 was a potent NF-κB antagonist for suppression of both IFN and early production of pro-inflammatory cytokines.

3.2 INTRODUCTION

Porcine epidemic diarrhea (PED) is an acute and highly contagious enteric disease characterized by severe enteritis, vomiting, watery diarrhea and a high mortality rate in neonatal piglets (Debouck and Pensaert, 1980; Junwei et al., 2006; Song and Park, 2012; Sun et al., 2012a). The current virulent PED outbreaks started in China in the late 2010 and quickly spread to other countries in Asia, causing significant economic losses in the swine industry (Sun et al., 2015; Sun et al., 2012a). PED emerged in the US for the first time in April 2013 and resulted in

This chapter has appeared as an article in Virology. The original citation is: Zhang, Q., Ma, J., Yoo, D., 2017. Inhibition of NF-κB activity by the porcine epidemic diarrhea virus nonstructural protein 1 for innate immune evasion. Virology 510, 111-126.

more than 8 million deaths of pig in less than 8 months of the first outbreak. (Chen et al., 2014; Marthaler et al., 2013; Mole, 2013; Stevenson et al., 2013).

Porcine epidemic diarrhea virus (PEDV) is a coronavirus belonging to the genus *Alphacoronavirus* of the *Coronaviridae* family (http://ictvonline.org/virustaxonomy.asp). The PEDV genome is a single-stranded, positive-sense RNA of ~28 kb in length with a 5'-cap and a 3'-polyadenylated tail. It encodes two polyproteins (pp1a and pp1a/b), an accessory protein (ORF3), and four structural proteins (spike S, envelope E, membrane M, and nucleocapsid N) (Duarte et al., 1993; Kocherhans et al., 2001). Pp1a and pp1a/b are processed to 16 nonstructural proteins (nsps) by the proteinase activity of nsp3 and nsp5. Among nsps, nsp1 is the most N-terminal and first cleavage product (Ziebuhr, 2005).

Virus-infected cells react quickly to invading viruses by producing type I interferons (IFN-α/β) and establish an antiviral state, which provides a first line of defense against viral infection. The viral nucleic acids are sensed by pattern-recognition receptors (PRRs) such as transmembrane toll-like receptors (TLRs) and cytoplasmic RNA/DNA sensors (Kawai and Akira, 2011). This recognition leads to the activation of cytosolic kinases which promotes the activation of IFN regulator factor 3 (IRF3), IRF7, and nuclear factor-κB (NF-κB), and their subsequent translocation to the nucleus allows them to bind to their respective positive regulatory domain (PRD) for production of type I IFNs (Honda et al., 2006). The activated IRF3/IRF7 bind to the PRD I/III sequences and induces the expression of type I IFN genes (Hermant and Michiels, 2014). For NF-κB, the activated form is translocated to the nucleus and triggers IFN-β expression by binding to the PRD II element (Escalante et al., 2002). Type I IFNs are then secreted and bind to their receptors on virus-infected cells as well as uninfected neighbor cells,

and activate the JAK/STAT pathway to produce hundreds of interferon-stimulating genes (ISGs) to establish an antiviral state (Stark and Darnell, 2012).

In unstimulated cells, NF-κB (p50/p65 heterocomplex) remains associated with the inhibitory protein IκBα masking the nuclear localization signal (NLS) of NF-κB and sequesters the NF-κB·IκBα complex in the cytoplasm. The NF-κB signaling pathway may be activated by intracellular products such as IL-1 and TNFα that are induced by viral infections or extracellular stress such as phorbol esters and UV (Campbell and Perkins, 2006; Ghosh et al., 1998). Activated NF-κB then induces the production of proinflammatory cytokines and regulates a variety of gene expressions, which affects cell survival, differentiation, immunity, and proliferation (Hayden and Ghosh, 2012). TNFα binds to its receptor and initiates a signaling cascade culminating the activation of IκB kinase complex (IKKα/β). The IKK complex then phosphorylates IκBα to mediate ubiquitination and degradation and releases NF-κB. Released NF-κB is transported to the nucleus, where it binds to target sequences and initiates transcriptions (Hayden and Ghosh, 2012; Napetschnig and Wu, 2013; Verstrepen et al., 2008).

To circumvent such responses of the cell, many viruses have developed various strategies to evade the host innate immunity. We have previously reported that PEDV suppresses the type I interferon and ISGs productions and have identified nsp1 as the potent viral IFN antagonist (Zhang et al., 2016). PEDV nsp1 causes the CREB-binding protein (CBP) degradation in the nucleus and antagonizes the IFN production and signaling (Zhang et al., 2016). Despite the importance of NF-κB during infection, regulation of NF-κB by PEDV is poorly understood. The PEDV N protein blocks the NF-κB activity and inhibits the IFN-β production and IFN stimulating genes (ISGs) expression (Ding et al., 2014). PEDV nsp5 is a 3C-like proteinase and cleaves the NF-κB essential modulator (NEMO) (Wang et al., 2015a), suggesting that PEDV has

the ability for NF-κB suppression. Although PEDV has been shown to activate NF-κB at a late stage of infection (Cao et al., 2015b; Xing et al., 2013), it is unclear whether it is time-dependent and TNFα-mediated. In the present study, we show the inhibition of NF-κB, and temporal regulation of type I IFNs and pro-inflammatory cytokines by PEDV. Among PEDV proteins, nsp1, nsp3, nsp5, nsp7, nsp14, nsp15, nsp16, ORF3, and E were identified as NF-κB antagonists with nsp1 being the most potent. We also showed that the conserved residues of nsp1 were crucial for NF-κB suppression. The nsp1-mediated NF-κB modulation may facilitate the replication and pathogenesis of PEDV.

3.3 MATERIALS AND METHODS

3.3.1 Cell culture, viral infection, and titration

Two different lines of African green monkey kidney cells, MARC-145 (Kim et al., 1993) and Vero (ATCC® CCL-81™), were grown in Dulbecco's modified Eagle's medium (DMEM) (Corning™ Cellgro™) supplemented with 10% heat-inactivated fetal bovine serum (FBS) (Gibco®) at 37°C in a humidified atmosphere of 5% CO_2. HeLa cells (NIH AIDS Research and Reference Reagent Program, Germantown, MD) were maintained in minimum essential medium (MEM) (Corning™ Cellgro™) with 10% heat-inactivated FBS. LLC-PK1 (Perantoni and Berman, 1979) is a porcine kidney epithelial cell line derived from the kidney of a normal healthy male pig of three weeks of age and was obtained from Dr. K. Chang (Kansas State University, Manhattan, KS). LLC-PK1 cells were maintained in MEM with 5% FBS. RAW264.7 cells were obtained from Dr. G. Lau (University of Illinois at Urbana-Champaign) and maintained in RPMI-1640 supplemented with 10% FBS.

The recombinant vesicular stomatitis virus expressing green fluorescent protein (VSV-GFP) was kindly provided by Dr. A. Garcia-Sastre (Mount Sinai Hospital, New York, NY). PEDV (USA/Colorado/2013; GenBank: KF272920) was obtained from Agricultural Research Service US Department of Agriculture (Ames, IA). PEDV was propagated in FBS-free DMEM (or MEM) supplemented with 0.3% tryptose phosphate broth (Sigma, St. Louis, MO), 0.02% yeast extract (Teknova, Hollister, CA) containing varying concentrations of trypsin 250 (Sigma-Aldrich, St. Louis, MO). The optimal trypsin concentration for Vero, MARC-145, and LLC-PK1 cells was 5 μg/ml, 2 μg/ml, and 1 μg/ml, respectively. For PEDV growth curve, cells were infected at either low MOI (0.01 MOI) or high MOI (5 MOI) for 1 h and incubated further. Culture supernatants were collected at indicated times post-infection and titrated using the 50% tissue culture infective dose ($TCID_{50}$) protocol. The viral titers were calculated using the Spearman-Karber equation (Mahy et al., 1996) and presented as the viral growth curve.

3.3.2 Antibodies and chemicals

Following antibodies were used for immunofluorescence assay (IFA) and Western blot (WB) analysis: mouse anti-PEDV N mAb (Medgene, Brookings, no. SD-1-5, 1:1,000 dilution for WB, 1:200 dilution for IFA); rabbit anti-p65 mAb (Cell Signaling Technology, no. 8242, 1:1,000 dilution for WB, 1:200 for IFA); mouse anti-hsp90 mAb (Santa Cruz, no. sc-69703, 1:1,000 for WB); rabbit anti-PARP pAb (Santa Cruz, no. sc-7150, 1:1,000 for WB); mouse anti-IκBα mAb (Thermo Scientific, no. MA5-15132, 1:1,000 for WB); mouse anti-p-IκBα mAb (Cell Signaling Technology, no. 9246, 1:1,000 dilution for WB); rabbit anti-IKKα pAb (Santa Cruz no. sc-7218, 1:200 for WB); mouse anti-IKKβ mAb (Santa Cruz no. sc-56918, 1:200 for WB); rabbit anti-p-IKKα (Ser180)/IKKβ (Ser181) Ab (Cell Signaling Technology, no. 2681, 1:1,000

dilution for WB); mouse anti-β-actin mAb (Santa Cruz no. sc-47778, 1:2,000 for WB); rat anti-FLAG Ab (Agilent Technologies, no. 200474, 1:2,000 for WB, 1:200 for IFA).

Human TNFα was purchased from Cell Signaling Technology (no. 8902) and used at 15 ng/ml or 20 ng/ml. Polyinosinic:polycytidylic acid (polyI:C) and DAPI (4', 6-diamidino-2-phenylindole) were purchased from Sigma (St. Louis, MO). Lipofectamine 2000 transfection reagent was purchased from Invitrogen (Carlsbad, CA). QIAamp Viral RNA mini kit and RNeasy mini kit were purchased from QIAGEN (Venlo, Limburg). Power SYBR Green PCR master mix was purchased from Life Technologies (Carlsbad, CA). Alexa Fluor 594-conjugated (goat anti-rabbit, red) and 488-conjugated (goat anti-mouse, green) secondary antibodies and Pierce™ ECL Western blotting substrate were purchased from Thermo Scientific (Waltham, MA).

3.3.3 Plasmid constructs

The firefly luciferase gene was under the control of the respective promoter as described below and used as a reporter. The plasmid pIFN-β-Luc contains the entire IFN-β enhancer-promoter sequence and was obtained from Dr. S. Ludwig at Heinrich-Heine-Universität, Düsseldorf, Germany (Ehrhardt et al., 2004). The plasmid pNF-κB-Luc (Stratagene, La Jolla, CA) contains the NF-κB enhancer, which is responsive to the stimulation of TNFα. The plasmid pPRD II-Luc contains two copies of the NF-κB binding region PRD II of the IFN-β promoter and was kindly provided by Dr. S. Perlman at University of Iowa, IA (Zhou and Perlman, 2007). The plasmid pswTNFα-Luc contains swine TNFα promoter sequences and was obtained from Dr. F. A. Osorio at University of Nebraska-Lincoln, NE (Subramaniam et al., 2010). The *Renilla* luciferase plasmid pRL-TK (Promega) contains the herpes simplex virus thymidine kinase

(HSV-tk) promoter and was included as an internal control. Constructs expressing individual proteins of PEDV are described elsewhere (Zhang et al., 2016). PRRSV N (P-N), PRRSV nsp1β (P-nsp1β), PRRSV nsp1α (P-nsp1α), and PRRSV nsp1α cystine mutant P-nsp1α(m) (C28S) are described elsewhere (Han et al., 2013; Song et al., 2010). The higher order structure of PEDV nsp1 was predicted using DNASTAR (https://www.dnastar.com; Madison, WI) based on the X-ray crystallographic structure of TGEV nsp1. PCR-based site-directed mutagenesis was performed to mutate amino acids of PEDV nsp1 and a series of nsp1 mutants were generated. The primers and the position of mutations for each mutant are shown in Table 3.1. Mutations were confirmed by DNA sequencing, and mutant protein expressions were examined by immunofluorescence assay and Western blot.

3.3.4 RNA extraction and quantitative real-time RT-PCR

Cells were washed with PBS and lysed with RLT lysis buffer (QIAGEN). Total cellular RNA was extracted using RNeasy mini kit according to the manufacturer's instructions (QIAGEN). Genomic DNA contaminants were removed by treatment with DNase I (Promega). One μg of RNA was used for reverse transcription using random primers and M-MLV reverse transcriptase (Promega). Real-time quantitative PCR was performed using cDNA and SYBR Green PCR mix in the ABI 7500 real-time PCR system according to the manufacturer's instruction (Life Technologies). The swine-specific real-time qPCR primers for IFN-α, IFN-β, TNFα, IL-1β, IL-6, IL-8, IL-15, IL-17, CXCL10, TGF-β3, MCP-1, RANTES, and β-actin are listed in Table 3.2. The β-actin gene was used as an internal control for each sample. Specific amplification was confirmed by the sequencing of PCR products and the melting curve analysis of qPCR. Threshold cycles for target genes and differences between C_t values (ΔC_t) were

determined. Relative levels of transcripts of target genes were shown as fold changes relative to respective controls by the $2^{-\Delta\Delta Ct}$ threshold method (Livak and Schmittgen, 2001).

3.3.5 Dual luciferase reporter assay

To identify the viral antagonists for NF-κB/PRD II promoter, dual luciferase reporter assays were conducted. HeLa cells were grown in 48-well plates to 80% confluency, and transfected with luciferase reporters, individual viral genes, and pRL-TK at a ratio of 10:10:1 using Lipofectamine 2000 according to the manufacturer's instruction (Invitrogen). Cells were stimulated with 0.5 μg/ml of poly(I:C) or 15 ng/ml of TNFα at 12 h post-transfection for 12 h, and then lysed in 60 μl 1X Passive lysis buffer for 20 min at room temperature (RT) with constant shaking. To examine the NF-κB/PRD II promoter activity during PEDV infection, MARC-145 cells were grown in 12-well plates to 80% confluency, and transfected with luciferase reporters and pRL-TK at a ratio of 10:1 using Lipofectamine 2000. Cells were infected with PEDV at 1 MOI at 6 h post-transfection for 12 h, and stimulated with poly(I:C) for 12 h or TNFα for 9 h . Cells were then lysed in 100 μl 1X Passive lysis buffer for 20 min at RT. Supernatants of the cell lysates were subjected to dual Luciferase assays according to the manufacturer's instructions (Promega). All the values were normalized using the *Renilla* luciferase activity as the internal control and presented in fold changes. The data are represented as the mean value with a standard deviation from three independent experiments.

3.3.6 Indirect immunofluorescence assay (IFA) and confocal microscopy

Cells were grown on coverslips placed in 12-well plates to 80% confluency for transfection or infection. For transfection, HeLa cells were transfected with individual plasmids

using Lipofectamine 2000 according to the manufacturer's instructions (Invitrogen). For infection, LLC-PK1 cells were infected with PEDV at 0.01 MOI. At indicated times post-treatment with poly(I:C) or TNFα, cells were washed once and fixed with 4% paraformaldehyde in PBS overnight at 4°C followed by permeabilization using 0.1% Triton X-100 for 15 min at RT. Cells were incubated in the blocking buffer (1% BSA in PBS) for 30 min at RT and then incubated with primary antibody diluted in 1% BSA for 1-3 h. After three washes, cells were incubated with fluorochrome-conjugated secondary antibody (Thermo Scientific) in the dark for 1 h at RT, followed by treatment with DAPI for 10 min to stain the nuclei. After washing with PBS, cover slips were mounted on microscope slides using Fluoromount-G mounting medium (Southern Biotech, Birmingham, AL) and examined for fluorescence using the Nikon A1R confocal fluorescence microscope. The confocal microscopy images were processed using NIS-Elements analysis software.

3.3.7 Cell fractionation, Co-immunoprecipitation, and western blot analysis

For cell fractionation, HeLa cells were grown in 6-well plates to 80% confluency for gene transfection. Cells were then stimulated with 15 ng/ml TNFα for 12 h and lysed and fractionated using the Nuclear/Cytosol Fractionation kit (BioVision, Milpitas, CA). Briefly, cells were washed once with cold PBS and collected with cell scrapers. Cell pellets were then resuspended in CEB-A buffer on ice for 10 min and after addition of CEB-B further incubated on ice for 1 min. The lysates were centrifuged at 4°C for 5 min at 16,000 x g, and the supernatants were collected as the cytosolic fraction. Cell pellets were resuspended in NEB buffer and vortexed for 30 s, which was repeated 5 times every 10 min. Cell pellets were centrifuged for 10 min at 4°C at 16,000 x g, and the supernatants were kept as the nuclear fraction.

For co-immunoprecipitation, cells were lysed in lysis buffer [50 mM Tris (pH 8.0), 150 mM NaCl, 5 mM Na_3VO_4, 1 mM PMSF, 100 mg/ml leupetin, 1% NP-40, 10% glycerol] supplemented with the proteinase inhibitors cocktail (Promega), followed by immunoprecipitation as described previously (Zhang et al., 2016). For Western blot, cells were harvested in RIPA buffer [20 mM Tris (pH 7.5), 150 mM NaCl, 1 mM EDTA, 1 mM phenylmethanesulphonyl fluoride (PMSF), 0.1% SDS, 0.5% sodium deoxycholate, 1% NP-40] containing the proteinase inhibitors cocktail (Promega). Cells were lysed on ice for 30 min, sonicated, and centrifuged to remove insoluble components. For Western blot, proteins were resolved by SDS-PAGE and transferred to an Immobilon-P membrane (Millipore). The membranes were blocked with 5% nonfat dry milk or 5% BSA in TBST (0.05% Tween-20) for 1 h and then incubated with primary antibody at 4°C overnight. After three washes, the membranes were incubated with horseradish peroxidase (HRP)-conjugated secondary antibody for 1 h at RT. The antibody-antigen complex was visualized using enhanced chemiluminescence detection reagents (Thermo). Images were taken by the FluorChem™ R System according to the manufacturer's instructions (ProteinSimple).

3.3.8 Statistical analysis

The student's *t* test was used for statistical analyses using GraphPad Prism 6. Asterisks indicate the statistical significance as follow: *, $P<0.05$, **, $P<0.01$ and ***, $P<0.001$.

3.4 RESULTS

3.4.1 Inhibition of Type I IFNs production by PEDV in LLC-PK1 cells

The primary target cells for PEDV in pigs are villous epithelial cells of the intestinal tract (Debouck and Pensaert, 1980; Lee et al., 2000; Sueyoshi et al., 1995). Vero cells are commonly used for the study of PEDV, but these cells are deficient for type I IFN genes, and we have previously identified MARC-145 as an additional cell line permissive for PEDV. In these cells, PEDV has been shown to inhibit type I IFN production (Zhang et al., 2016). However, MARC-145 cells are originated from monkey kidney epithelium, and porcine epithelial cells will serve a better model to study the innate immune regulation for PEDV. To this aim, we identified LLC-PK1 as a permissive cell line for PEDV. LLC-PK1 is of porcine kidney epithelial cells, and we found that these cells efficiently supported PEDV infection. Even at an MOI of 0.01, almost 100% of LLC-PK1 cells became infected by 24 h of infection (data not shown). Western blot analysis of PEDV N protein confirmed the productive infection in LLC-PK1 cells (Fig. 3.1A). To examine the growth of PEDV, LLC-PK1, MARC-145, and Vero cells were infected with the virus at a low MOI (0.01), and the culture supernatants were collected to determine the titers at different times of infection. The growth curves show the productive infection of PEDV in these cells (Fig. 3.1B). Similar growth kinetics was observed for Vero and MARC-145 cells. PEDV induced extensive cell fusion in Vero cells and these cells died by 24 h post-infection (hpi). LLC-PK1 cells supported PEDV growth most efficiently, and the peak viral titer was as high as $10^{7.5}$ $TCID_{50}$/ml at 48 hpi (Fig. 3.1B), compared to 10^{5} $TCID_{50}$/ml in MARC-145 cells. The one-step growth curve for PEDV was determined by infecting with a high MOI of 5. Syncytia formation characteristic for PEDV was evident as early as 9 hpi in PEDV-infected cells (Fig. 3.1C, arrows). The one step growth curve showed that PEDV replicated in LLC-PK1 cells most

effectively compared to MARC-145 and Vero cells (Fig. 3.1D). To examine the type I IFN regulation in LLC-PK1 by PEDV, cells were infected with the virus, and RT-qPCR was conducted for both IFN-α and IFN-β mRNAs. While poly(I:C) induced the production of IFN-α and INF-β in uninfected LLC-PK1 cells as anticipated, hardly any IFN-α/β were produced in PEDV-infected LLC-PK1 cells especially at 8-24 hpi (Fig. 3.1E). Even at 5 MOI, PEDV infection did not induce type I IFNs (Fig. 3.1F) and also inhibited the production of type I IFNs even when stimulated with poly(I:C) (Fig. 3.1G, 3.1H), further confirming the suppression of type I IFN production by PEDV.

3.4.2 Inhibition of early production of pro-inflammatory cytokines by PEDV

Evidence suggests that PEDV modulates innate immune response for optimal viral replication (Annamalai et al., 2015; Zhang et al., 2016; Zhang and Yoo, 2016). PEDV may also have the ability to modulate the production of pro-inflammatory cytokines for viral pathogenesis and virulence. To determine this possibility, we assessed the expression of pro-inflammatory cytokines in virus-infected cells. LLC-PK1 cells were infected with PEDV, and total RNA was prepared at different times to determine different cytokine gene expressions by RT-qPCR using specific primers (Table 3.2). PEDV infection caused down-regulation of TNFα during 8-12 hpi, but later times of 24-30 hpi, its expression was upregulated (Fig. 3.2A). The IL-1β mRNA levels were significantly downregulated at early times (8-24 hpi) and returned to the basal level by 30 hpi (Fig. 3.2B). The IL-6 mRNA expression was also suppressed at 8-18 hpi but became activated at 30 hpi (Fig. 3.2C). Similarly, the IL-15 expression was inhibited at early times (8-18 hpi) but activated later times of infection (24-30 hpi) (Fig. 3.2D). The IL-17 expression was also suppressed at 8-24 hpi but upregulated at 30 hpi (Fig. 3.2E), and the TGF-β3 expression was

inhibited at 12 and 24 hpi (Fig. 3.2F). These results demonstrate that PEDV regulated the production of pro-inflammatory cytokines in a time-dependent manner. This was confirmed in two other cell types, MARC-145 and Vero, using TNFα mRNA. PRRSV is known to suppress TNFα production (Subramaniam et al., 2010) and VSV is known to activate TNFα production (Garcia et al., 2009), and thus both viruses were included as controls. As anticipated, PRRSV inhibited the expression of TNFα at 18 hpi, whereas VSV activated the TNFα expression continuously over time (Fig. 3.2G). In both PEDV-infected MARC-145 cells and Vero cells, the TNFα expression was suppressed at early times (6-18 hpi) and became activated later (24 hpi), confirming the suppression of pro-inflammatory cytokines by PEDV at early times.

3.4.3 Temporal regulation of TNFα-induced NF-κB activation by PEDV

The NF-κB signaling is a central pathway regulating the production of proinflammatory cytokines (Blackwell and Christman, 1997). Viral infections can trigger NF-κB activation and produce TNFα and IL-1, which in turn may activate NF-κB in a positive regulatory loop (Barnes and Karin, 1997). This positive feedback mechanism may amplify and perpetuate local inflammatory reactions. To understand the basis for PEDV suppression of early proinflammatory cytokines, we first examined whether PEDV induced the NF-κB nuclear translocation. LLC-PK1 cells were infected with PEDV and treated with TNFα, followed by co-staining with anti-p65 mAb and anti-PEDV N mAb. Without TNFα treatment, p65 remained in the cytoplasm as anticipated. When stimulated with TNFα, however, p65 was translocated to the nucleus in uninfected cells (Fig. 3.3A, white arrows). Interestingly in PEDV-infected cells, p65 remained in the cytoplasm, and even after stimulation with TNFα, p65 was not translocated to the nucleus and remained in the cytoplasm in virus-infected cells (Fig. 3.3A, yellow arrows), indicating that

NF-κB activation by TNFα was inhibited by PEDV. Only a minimal fraction of PEDV-infected cells showed p65 in the nucleus at late infection. The ratios for p65 nuclear translocation were quantified in PEDV-infected cells (Fig. 3.3B). PEDV did not induce p65 nuclear translocation through 12 hpi, and only approximately 4% of PEDV-infected cells showed p65 in the nucleus at 18-24 hpi in the absence of TNFα stimulation. The suppression of p65 in PEDV-infected cells after TNFα stimulation was proportional to viral replication with the peak at 10 hpi followed by a gradual decrease. This result indicates that PEDV suppresses early NF-κB activation. Two other cell types permissive for PEDV were examined for p65 nuclear translocation. Similar to LLC-PK1, both MARC-145 and ST cells showed the lack of p65 nuclear translocation when infected with PEDV and stimulated with TNFα (data not shown), indicating that the PEDV-mediated NF-κB suppression was cell type-independent. The p65 phosphorylation remained unchanged at the basal level in PEDV-infected cells throughout the infection (data not shown), which further confirms the cell-type independent suppression of NF-κB by PEDV.

3.4.4 Identification of PRD II and NF-κB antagonists for PEDV

Once IRF3/7 and NF-κB translocate to the nucleus, they bind to their respective PRD domains for expression of type I IFNs. Activated IRF3/7 binds to PRD I/III element in the nucleus, whereas NF-κB binds to the PRD II element for IFN gene expression. Evidence shows that type I IFN suppression by PEDV is mediated through the IRF3/7 singling pathways (Cao et al., 2015a; Xing et al., 2013; Zhang et al., 2016). To examine whether PEDV inhibited PRD II, luciferase assays were performed. It was apparent that the PRD II activity was suppressed even when stimulated with poly(I:C) in PEDV-infected cells (Fig. 3.4A), demonstrating the significant inhibition of NF-κB-mediated IFN production by PEDV. We previously identified ten different

PEDV proteins as IFN antagonists (Zhang et al., 2016), and these proteins suppressed the PRD I/III activity. Thus to identify PRD II antagonists among the ten viral protein, PRD II luciferase assays were conducted for these proteins. PRRSV nsp1α (P-nsp1α) is known to inhibit PRD II and included as a positive control, and its cysteine mutant P-nsp1α(m) (C28S) was included as a negative control (Han et al., 2013; Song et al., 2010). Upon stimulation, PRD II-dependent luciferase activities were reduced in cells expressing nsp1, nsp3, nsp14, nsp15, ORF3, E, and N protein, compared to those of pXJ41 empty vector- and GST gene-transfected cells (Fig. 3.4B). These results indicate that NF-κB-mediated type I IFNs suppression also participate in type I IFN suppression by these viral proteins.

In uninfected cells, NF-κB was activated up to 150 folds by TNFα stimulation (Fig. 3.5A). In PEDV-infected cells, however, NF-κB activation was blocked even after TNFα stimulation (Fig. 3.5A), suggesting a possible suppression of proinflammatory cytokines, in addition to the suppression of type I IFNs, by PEDV at early time of infection. It was of interest to first identify viral proteins inhibiting NF-κB, and therefore individual PEDV genes were examined. As anticipated, TNFα upregulated NF-κB in cells expressing GST and P-nsp1α (m), whereas P-nsp1α suppressed the NF-κB activity (Fig. 3.5B). Of nsps of PEDV, nsp1, nsp3, nsp5, nsp7, nsp14, nsp15 and nsp16 appeared to downregulate the NF-κB activity, and similarly, the ORF3 protein also downregulated NF-κB (Fig. 3.5B). Of structural proteins, only E protein was found to suppress the NF-κB activity (Fig. 3.5C). Among all NF-κB antagonists, nsp1 and nsp14 appeared to be the most potent inhibitors.

3.4.5 Suppression of pro-inflammatory cytokines of PEDV nsp1

PEDV nsp1 is a nuclear-cytoplasmic protein and antagonizes type I IFN production by degrading the CREB-binding protein in the nucleus (Zhang et al., 2016). In the present study, PEDV nsp1 also appeared to inhibit the activation of PRD II and NF-κB (Fig. 3.4B and Fig. 3.5B). It seems that nsp1 blocks NF-κB so as to inhibit the production of IFNs and proinflammatory cytokines. Thus, it was of interest to examine whether nsp1 suppressed TNFα expression. PRRSV nsp1β (P-nsp1β) has been shown to suppress TNFα activation by inhibiting NF-κB and Sp1, and PRRSV N (P-N) does not interfere with TNFα activation (Subramaniam et al., 2010), and thus both constructs were included as controls. Similar to P-nsp1β, PEDV nsp1 appeared to suppress the TNFα activation when stimulated with LPS (Fig. 3.6A). Suppression of proinflammatory cytokines by nsp1 was examined by RT-qPCR in nsp1-gene transfected cells, and the results showed that nsp1 significantly suppressed TNFα mRNA transcription (Fig. 3.6B), validating the nsp1 antagonism against TNFα expression. PEDV nsp1 also suppressed the expression of IL-8, CXCL10, MCP-1, and RANTES (Fig. 3.6B), indicating that PEDV nsp1 was able to antagonize TNFα-mediated NF-κB activation and suppressed the proinflammatory cytokines.

3.4.6 Inhibition of IκBα phosphorylation and degradation by PEDV nsp1 and blockage of p65 nuclear transport

Stimulation of cytokine receptors such as those in the TNF receptor superfamily by TNFα or IL-1 leads to activation of the IKK complex (IKKα/β). Activated IKK induces IκBα phosphorylation, resulting in its proteasomal degradation and release of NF-κB for nuclear translocation and subsequent activation of target gene expressions (Napetschnig and Wu, 2013).

The p65 subunit of NF-κB is a key transcription factor for downstream signaling, and in the present study, PEDV appears to inhibit p65 nuclear translocation (Fig. 3.3). To investigate the mechanism of NF-κB suppression by nsp1, nuclear translocation of p65 was first examined in nsp1-expressing cells. Without TNFα stimulation, nsp1, PEDV N, and PRRSV nsp1α did not activate p65, and it remained in the cytoplasm. When the N-expressing cells were stimulated with TNFα, p65 was activated and normally translocated to the nucleus as anticipated (Fig. 3.7A). In contrast, p65 was remained in the cytoplasm in PRRSV nsp1α-expressing control cells and PEDV nsp1-expressing cells after TNFα stimulation, indicating that PEDV nsp1 suppressed the p65 nuclear translocation. Only 10-13% of nsp1-expressing cells showed the p65 in the nucleus, whereas more than 90% of control cells showed p65 in the nucleus after TNFα stimulation (Fig. 3.7B), confirming that PEDV nsp1 blocked p65 nuclear translocation. The cell fractionation study also confirmed the blockage of p65 nuclear translocation in nsp1-expressing cells (Fig. 3.7C).

Activated IKKβ phosphorylates IκBα for its degradation via ubiquitination. To examine whether nsp1-mediated NF-κB suppression was due to the prevention of IκBα phosphorylation and subsequent degradation, IκBα phosphorylation was examined by Western blot. In contrast to cells transfected with the empty vector, phosphorylation of IκBα was reduced, and the amount of IκBα was stable in nsp1-expressing cells as well as in PRRSV nsp1α-expressing control cells when treated with TNFα (Fig. 3.7D). This result demonstrates that nsp1 inhibited the IκBα phosphorylation. Similar to PRRSV nsp1α, the densitometric analysis for p-IkBα showed the significant inhibition of IκBα phosphorylation by nsp1 after TNFα treatment for 5 min (Fig. 3.7E). The level of IκBα phosphorylation was further decreased by the increasing amount of nsp1 (Fig. 3.7F), suggesting that the suppression of IκBα phosphorylation by nsp1 was dose-

dependent. TNFα caused the IκBα phosphorylation, but no phosphorylation of IκBα was observed in PEDV-infected cells (Fig. 3.7G), which confirmed that nsp1 suppressed IκBα phosphorylation. To examine whether nsp1 interferes with IKK activation, nsp1-expressing cells were stimulated with TNFα, and the IKKα/β phosphorylation was examined. The expression of IKKα/β was stable, and the phosphorylation of IKKα/β normally occurred in nsp1-expressing cells (Fig. 3.7H). The inhibition of IκBα phosphorylation and degradation was also observed (Fig. 3.7H) and the densitometric analysis also showed this inhibition (Fig. 3.7I). This indicates that the inhibition by nsp1 takes place between steps of IKK and IκBα in the NF-κB signaling. Together, our data demonstrate that PEDV nsp1 interferes with the IκBα phosphorylation and degradation, resulting in the inhibition of p65 nuclear translocation.

3.4.7 The highly conserved residues of nsp1 are crucial for NF-κB suppression

Coronavirus nsp1 is the N-terminal cleavage product of the polyproteins pp1a and pp1ab and is one of the most divergent proteins among the four different genera in the *Coronaviridae* family (Ziebuhr, 2005). Nsp1 proteins of α-CoV are similar in their lengths and thus may share some functions (Narayanan et al., 2015). Similar to PEDV nsp1, transmissible gastroenteritis virus (TGEV) nsp1 also inhibits the IFN-β production (Zhang and Yoo, 2016). Thus, we made structural comparisons of PEDV nsp1 and TGEV nsp1. TGEV nsp1 displayed a six-stranded β-barrel fold with a long α-helix on the rim of the barrel (Fig. 3.8A, left panel; Jansson, 2013), and PEDV nsp1 showed a similar structure, except two missing β-sheets (Fig. 3.8A, right panel), suggesting that PEDV nsp1 may have a unique mechanism for immune modulation. As with TGEV nsp1, the surface of PEDV nsp1 displayed two highly conserved areas. The first area was consisted of four conserved residues D13/E15/N93/N95, and the second area was consisted of

three conserved residues L98/E99/E100. These two areas made up two conserved circles placed on a protruding ridge and were potential surfaces for interaction with a partner molecule. Besides, two highly conserved residues (G38/F39) were connected to the hydrophobic core of PEDV nsp1, whereas G87 was highly conserved. We hypothesized that the change of the conserved residues might revert the IFN suppression function of nsp1. To examine this hypothesis, 13 nsp1 mutants were made based on the structural prediction. The mutated genes were individually expressed in cells and examined for their cellular distributions by confocal microscopy. Consistent with the previous report (Zhang et al., 2016), PEDV nsp1 appeared as a nuclear-cytoplasmic protein (Fig. 3.8B). Among the nsp1 mutants, T23A, T68A, K70A, T68A/K70A, and L101A remained nuclear-cytoplasmic. G38A/F39A, F44A, G87A, G87E, L98A/E99A/E100A, and the deletion mutant Δ37-75 exhibited nuclear punctate patterns. N93A/N95A was perinuclear whereas Δ37-51 became cytoplasmic, suggesting the deletion region was crucial for nuclear localization of nsp1. The results indicated that the highly conserved residues are crucial to maintain the higher order structure of nsp1. To determine the crucial residues for nsp1-mediated IFN suppression, luciferase assays for NF-κB and IFN-β were performed for individual mutants. While T23A, T68A, G87A, K70A, T68A/K70A, and L101A still retained the function of NF-κB suppression (Fig. 3.8C), G38A/F39A, F44A, G87E, N93A/N95A, L98A/E99A/E100A, and Δ37-75 lost the NF-κB suppression, indicating that the conserved residues in nsp1 are crucial for NF-κB suppression. The deletion mutant Δ37-51 retained NF-κB inhibition, further confirming that the suppression of NF-κB is a cytoplasmic event. N93A/N95A and L98A/E99A/E100A did not suppress the IFN-β production (Fig. 3.8D), indicating that the conserved residues are also crucial for type I IFN suppression. Unlike the NF-κB suppression, T23A, T68A, T68A/K70A, and G87A lost the IFN suppression function. Additionally, Δ37-51 was cytoplasmic and lost the IFN

suppression function, confirming that the IFN suppression by nsp1 is a nuclear event (Zhang et al., 2016). Our study indicates that the suppression of innate immune responses by PEDV nsp1 relies on its highly conserved residues.

3.5 DISCUSSION

The innate immune system forms the first line of antiviral defense of a host. It activates the production of type I IFNs and proinflammatory cytokines controlled by IRF3/IRF7 and NF-κB. Many viruses have evolved to counteract the host innate immunity for optimal viral adaptation and replication. Studies have shown that PEDV inhibits type I IFN production in virus-infected cells. Of 22 PEDV proteins, ten proteins appear to suppress the IFN production. The nsp1 protein antagonizes the IRF3 signaling by degrading CBP in the nucleus via the proteasome-dependent pathway (Zhang et al., 2016), and the nsp5 protein antagonizes NF-κB to suppress type I IFN production by cleaving NEMO (Wang et al., 2015a). The N protein suppresses IRF3 and NF-κB and inhibits IFN-β production (Ding et al., 2014). PEDV infection leads to activation of NF-κB at later times post-infection (Cao et al., 2015b; Xing et al., 2013). However, the basis for temporal regulation of NF-κB for the production of type I IFNs and proinflammatory cytokines is unknown. In the present study, we show that PEDV blocks TNFα-mediated p65 nuclear translocation and have subsequently identified nine NF-κB antagonists. Among these, nsp1 is the most potent NF-κB inhibitor, which blocks the p65 nuclear translocation by inhibiting the phosphorylation and degradation of IκBα.

Both coronaviruses and arteriviruses in the order *Nidovirales* are sensitive to type I IFNs and modulate the IFN response. Equine arteritis virus (EAV) inhibits type I IFN production in virus-infected equine endothelial cells (Go et al., 2014). Porcine reproductive and respiratory

syndrome virus (PRRSV) is also sensitive to type I IFNs and modulate the IFN production in cells and pigs (Albina et al., 1998; Lee et al., 2004; Overend et al., 2007). Mouse hepatitis coronavirus (MHV) induces extremely low levels of type I IFNs in macrophages, microglia, and oligodendrocytes of infected mice (Li et al., 2010; Roth-Cross et al., 2008; Zhou and Perlman, 2007). SARS-CoV and MERS-CoV also do not induce type I IFN responses in virus-infected cells (Cinatl et al., 2004; Lau et al., 2013; Zhou et al., 2014). TGEV can induce a high level of IFN-α in newborn pigs (La Bonnardiere and Laude, 1981). However, the IFN expression is delayed and the IFN response inhibits TGEV replication in the early stage of infection (Zhu et al., 2017). Protein 7 and nsp1 of TGEV have been shown to counteract the host antiviral response (Cruz et al., 2013; Cruz et al., 2011; Zhang and Yoo, 2016). Viruses often code for multiple IFN antagonists, and PEDV also encodes at least 10 IFN antagonists (Cao et al., 2015a; Xing et al., 2013; Zhang et al., 2016). Activated NF-κB binds to PRD II in the nucleus, which is essential for NF-κB-mediated IFN-β production. The p65 subunit of NF-κB specifically functions as a key element for early phase IFN production after infection. The PEDV N protein inhibits NF-κB (Ding et al., 2014), suggesting that the NF-κB inhibition may lead to the suppression of type I IFNs. In the present study, we have shown that PEDV blocks NF-κB activation and suppresses NF-κB-mediated type I IFN production. Of the ten IFN suppressors, nsp7, nsp16, and M do not interfere with PRD II, suggesting the specific target of IRF3/7. Thus, targeting PRD II via NF-κB and PRD I/III via IRF3/7 results in synergistic effects on the viral IFN antagonism to allow efficient replication of the invading virus.

The p65 subunit of NF-κB undergoes various post-translational modifications for activation. Not only for type I IFN induction, but NF-κB is also a key regulator for proinflammatory cytokines including TNFα, IL-6, and IL-8 (Lappas et al., 2002).

Proinflammatory cytokines initiate inflammation and disease progression during viral infection. IL-12 plays a critical role in the early inflammatory response and the generation of Th1 cells leading to cell-mediated immunity (Hsieh et al., 1993). Activation of NF-κB is critical for host defense and thus occurs rapidly after stimulation without additional protein translation. In turn, NF-κB is an attractive viral target for optimal replication during infection. For SARS-CoV, N protein activates NF-κB (Liao et al., 2005), whereas M protein suppresses NF-κB probably through a direct interaction with IKKβ (Fang et al., 2007). PEDV has also been shown to activate NF-κB later time post-infection (Cao et al., 2015b; Xing et al., 2013), and the N protein is the NF-κB activator for up-regulation of IL-8 and Bcl-2 (Xu et al., 2013b). The basis for PEDV-mediated NF-κB modulation remains uncharacterized. We show in the present study that PEDV blocks the NF-κB activation and suppresses the production of early proinflammatory cytokines. The PEDV replication cycle is less than 12 h (Fig. 3.1D), and the inhibition of NF-κB during the early stage of infection may play a role to help viral replication. Nine viral proteins have been identified to regulate NF-κB, and it is of interest to study their individual mode of action for NF-κB.

For activation of NF-κB, the release of IκBα from NF-κB is crucial. In the latent state, NF-κB is sequestered in the cytosol by IκBα. In response to stimulation by TNFα or IL-1, a series of membrane-proximal events lead to activation of the IKK complex (IKKα/β/γ). The IKK complex is responsible for the phosphorylation of two serine residues in IκBα, which in turn leads to Lys48-linked polyubiquitination and degradation by the proteasome. Proteasomal degradation of IκBα frees and translocates NF-κB to the nucleus for binding to the κB DNA element in the specific promoters and enhancers of target genes (Napetschnig and Wu, 2013). Viruses have evolved to develop sophisticated strategies to modulate NF-κB signaling, and

ample examples are available. PRRSV nsp1α inhibits IκBα phosphorylation and degradation for suppression of type I IFNs (Song et al., 2010). Bocavirus NS1 and NS1-70 protein blocks the binding of p65 to the κB DNA element and inhibits TNFα-mediated activation of NF-κB (Liu et al., 2016). Molluscum contagiosum poxvirus (MCV) MC160 protein degrades IKKα and prevents TNFα-induced NF-κB activation (Le Negrate, 2012). Influenza virus NS1 protein specifically interacts with IKKα and IKKβ for inhibition of IKKβ-mediated phosphorylation and degradation of IκBα (Gao et al., 2012).

PEDV nsp1 inhibits the phosphorylation and subsequent degradation of IκBα and blocks p65 from nuclear translocation. PEDV nsp1 does not interfere the phosphorylation of IKKα/β complex (Fig. 3.7H) nor interact with IκBα or IKKα/β (data not shown), suggesting a possible modulation of posttranslational modifications of IκBα such as SUMOylation. Unlike ubiquitination and degradation of IκBα, SUMOylation of IκBα inhibits NF-κB activation (Desterro et al., 1998). Breast cancer-associated gene 2 (BCA2) functions as an E3 SUMO-ligase and enhances the SUMOylation of IκBα, leading to improved sequestration of NF-κB in the cytoplasm, thereby preventing the expression of NF-κB-responsive genes (Colomer-Lluch and Serra-Moreno, 2017). It is of interest to examine whether PEDV nsp1 recruits an E3 SUMO-ligase and enhances SUMOylation of IκBα.

In coronaviruses, nsp1 proteins of α-CoV and β-CoV are potent IFN antagonists. The β-CoV nsp1 protein regulates cellular and viral gene expressions. SARS-CoV nsp1 is consisted of 180 amino acids and inhibits the translation of capped cellular mRNAs by blocking the formation of the 80S complex. It also recruits a cellular endonuclease to induce an endonucleolytic cleavage of host mRNAs (Narayanan et al., 2015). Unlike SARS-CoV nsp1, MERS-CoV nsp1 selectively targets host mRNAs for translation inhibition and mRNA

degradation but spares mRNAs of cytoplasmic origin (Lokugamage et al., 2015). The α-CoV nsp1 protein also inhibits the expression of reporter genes. The C-terminal portion of β-CoV nsp1 is crucial for host mRNA cleavage, and this region is lost in α-CoV nsp1, suggesting that α-CoV nsp1 may have evolved a distinct mechanism for immune evasion. Unlike SARS-CoV nsp1, TGEV nsp1 does not bind to the 40S ribosomal subunit for suppression of host gene expression (Huang et al., 2011a). Surface electrostatics, shapes, and amino acid conservations between α-CoV nsp1 and β-CoV nsp1 may contribute to different mechanisms for nsp1-induced suppression of host gene expression (Jansson, 2013). The structure of TGEV nsp1 is characterized by an irregular six-stranded β-barrel flanked by an α-helix. Most conserved residues are centered on the highly conserved β7 strand, which is likely involved in its structural stability. Two highly conserved patches on the surface of TGEV nsp1 are placed on a producing ridge formation, which forms potential sites for interaction with cellular proteins (Jansson, 2013). PEDV nsp1 also shows two highly conserved surface patches, and mutations of these regions alter their cellular distributions and functions for IFN and NF-κB suppressions. It is of interest to identify the cellular proteins that may interact with PEDV nsp1. The PEDV full-length infectious clone is available (Beall et al., 2016; Jengarn et al., 2015) and it will be useful to study nsp1 function in pigs using replicating mutant viruses.

In conclusion, we have shown that PEDV inhibits NF-κB activity and early production of proinflammatory cytokines. PEDV modulates TNFα-mediated p65 nuclear localization, and we have identified nine viral NF-κB antagonists. PEDV nsp1 interferes the phosphorylation and degradation of IκBα and blocks NF-κB activation. The conserved residues of nsp1 are crucial for nsp1-mediated NF-κB activity. Our study provides a better understanding for PEDV-mediated innate immune modulation and the basis for PEDV pathogenesis.

3.6 FIGURES AND TABLES

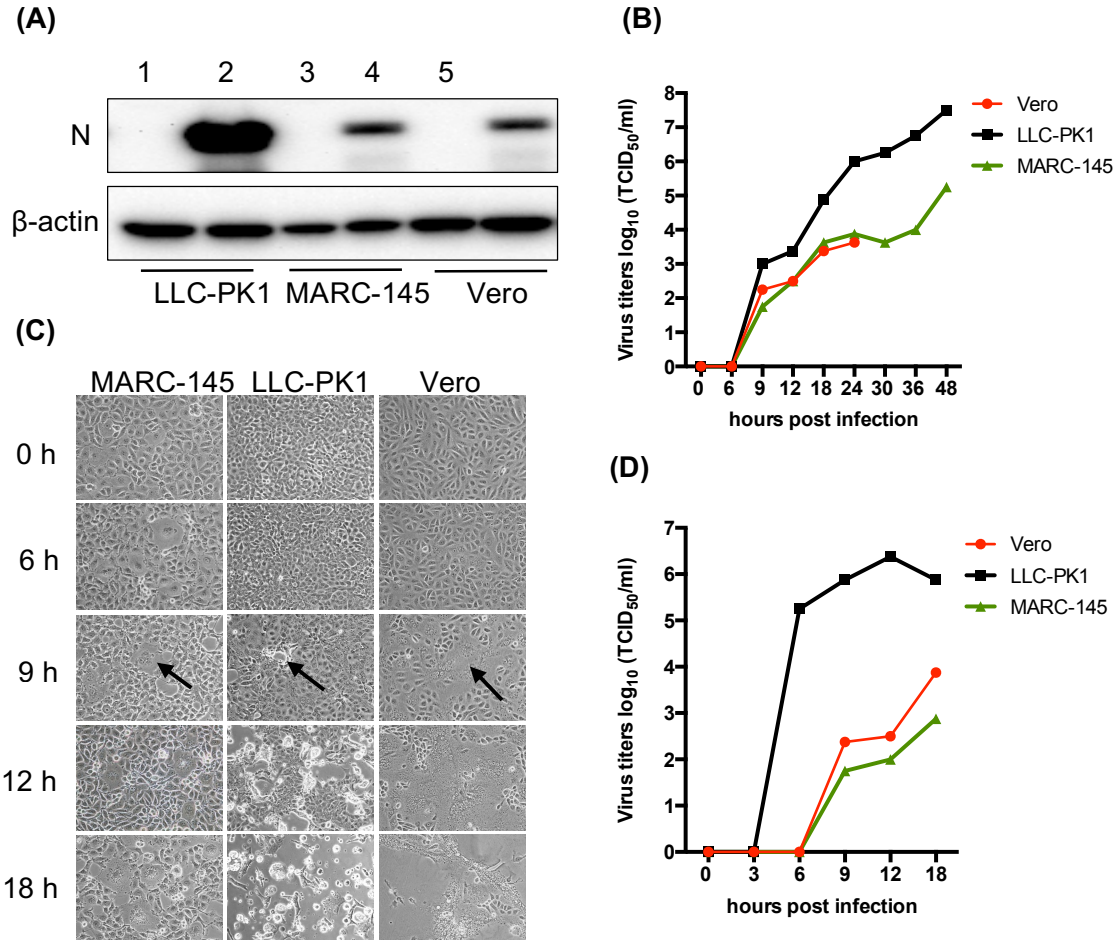

Fig. 3.1: Suppression of type I IFN production in LLC-PK cells by PEDV. (A), Expression of N protein in PEDV-infected cells. Cells were infected with PEDV at an MOI of 0.01 for 24 h, and Western blot was conducted using anti-N mAb. (B), multistep growth kinetics of PEDV in different lines of cells. MARC-145, Vero, and LLC-PK1 cells were infected with PEDV at an MOI of 0.01 and cell culture supernatants were collected at different times. Viral titers were determined in respective cells by the 50% tissue culture infectious dose ($TCID_{50}$) protocol. (C), Cytopathic effects (CPE) of PEDV on different types of cells. Cells were infected with PEDV at an MOI of 5 and CPE was observed at different times. Arrows show multinucleated cells. (D), One step growth curve of PEDV. Cells were infected with PEDV at an MOI of 5, and culture supernatants were collected at indicated times to determine $TCID_{50}$. (E) and (F), Suppression of type I IFN production by PEDV. LLC-PK1 cells were grown in 12-well plates and infected with PEDV either at a low MOI (0.01 MOI, panel E) or a high MOI (5 MOI, panel F). Cells were harvested at indicated times, and expressions of IFN-α and IFN-β were determined by RT-qPCR. Cells stimulated with poly(I:C) for 12 h were used as positive controls. (G) and (H), Stimulation for type I IFN production by poly(I:C) and suppression by PEDV. LLC-PK1 cells were infected with PEDV at an MOI of 0.01 for 12 h, and stimulated with poly(I:C) for 12 h. Cells were harvested and expression of IFN-α (G) and IFN-β (H) were determined by RT-qPCR.

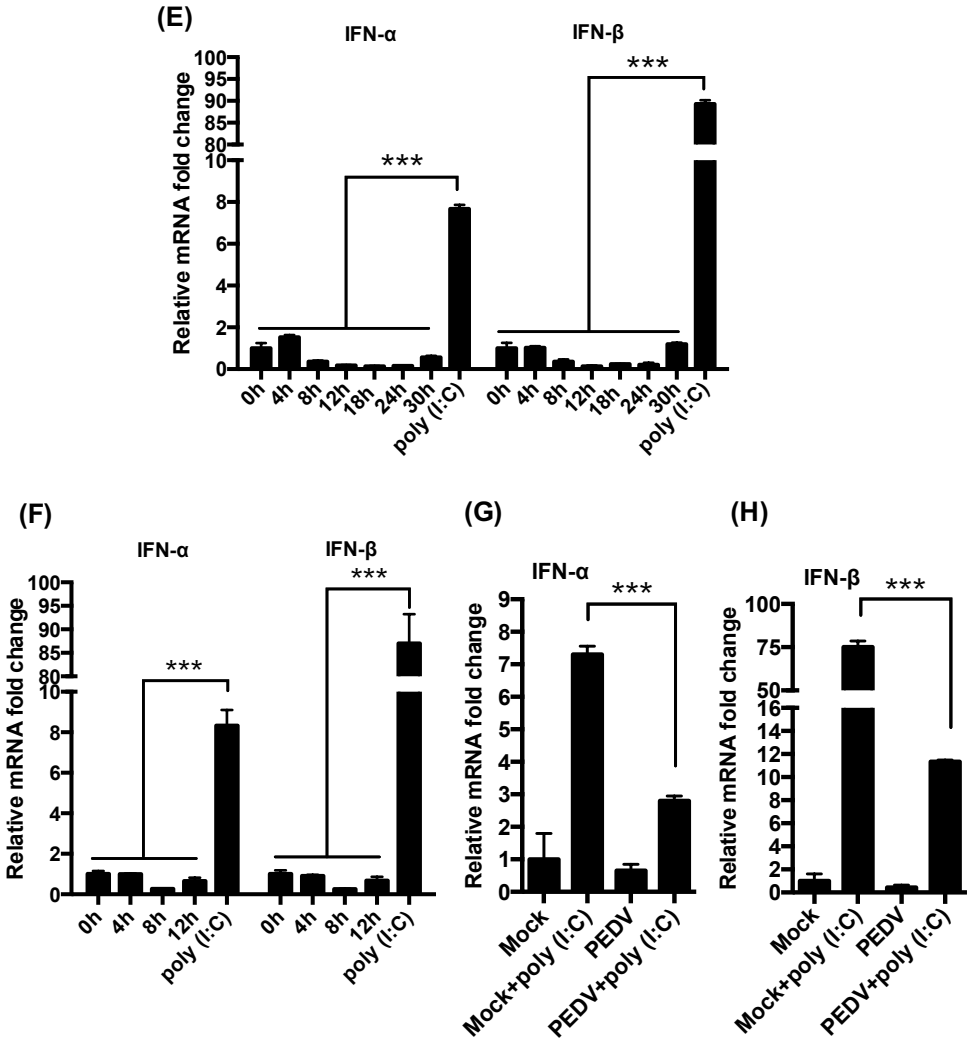
(E)
IFN-α
IFN-β
Relative mRNA fold change
***
***
0h 4h 8h 12h 18h 24h 30h poly (I:C)
(F)
IFN-α
IFN-β
***
***
0h 4h 8h 12h poly (I:C)
(G)
IFN-α
***
Relative mRNA fold change
Mock
Mock+poly (I:C)
PEDV
PEDV+poly (I:C)
(H)
IFN-β
***
Relative mRNA fold change
Mock
Mock+poly (I:C)
PEDV
PEDV+poly (I:C)

Fig. 3.1 (cont.)

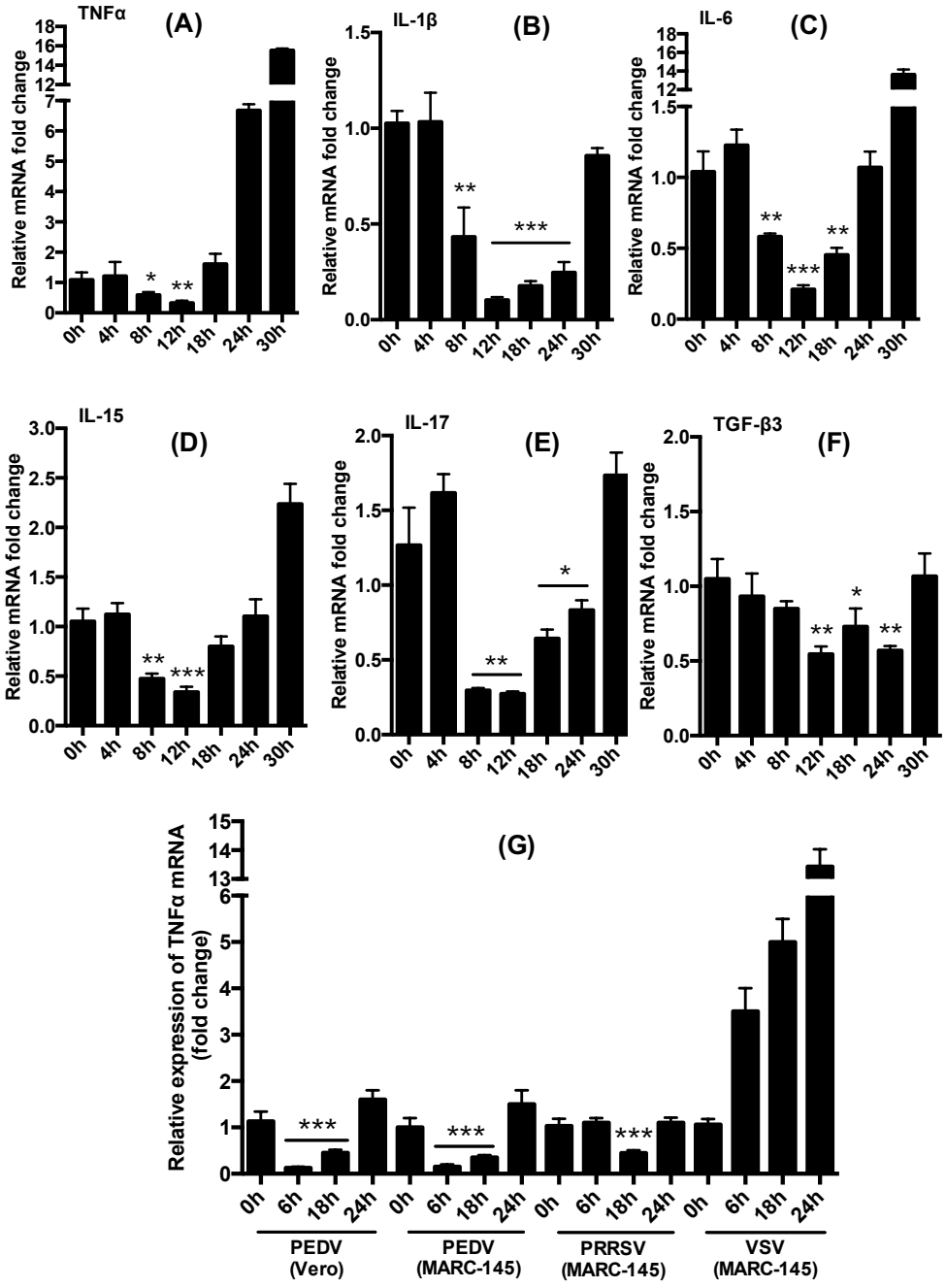

Fig. 3.2: Inhibition of early production of proinflammatory cytokines by PEDV. (A) through (F), Inhibition of pro-inflammatory cytokines at early times of infection. LLC-PK1 cells were infected with PEDV at an MOI of 0.01 and cells were harvested at indicated times for expression of pro-inflammatory cytokines by RT-qPCR. (G), Inhibition of the induction of TNFα by PEDV in Vero and MARC-145 cells. Cells were infected with PEDV at an MOI of 1 for indicated times and the production of TNFα was determined by RT-qPCR. PRRSV as a known inhibitor of TNFα and VSV as a known stimulator were included as controls. Asterisks indicate statistical significance calculated by the Student's *t* test. *, $P<0.05$; **, $P<0.01$; ***, $P<0.001$.

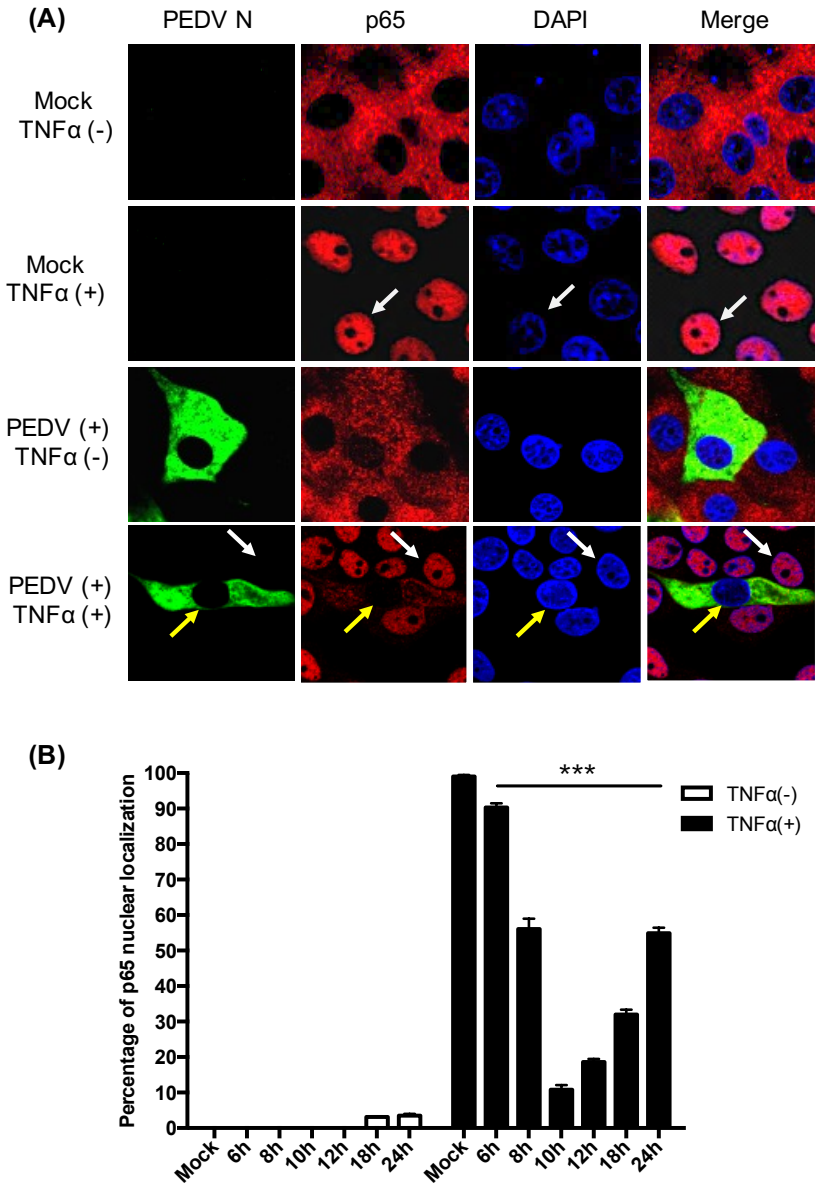

Fig. 3.3: PEDV-mediated inhibition of TNFα-stimulated p65 nuclear translocation. (A), Inhibition of TNFα-stimulated p65 nuclear localization by PEDV. LLC-PK1 cells were infected with PEDV for 12 h and stimulated with TNFα as the concentration of 15 ng/ml for 20 min. Cells were fixed and stained with anti-N antibody and anti-p65 antibody. White arrows indicate the non-infected cells, yellow arrows indicate the PEDV-infected cells. (B), LLC-PK1 cells were infected with PEDV and stimulated with TNFα at different times. Percentages of cells showing p65 nuclear localization were quantified by randomly counting 200 PEDV-infected cells. The data were obtained from three independent experiments. Asterisks indicate statistical significance calculated by the Student's *t* test. *, $P<0.05$; **, $P<0.01$; ***, $P<0.001$.

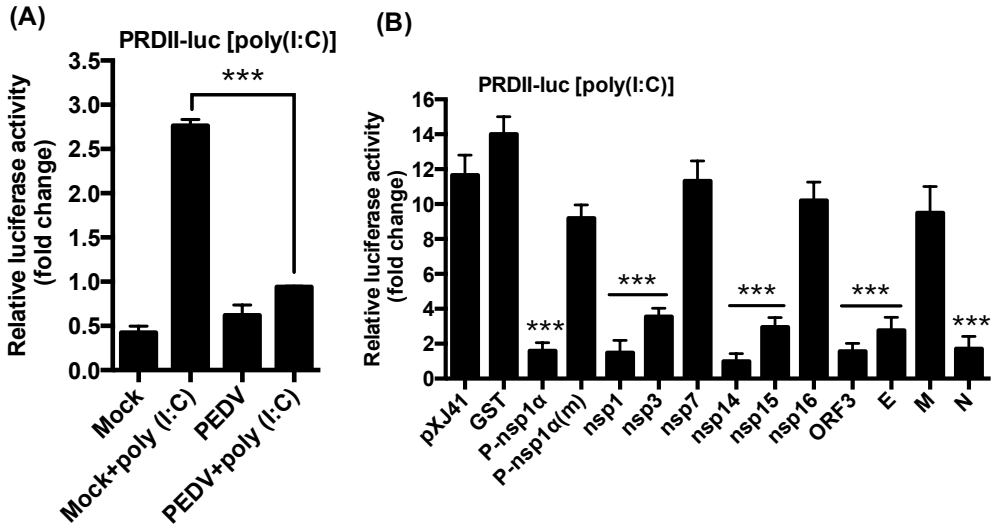

Fig. 3.4: Inhibition of NF-κB-mediated IFN production by PEDV. (A), Inhibition of PRD II promoter by PEDV. MARC-145 cells were co-transfected with the pPRD II-Luc reporter plasmid along with the pRL-TK internal control for 6 h followed by PEDV infection at an MOI of 1 for 12 h. Cells were then stimulated with poly(I:C) for 12 h, and cell lysates were subjected to dual-luciferase reporter assays. Results from three independent experiments were presented as the mean relative luciferase values. Asterisks indicate statistical significance calculated by the Student's *t* test. *, $P<0.05$; **, $P<0.01$; ***, $P<0.001$. (B), Inhibition of PRD II promoter by PEDV proteins. HeLa cells were co-transfected with the pPRD II-Luc reporter along with individual type I IFN antagonist for PEDV followed by stimulation with poly(I:C). Cell lysates were prepared and subjected to luciferase assays. PRRSV nsp1α (P-nsp1α) is known to inhibit the PRD II promoter and was included as a positive control. Its mutant P-nsp1α(m) (C28S) was included as a negative control (Han et al., 2013; Song et al., 2010). Results from three independent experiments were presented as the mean relative luciferase values with standard deviation. Asterisks indicate statistical significance calculated by the Student's *t* test. *, $P<0.05$; **, $P<0.01$; ***, $P<0.001$.

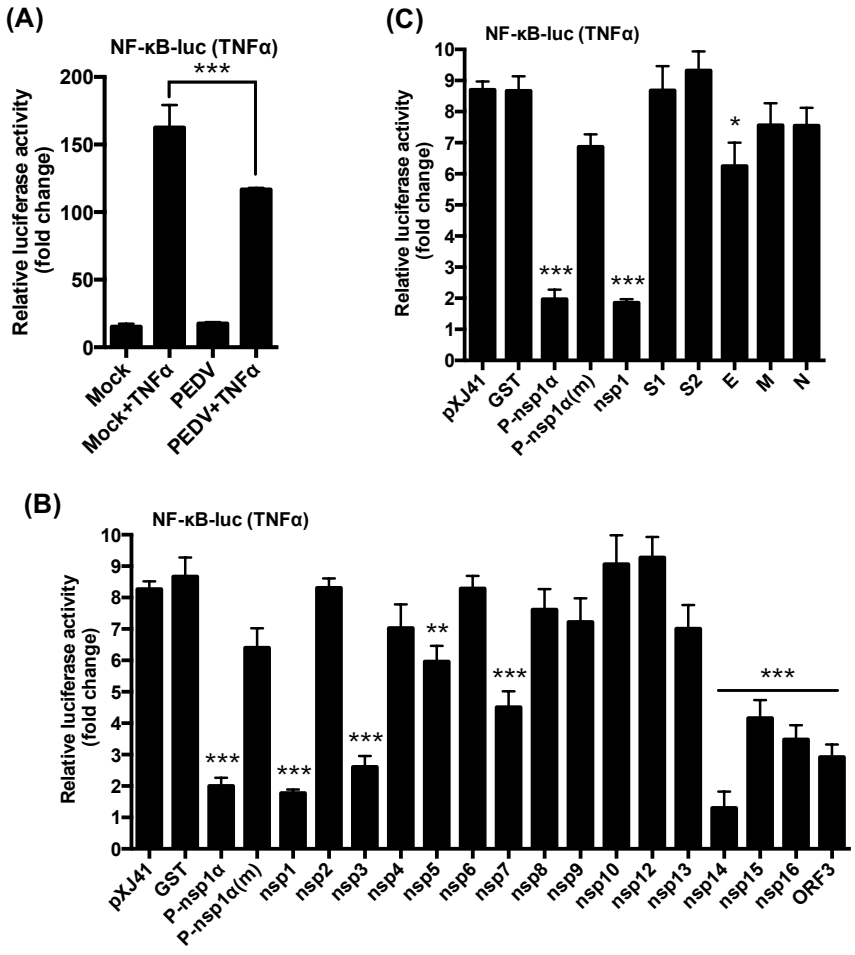

Fig. 3.5: Identification of NF-κB antagonists of PEDV. (A), Suppression of TNFα-stimulated NF-κB activity by PEDV. MARC-145 cells were co-transfected with pNF-κB-Luc along with pRL-TK in 12-well plates for 6 h followed by PEDV infection at an MOI of 1 for 12 h. Cells were then stimulated with TNFα at the concentration of 15 ng/ml for 9 h, and cell lysates were prepared for dual-luciferase reporter assays. Results from three independent experiments were presented as the mean relative luciferase values with standard deviation. Asterisks indicate statistical significance calculated by the Student's *t* test. *, $P<0.05$; **, $P<0.01$; ***, $P<0.001$. (B) and (C), Regulation of TNFα-induced NF-κB activity by individual PEDV proteins. HeLa cells were grown in 48-well plates and co-transfected with pNF-κB-Luc along with individual PEDV genes and pRL-TK at a ratio of 10:10:1. For nsp3, nsp5, and nsp16, transfection was conducted as described previously (Zhang et al., 2016). PRRSV nsp1α (P-nsp1α) is a known NF-κB promoter suppressor, and its mutant P-nsp1α(m) reverts its suppressive function. Both constructs were included as controls. Cells were stimulated with poly(I:C) (0.5μg/ml) at 12 h post-transfection for 12 h and dual luciferase activities were determined. Results from three independent experiments were presented as the mean relative luciferase values with standard deviation. Asterisks indicate statistical significance calculated by the Student's *t* test using GST as a control. *, $P<0.05$; **, $P<0.01$; ***, $P<0.001$.

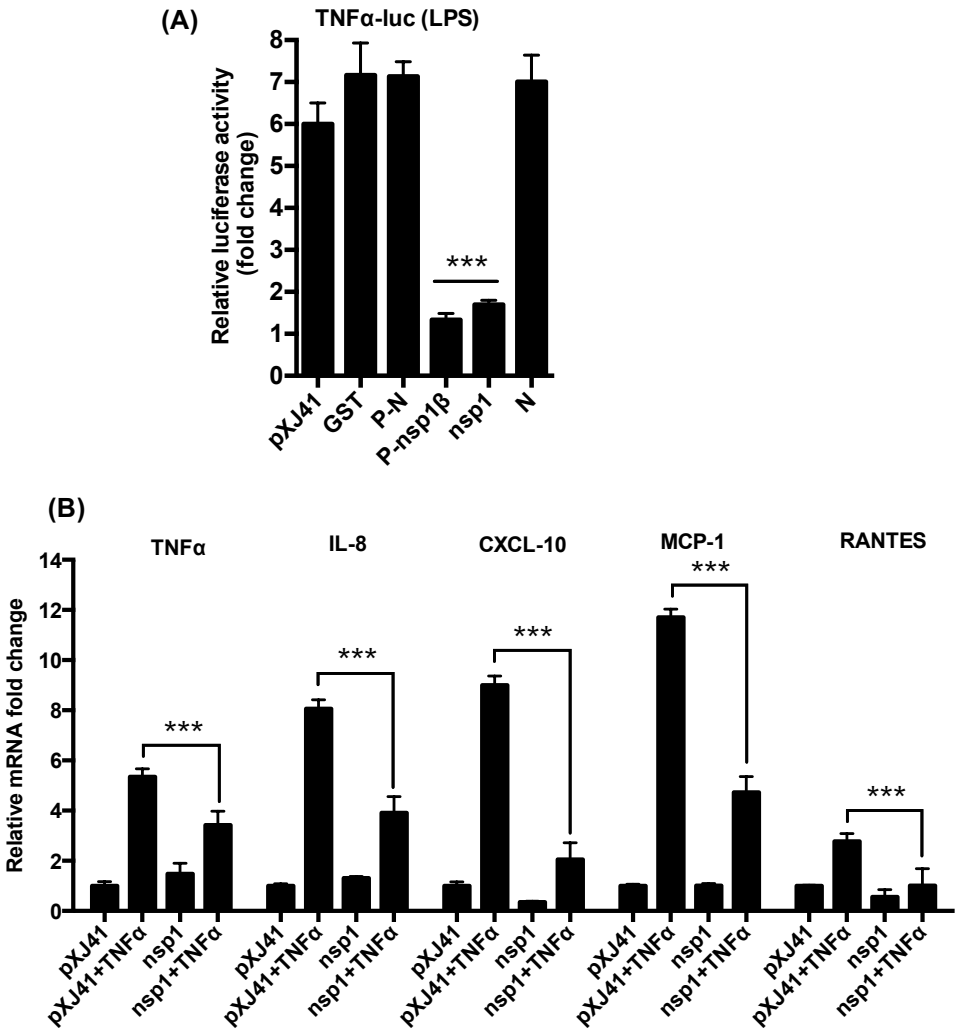

Fig. 3.6: Suppression of proinflammatory cytokines by PEDV nsp1. (A), Suppression of TNFα promoter by nsp1. RAW cells were co-transfected with pswTNFα-Luc and individual viral genes along with pRL-TK for 24 h followed by stimulation with LPS (1 μg/ml) for 6 h. Firefly luciferase activities were determined and normalized using the *Renilla* luciferase internal control. PRRSV nsp1β (P-nsp1β) is known to suppress TNFα promoter and was included as a control (Subramaniam et al., 2010). Results from three independent experiments were presented as the mean relative luciferase values. Asterisks indicate statistical significance calculated by the Student's *t* test. *, $P<0.05$; **, $P<0.01$; ***, $P<0.001$. (B), Inhibition of proinflammatory cytokines by nsp1. LLC-PK1 cells were transfected with PEDV nsp1 gene for 12 h and stimulated with TNFα (15 ng/ml) and for 12h. Expressions of proinflammatory cytokines were determined by RT-qPCR. Asterisks indicate statistical significance calculated by the Student's *t* test. *, $P<0.05$; **, $P<0.01$; ***, $P<0.001$.

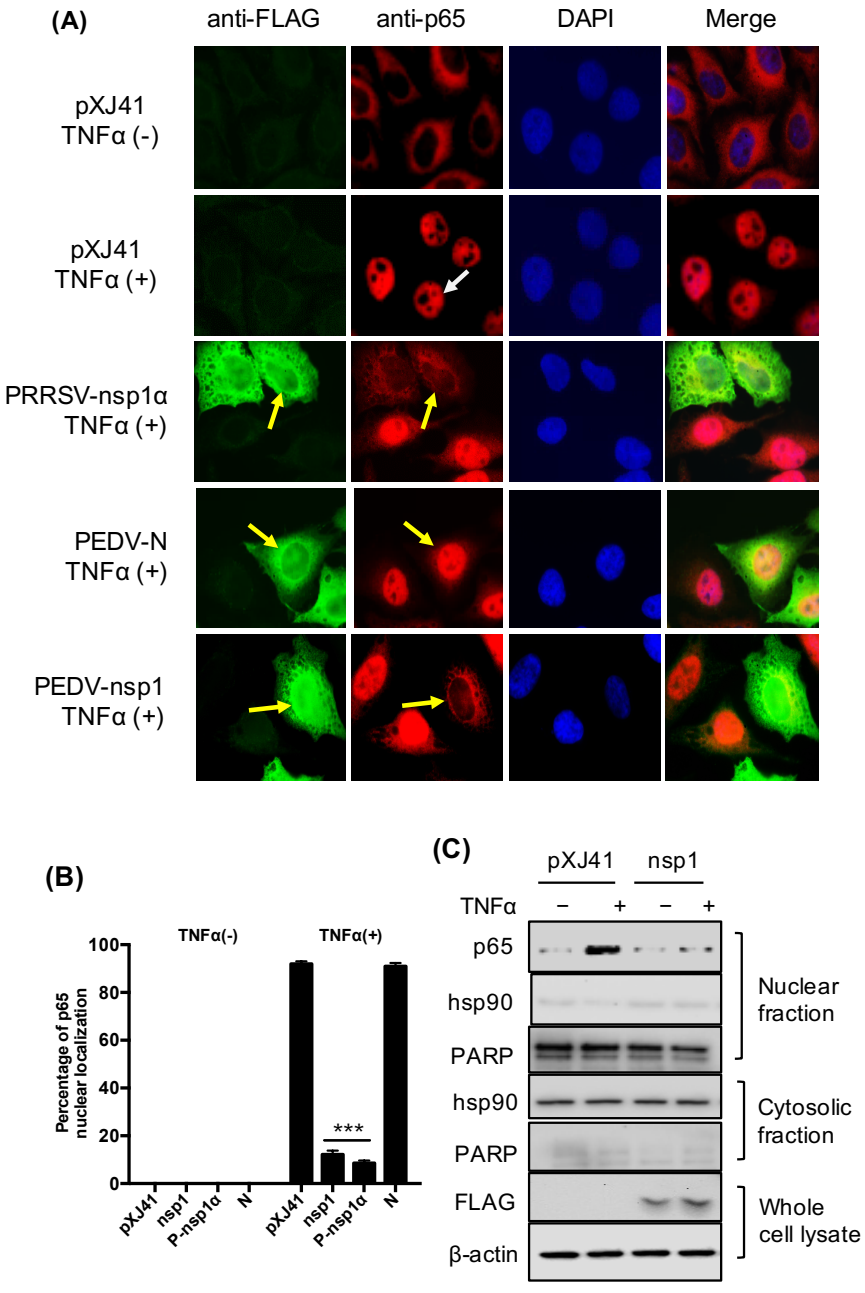
(A)
anti-FLAG
anti-p65
DAPI
Merge
pXJ41
TNFα (-)
pXJ41
TNFα (+)
PRRSV-nsp1α
TNFα (+)
PEDV-N
TNFα (+)
PEDV-nsp1
TNFα (+)
(B)
TNFα(-)
TNFα(+)
Percentage of p65 nuclear localization
100
80
60
40
20
0
***
pXJ41
nsp1
P-nsp1α
N
pXJ41
nsp1
P-nsp1α
N
(C)
pXJ41
nsp1
TNFα
–
+
–
+
p65
hsp90
PARP
hsp90
PARP
FLAG
β-actin
Nuclear fraction
Cytosolic fraction
Whole cell lysate

Fig. 3.7 (cont.)

Fig. 3.7 (cont.): Inhibition of p65 nuclear translocation by nsp1 and inhibition of IκBα phosphorylation. (A) and (B), PEDV nsp1 blocks p65 nuclear translocation. HeLa cells were co-transfected with pXJ41 (empty plasmid), nsp1, N, and PRRSV nsp1α for 24 h followed by stimulation with TNFα (15 ng/ml) for 20 min. Cells were then subjected to immunostaining. PRRSV nsp1α is known to inhibit p65 nuclear translocation and was included as a positive control. White arrows indicate p65 in mock-transfected cells, and yellow arrows indicate p65 in gene-transfected cells (panel A). The percentages of cells showing p65 activation were calculated by examining 200 gene-transfected cells in three independent experiments (panel B). Asterisks indicate statistical significance calculated by the Student's *t* test. *, $P<0.05$; **, $P<0.01$; ***, $P<0.001$. (C), Cell fractionation and Western blot. HeLa cells were transfected with PEDV nsp1 gene for 24 h and then stimulated with TNFα for 12 h. Cells were subjected to nuclear-cytoplasmic fractionation to determine subcellular distribution of p65. Hsp90 is a cytosolic protein and was included as the cytosolic marker and PARP was included as a nuclear protein marker. (D), PEDV nsp1 inhibits IκBα phosphorylation and subsequent degradation. HeLa cells were transfected with PEDV nsp1 gene or PRRSV nsp1α (P-nsp1α) for 24 h and then stimulated with TNFα for indicated times. Cells were lysed and subjected to Western blot using IκBα antibody and phophso-IκBα antibody. P-nsp1α is known to inhibit IκBα phosphorylation and was included as a control. (E) and (I), Inhibition of IκBα phosphorylation by nsp1 by the densitometric analysis using the β-actin as an internal control. 7E corresponds to 7D, and 7I corresponds to 7H. Results from three independent experiments were presented as the mean values with standard deviation. Asterisks indicate statistical significance calculated by the Student's *t* test comparing to the pXJ41 empty-vector-transfected cells. *, $P<0.05$; **, $P<0.01$; ***, $P<0.001$. (F) Inhibition of IκBα phosphorylation by nsp1 is dose-dependent. HeLa cells were transfected with an increasing amount of nsp1 and treated with TNFα for 5 min. Cells were lysed and subjected to Western blot using anti-IκBα and anti-phospho-IκBα antibodies. (G) Inhibition of IκBα phosphorylation by nsp1. LLC-PK1 cells were infected with PEDV at an MOI of 5 and cells were lysed at indicated times, followed by Western blot using anti-IκBα and anti-phospho-IκBα antibodies. Mock-infected cells with the treatment of TNFα for 5 min were used as a control. (H), PEDV nsp1 does not interfere phosphorylation of IKKα/IKKβ. HeLa cells were transfected with PEDV nsp1 gene for 24 h and then stimulated with TNFα for indicated times. Cells were lysed and subjected to Western blot using antibodies for p-IKKα/IKKβ, IKKα, IKKβ, IκBα, and p-IκBα.

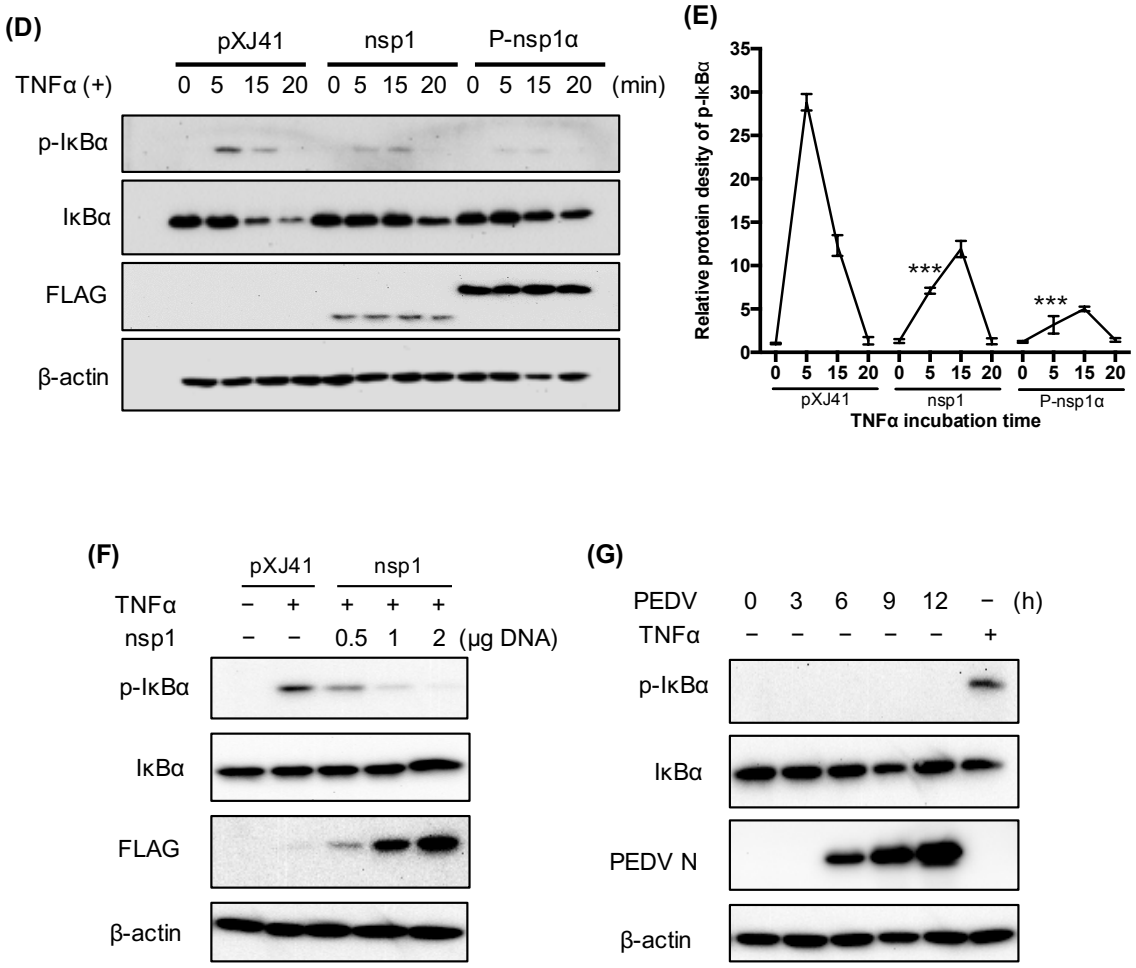
(D)
pXJ41
nsp1
P-nsp1α
TNFα (+)
0 5 15 20 0 5 15 20 0 5 15 20 (min)
p-IκBα
IκBα
FLAG
β-actin
(E)
Relative protein desity of p-IκBα
35
30
25
20
15
10
5
0
***
***
0 5 15 20 0 5 15 20 0 5 15 20
pXJ41
nsp1
P-nsp1α
TNFα incubation time
(F)
pXJ41
nsp1
TNFα − + + + +
nsp1 − − 0.5 1 2 (μg DNA)
p-IκBα
IκBα
FLAG
β-actin
(G)
PEDV 0 3 6 9 12 − (h)
TNFα − − − − − +
p-IκBα
IκBα
PEDV N
β-actin

Fig. 3.7 (cont.)

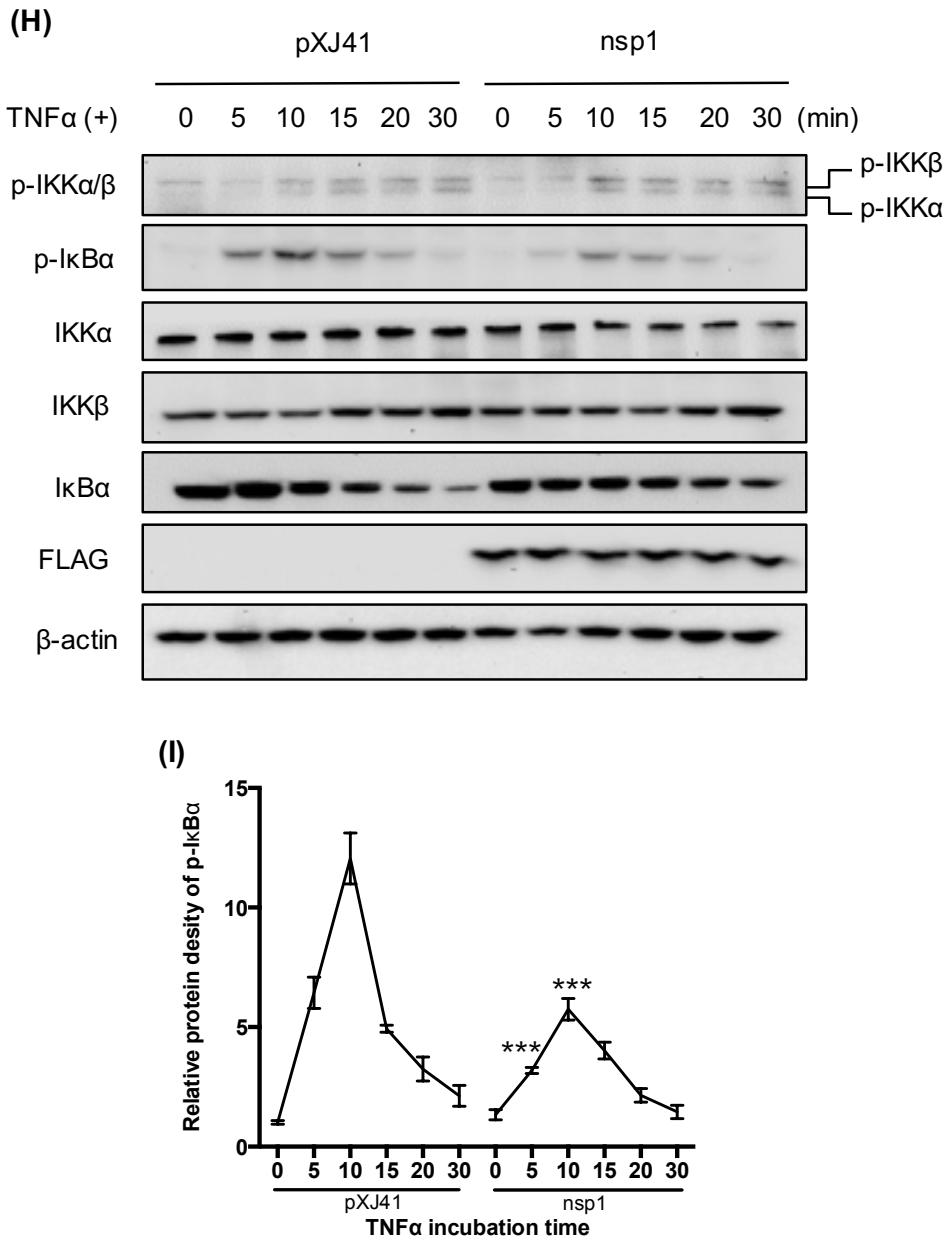
(H)
pXJ41
nsp1
TNFα (+)
0 5 10 15 20 30 0 5 10 15 20 30 (min)
p-IKKα/β
p-IKKβ
p-IKKα
p-IκBα
IKKα
IKKβ
IκBα
FLAG
β-actin
(I)
Relative protein desity of p-IκBα
15
10
5
0
***
***
0 5 10 15 20 30 0 5 10 15 20 30
pXJ41
nsp1
TNFα incubation time

Fig. 3.7 (cont.)

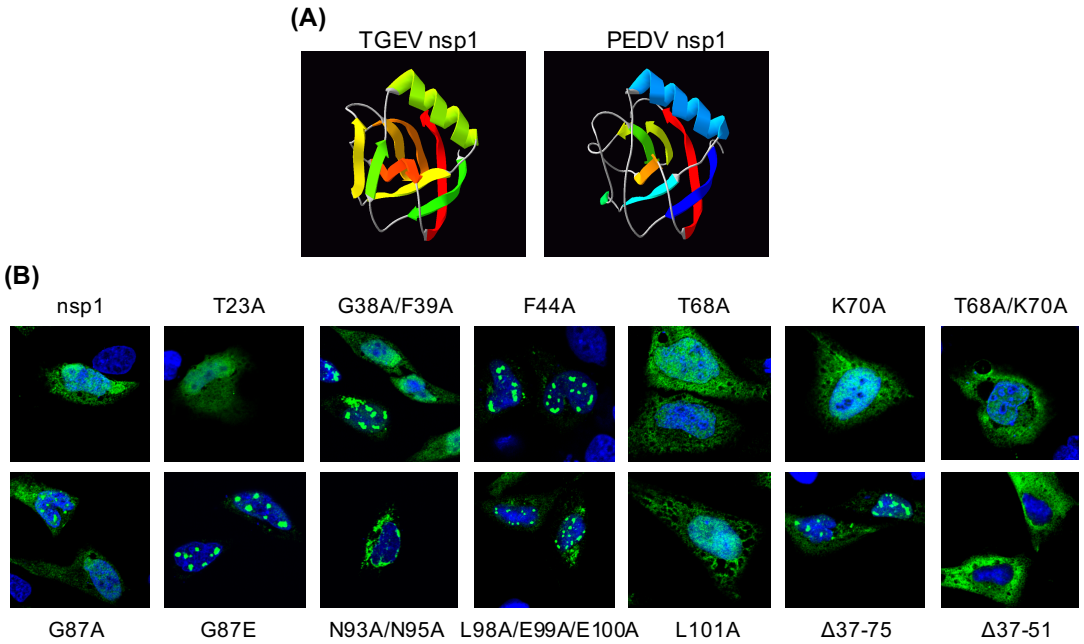

Fig. 3.8: Highly conserved residues of nsp1 are crucial for NF-κB suppression. (A), Predication of higher order structure of PEDV nsp1 based on the TGEV nsp1 structure. (B), Cellular distribution of nsp1 mutants. Nsp1 mutants were expressed individually in HeLa cells followed by immunostaining. Confocal images showed their cellular distributions. (C) through (D), Conserved residues are crucial for nsp1-mediated NF-κB/IFN-β suppression. HeLa cells were grown in 48-well plates and co-transfected with pNF-κB-Luc (panel C) or pIFN-β-Luc (panel D) along with individual PEDV nsp1 mutants and pRL-TK at a ratio of 10:10:1. Cells were stimulated with TNFα (panel C) or poly(I:C) (panel D) at 12 h post-transfection for 12 h, and cell lysates were subjected to dual-luciferase reporter assays. Results from three independent experiments are presented as the mean relative luciferase values with standard deviation. Asterisks indicate statistical significance calculated by the Student's *t* test using nsp1 as a control. *, $P<0.05$; **, $P<0.01$; ***, $P<0.001$.

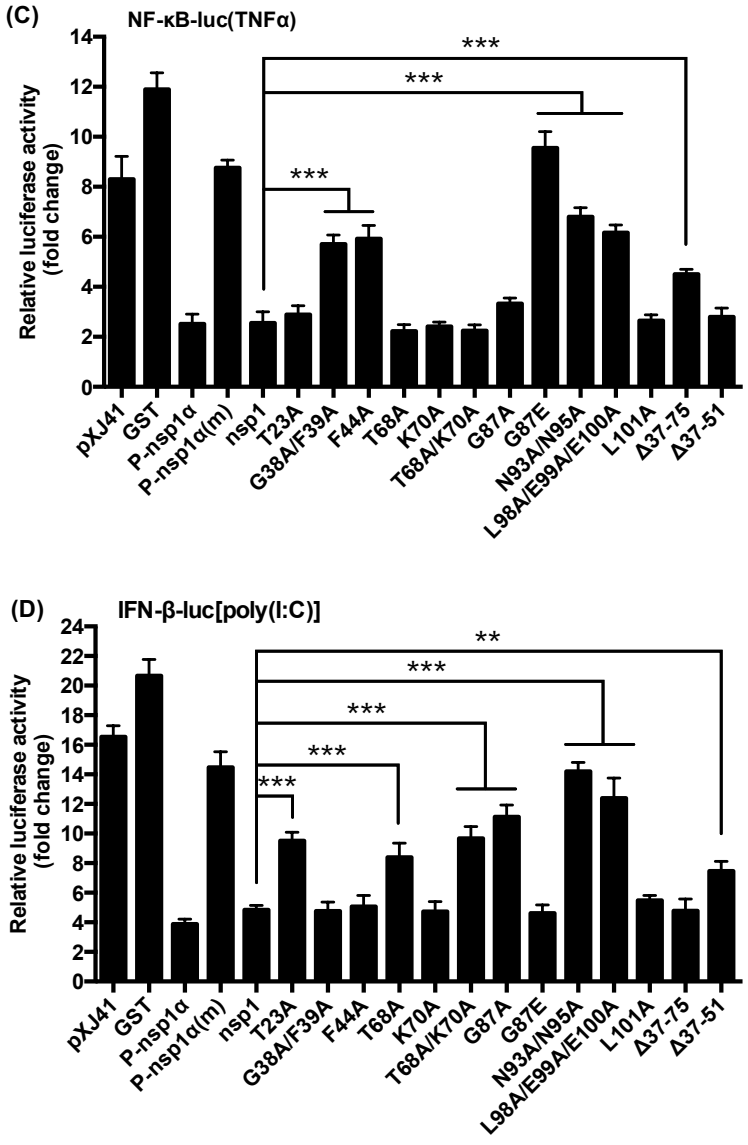
(C)
NF-κB-luc(TNFα)
Relative luciferase activity (fold change)
0
2
4
6
8
10
12
14
***
***
***
pXJ41
GST
P-nsp1α
P-nsp1α(m)
nsp1
T23A
G38A/F39A
F44A
T68A
K70A
T68A/K70A
G87A
G87E
N93A/N95A
L98A/E99A/E100A
L101A
Δ37-75
Δ37-51
(D)
IFN-β-luc[poly(I:C)]
Relative luciferase activity (fold change)
0
2
4
6
8
10
12
14
16
18
20
22
24
**
***
***
***
***
pXJ41
GST
P-nsp1α
P-nsp1α(m)
nsp1
T23A
G38A/F39A
F44A
T68A
K70A
T68A/K70A
G87A
G87E
N93A/N95A
L98A/E99A/E100A
L101A
Δ37-75
Δ37-51

Fig. 3.8 (cont.)

Table 3.1: Primers used for the PEDV nsp1 mutants by PCR site-directed mutagenesis.

Nsp1 mutants	Primer sequence (5'-3')
T23A-F	GACGGCTTCACTAGCAGCGCAAAAGCCAAAAGCTG
T23A-R	CAGCTTTTGGCTTTTGCGCTGCTAGTGAAGCCGTC
G38A/F39A-F	GAAACGGCAGTGCATAGCTGCACTAGCGGCGGCCTC
G38A/F39A-R	GAGGCCGCCGCTAGTGCAGCTATGCACTGCCGTTTC
F44A-F	CGAGATCGAAGGACACGGCACGGCAGTGCATAAATCCA
F44A-R	TGGATTTATGCACTGCCGTGCCGTGTCCTTCGATCTCG
T68A-F	CACTAAGCTTGGTAGCGCCGACCACCACCAT
T68A-R	ATGGTGGTGGTCGGCGCTACCAAGCTTAGTG
K70A-F	CACATACGCACTAAGCGCGGTAGTGCCGACCACC
K70A-R	GGTGGTCGGCACTACCGCGCTTAGTGCGTATGTG
T68A/K70A-F	CACATACGCACTAAGCGCGGTAGCGCCGACCACCACCATG
T68A/K70A-R	CATGGTGGTGGTCGGCGCTACCGCGCTTAGTGCGTATGTG
G87A-F	GTTAGAAAATAACAGCCAAGCACAAATGTTTTTGGGGCG
G87A-R	CGCCCCAAAAACATTTGTGCTTGGCTGTTATTTTCTAAC
G87E-F	AGTTAGAAAATAACAGCCACTCACAAATGTTTTTGGGGCGGCTAC
G87E-R	GTAGCCGCCCCAAAAACATTTGTGAGTGGCTGTTATTTTCTAACT
N93A/N95A-F	TAAGCTCTAACTCTTCGAGGAAGTAAGCACAGGCAGAAAATAACAGCCAACCACAAATGT
N93A/N95A-R	ACATTTGTGGTTGGCTGTTATTTTCTGCCTGTGCTTACTTCCTCGAAGAGTTAGAGCTTA
L98A-F	ACCAAAAGTAAGCTCTAACTCTTCGGCGAAGTAATTACAGTTAGAAAATAAC
L98A-R	GTTATTTTCTAACTGTAATTACTTCGCCGAAGAGTTAGAGCTTACTTTTGGT
E99A/E100A-F	CGACCAAAAGTAAGCTCTAACGCTGCGAGGAAGTAATTACAGTTAG
E99A/E100A-R	CTAACTGTAATTACTTCCTCGCAGCGTTAGAGCTTACTTTTGGTCG
L101A-F	CGACGACCAAAAGTAAGCTCTGCCTCTTCGAGGAAGTAATTACA
L101A-R	TGTAATTACTTCCTCGAAGAGGCAGAGCTTACTTTTGGTCGTCG
Δ37-75F	CCATGTTACATTGGCTTTTGCCAATGAAGCCGTCTCATA
Δ37-75R	TATGAGACGGCTTCATTGGCAAAAGCCAATGTAACATGG
Δ37-51F	CATGTTACATTGGCTTTTGCCAATGCTTTTGGCTTTTGCACTG
Δ37-51R	CAGTGCAAAAGCCAAAAGCATTGGCAAAAGCCAATGTAACATG

Table 3.2: Real-time PCR primer sets for cytokine genes used in this study.

Genes	Forward primer (5'-3')	Reverse primer (5'-3')	Accession no./references
sIFN-α*	GCCTCCTGCACCAGTTCTACA	TGCATGACACAGGCTTCCA	(Loving et al., 2006)
sIFN-β	AGTGCATCCTCCAAATCGCT	GCTCATGGAAAGAGCTGTGGT	(de Los Santos et al., 2006)
sTNFα	AACCTCAGATAAGCCCGTCG	ACCACCAGCTGGTTGTCTTT	(Gudmundsdottir and Risatti, 2009)
sIL-1β	ACCTGGACCTTGGTTCTCTG	CATCTGCCTGATGCTCTTGT	NM_214055.1
sIL-6	CTGGCAGAAAACAACCTGAACC	TGATTCTCATCAAGCAGGTCTCC	(Duvigneau et al., 2005)
sIL-8	CCGTGTCAACATGACTTCCAA	GCCTCACAGAGAGCTGCAGAA	(Royaee et al., 2004)
sIL-15	GCTGTATCAGTGCAGGTCTTCCT	TTTCAGTATACAATGTGGCATCCA	(Gudmundsdottir and Risatti, 2009)
sIL-17	AATGCTGAAGGGAAGGAAGA	CCCACTGTCACCATCACTTT	NM_001005729.1
sCXCL10	CTGCATCAAGATCAGTGACAGAC	TTGTGGCAATGATCTCAACAT	NM_001008691.1
sMCP-1	GCAGCAAGTGTCCTAAAGAAGCA	GCTTGGGTTCTGCACAGATCT	(Gudmundsdottir and Risatti, 2009)
sRANTES	AGCATCAGCCTCCCCATATG	TTGCTGCTGGTGTAGAAATATTCC	(Gudmundsdottir and Risatti, 2009)
sTGFβ3	CCTTCGACGTCACAGACACT	TGTGACACGGACAATGAATG	XM_005666355.2
mTNFα	CCTCTTCAAGGGCCAAGGCT	TGGGCTCATACCAGGGCTTG	U19850.1
β-actin	ATCGTGCGTGACATTAAG	ATTGCCAATGGTGATGAC	(Zhang et al., 2016)

(Note: 's' in the front of each gene denotes swine specific primers; 'm' for TNFα indicates monkey specific primers; β-actin primers were universal for swine, monkey, and human.)

CHAPTER 4: TYPE III INTERFERON RESTRICTION BY PORCINE EPIDEMIC DIARRHEA VIRUS INFECTION IS MEDIATED THROUGH IRF1 BY NSP1 PROTEIN

4.1 ABSTRACT

Type III interferons (IFN-λs) play a vital role to maintain the antiviral state of the mucosal epithelial surface in the gut, and in turn, enteric viruses may have evolved to evade the type III IFN responses during infection. For the study of the immune evasion of porcine epidemic diarrhea virus (PEDV) from type III IFN response, a line of porcine intestinal epithelial cells was developed as a model for PEDV replication. IFN-λ1 and IFN-λ3 inhibited the PEDV replication, indicating the anti-PEDV activity of type III IFNs. Of the 21 PEDV proteins, nsp1, nsp3, nsp5, nsp8, nsp14, nsp15, nsp16, ORF3, E, M, and N were found to suppress the type III IFN activities, and the IRF1 signaling mediated the suppression. PEDV specifically inhibited IRF1 nuclear translocation. Peroxisomes are the innate antiviral signaling platforms for activation of IRF1-mediated IFN-λ production, and peroxisomes were found to decrease in number in PEDV-infected cells. PEDV nsp1 blocked the nuclear translocation of IRF1 and reduced the number of peroxisomes to suppress the IRF1-mediated type III IFN. Mutational studies showed the conserved residues of nsp1 were crucial for IRF1-mediated IFN-λ suppression. Our study for the first time provides the evidence that the porcine enteric virus PEDV downregulates and evades the IRF1-mediated type III IFN responses by reducing the peroxisomes.

This chapter has been accepted to publish as a research article in Journal of Virology. The original citation is: Zhang, Q., Ke, H., Blikslager, A., Fujita, T., Yoo, D., 2017a. Type III Interferon Restriction by Porcine Epidemic Diarrhea Virus and the Role of Viral Protein nsp1 in IRF1 Signaling. J. Virol.

4.2 INTRODUCTION

A classic antiviral response in mammals is mediated by type I interferons (IFNs). Upon infection, host cells react quickly by producing type I IFNs (IFN-α/β), which triggers the production of hundreds of interferon-stimulating genes (ISGs) through the JAK-STAT pathway (Stark and Darnell, 2012). Thus, type I IFNs and ISGs are the major components for the establishment of a host antiviral state and provide the first line of defense against viral infections. Recently, types III IFNs (IFN-λ) have been identified as a distinct class of antiviral cytokines and inducers for expression of ISGs. Type III IFNs in humans constitute IFN-λ1 (interleukin 29 [IL-29]), IFN-λ2 (IL-28A), IFN-λ3 (IL-28B), and IFN-λ4 (Hermant and Michiels, 2014; Kotenko et al., 2003; Prokunina-Olsson et al., 2013; Sheppard et al., 2003). For swine, IFN-λ1 and IFN-λ3 have been described, but whether IFN-λ2 is expressed or deficient in pigs is unclear (Sang et al., 2010). The induction process and mechanism of action for type I IFNs and type III IFNs are similar (Mordstein et al., 2010; Onoguchi et al., 2007; Sommereyns et al., 2008). While the induction of type I IFNs requires all components of IFN enhanceosome, type III IFNs can be produced by independent actions of IRF (interferon regulatory factor) and NF-κB (Thomson et al., 2009). Similar to type I IFNs, IRF3, IRF7, and NF-κB too are essential for type III IFNs, but IRF1 plays a particular role (Odendall et al., 2014). The mitochondrial antiviral-signaling (MAVS) protein localizes to the both mitochondria and peroxisomes and participates in activating an antiviral response. Mitochondrial MAVS is responsible for activation of a stable response mediated by type I IFNs, whereas peroxisomal MAVS induces a type III IFN-dependent antiviral response (Dixit et al., 2010; Seth et al., 2005). Peroxisomal MAVS in the intestinal epithelial cells is particularly crucial for IRF1-dependent activation of type III IFN response (Odendall et al., 2014).

A main difference between the type I and type III IFN systems is that receptors for type I IFNs are seemingly ubiquitously expressed whereas receptors for type III IFNs are confined mostly to the mucosal epithelium (Sommereyns et al., 2008). Thus, type III IFN response is mostly limited to epithelial cells due to the highly restricted expression of specific receptors. Recent studies show that intestinal epithelial cells (IECs) express extremely low levels of type I IFN receptors and thus respond poorly to type I IFNs (Mahlakoiv et al., 2015). IECs produce abundantly type III IFNs but poorly type I IFNs, and thus selectively respond to type III IFNs. The robust response of type III IFNs to invading pathogens is due to the differentiation of IECs and upregulation of the biogenesis of peroxisomes (Odendall et al., 2014). For antiviral defense, IECs in the gut mucosa mainly respond to type III IFNs after viral infection, whereas other cell types in the gut rely on type I IFNs (Mahlakoiv et al., 2015). In turn, viruses have evolved to evade the type III IFN response. Hepatitis C virus NS3-4A cleaves peroxisomal MAVS to inhibit the peroxisome-dependent antiviral cellular response (Ferreira et al., 2016), and flavivirus also impairs the peroxisomal biogenesis for suppression of type III IFNs (You et al., 2015).

Porcine epidemic diarrhea (PED) is an acute and highly contagious enteric viral disease characterized by watery diarrhea, vomiting, and dehydration, resulting in the high mortality in neonatal piglets (Debouck and Pensaert, 1980; Song and Park, 2012; Stevenson et al., 2013). PED was first recognized in England in 1971 but limited mostly to some parts of Europe until the 1990s when it appeared in Asia. In 2010, highly virulent PED outbreaks occurred in China (Sun et al., 2015; Sun et al., 2012a). In the US, PED was recognized first in April 2013, and in the following eight months, caused more than 8 million deaths of pigs resulting in the substantial economic losses (Chen et al., 2014; Marthaler et al., 2013; Mole, 2013; Stevenson et al., 2013). The causative agent is PED virus (PEDV) which is an enveloped, positive-sense, single-strand

RNA virus grouped in the genus *Alphacoronavirus* of the family *Coronaviridae* in the order *Nidovirale* (http://ictvonline.org/virustaxonomy.asp). The PEDV genome is 28 kb in length and codes for two large polyproteins pp1a and pp1ab, an accessory protein ORF3, and four structural proteins: spike (S), membrane (M), envelope (E), and nucleocapsid (N) (Kocherhans et al., 2001). The two large polyproteins are further processed to 16 nonstructural proteins, nsp1 through nsp16, by the proteinase activities of nsp3 and nsp5.

We have previously shown that PEDV inhibits the type I IFN response in cells and that nsp1 is the major IFN antagonist (Zhang et al., 2016). The primary target cells for PEDV, however, are intestinal villous epithelial cells of swine and, to some extent, macrophages infiltrated to the lamina propria (Debouck and Pensaert, 1980; Lee et al., 2000; Sueyoshi et al., 1995). So thus far, no information is available whether and how PEDV modulates type III IFN response in intestinal epithelial cells of swine. In the present study, we developed PEDV-susceptible porcine intestinal epithelial cells and showed in these cells that PEDV suppressed type III IFN production. We further demonstrated that PEDV inhibited the IRF1 activation and reduced the peroxisomes in number. Our findings indicate that PEDV evades the IRF1-mediated type III IFN response in porcine intestinal epithelial cells by reducing the number of peroxisomes, which is likely the key mechanism to thwart early antiviral signaling that emanates from these organelles.

4.3 MATERIALS AND METHODS

4.3.1 Cell culture

Porcine kidney epithelial cells (LLC-PK1), derived from a healthy male pig of three to four weeks of age (Perantoni and Berman, 1979), were obtained from Dr. K. Chang (Kansas

State University, Manhattan, KS). LLC-PK1 was maintained in modified Eagle's medium (MEM; Corning Cellgro) with 5% heat-inactivated fetal bovine serum (FBS; Gibco) at 37°C in a humidified atmosphere of 5% CO_2. African green monkey kidney epithelial cells (MARC-145; Kim et al., 1993) and Vero (ATCC® CCL-81™) were grown in high-glucose Dulbecco's modified Eagle's medium (DMEM; Corning Cellgro) supplemented with 10% heat-inactivated FBS. IPEC-J2 cells were obtained from Dr. A. Blikslager (North Carolina State University, Raleigh, NC). IPEC-J2 is a continuous line of epithelial cells derived from the jejunum of a 12 hours old, colostrum-unsuckled, mixed breed piglet (Schierack et al., 2006). These cells were maintained in DMEM/F12 with 5% FBS supplemented with 5 mg/ml of insulin/selenium/transferrin (Life Technologies) and 5 ng/ml of epidermal growth factor (Life Technologies). IPEC-DQ, a subline of IPEC-J2 cells, was maintained in RPMI-1640 supplemented with 10% FBS.

4.3.2 Virus stocks, titration, and infection of cells

The Colorado strain of PEDV (USA/Colorado/2013; GenBank: KF272920) was obtained from Agricultural Research Service, US Department of Agriculture (Ames, IA). PEDV was propagated in FBS-free DMEM supplemented with 0.3% tryptose phosphate broth (Sigma, St. Louis, MO), 0.02% yeast extract (Teknova, Hollister, CA) with different concentrations of trypsin 250 (Sigma-Aldrich, St. Louis, MO). LLC-PK1 and Vero cells were used for PEDV propagation and titration. The optimal trypsin concentrations for Vero, IPEC-J2, MARC-145, LLC-PK1, and IPEC-DQ cells were 5 μg/ml, 5 μg/ml, 2 μg/ml, 1 μg/ml, and 1 μg/ml, respectively. For the anti-PEDV activity of IFN-λ1 and IFN-λ3, cell culture supernatants were collected at indicated times post-infection and titrated according to the 50% tissue culture

infective dose ($TCID_{50}$) protocol. The viral titers were calculated using the Spearman-Karber equation.

4.3.3 Antibodies and chemicals

The following antibodies were used for immunofluorescence assay (IFA) and Western blot (WB): mouse anti-PEDV N mAb (Medgene, Brookings, SD; SD-1-5, 1:1,000 dilution for WB, 1:200 dilution for IFA), mouse anti-β-actin mAb (C-4) (Santa Cruz; sc-47778, 1:2,000 for WB), rat anti-FLAG Ab (Agilent Technologies; 200474, 1:2,000 for WB, 1:200 for IFA), rabbit anti-IRF1 pAb (C-20) (Santa Cruz; sc-497, 1:1,000 for WB, 1:200 for IFA), rabbit anti-PMP70 pAb as a peroxisomal membrane marker (Novus Biologicals; NBP187258, 1:200 for IFA), mouse anti-pan cytokeratin mAb (C-11) (ThermoFisher Scientific; MA5-12231, 1:50 for IFA), mouse anti-Sucrase-Isomaltase mAb (A-12) (Santa Cruz; sc-393424, 1:50 for IFA), and Alexa Fluor 594-conjugated (goat anti-rabbit) and 488-conjugated (goat anti-mouse) secondary antibodies (Thermo Scientific; 1:200 for IFA).

Recombinant IL-29/IFN-λ1 protein (no. 1598IL025) and recombinant IL-28B/IFN-λ3 protein (no. 5259IL025) were purchased from Bio-Techne (Minneapolis, MN). Polyinosinic:polycytidylic acid [poly(I:C)] and DAPI (4', 6-diamidino-2-phenylindole) were purchased from Sigma (St. Louis, MO). QIAamp Viral RNA mini kit and RNeasy mini kit were purchased from QIAGEN. Power SYBR Green PCR master mix was purchased from Life Technologies (Carlsbad, CA). Pierce ECL Western blotting substrate, methanol, and Triton X-100 were purchased from Thermo Scientific (Waltham, MA). The fluoromount-G mounting medium was purchased from Southern Biotech (Birmingham, AL).

4.3.4 Plasmids and transfections

Plasmids expressing individual proteins of PEDV were constructed by cloning genes as a fusion with a FLAG tag under the CMV promoter as described previously (Zhang et al., 2016). The PEDV nsp1 mutants were made by PCR-based site-directed mutagenesis and described elsewhere (Zhang et al., 2017b). Expression of each viral protein was confirmed by immunofluorescence and Western blot analysis. Firefly luciferase-based reporter assays were described elsewhere (Zhang et al., 2016). The wild type IFN-λ1 luciferase reporter construct (p-55λ1-(-225/-36)-Luc) and its mutants (p-55λ1mut.IRF-Luc, p-55λ1mut.NF-κB-Luc, and p-55λ1mut.IRF/mut.NF-κB-Luc) were described previously (Onoguchi et al., 2007). The plasmid pIRF1-Luc contained multiple copies of the IRF1 cis-acting enhancer element for measurement of the IRF1 transcriptional activity and was purchased from Thermo Scientific (Waltham, MA). The *Renilla* luciferase plasmid pRL-TK (Promega) contained the herpes simplex virus thymidine kinase (HSV-tk) promoter and was included to serve as an internal control. The activated stimulator pMAVS was obtained from Dr. J. Shisler (University of Illinois, Urbana, IL), and pMDA5 and pIKKε were kindly provided by Dr. B. Gotoh (Shiga University of Medical Science, Shiga, Japan). The activated pIRF3 was obtained from Dr. Y. Fang (Kansas State University, Manhattan, KS). The constitutively activated pRIG-I and pTBK1 were provided by Dr. S. Xiao (Huazhong Agricultural University, Wuhan, China). Transfections were performed using Lipofectamine 2000 according to the manufacturer's instructions (Invitrogen, Carlsbad, CA).

4.3.5 RNA isolation and quantitative PCR

Cells were washed once with PBS and lysed directly in cell culture dishes. Total RNA was isolated using the RNeasy mini kit according to the manufacturer's instructions (QIAGEN).

Possible contamination of cellular DNA was removed by treatment with DNase I. One μg of total RNA was transcribed to cDNA using M-MLV reverse transcriptase and random primers (Promega). The synthesized cDNA was subjected to quantitative PCR using the SYBR Green PCR mix according to the manufacturer's instructions (Life Technologies) in the ABI 7500 real-time PCR system. The RT-qPCR primers were listed in Table 4.1. The β-actin gene was used as an internal control for each experiment. The specificity was confirmed by the sequencing of PCR products and the melting curve analysis for qPCR. The threshold cycles for target genes and the difference in their C_t values (ΔC_t) were determined. Relative transcriptions of target genes were presented as fold changes relative to the respective controls using the $2^{-\Delta\Delta Ct}$ threshold method (Livak and Schmittgen, 2001).

4.3.6 Dual luciferase reporter assay

To examine activation of the IFN-λ1 promoter and its mutants during PEDV infection, MARC-145 cells were grown in 24-well plates to 80% confluency and transfected with luciferase reporter and pRL-TK at a ratio of 1:0.1 for 6 h. Cells were then infected with PEDV at 1 MOI for 12 h followed by stimulation with poly(I:C) for 12 h. For screening of viral antagonists for IFN-λ1, HeLa cells were grown in 48-well plates to 80% confluency and transfected with a luciferase reporter, individual viral gene, and pRL-TK at a ratio of 1:1:0.1 for 12 h using Lipofectamine 2000. To ensure a similar protein expression level of all the viral proteins, the transfection was conducted as described previously (Zhang et al., 2016) and protein expression level was validated for each luciferase assays. Of note, three-times more plasmids were transfected for nsp3 and nsp16 gene to ensure the comparable level of protein expression. Cells were stimulated with 0.5 μg/ml of poly(I:C) for 12 h. For examination of the IFN-λ

singling by nsp1, cells were transfected for 24 h with luciferase reporters, individual viral gene, activator, and pRL-TK at a ratio of 1:1:1:0.1. Transfection was performed using Lipofectamine 2000 according to the manufacturer's instructions (Invitrogen). For dual luciferase assay, cells were lysed in 50 μl of Passive lysis buffer for 20 min at room temperature (RT) with gentle shaking and placed on ice. Twenty μl of the cell lysates were used for dual luciferase assays according to the manufacturer's instructions (Promega). Luciferase values were normalized using *Renilla* as the internal control. Results were presented as the mean values of fold-changes with standard deviations. Data were obtained from three independent experiments each in triplicate.

4.3.7 Indirect immunofluorescence assay (IFA) and confocal microscopy

Cells were grown on coverslips placed in 12-well plates to 80% confluency for PEDV infection. For staining of pan Cytokeratin and Sucrase-Isomaltase, cells were fixed with 4% paraformaldehyde in PBS overnight at 4°C and permeabilized using 100% methanol at -20°C for 20 min. For transfection, cells were seeded on coverslips and grown to 80% confluency. A transfection mix was added to cells for 4 h followed by replacement with fresh medium, and cells were incubated for 12 h to allow gene expression. Cells were then transfected with poly(I:C) for 12 h and further incubated with fresh infection medium for additional 12 h. Cells were fixed with 4% paraformaldehyde in PBS overnight at 4°C and permeabilized using 0.1% Triton X-100 for 15 min at RT. Cells were incubated with 1% BSA in PBS for 30 min at RT and then with primary antibody for 1 h. After three washes with PBS, cells were incubated with fluorochrome-conjugated secondary antibody in the dark for 1 h. The cell nuclei were stained with DAPI for 10 min. The coverslips were mounted on the microscope slides using Fluoromount-G mounting

medium. Fluorescence was visualized using a Nikon A1R fluorescence microscope. Confocal microscope images were processed using NIS-Elements analysis software (Nikon).

4.3.8 SDS-PAGE and Western blot analysis

Cells were lysed at indicated times in RIPA buffer [20 mM Tris (pH 7.5), 150 mM NaCl, 1 mM EDTA, 1 mM phenylmethane sulfonyl fluoride (PMSF), 0.1% SDS, 0.5% sodium deoxycholate, 1% NP-40] containing the proteinase inhibitors cocktail (Promega) on ice for 30 min. The cell lysates were then sonicated and centrifuged at 4°C at 12,000 rpm (Eppendorf, 5415R) for 10 min to remove insoluble components. Protein concentrations were determined using the Pierce BCA protein assay kit (Thermo Scientific). Proteins were resolved by SDS-PAGE and transferred onto an Immobilon-P membrane (Millipore). The membranes were blocked with 5% nonfat dry milk in TBST for 1 h and incubated with primary antibody at 4°C overnight. The membranes were then incubated with horseradish peroxidase (HRP)-conjugated secondary antibody for 1 h at RT. Proteins were visualized by enhanced chemiluminescence detection reagents (Thermo), and images were obtained by FluorChem™ R System according to the manufacturer's instructions (ProteinSimple).

4.3.9 Statistical analysis

Statistical analyses were conducted using GraphPad Prism 6 for ANOVA analyses. Asterisks indicate the statistical significance. *, $P<0.05$, **, $P<0.01$, and ***, $P<0.001$.

4.4 RESULTS

4.4.1 Porcine intestinal epithelial cells (IPEC-DQ) and infection of PEDV

Vero cells are widely used for PEDV isolation and propagation (Hofmann and Wyler, 1988; Kusanagi et al., 1992), and ST and PK-15 cells also support PEDV replication (Liu et al., 2015). We have reported MARC-145 (a subline of MA-104 African green monkey kidney cells) as an alternative cell line permissive for PEDV infection (Zhang et al., 2016). Due to the different degree of cytotoxicity to transfection and variable efficiencies for infection of PEDV, different cell types were used for different experiments. However, the primary target cells for PEDV in pigs are villous epithelial cells of the intestinal tract (Debouck and Pensaert, 1980; Lee et al., 2000; Sueyoshi et al., 1995). Thus, Vero, MARC-145, LLC-PK1, and ST cells may be less suitable to study for cell-virus interactions especially innate immunity in the intestinal epithelia and needed to be validated in a porcine intestinal epithelial cell model. IPEC-J2 is the line of porcine intestinal epithelial cells established from the jejunum of a colostrum-deprived neonatal pig at 12 h of age. Some researchers reported that IPEC-J2 cells were susceptible to PEDV (Guo et al., 2016; Zhao et al., 2014). However, we and others found that these cells were not susceptible to PEDV (Zhang and Yoo, 2016; Personal communications with D. Diel at South Dakota State University and M. Torremorell at University of Minnesota). IPEC-J2 cells were non-homogeneous, and as shown by IFA, only a few number of cells were shown to be PEDV-positive. We subcloned IPEC-J2 cells by limited serial dilutions and were able to obtain a homogeneous subclone of cells, designated IPEC-DQ. These cells were examined first for their characteristics. Cytokeratin is the intracytoplasmic cytoskeleton protein of epithelial tissues, and the pan cytokeratin mAb staining showed the abundant expression of cytokeratins in IPEC-DQ as in LLC-PK1 and IPEC-J2, (Fig. 4.1A). Sucrase-isomaltase is a transmembrane glycoprotein

located in the brush border of the small intestine, and IPEC-DQ cells, as well as IPEC-J2, showed the expression of Sucrase-isomaltase, whereas it was absent in the LLC-PK1 kidney epithelial cells. The growth kinetics of IPEC-DQ cells was similar to that of IPEC-J2 cells with the same doubling time of approximately 53 h (data not shown). Based on these data, we concluded that IPEC-DQ retained the porcine intestinal epithelial phenotype. For examination of the susceptibility of IPEC-DQ for PEDV, cells were infected, and at 24 h postinfection, IFA and Western blot were conducted using viral specific antibody. Specific fluorescence was observed in PEDV-infected IPEC-DQ cells, indicating the efficient replication of PEDV in these cells. In contrast, IPEC-J2 cells did not show any PEDV-specific fluorescence even at an MOI of 5 (Fig. 4.1B). Western blot analysis further confirmed the efficient and productive infection of PEDV in IPEC-DQ cells (Fig. 4.1C).

Recent studies suggest that IFN induction and signaling in the intestinal epithelial cells are unique, and type III IFNs play a key role maintaining the antiviral state in the gut (Mahlakoiv et al., 2015; Nice et al., 2015; Pott et al., 2011). Intestinal epithelial cells express the high level of IFN-λ but not IFN-α/β upon poly(I:C) stimulation or enteric viral infections (Mahlakoiv et al., 2015). Thus to examine whether IPEC-DQ cells also produced IFN-λ selectively, the induction levels for different types of IFNs were determined after stimulation with poly(I:C). More than 1,700-folds increase of IFN-λ3 was observed in IPEC-DQ cells compared to IFN-α (Fig. 4.1D), suggesting that IPEC-DQ cells produced type III IFNs efficiently. These results showed that IPEC-DQ cells supported PEDV infection and induced the production of type III IFNs, demonstrating IPEC-DQ as a suitable cell model for the study of innate immune modulation by PEDV in the gut.

4.4.2 Antiviral activities of type III IFNs against PEDV

For examination of the antiviral activities of type III IFNs against PEDV infection, cells were primed for 12 h with either IFN-λ1 or IFN-λ3 and inoculated with PEDV. Cells were washed once and were replenished with fresh infection medium containing respective IFN-λ. Cell culture supernatants were collected at 12 h, 18 h, 24 h, 36 h, and 48 h postinfection and viral titers were determined. The PEDV titers were reduced by IFN-λ1 and IFN-λ3 over time, indicating that these IFNs inhibited PEDV production (Fig. 4.2A). IFN-λ3 had a stronger antiviral activity against PEDV than IFN-λ1. For evaluation of whether this IFN-λ-mediated antiviral activity was dose-dependent, cells were pretreated with 10, 100, and 1000 ng/ml of IFN-λ1 or IFN-λ3 for 12 h, and were then infected with PEDV for 24 h in the presence of respective IFN. The treatment of cells with IFN-λ inhibited PEDV infection in a dose-dependent manner, being the higher concentration of IFN-λ the stronger inhibition of PEDV replication (Fig. 4.2B). The immunofluorescence signal for PEDV N protein was decreased relative to the increase of IFN-λ1 and IFN-λ3 (Fig. 4.2C), further confirming that type III IFNs restricted PEDV infection in a dose-dependent manner. The anti-PEDV activity of type III IFNs was examined in three different treatment conditions. Cells were treated with IFN-λ1 or IFN-λ3 at 100 ng/ml for 12 h before, at the time, or after PEDV inoculation, and the culture supernatants were collected at 24 h postinfection for viral titration. Both IFN-λ1 and IFN-λ3 inhibited PEDV replication at comparable levels regardless of different treatment conditions, being the highest inhibition by treatment before infection (Fig. 4.2D). RT-qPCR was conducted for PEDV N gene expression, and both IFN-λ1 and IFN-λ3 reduced the amount of N mRNA in a dose-dependent manner (Fig. 4.2E) and in all three conditions (Fig. 4.2F). These data confirm that type III IFNs possess productive anti-PEDV activities.

4.4.3 Inhibition of type III IFN production by PEDV

Type III IFNs play a critical role to maintain the antiviral state of the epithelium in the gut (Mahlakoiv et al., 2015; Nice et al., 2015; Pott et al., 2011). We have also shown that they inhibit PEDV infection (Fig. 4.2). Thus we hypothesized that PEDV might have evolved to modulate the type III IFN response of the host. To investigate this possibility, we first assessed the expression of type III IFNs in PEDV-infected IPEC-DQ cells. Cells were inoculated with PEDV at an MOI of 5, and cell lysates were harvested at various times postinfection for RT-qPCR. Transfection with poly(I:C) was used as a positive control, and the poly(I:C) stimulation induced the strong production of all subtypes of IFN-λ (IFN-λ1, IFN-λ3, and IFN-λ4), with the highest production for IFN-λ3 (Figs. 4.3A, 4.3B, and 4.3C). Infection of IPEC-DQ cells with PEDV caused slight induction of all subtypes of IFN-λ at 3 hpi but quickly downregulated their induction at 9 hpi and 12 hpi. We also evaluated the type III IFN induction in LLC-PK1 cells. At the MOI of 0.01, no apparent induction was observed throughout the observation period. Transcripts for each subtype of IFN-λ were also negligible at 12-24 hpi (data not shown). At the high MOI of 5, type III IFNs were still not inducible, and the levels of respective mRNAs were negligible (data not shown), suggesting the suppression of type III IFN responses by PEDV was not cell type-dependent. For examination of whether PEDV could induce the activation of type III IFN at any time of infection, cells were transfected with the IFN-λ1 luciferase reporter and inoculated with PEDV to determine the viral regulation of reporter activity. The IFN-λ1 promoter-driven luciferase activity was barely detectable in PEDV-infected cells compared to the intense activity in poly(I:C)-stimulated cells (Fig. 4.3D), suggesting that PEDV infection failed to induce IFN-λ1 expression.

The observation that PEDV did not induce the type III IFN response indicated that PEDV had an ability to suppress type III IFN response during infection. For this possibility, IFN-λ1 reporter assays were performed in PEDV-infected cells. Cells were transfected with the luciferase reporter and inoculated with PEDV, followed by stimulation with poly(I:C). Treatment of mock-infected cells with poly(I:C) upregulated the IFN-λ1 promoter activity up to 125 folds. In sharp contrast, the IFN-λ1 activity in PEDV-infected cells was significantly suppressed even after stimulation with poly(I:C) (Fig. 4.3E), suggesting the virus-mediated suppression of type III IFN response. For confirmation of the IFN-λ suppression by PEDV, RT-qPCR for IFN-λ transcripts was conducted in cells infected with the virus and stimulated with poly(I:C). The poly(I:C) stimulation upregulated the expression of IFN-λ1, IFN-λ3, and IFN-λ4 in mock-infected cells as anticipated, however, PEDV infection significantly inhibited their expressions (Figs. 4.3F, 4.3G, and 4.3H), confirming the suppression of type III IFN response by PEDV.

4.4.4 Identification of type III IFN antagonists of PEDV

For identification of the type III IFN viral antagonists, individual proteins of PEDV were examined for IFN-λ suppression by reporter assays. The expression levels of individually cloned viral protein were first examined by Western blot (Fig. 4.4A) using anti-FLAG antibody as described previously (Zhang et al., 2016). All genes were expressed well as anticipated. The poly(I:C) stimulation upregulated the IFN-λ1 transcription in cells expressing GST or empty-vector transfected cells as expected, indicating that cells typically recognize dsRNA and activate the IFN-λ1 promoter. Of the nsps, nsp1, nsp3, nsp5, nsp8, nsp14, nsp15, and nsp16 were shown to downregulate the IFN-λ1 promoter activity (Fig. 4.4B), and the accessory protein ORF3 also inhibited the IFN-λ1 activity. Of the structural proteins, E, M, and N were identified as type III

IFN antagonists (Fig. 4.4C).

Among the type III IFN antagonists, nsp1 appeared to be one of the most potent suppressor (Fig. 4.4B). We examined whether the suppression of IFN-λ1 activity by nsp1 was dose-dependent. Cells were co-transfected with p-55λ1-(-225/-36)-Luc and increasing amounts of nsp1 gene, and luciferase assays were performed. The luciferase activities decreased when the amounts of nsp1 increased (Fig. 4.4D), indicating that PEDV nsp1-mediated IFN-λ1 inhibition was dose-dependent. To further confirm the suppression of type III IFN expression by nsp1, RT-qPCR was conducted for mRNA quantification. While poly(I:C) alone upregulated the IFN-λ1, IFN-λ3, and IFN-λ4 expression, nsp1 inhibited their expressions significantly (Figs. 4.4E, 4.4F, and 4.4G). Taking together, these data demonstrate that PEDV encodes multiple antagonists for suppression of type III IFN, and nsp1 is the most potent antagonist.

4.4.5 Suppression of type III IFN production mediated by the interference of IRF and NF-κB

Expression of IFN-λ is dependent on the activation of the transcriptional factors IRF1, IRF3, IRF7, or NF-κB. A cluster of the IRF-binding and NF-κB-binding sites has been identified as the cis-acting elements for IFN-λ expression (Onoguchi et al., 2007). For determination of the transcription factors required for PEDV-mediated IFN-λ1 inhibition, a series of promoter mutants was used for reporter assays. The wild type reporter p-55λ1-(-225/-36)-Luc contains the binding sites for both IRF and NF-κB for IFN-λ1 expression. The reporter mutants p-55λ1mut.IRF-Luc, p-55λ1mut.NF-κB-Luc, and p-55λ1mut.IRF/mut.NF-κB-Luc contain the binding-site mutation for IRF, NF-κB, and both IRF and NF-κB, respectively. Cells were transfected with individual reporter mutants and infected with PEDV, followed by stimulation

with poly(I:C) and determination of the luciferase activities. Although the mutation of the IRF-binding or NF-κB binding abrogated the IFN-λ1 activation compared to the activity by wild-type promoter (Fig. 4.3E), the mutants still retained the ability to activate IFN-λ1 when stimulated with poly(I:C) (Fig. 4.5A). PEDV infection, however, suppressed the luciferase activity of the mutants. These results indicate that both IRF and NF-κB are involved in the PEDV-mediated IFN-λ suppression. Expression of type III IFNs in the intestinal epithelial cells is mainly dependent on IRF1 activation, whereas IRF3 and IRF7 play a minimal role (Odendall et al., 2014). We thus examined whether the PEDV suppression of type III IFN response was due to the IRF1 interference. Poly(I:C) stimulation of cells upregulated the IRF1 activity as anticipated. In virus-infected cells, however, IRF1 activity was significantly inhibited (Fig. 4.5B).

To determine if other viral antagonists for IFN-λ also suppressed the IRF1 activity, reporter assays were conducted. A strong luciferase activity was observed in cells transfected with the empty vector or in the GST-expressing cells as anticipated when stimulated with poly(I:C) (Fig. 4.5C). In contrast, the IRF1 activity was suppressed by nsp3, nsp5, nsp14, nsp15, nsp16, ORF3, E, and M in addition to nsp1 even after poly(I:C) stimulation. Of the total of 11 viral IFN-λ antagonists, nsp8 and N did not inhibit the IRF1 activity, suggesting that these two proteins may function through other pathways than the IRF1-mediated pathway. Nsp1 was also examined for its ability for suppression of IRF-mediated and NF-κB-mediated IFN-λ1 responses. Indeed, PEDV nsp1 suppressed the activities of the IFN-λ1 promoter mutants (Fig. 4.5D), indicating that nsp1 inhibited type III IFNs by suppressing both IRF1 and NF-κB.

4.4.6 Inhibition of RIG-I/MDA5 and suppression of IRF1

Since PEDV nsp1 appeared to be a potent suppressor for type III IFNs and inhibited the IRF1 activity, the IRF3 and IRF1 signaling pathways were examined. We first determined the IRF3 signaling. IRF3-mediated type III IFN signaling is activated when transfected with a constitutively activated adaptor protein. Cells were co-transfected with p-55λ1-(-225/-36)-Luc, PEDV nsp1 gene, and a plasmid expressing activated RIG-I, MDA5, MAVS, TBK1, IKKε, or IRF3 along with the pRL-TK internal control, and reporters were determined. The transfection of these active molecules significantly upregulated the IFN-λ1 promoter activities (Fig. 4.6A-4.6E). In contrast, these activities were suppressed when PEDV nsp1 was expressed. These results indicated that PEDV nsp1 possessed the ability to suppress IRF3-dependent type III IFN expression. PEDV nsp1 also inhibited the IFN-λ1 promoter activated by IRF3 (Fig. 4.6F), which suggests that IRF3-mediated type III IFN suppression might be a nuclear event.

PEDV nsp1 has been found to degrade the CREB-binding protein (CBP) in the nucleus, resulting in the suppression of type I IFN production (Zhang et al., 2016). The IRF3-mediated type III IFN production also relies on the enhanceosome formation (Odendall et al., 2014) and thus the CBP degradation by nsp1 in the nucleus may also affect type III IFN suppression. However, IRF1-mediated type III IFN induction can be independent of the enhanceosome assembly (Thomson et al., 2009). We thus investigated whether PEDV nsp1 inhibited the RIG-I/MDA5-mediated IRF1 activation. Transfection with an activated form of RIG-I or MDA5 was found to upregulate the IRF1 activity, and PEDV nsp1 suppressed this activity (Figs. 4.6G-4.6H). The overexpression of MAVS also upregulated the IRF1 activity, but PEDV nsp1 suppressed the IRF1 activity (Fig. 4.6I). Since MAVS in the peroxisomes is crucial for activation of IRF1-

mediated IFN-λ production (Odendall et al., 2014), our finding suggests that the suppression of IRF1-mediated type III IFN production occurs downstream of the MAVS activation.

4.4.7 Inhibition of IRF1 nuclear translocation by PEDV and nsp1

To investigate the basis of inhibition of IRF1-mediated type III IFN response by PEDV, the expression kinetics of IRF1 was examined in virus-infected cells. IPEC-DQ cells were infected with PEDV at an MOI of 5, and Western blot was conducted to investigate IRF1 expression at different times. The expression of PEDV N protein indicated the productive infection. The expression level of IRF1 was not altered by PEDV infection (Fig. 4.7A). The IRF1 protein contains a functional nuclear localization signal (NLS) located immediately downstream of the DNA-binding domain and is usually hidden to result IRF1 diffusely distributed in the cytoplasm. When stimulated, IRF1 is instantly activated and translocates to the nucleus (Lau et al., 2000). To examine whether PEDV blocked the IRF1 nuclear translocation, IPEC-DQ cells were infected with PEDV for 12 h and stimulated with poly(I:C), followed by antibody staining for IRF1. IRF1 became translocated to the nucleus when stimulated by poly(I:C) (Fig. 4.7B, second panel, yellow arrow). Similarly in PEDV-infected cells, IRF1 remained in the cytoplasm (Fig. 4.7B, third panel), indicating that PEDV infection failed to activate IRF1 nuclear translocation. Furthermore, IRF1 in virus-infected cells remained in the cytoplasm even after poly(I:C) stimulation (Fig. 4.7B, bottom panel, white arrow), indicating that the IRF suppression by PEDV was a cytoplasmic event. In IPEC-DQ cells, IRF1 was typically diffused throughout the cell, but poly(I:C) stimulation rendered IRF1 to the nucleus (Fig. 4.7C, second panel, yellow arrow). The IRF1 expression and its cellular distribution, however, were not altered in nsp1-expressing cells (Fig. 4.7C, third panel), and when nsp1-

expressing cells were stimulated, IRF1 in the nucleus was significantly reduced (Fig. 4.7C, bottom panel, white arrow). This data suggests that the IRF1-mediated type III IFN antagonism by nsp1 occurred upstream of the IRF1 activation.

4.4.8 Reduction of peroxisomes in number in PEDV-infected cells

MAVS localizes in the mitochondria and peroxisomes for a coordinated activation of effective innate immune responses (Dixit et al., 2010; Seth et al., 2005). The mitochondrial and peroxisomal MAVS pathways result in different but complementing responses: mitochondrial MAVS is associated with the activation of a stable response with delayed kinetics (type I IFN-dependent), while peroxisomal MAVS is responsible for a rapid but short-lived antiviral response (type III IFN-dependent) (Dixit et al., 2010). The peroxisomal MAVS in the intestinal epithelial cells preferentially triggers the IRF1-mediated expression of IFN-λ genes (Odendall et al., 2014). Differentiation of intestinal epithelial cells upregulates the biogenesis of peroxisomes and promotes robust type III IFN response to invading pathogens, and thus adequate numbers of peroxisome-associated MAVS are essential for type III IFN response. For examination of the peroxisomes in PEDV-infected cells, IPEC-DQ, LLC-PK1, and MARC-145 cells were infected with the virus, and the numbers and morphologies of peroxisomes were examined. The PMP70 peroxisomal membrane protein is one of the major components of the peroxisomal membrane and indicates the proliferation of peroxisomes (Imanaka et al., 2000), thus is used as a peroxisomal marker. In mock-infected cells, peroxisomes were abundantly distributed throughout the cytoplasm (Fig. 4.8A). In contrast, much less number of peroxisomes was observed in PEDV-infected MARC-145, LLC-PK1, and IPEC-DQ cells. One hundred fifty PEDV-infected cells were randomly chosen, and the average number of peroxisomes per cell

was calculated. The results showed 30-50% reduction of peroxisomes in PEDV-infected cells (Fig. 4.8B). This study indicates that PEDV reduces the peroxisomes in number in PEDV-infected cells.

4.4.9 Conserved residues of nsp1 are crucial for reduction of peroxisomes and IRF1-mediated IFN-λ suppression

Since PEDV nsp1 inhibited IRF1 by activated MAVS (Fig. 4.6I), nsp1 might be the protein reducing the number of peroxisomes. To investigate this, IPEC-DQ cells were transfected with nsp1 gene or its mutants and stained for PMP70. The peroxisomes were abundant and normally distributed throughout the cytoplasm in control cells (Fig. 4.9A, top panel), whereas in nsp1-expressing cells, the number of peroxisomes decreased (Fig. 4.9A, second panel). Previously, we determined the predicted tertiary structure of nsp1 and reported that the conserved residues were critical for NF-κB regulation (Zhang et al., 2017b). The cellular distribution of nsp1 mutants in IPEC-DQ cells was consistent in HeLa cells (Fig. 4.9A). The mutant K70A was normally distributed and retained its ability to reduce the peroxisomes in number (Fig. 4.9A, third panel). The deletion mutant Δ37-51 was localized in the cytoplasm and also reduced the peroxisomes in number (Fig. 4.9A, fifth panel). The perinuclear mutant N93A/N95A (Fig. 4.9A, fourth panel) and other mutants G38A/F39A, F44A, G87A, L98A/E99A/E100A, and Δ37-75 showed punctate patterns in the nucleus and did not interfere the peroxisomes in number (Fig. 4.9A, sixth-tenth panel). The numbers of peroxisomes were quantified in nsp1- and mutant nsp1-expressing cells and the data indicate that the conserved residues of nsp1 were crucial for the reduction of peroxisomes in number (Fig. 4.9B).

To further identify the residues for nsp1-mediated IFN-λ suppression, reporter assays were conducted using the IFN-λ1 and IRF1 luciferase constructs. Cells were co-transfected with individual nsp1 constructs along with p-55λ1-(-225/-36)-Luc or pIRF1-Luc and then stimulated with poly(I:C) for reporter assays. The nsp1 and its mutants exhibited comparable expression levels (Fig. 4.9C). Among the nsp1 mutants, T68A, K70A, T68A/K70A, and L101A appeared to inhibit the IFN-λ1 expression (Fig. 4.9D). The deletion mutant Δ37-51 localized in the cytoplasm but retained the IFN-λ1 suppression activity, which confirms that the suppression of type III IFNs by nsp1 is a cytosolic event. The cellular distribution of N93A/N95A was mostly perinuclear and reverted the suppression of type III IFNs. The cellular distributions of G38A/F39A, F44A, G87A, L98A/E99A/E100A, and Δ37-75 were punctate in the nucleus and their activity for suppression of type III IFNs was significantly reverted (Fig. 4.9D), suggesting that the highly conserved residues of nsp1 were crucial for IFN-λ suppression. Furthermore, G38A/F39A, F44A, G87A, N93A/N95A, L98A/E99A/E100A, and Δ37-75 reverted their IRF1 suppression activities (Fig. 4.9E), suggesting that the mutated amino acid residues were crucial for the IRF1-mediated suppression of type III IFN production.

4.5 DISCUSSION

Antiviral responses are primarily mediated by type I IFNs (IFN-α/β), leading to expression of hundreds of ISGs for the establishment of an antiviral state. Recent evidence, however, shows that type III IFNs play a critical role in innate antiviral immunity in the intestinal epithelial cells in the gut. Peroxisomes are the signaling platforms for innate antiviral activity, and the peroxisomal MAVS triggers type III IFN production for rapid ISG expression independent of type I IFNs (Dixit et al., 2010). The peroxisomal MAVS is essential for IRF1-

mediated type III IFN response (Odendall et al., 2014), which plays a pivotal role in restricting viral infections in the epithelial cells at the mucosal surfaces (Lazear et al., 2015). PEDV is an enteric virus causing severe diarrhea in pigs, but virtually no information is available as to whether and how the virus modulates the type III IFN response in the intestinal epithelial cells. In the present study, we have first developed a subline of porcine intestinal epithelial cells (IPEC-DQ). These cells confer the productive infection of PEDV and serve as an excellent cell model for porcine enteric viruses. The IFN-λ proteins can inhibit PEDV replication in a dose-dependent manner, and thus they are potent antiviral cytokines. In turn, PEDV inhibits type III IFN production, and the inhibition is mediated by interfering IRF and NF-κB. PEDV reduces the number of peroxisomes for suppression of IRF1-mediated type III IFN production. The conserved residues of PEDV nsp1 appear to be crucial for the reduction of peroxisomes in number and thus the suppression of IRF1-mediated type III IFNs.

For humans, type III IFNs constitute four subtypes: IFN-λ1 (interleukin 29 [IL-29]), IFN-λ2 (IL-28A), IFN-λ3 (IL-28B), and IFN-λ4 (Hermant and Michiels, 2014; Kotenko et al., 2003; Prokunina-Olsson et al., 2013; Sheppard et al., 2003). For swine, IFN-λ1 and IFN-λ3 have previously been described (Sang et al., 2010), and in the present study, we have identified the IFN-λ4 gene expression in porcine intestinal cells by RT-qPCR (Fig. 4.3C), implicating the importance of the type III IFN system for swine as well. We have not been able to identify IFN-λ2 in IPEC-DQ cells. The antiviral function of type III IFNs was initially thought to be analogous to that of type I IFNs when they were discovered. It appears, however, that type III IFNs mainly exerts the antiviral activity in the epithelial cells at the mucosal surfaces via induction of ISGs by activating JAK-STAT signaling pathway (Lazear et al., 2015). To activate the JAK-STAT pathway, type I IFNs signal through a heterodimeric IFNAR receptor consisting

of IFNAR1 and IFNAR2, whereas type III IFNs signal through a distinct heterodimer of IFNLR receptor of IFNLR1 and IL10R2. The IL-10R2 is widely distributed in different cell types, whereas IFNRL1 is mostly restricted to epithelial cells (Sommereyns et al., 2008), which renders type III IFNs selectively exert their antiviral functions to epithelial cells. The receptors for type I IFNs are expressed in all nucleated cells. However, their expressions are minimal in IECs and thus type I IFNs fail to protect these cells from enteric viral infections (Mahlakoiv et al., 2015). The gut mucosa is equipped with the compartmentalized IFN system in which the intestinal epithelial cells mainly respond to type III IFNs that are produced after viral infection, whereas other cells mostly rely on type I IFNs for antiviral defense (Mahlakoiv et al., 2015). The cell tropism of enteric viruses determines the potency of antiviral activity of the different type of IFNs in the gut. Rotavirus mainly infects IECs (Lopez and Arias, 2006), and thus the infection is controlled exclusively by type III IFNs (Angel et al., 1999; Pott et al., 2011). Reovirus replicates in both epithelial and non-epithelial cells (Forrest and Dermody, 2003), and thus type I and type III IFNs cooperatively control the reovirus infection such that type III IFNs restrict the infection in epithelial cells whereas type I IFNs exert the antiviral activity in non-epithelial cells (Mahlakoiv et al., 2015). The recombinant swine type III IFNs have been shown to restrict the PEDV infection in both Vero and IPEC-J2 cells (Li et al., 2017a; Shen et al., 2016). We have also shown that type III IFNs restrict the PEDV infection in a dose-dependent manner (Fig. 4.2B), which further confirms the strong anti-PEDV activities of type III IFNs. The swine type III IFNs also have greater antiviral activities against PEDV than IFN-α, which is probably since type III IFNs can induce differential and more potent ISG expressions than IFN-α in intestinal epithelial cells (Li et al., 2017a). In our study, IFN-λ3 restricts PEDV infection more efficiently than IFN-λ1 (Fig. 4.2A), which is consistent with the previous finding that IFN-λ3 exhibits a

more potent antiviral activity than IFN-λ1 (Li et al., 2017a; Palma-Ocampo et al., 2015). The potent antiviral activities of type III IFNs indicate therapeutic applications of these cytokines to enteric viral infections.

Type III IFNs exhibit potent antiviral activities against many viruses, in particular for viruses infecting the epithelial cells of the respiratory, blood brain barrier, liver, urogenital tracts, and gastrointestinal tracts (Lazear et al., 2015). Given the potent antiviral activity of type III IFNs, viruses have evolved to encode viral antagonists for evasion from type III IFN responses. The treatment with recombinant IFN-λ1 inhibits the replication of foot and mouth disease virus (FMDV), and in turn, FMDV has evolved to interrupt the antiviral function of IFN-λ1 (Wang et al., 2011). FMDV infection does not induce type III IFNs, and several viral antagonists have been identified to inhibit the IFN-λ1 expression (Wang et al., 2011). Among them, the leader proteinase L^{pro} is the most potent viral antagonist and disrupts the activation of IRF and NF-κB. The catalytic activity of the proteinase and the SAP (SAF-A/B, Acinus, and PIAS) domain are crucial for the L^{pro}-mediated IFN-λ1 suppression (Wang et al., 2011). The Yaba-like disease virus (YLDV) is a primate pox virus that exclusively infects the skin. The secreted glycoprotein Y136 of YLDV binds to IFN-α/β for inhibition of IFNAR signaling and also binds to type III IFNs to inhibit the antiviral response (Bandi et al., 2010; Huang et al., 2007). Similarly, we have described that PEDV suppresses the type III IFN response, suggesting a potential therapeutic application of type III IFNs to treatment and prevention of PED. PEDV codes for many antagonists for type I IFN antagonists (Zhang et al., 2016). Due to the similar induction and signaling pathways between the type I and type III IFNs, PEDV may take similar evasion strategies. Indeed, many of the type III IFN antagonists also suppress the type I IFN production (Fig. 4.4B-C), suggesting the common mechanisms between IFN-α/β and IFN-λs. The type I IFN

antagonists of PEDV inhibit the IRF3-mediated and the NF-κB-mediated pathways (Ding et al., 2014; Xing et al., 2013; Zhang et al., 2016), and we have shown here that PEDV also inhibits the IFN-λ expression by interfering IRF1 and NF-κB (Fig. 4.5A). PEDV nsp1 suppresses the IRF3-mediated type I IFN production by degrading CREB-binding protein in the nucleus (Zhang et al., 2016), and also inhibits IRF3-mediated IFN-λ1 activation (Fig. 4.6A-F). These findings suggest that the nsp1-mediated CBP degradation in the nucleus may also result in the suppression of type III IFN response.

Similar to type I IFNs, type III IFNs also require IRF3, IRF7, and NF-κB for induction (Onoguchi et al., 2007; Sommereyns et al., 2008). However, the induction of type III IFNs does not need all the components of enhanceosome (Thomson et al., 2009). Epithelial cells preferentially induce the production of IFN-λ to IFN-α/β. Viruses thus may selectively cause the type III IFN production. Hepatitis B virus (HBV) infection of hepatocytes induces the production of IFN-λ, but not IFN-α/β (Sato et al., 2015). Hepatitis C virus (HCV) infection also preferentially induces the production of IFN-λ to IFN-α/β (Park et al., 2012). We have found that the induction of type III IFNs in IPEC-DQ cells is much more potent than that of type I IFNs (Fig. 4.1D), which confirms that intestinal epithelial cells abundantly induce type III IFNs upon stimulation. It may be due to the relative abundance of peroxisomes in the intestinal epithelial cells. The activation of mitochondrial MAVS induces the type I IFN production, whereas the activation of peroxisomal MAVS predominantly induces the IFN-λ production (Odendall et al., 2014). IRF1 is the first identified IRF but does not induce the production of type I IFNs (Reis et al., 1994). IRF1 is also an ISG which is a prominent antiviral effector against many viruses (Schoggins and Rice, 2011). IRF1 can be induced by viral infections and translocates to the nucleus to activate the antiviral response (Li et al., 2015). The porcine IRF1 does not induce type

I IFN production but inhibits the replication of swine viruses, including swine influenza virus, pseudorabies virus, and transmissible gastroenteritis virus (Li et al., 2015). IRF1 is dispensable for type I IFN production but plays a crucial role in regulating MAVS-dependent signaling of peroxisomes for type III IFNs (Dixit et al., 2010; Odendall et al., 2014). Peroxisomes are the signaling platforms for the IRF1-dependent IFN-λ production. The differentiation process of IECs upregulates the biogenesis of peroxisomes for the robust response of type III IFNs (Odendall et al., 2014), which highlights the importance of type III IFNs for the innate antiviral state in the intestinal epithelial cells. Viruses may target the IRF1 activation, peroxisomal MAVS activation, or peroxisomal biogenesis for suppression of type III IFNs. Hepatitis C virus (HCV) NS3-4A can traffic and localize in the peroxisomes and specifically cleaves the peroxisomal MAVS and releases it into the cytosol (Ferreira et al., 2016). This action is intense to inhibit the peroxisome-dependent antiviral response and dampens the type III IFN responses. In flavivirus-infected cells, the peroxisomes are reduced in number and redistributed, resulting in the suppression of type III IFNs (You et al., 2015). Capsid proteins of West Nile virus (WNV) and Dengue virus (DENV) bind to the Pex19 peroxisome biogenesis factor and impair the biogenesis of peroxisomes. The level of the peroxisomal matrix enzyme is also reduced in infected cells (You et al., 2015). PEDV also decreases the number of peroxisomes for evasion of IRF1-mediated type III IFN response in intestinal epithelial cells (Fig. 4.8). This finding suggests that the targeting of peroxisomes is likely a key strategy for viral evasion from type III IFN responses. PEDV nsp1 blocks the IRF1 nuclear localization (Fig. 4.7C) and impairs the biogenesis of peroxisomes (Fig. 4.9A), indicating that targeting the peroxisome biogenesis is crucial for nsp1-mediated type III IFN response. The conserved residues are essential for nsp1-mediated suppression of NF-κB (Zhang et al., 2017b), IFN-λ (Fig. 4.9D), and IRF (Fig. 4.9E), which

suggests that the conserved structures are crucial for nsp1-mediated innate immune evasion for PEDV.

Peroxisomes are intracellular organelles that play a central role in regulating various metabolic activities in mammalian cells. They act in concert with mitochondria to control the metabolism of lipids and reactive oxygen species. Most RNA viruses replicate in the cellular membrane organelles or rely on them for entry and assembly. Coronaviruses and arteriviruses replicate in the double membrane vesicles (DMVs) and are assembled and released through the membrane trafficking, which is associated with the endoplasmic reticulum (ER) and Golgi complex. Despite the absence of evidence indicating that mammalian viruses replicate in the peroxisomes, some viruses interact with the peroxisomes. The influenza virus NS1 protein has been shown to bind to the peroxisomal enzyme 17-β-hydroxysteroid dehydrogenase (Wolff et al., 1996), which may alter the peroxisome-specific lipid metabolism for viral replication (Tanner et al., 2014). The rotavirus spike protein VP4 contains peroxisome-targeting sequences, which may also associate with lipid metabolism or cholesterol formation for viral infectivity (Lazarow, 2011). The HIV Nef protein interacts with thioesterase, which is the peroxisomal matrix protein (Liu et al., 1997; Watanabe et al., 1997). This interaction is associated with the downregulating of CD4 in HIV-infected cells (Cohen et al., 2000; Liu et al., 2000). The interactions between viruses and peroxisomes may dampen the innate antiviral signaling of the peroxisomes. In our study, PEDV and nsp1 reduce the number of peroxisomes for suppression of type III IFN production. PEDV replication and the nsp1 protein may impair the biogenesis of peroxisomes by direct interaction with essential peroxisome biogenesis factors, such as Pex19. It is also possible that PEDV and nsp1 protein trigger the disassembly of peroxisomes by disrupting the peroxisomal structure. The disassembly can be visualized by electron microscopy, and it will be

of interest to examine the structural disassembly. Identification of cellular proteins interacting with nsp1 in the peroxisomes and other viral factors affecting the antiviral signaling from peroxisomes will also be interesting.

Coronavirus nsp1 is the first N-terminal cleavage product of pp1a and pp1a/b polyproteins (Ziebuhr, 2005). It is one of the most divergent viral proteins in four different genera and does not harbor any known cellular functional motifs (Connor et al., 2007). Only *Alphacoronavirus* and *Betacoronavirus* code for nsp1, whereas *Gammacoronavirus* and *Deltacoronavirus* do not contain the nsp1 gene (Woo et al., 2010; Woo et al., 2012; Ziebuhr et al., 2005; Ziebuhr et al., 2007). For *Betacoronavirus* nsp1, the regulation of host cell and viral gene expressions has been documented, and nsp1 is also a potent IFN antagonist. SARS-CoV nsp1 inhibits the reporter gene expression under the constitutive and IFN-β promoters (Kamitani et al., 2006), and employs a two-pronged strategy to inhibit host gene expression. It tightly associates with the 40S ribosomal subunit for inhibition of mRNA translation and induction of an endonucleolytic RNA cleavage of cellular mRNAs (Huang et al., 2011b; Kamitani et al., 2009). Murine hepatitis coronavirus (MHV) nsp1 affects the cellular gene expression by suppressing IFN-β, IFN-stimulated response element (ISRE), and SV40 promoter (Zust et al., 2007). MERS-CoV nsp1 inhibits host gene expression by selectively targeting mRNAs transcribed in the nucleus for translation inhibition and mRNA degradation, but spares exogenous mRNAs introduced directly into the cytoplasm or virus-like mRNAs that originate in the cytoplasm (Lokugamage et al., 2015). However, nsp1 in *Alphacoronavirus* and *Betacoronavirus* lack an overall sequence similarity, and neither conserved motifs nor domains are found in viruses of *Alphacoronavirus*. Interestingly, the domains in SARS-CoV nsp1 responsible for suppression of host gene expression and type I IFN production are absent in PEDV nsp1 (Huang et al., 2011b;

Narayanan et al., 2008). Thus, it is plausible that nsp1 of *Alphacoronavirus* may have distinct functions regulating host innate immune response and gene expression. Transmissible gastroenteritis virus (TGEV), a porcine *Alphacoronavirus*, strongly inhibits host protein synthesis without binding to 40S ribosomal subunit in a cell-free *in vitro* translation system (Huang et al., 2011a). However, this translational suppression does not contribute to IFN suppression because TGEV induces a rapid and massive production of type I IFN both *in vitro* and *in vivo* (Charley and Laude, 1988; La Bonnardiere and Laude, 1981). SARS-CoV nsp1 potently inhibits host gene expression universally, including the endogenous protein β-actin (Narayanan et al., 2008). For PEDV however, the suppression of protein translation by nsp1 may not be a universal event since the expression level of endogenous β-actin is unchanged after virus infection and nsp1-gene transfection (Zhang et al., 2016; Zhang et al., 2017b). Thus, it remains to be examined whether PEDV nsp1 also has similar functions as other coronaviruses for shutting off host gene translation and whether these biological activities contribute to the regulation of IFN response.

In summary, we show that PEDV suppresses the IRF1-mediated type III IFN production and this suppression is correlated to decreased numbers of peroxisomes in the swine intestinal epithelial cells. PEDV codes for many antagonists for type III IFNs and IRF1. PEDV nsp1 inhibits the RIG-I/MDA5-mediated activation of type III IFNs and IRF1 activities. Our data provide novel information on the innate immune evasion of PEDV in the intestinal epithelial cells, which may form the foundation for future development of effective therapies and control of PED.

4.6 FIGURES AND TABLES

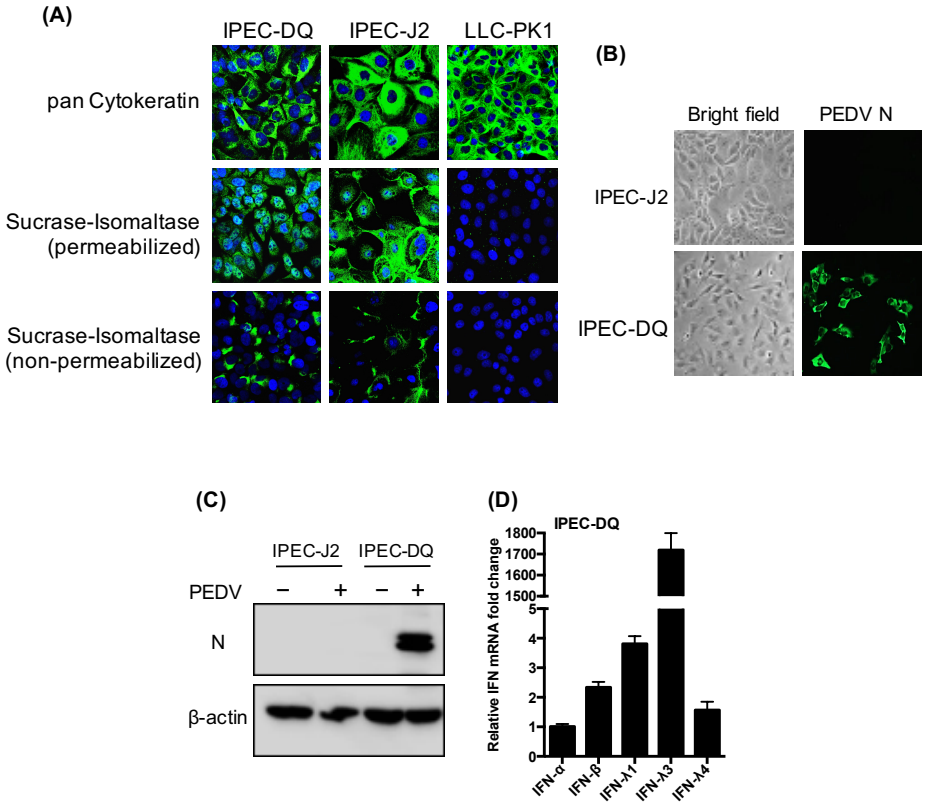

Fig. 4.1: Efficient replication of PEDV in porcine intestinal epithelial cells IPEC-DQ. (A), IPEC-DQ cells retained the intestinal epithelial phenotype. LLC-PK1, IPEC-J2, and IPEC-DQ cells were grown on coverslips and fixed with 4% paraformaldehyde in PBS at 4 °C overnight. The cells were then permeabilized with cold methanol for 15 min at -20 °C. Immunostaining was conducted to detect the presence of pan cytokeratin (epithelial cell marker) and Sucrase-Isomaltase (intestinal cell differentiation marker). (B), Expression of the viral nucleocapsid (N) protein in PEDV-infected IPEC-DQ cells. IPEC-J2 and IPEC-DQ cells were infected with PEDV at MOI of 5 and 1, respectively. Cells were then fixed at 24 h postinfection (hpi) with 4% paraformaldehyde and were stained with mouse anti-N mAb. (C), Expression of N protein in PEDV-infected IPEC-DQ cells by Western blot. IPEC-J2 and IPEC-DQ cells were infected with PEDV at MOI of 5 and 1, respectively, and Western blot was conducted using anti-N mAb at 24 hpi. (D), Induction of IFN in IPEC-DQ cells. Cells were stimulated with poly(I:C) for 12 h and were harvested to determine activation of the type I and type III IFNs by RT-qPCR. The relative IFN induction levels were normalized to those of IFN-α.

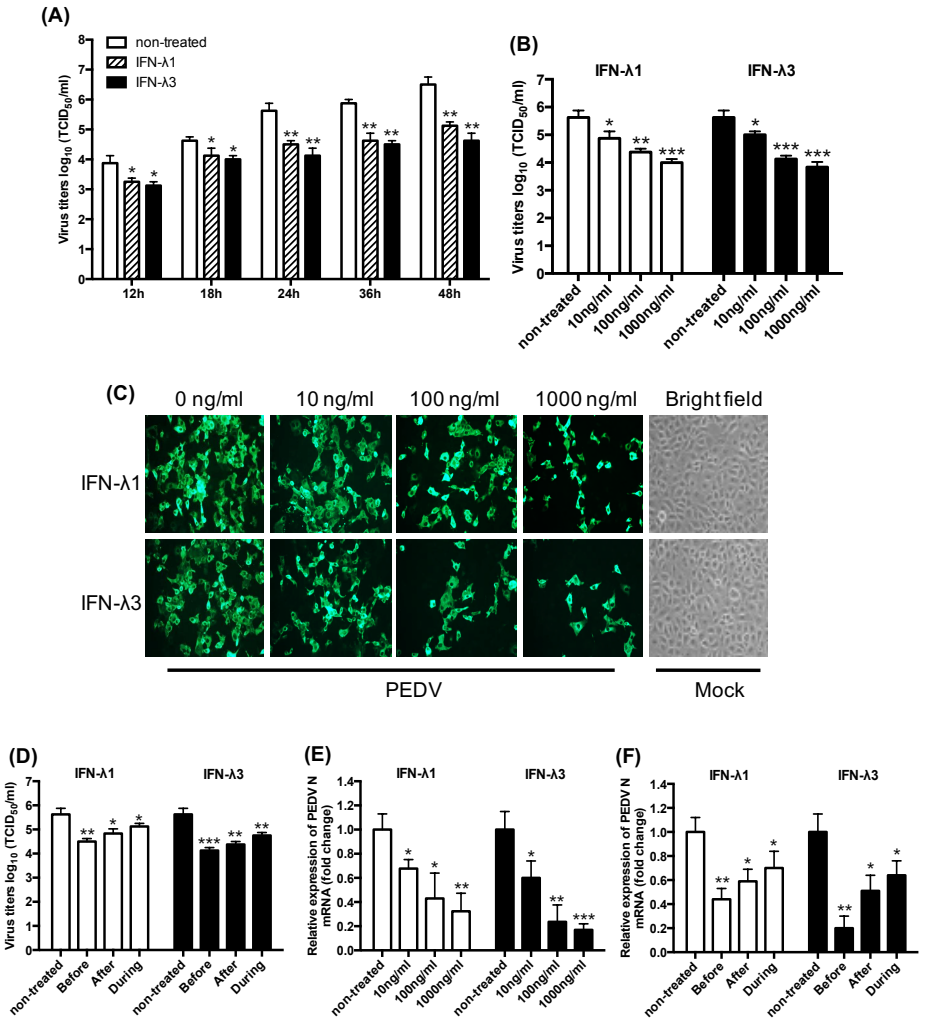

Fig. 4.2: Type III IFNs exert an antiviral role against PEDV. (A), Suppression of type III IFNs during PEDV infection. MARC-145 cells were seeded in 12-well plates and were treated with 100 ng/ml of IFN-λ1 or IFN-λ3 for 12 h. The cells were then infected with PEDV at 1 MOI for 1 h, washed, and replenished with fresh infection medium containing indicated subtypes of IFN-λ. Cell culture supernatants were collected at 12, 18, 24, 36, and 48 h postinfection and were titrated for $TCID_{50}$. (B)-(C), Restriction of PEDV infection by type III IFNs is dose-dependent. MARC-145 cells were seeded in 12-well plates and were treated with different amounts of IFN-λ1 or IFN-λ3 for 12 h. The cells were then infected with PEDV at 1 MOI for 1 h, washed, and replenished with fresh infection medium containing the indicated IFN. Cell culture supernatants were collected at 24 h post-infection and were titrated for $TCID_{50}$ (panel B). The cells were fixed for immunostaining with anti-N mAb and visualized under a fluorescence microscope (panel C). (D), Inhibition of PEDV infection by type III IFNs under three different treatment conditions. MARC-145 cells were pretreated with IFN-λ1 or IFN-λ3 (100 ng/ml) for 12 h and then inoculated with PEDV at an MOI of 1, washed, and replenished with fresh infection medium without IFN (Before). MARC-145 cells were coincubated PEDV with IFN-λ1 or IFN-λ3 (100 ng/ml) for 1 h, washed, and replenished with fresh infection medium without IFN (During). Alternatively, cells were inoculated first with PEDV for 1 h, and were treated with IFN-λ1 or IFN-λ3 (100 ng/ml) during incubation for 12 h (After). (E)-(F), Relative expression of the nucleocapsid (N) mRNA in PEDV-infected cells determined by RT-qPCR. The experiments for panel B and panel D form a pair, and the cells were harvested for RT-qPCR for PEDV N mRNA transcript. β-actin was used as an internal control for normalization.

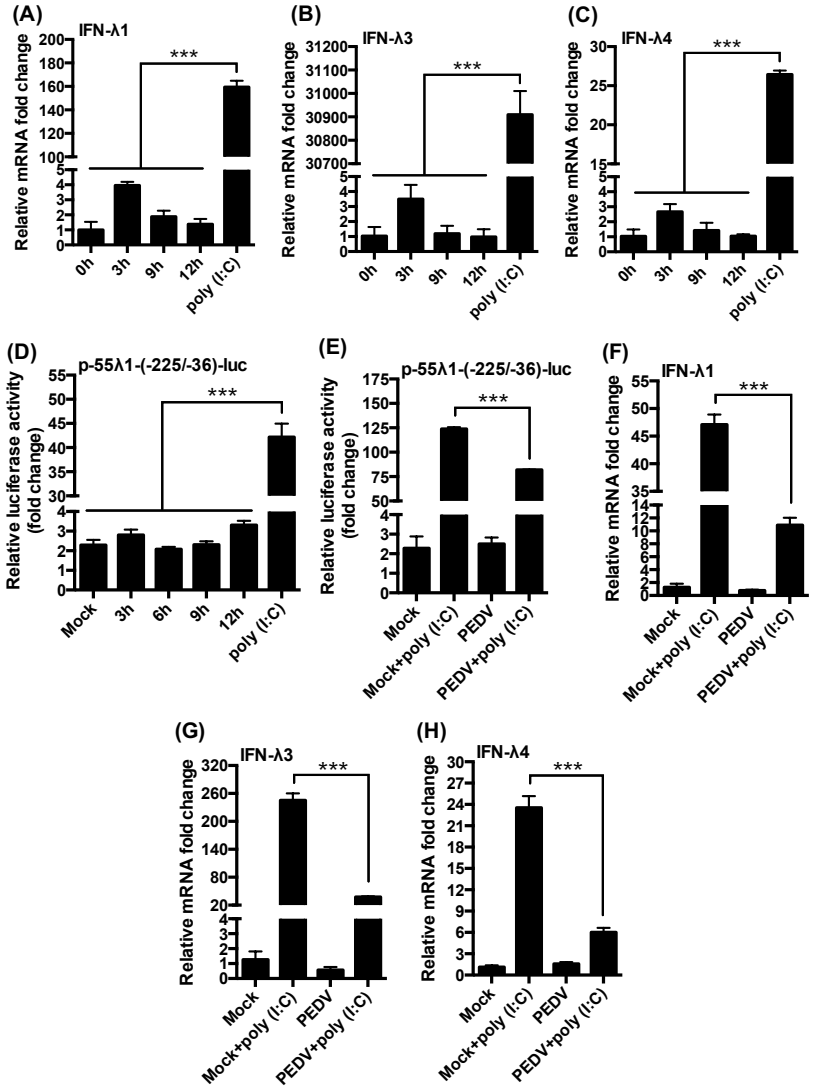

Fig. 4.3: Inhibition of type III IFN production by PEDV. (A)-(C), PEDV does not induce type III IFN production in intestinal epithelial cells. IPEC-DQ cells were infected with PEDV at an MOI of 5, and total cellular RNA was prepared at indicated times post-infection to determine the type III IFN mRNA by RT-qPCR. (D), PEDV does not activate IFN-λ1 promoter. MARC-145 cells were grown in 12-well plates and cotransfected with p-55λ1-(-225/-36)-Luc and pRL-TK for 6 h followed by PEDV infection at an MOI of 1. Cells were harvested at 3, 6, 9, and 12 h postinfection for dual-luciferase reporter assays. Mock-infected cells transfected with poly(I:C) for 12 h were used as a positive control. (E), PEDV inhibits IFN-λ1 promoter. MARC-145 cells were grown in 12-well plates and transfected with p-55λ1-(-225/-36)-Luc for 6 h followed by infection. The gene-transfected and PEDV-inoculated cells were then stimulated with poly(I:C) for 12 h, and cell lysates were prepared for dual-luciferase reporter assays. (F)-(H), PEDV suppresses the induction of type III IFN mRNA as determined by RT-qPCR. LLC-PK1 cells were grown in 12-well plates for infection for 12 h and then stimulated with poly(I:C) for 12 h. Total cellular RNA was prepared for RT-qPCR. Results were obtained from three independent experiments in triplicate each and were presented as mean values with standard deviation. Asterisks indicate statistical significance. *, $P<0.05$; **, $P<0.01$; ***, $P<0.001$.

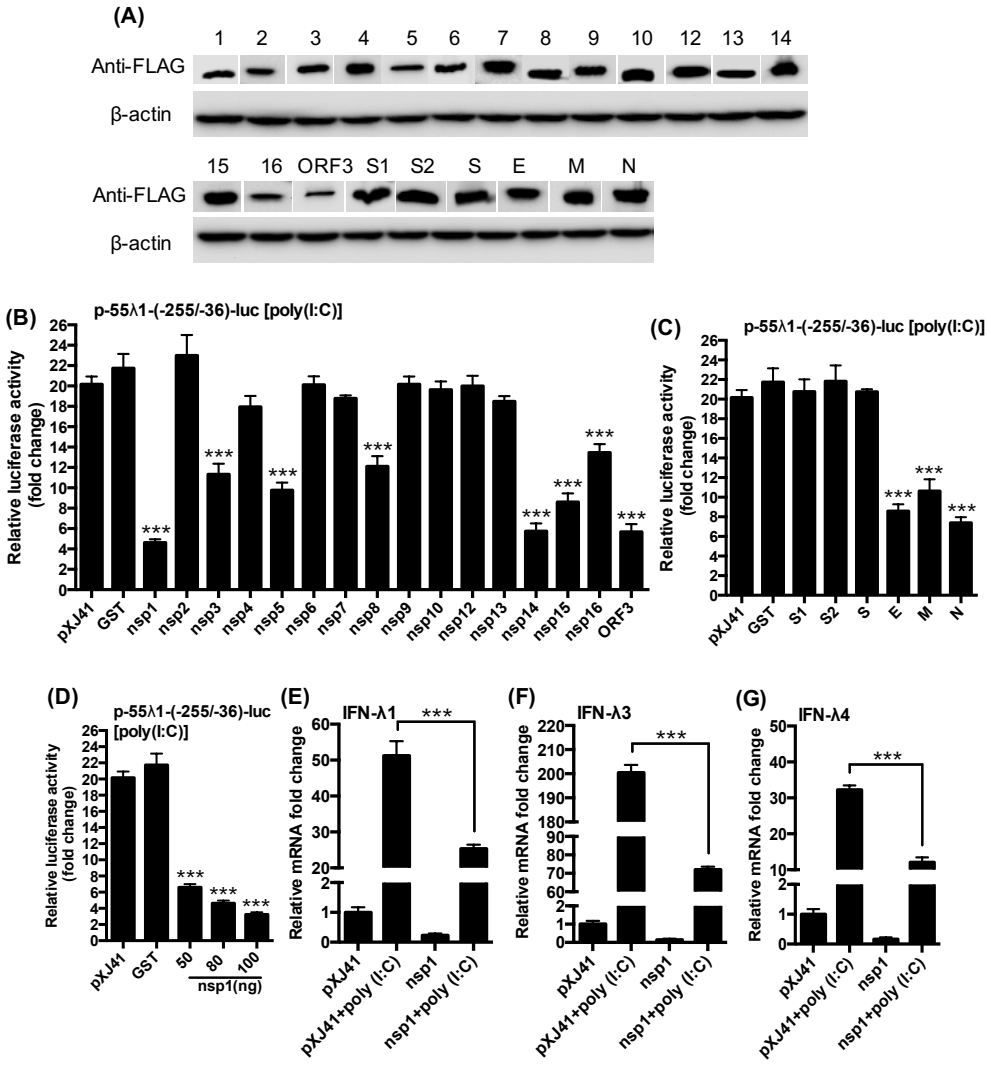

Fig. 4.4: Identification of PEDV nsp1 as a potent type III IFN antagonist. (A), Expression of individually cloned PEDV proteins in gene-transfected cells. Each gene was transfected to HeLa cells and the protein expression was determined by Western blot using anti-FLAG antibody. Transfection was conducted as described previously (Zhang et al., 2016). Numbers indicate respective nonstructural proteins representing nsp1 through nsp16. (B)-(C), Suppression of IFN-λ1 promoter activity by an individual PEDV protein. HeLa cells were grown in 24-well plates and cotransfected with p-55λ1-(-225/-36)-Luc and different PEDV genes along with pRL-TK at the ratio of 1:1:0.1. At 12 h posttransfection, cells were stimulated with poly(I:C) (0.5 μg/ml) for 12 h and the luciferase activities were measured. (D), Dose-dependent inhibition of IFN-λ1 promoter activity by PEDV nsp1. HeLa cells were grown in 24-well plates and cotransfected with p-55λ1-(-225/-36)-Luc along with pRL-TK at the ratio of 1:0.1 with an increasing amount of PEDV nsp1 gene. At 12 h post-transfection, cells were stimulated with poly(I:C) (0.5 μg/ml) for 12 h and the luciferase activities were measured. The pXJ41 empty vector was used as a control. (E)-(G), Suppression of type III IFN production by PEDV nsp1. LLC-PK1 cells were grown in the 12-well plates and transfected with the pXJ41 empty vector or PEDV nsp1 gene for 12 h. Cells were then stimulated with poly(I:C) for 12 h. Total cellular RNA was prepared for RT-qPCR to determine mRNAs for IFN-λ1 (E), IFN-λ3 (F), IFN-λ4 (G). Results were normalized using β-actin mRNA and expressed as relative changes in mRNA levels to those in cells without stimulation. Data were obtained from three independent experiments, each in triplicate.

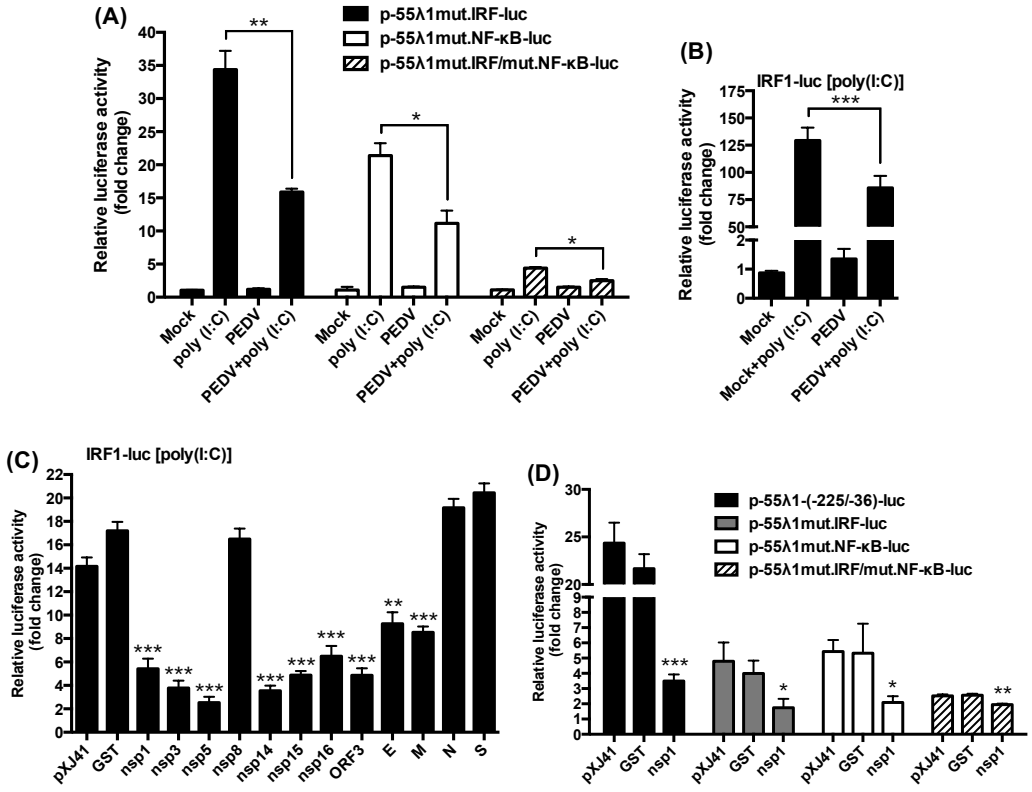

Fig. 4.5: Suppression of IFN-λ1 is mediated via IRF and NF-κB interference. (A), Suppression of IRF- and NF-κB-mediated IFN-λ1 activity by PEDV. MARC-145 cells were transfected with p-55λ1mut.IRF-Luc, p-55λ1mut.NF-κB -Luc, or p-55λ1mut.IRF/mut.NF-κB-Luc for 6 h and infected with PEDV at an MOI of 1 for 12 h. Cells were then stimulated with poly(I:C) for 12 h, and cell lysates were prepared for dual-luciferase reporter assays. (B), PEDV blocks IRF1 activation. MARC-145 cells were transfected with pIRF1-Luc and infected with PEDV for dual-luciferase reporter assays. (C), Identification of IRF1 antagonists. HeLa cells were grown in 24-well plates and cotransfected with pIRF1-Luc, along with an individual PEDV gene and pRL-TK at the ratio of 1:1:0.1. At 12 h posttransfection, cells were stimulated with poly(I:C) and the luciferase activities were measured. (D), Inhibition of IFN-λ1 activity is mediated by IRF and NF-κB interference. HeLa cells were co-transfected with p-55λ1-(-225/-36)-Luc or its mutants along with PEDV nsp1 gene for dual luciferase assay. The reporter experiments were repeated three times, each time in triplicate. Asterisks indicate the statistical significance using the pXJ41 empty vector as a control. *, $P<0.05$; **, $P<0.01$; ***, $P<0.001$.

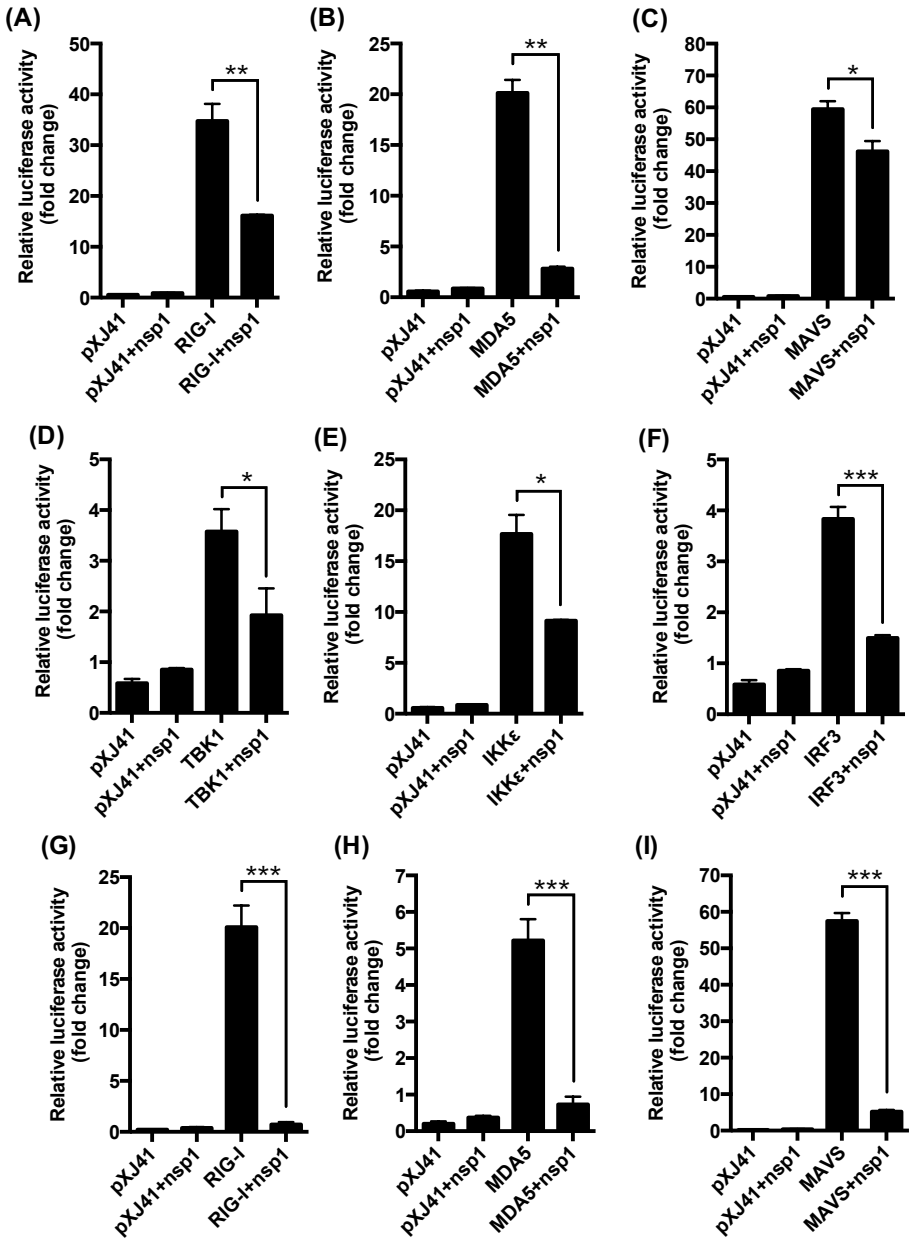

Fig. 4.6: Inhibition of RIG-I/MDA5-mediated IFN-λ1 and IRF1 activities by nsp1. (A)-(F), Inhibition of RIG-I/MDA5-mediated IFN-λ1 activation by nsp1. HeLa cells were cotransfected with an active form of RIG-I (A), MDA5 (B), MAVS (C), TBK1 (D), IKKε (E), or IRF3 (F), along with the nsp1 gene and the p-55λ1-(-225/-36)-Luc reporter. Cell lysates were prepared to measure the luciferase activities. (G)-(I), PEDV nsp1 inhibits RIG-I/MDA5-mediated IRF1 activation. HeLa cells were cotransfected with an active form of RIG-I (G), MDA5 (H), or MAVS (I), along with the nsp1 gene and IRF1-Luc reporter for luciferase assays.

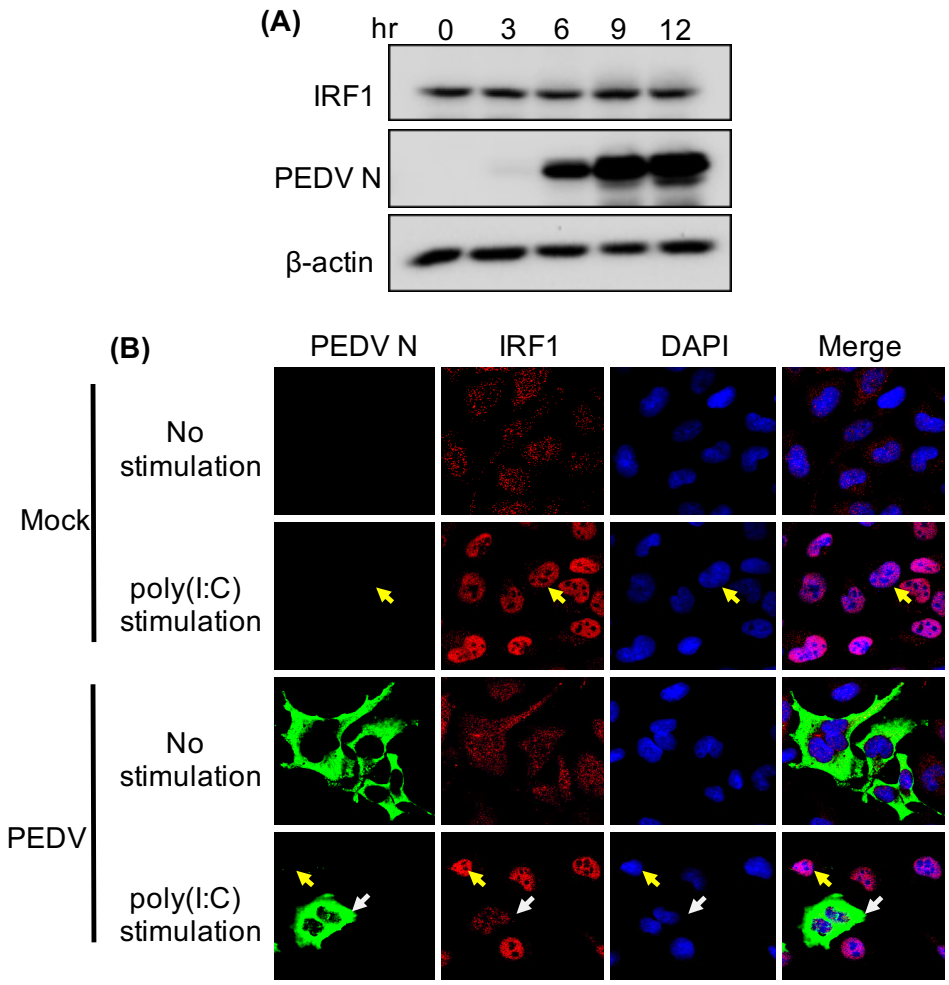

Fig. 4.7: Inhibition of IRF1 nuclear translocation by PEDV and nsp1. (A), IPEC-DQ cells grown in 12-well plates were infected with PEDV at 5 MOI, and lysed at indicated times for detection of IRF1 and PEDV N protein by Western blot. (B), PEDV blocks IRF1 nuclear translocation. IPEC-DQ cells were grown on coverslips and infected with PEDV for 12 h followed by stimulation with poly(I:C). Cells were then fixed and stained with anti-N antibody and anti-IRF1 antibody. Nuclei were stained with DAPI. Yellow arrows indicate IRF1 in the nucleus, and white arrows indicate IRF1 in the cytoplasm. (C), Inhibition of IRF1 nuclear translocation by PEDV nsp1. IPEC-DQ cells grown on coverslips were transfected with the PEDV nsp1 gene and then stimulated with poly(I:C). Cells were then fixed and stained with anti-Flag antibody and anti-IRF1 antibody. Yellow arrows indicate IRF1 in the nucleus after stimulation in the absence of nsp1 expression. White arrows indicate IRF1 in the cytoplasm in nsp1-expressing cells.

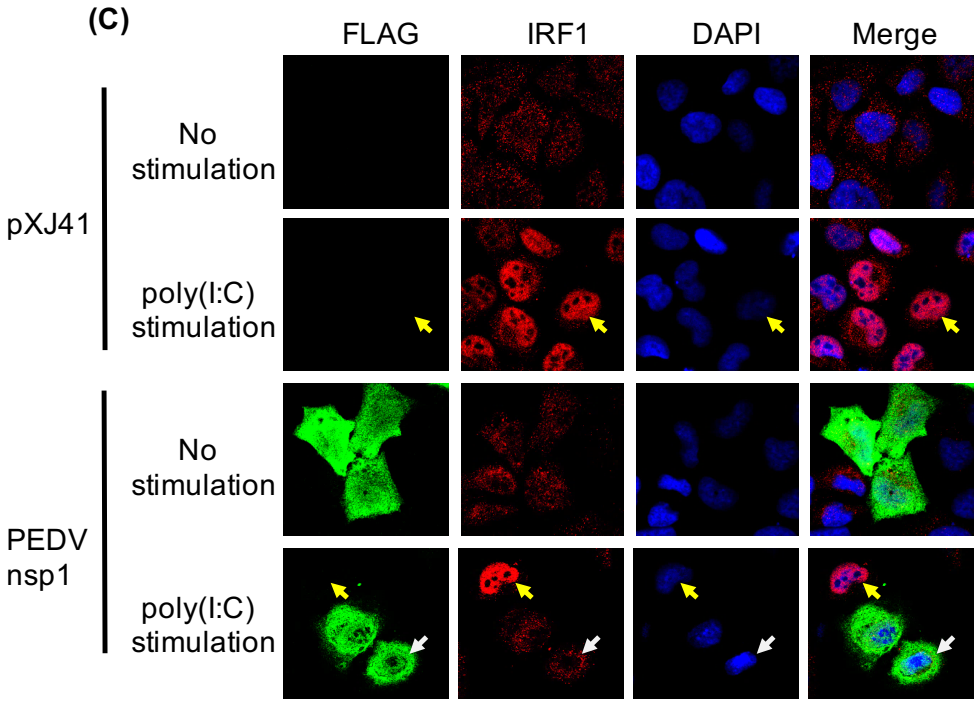
(C)
FLAG
IRF1
DAPI
Merge
pXJ41
No stimulation
poly(I:C) stimulation
PEDV nsp1
No stimulation
poly(I:C) stimulation

Fig. 4.7 (cont.)

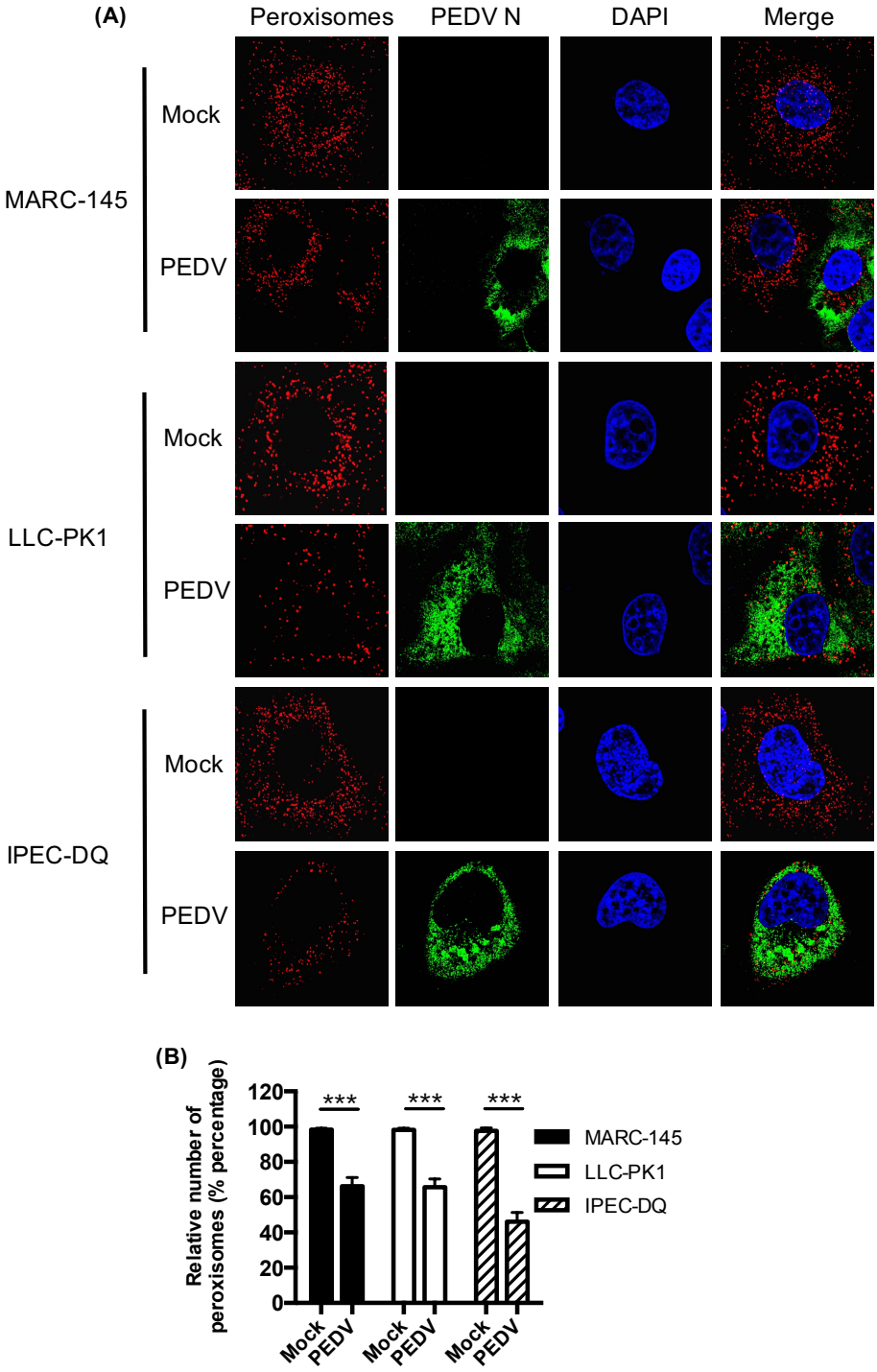

Fig. 4.8: Peroxisomes are decreased in number in PEDV-infected cells. (A), The reduction of peroxisomes in PEDV-infected cells. MARC-145, LLC-PK1, and IPEC-DQ cells grown on coverslips were infected with PEDV for 24 h and incubated with anti-PMP70 (peroxisome marker) antibody and anti-N antibody for immunostaining. (B), The relative numbers of peroxisomes in PEDV-infected cells. The number of peroxisomes in PEDV-infected cells was compared to that of non-infected cells. One hundred fifty PEDV-infected cells were randomly chosen, and the number of peroxisomes was quantified per cell. Asterisks indicate statistical significance. *, $P<0.05$; **, $P<0.01$; ***, $P<0.001$.

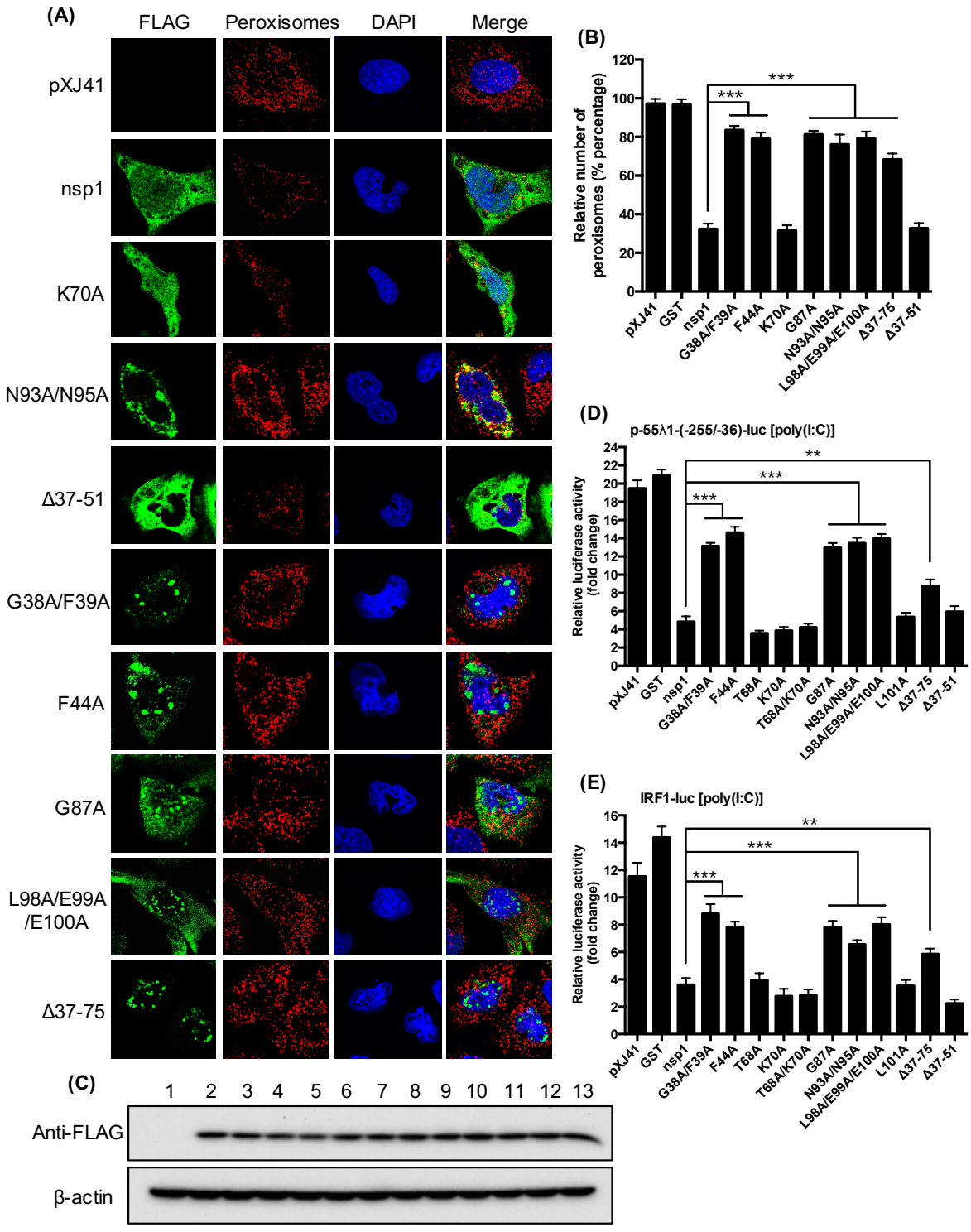
(A)
FLAG
Peroxisomes
DAPI
Merge
pXJ41
nsp1
K70A
N93A/N95A
Δ37-51
G38A/F39A
F44A
G87A
L98A/E99A
/E100A
Δ37-75
(B)
Relative number of peroxisomes (% percentage)
pXJ41
GST
nsp1
G38A/F39A
F44A
K70A
G87A
N93A/N95A
L98A/E99A/E100A
Δ37-75
Δ37-51
(C)
1 2 3 4 5 6 7 8 9 10 11 12 13
Anti-FLAG
β-actin
(D)
p-55λ1-(-255/-36)-luc [poly(I:C)]
Relative luciferase activity (fold change)
T68A
T68A/K70A
L101A
(E)
IRF1-luc [poly(I:C)]

Fig. 4.9 (cont.)

Fig. 4.9 (conti.): Conserved residues of nsp1 are crucial for the reduction of peroxisomes and IFN-λ suppression. (A), Conserved residues of nsp1 are critical for the reduction of peroxisomes. IPEC-DQ cells were grown on coverslips and transfected with the PEDV nsp1 gene or one of its mutants for 24 h. Cells were then stained with anti-PMP70 (peroxisome marker) and anti-FLAG antibody for 1 h. Alexa Fluor 594-conjugated goat anti-rabbit antibody and 488-conjugated goat anti-mouse secondary antibody were used to visualize peroxisomes and nsp1, respectively. Nuclei were stained with DAPI. (B), The relative number percentages of peroxisomes in nsp1-expressing cells. The number of peroxisomes in nsp1-expressing cells was compared to that in pXJ41-transfected cells. One hundred fifty nsp1-expressing cells were randomly chosen, and numbers of peroxisomes were quantified. (C), Expression levels of PEDV wild-type nsp1 and its mutants in gene-transfected cells. HeLa cells were cotransfected with either p-55λ1-(-225/-36)-Luc or IRF1-Luc with each mutant of nsp1. After stimulation with poly(I:C), cell lysates were prepared for Western blot with anti-FLAG antibody to individual mutant of nsp1. Lanes 1 through 13 represent empty vector pXJ41, wild-type nsp1, G38A/F39A, F44A, T68A, K70A, T68A/K70A, G87A, N93A/N95A, L98A/E99A/E100A, L101A, Δ37-75, and Δ37-51, respectively. β-actin was as a loading control. (D)-(E), Conserved residues in nsp1 are crucial for IFN-λ suppression. HeLa cells were cotransfected with p-55λ1-(-225/-36)-Luc (panel D) or IRF1-Luc (panel E), along with a nsp1 mutant. Cells were then stimulated with poly(I:C), and cell lysates were prepared to measure the luciferase activities. Data were obtained from three independent experiments and are presented as the mean values with standard deviation. Asterisks indicate the statistical significance with relative luciferase value of nsp1. *, $P<0.05$; **, $P<0.01$; ***, $P<0.001$.

Table 4.1: Real-time PCR primer sets for cytokine genes used in this study.

Gene	Forward primer (5'-3')	Reverse primer (5'-3')	Accession no./References
IFN-λ1	GGTGCTGGCGACTGTGATG	GATTGGAACTGGCCCATGTG	Wang et al., 2011
IFN-λ3	ACTTGGCCCAGTTCAAGTCT	CATCCTTGGCCCTCTTGA	FJ853389.1
IFN-λ4	GCTATGGGACTGTGGGTCTT	AGGGAGCGGTAGTGAGAGAG	NC_010456.4
N	GCAGCAAGTGTCCTAAAGAAGCA	GCTTGGGTTCTGCACAGATCT	KF272920
β-actin	ATCGTGCGTGACATTAAG	ATTGCCAATGGTGATGAC	Zhang et al., 2016

CHAPTER 5: GENERAL CONCLUSION

Innate immunity forms the first line of host defense to restrict the viral infections. Among many cytokines, type I and type III IFNs carry the antiviral activities and are the major components of the antiviral innate immunity. In turn, viruses have evolved to modulate the cellular signaling processes and pathways to evade host innate immunity. PEDV appears to evade the type I IFN response in multiple ways for efficient replication. PLP2 (papain-like proteinase 2) of PEDV antagonizes the type I IFN response by deubiquitinating RIG-I and STING, and PEDV N protein suppresses the IRF3 and NF-κB activities and antagonizes the IFN-β production by disrupting the interaction between IRF3 and TBK1. PEDV nsp5 protein cleaves NEMO for suppression of NF-κB-mediated type I IFN production. It is unknown whether PEDV encodes additional IFN antagonists and their mechanism of action.

In the present study, we first identified MARC-145 cells as susceptible cells for PEDV replication. These cells have an intact IFN signaling system, and during infection of these cells, PEDV suppresses IFN-β production. Of all PEDV proteins, ten viral proteins inhibit the IFN-β and IRF3 promoter activities. Coronavirus nsp1 is the N-terminal cleavage product of polyproteins and is one of the most divergent genes among four different genera. The nsp1 protein of β-CoV is a potent IFN antagonist, and interestingly, PEDV nsp1 is also the potent IFN antagonist. PEDV nsp1 does not interfere the IRF3 phosphorylation and nuclear translocation, but interrupts the enhanceosome assembly of IRF3 and CREB-binding protein (CBP). PEDV induces the CBP degradation in virus-infected cells and PEDV nsp1 degrades CBP in the nucleus in a proteasome-dependent manner. The degradation of CBP is a novel mechanism for coronavirus and likely plays a key role for suppression of type I IFN production by PEDV.

Despite the importance of NF-κB during infection, regulation of NF-κB by PEDV is poorly understood. It is unclear whether it is time-dependent and TNFα-mediated. PEDV inhibits both NF-κB activities and early production of proinflammatory cytokines in the porcine epithelial cell model. PEDV does not induce the p65 activation in infected cells and but inhibits the p65 nuclear localization after TNFα stimulation. PEDV also blocks the PRD II-mediated NF-κB activity. Among the PEDV proteins, nsp1, nsp3, nsp5, nsp7, nsp14, nsp15, nsp16, ORF3, and E have been identified as NF-κB antagonists, and nsp1 is the most potent suppressor of proinflammatory cytokines. Nsp1 interferes the phosphorylation and degradation of IκBα, and thus blocks the p65 activation. PEDV nsp1 does not interfere the IKKα/β phosphorylation. The expression of IKKα/β is stable, and the phosphorylation of IKKα/β normally occurs in nsp1-expressing cells, which indicates that the antagonism occurs between IKKα/β and IκBα. Mutational studies demonstrate the essential requirements of the conserved residues of nsp1 for NF-κB suppression. The nsp1-mediated NF-κB modulation may facilitate the replication and pathogenesis of PEDV.

Accumulating data show that type III interferons (IFN-λs) play a crucial role in the intestinal antiviral state, and in turn, enteric viruses may have evolved to evade the type III IFN response during infection. PEDV targets intestinal epithelial cells (IEC) *in vivo,* and IECs induce and selectively respond to type III IFNs. We have first developed a line of porcine intestinal epithelial cells (IPEC-DQ) as a cell model for PEDV replication. Both IFN-λ1 and IFN-λ3 inhibit PEDV replication in a dose-dependent manner, indicating the anti-PEDV activity of type III IFNs. Eleven PEDV proteins suppress the type III IFN activities. PEDV specifically inhibits IRF1 nuclear translocation. Peroxisomes are the innate antiviral signaling platforms for activation of IRF1-mediated IFN-λ production, and PEDV reduces the peroxisomes in number in

PEDV-infected cells. PEDV nsp1 blocks the nuclear translocation of IRF1 and reduces the number of peroxisomes to suppress the IRF1-mediated type III IFN. The conserved residues of nsp1 are crucial for IRF1-mediated IFN-λ suppression.

In summary, we have shown that PEDV inhibits the production of both type I and type III IFNs, and that their mechanisms of action differ. PEDV induces the degradation of CBP in the nucleus and inhibits the NF-κB activation for suppression of both type I IFNs and proinflammatory cytokines. PEDV reduces the number of peroxisomes for suppression of IRF1-mediated type III IFN production in intestinal epithelial cells. PEDV nsp1 is a potent IFN antagonist for IRF1, IRF3, IRF7, and NF-κB, and conserved residues are crucial for this action. These studies are of great value to facilitate the design of new strategies for control of not only PED, but also other enteric viral infections.

REFERENCES

Aich, P., Wilson, H.L., Kaushik, R.S., Potter, A.A., Babiuk, L.A., Griebel, P., 2007. Comparative analysis of innate immune responses following infection of newborn calves with bovine rotavirus and bovine coronavirus. J. Gen. Virol. 88, 2749-2761.

Albina, E., Carrat, C., Charley, B., 1998. Interferon-alpha response to swine arterivirus (PoAV), the porcine reproductive and respiratory syndrome virus. J. Interferon Cytokine Res. 18, 485-490.

Alonso, S., Izeta, A., Sola, I., Enjuanes, L., 2002. Transcription regulatory sequences and mRNA expression levels in the coronavirus transmissible gastroenteritis virus. J. Virol. 76, 1293-1308.

An, K., Fang, L., Luo, R., Wang, D., Xie, L., Yang, J., Chen, H., Xiao, S., 2014. Quantitative proteomic analysis reveals that transmissible gastroenteritis virus activates the JAK-STAT1 signaling pathway. J. Proteome Res. 13, 5376-5390.

Angel, J., Franco, M.A., Greenberg, H.B., Bass, D., 1999. Lack of a role for type I and type II interferons in the resolution of rotavirus-induced diarrhea and infection in mice. J. Interferon Cytokine Res. 19, 655-659.

Angelini, M.M., Akhlaghpour, M., Neuman, B.W., Buchmeier, M.J., 2013. Severe acute respiratory syndrome coronavirus nonstructural proteins 3, 4, and 6 induce double-membrane vesicles. MBio 4, e00524-13.

Ank, N., Iversen, M.B., Bartholdy, C., Staeheli, P., Hartmann, R., Jensen, U.B., Dagnaes-Hansen, F., Thomsen, A.R., Chen, Z., Haugen, H., Klucher, K., Paludan, S.R., 2008. An important role for type III interferon (IFN-lambda/IL-28) in TLR-induced antiviral activity. J. Immunol. 180, 2474-2485.

Annamalai, T., Saif, L.J., Lu, Z., Jung, K., 2015. Age-dependent variation in innate immune responses to porcine epidemic diarrhea virus infection in suckling versus weaned pigs. Vet. Immunol. Immunopathol. 168, 193-202.

Baldridge, M.T., Nice, T.J., McCune, B.T., Yokoyama, C.C., Kambal, A., Wheadon, M., Diamond, M.S., Ivanova, Y., Artyomov, M., Virgin, H.W., 2015. Commensal microbes and interferon-lambda determine persistence of enteric murine norovirus infection. Science 347, 266-269.

Bandi, P., Pagliaccetti, N.E., Robek, M.D., 2010. Inhibition of type III interferon activity by orthopoxvirus immunomodulatory proteins. J. Interferon Cytokine Res. 30, 123-134.

Barnes, P.J., Karin, M., 1997. Nuclear factor-kappaB: a pivotal transcription factor in chronic inflammatory diseases. N. Engl. J. Med. 336, 1066-1071.

Baudoux, P., Carrat, C., Besnardeau, L., Charley, B., Laude, H., 1998. Coronavirus pseudoparticles formed with recombinant M and E proteins induce alpha interferon synthesis by leukocytes. J. Virol. 72, 8636-8643.

Beall, A., Yount, B., Lin, C.M., Hou, Y., Wang, Q., Saif, L., Baric, R., 2016. Characterization of a pathogenic full-length cDNA clone and transmission model for porcine epidemic diarrhea virus strain PC22A. MBio 7, e01451-15.

Bedford, D.C., Brindle, P.K., 2012. Is histone acetylation the most important physiological function for CBP and p300? Aging 4, 247-255.

Blackwell, T.S., Christman, J.W., 1997. The role of nuclear factor-kappa B in cytokine gene regulation. Am. J. Respir. Cell Mol. Biol. 17, 3-9.

Boddy, M.N., Howe, K., Etkin, L.D., Solomon, E., Freemont, P.S., 1996. PIC 1, a novel ubiquitin-like protein which interacts with the PML component of a multiprotein complex that is disrupted in acute promyelocytic leukaemia. Oncogene 13, 971-982.

Boehme, K.W., Compton, T., 2004. Innate sensing of viruses by toll-like receptors. J. Virol. 78, 7867-7873.

Boisvert, F.M., Kruhlak, M.J., Box, A.K., Hendzel, M.J., Bazett-Jones, D.P., 2001. The transcription coactivator CBP is a dynamic component of the promyelocytic leukemia nuclear body. J. Cell Biol. 152, 1099-1106.

Bosch, B.J., van der Zee, R., de Haan, C.A., Rottier, P.J., 2003. The coronavirus spike protein is a class I virus fusion protein: structural and functional characterization of the fusion core complex. J. Virol. 77, 8801-8811.

Bosworth, B.T., MacLachlan, N.J., Johnston, M.I., 1989. Induction of the 2-5A system by interferon and transmissible gastroenteritis virus. J. Interferon Res. 9, 731-739.

Brian, D.A., Baric, R.S., 2005. Coronavirus genome structure and replication. Curr. Top. Microbiol. Immunol. 287, 1-30.

Brockway, S.M., Lu, X.T., Peters, T.R., Dermody, T.S., Denison, M.R., 2004. Intracellular localization and protein interactions of the gene 1 protein p28 during mouse hepatitis virus replication. J. Virol. 78, 11551-11562.

Calzada-Nova, G., Schnitzlein, W., Husmann, R., Zuckermann, F.A., 2010. Characterization of the cytokine and maturation responses of pure populations of porcine plasmacytoid dendritic cells to porcine viruses and toll-like receptor agonists. Vet. Immunol. Immunopathol. 135, 20-33.

Campbell, K.J., Perkins, N.D., 2006. Regulation of NF-kappaB function. Biochem. Soc. Symp. 73, 165-180.

Cantell, K., Hirvonen, S., Kauppinen, H.L., Myllyla, G., 1981. Production of interferon in human leukocytes from normal donors with the use of Sendai virus. Methods Enzymol. 78, 29-38.

Cao, L., Ge, X., Gao, Y., Herrler, G., Ren, Y., Ren, X., Li, G., 2015a. Porcine epidemic diarrhea virus inhibits dsRNA-induced interferon-beta production in porcine intestinal epithelial cells by blockade of the RIG-I-mediated pathway. Virol. J. 12, 127.

Cao, L., Ge, X., Gao, Y., Ren, Y., Ren, X., Li, G., 2015b. Porcine epidemic diarrhea virus infection induces NF-kappaB activation through the TLR2, TLR3, and TLR9 pathways in porcine intestinal epithelial cells. J. Gen. Virol. 96, 1757-1767.

Cervantes-Barragan, L., Zust, R., Weber, F., Spiegel, M., Lang, K.S., Akira, S., Thiel, V., Ludewig, B., 2007. Control of coronavirus infection through plasmacytoid dendritic-cell-derived type I interferon. Blood 109, 1131-1137.

Charley, B., Laude, H., 1988. Induction of alpha interferon by transmissible gastroenteritis coronavirus: role of transmembrane glycoprotein E1. J. Virol. 62, 8-11.

Charley, B., Riffault, S., Van Reeth, K., 2006. Porcine innate and adaptative immune responses to influenza and coronavirus infections. Ann. N. Y. Acad. Sci. 1081, 130-136.

Chen, H., Kinzer, C.A., Paul, W.E., 1996. p161, a murine membrane protein expressed on mast cells and some macrophages, is mouse CD13/aminopeptidase N. J. Immunol. 157, 2593-2600.

Chen, J., Liu, X., Shi, D., Shi, H., Zhang, X., Li, C., Chi, Y., Feng, L., 2013. Detection and molecular diversity of spike gene of porcine epidemic diarrhea virus in China. Viruses 5, 2601-2613.

Chen, Q., Gauger, P., Stafne, M., Thomas, J., Arruda, P., Burrough, E., Madson, D., Brodie, J., Magstadt, D., Derscheid, R., Welch, M., Zhang, J., 2015. Pathogenicity and pathogenesis of a United States porcine deltacoronavirus cell culture isolate in 5-day-old neonatal piglets. Virology 482, 51-59.

Chen, Q., Li, G., Stasko, J., Thomas, J.T., Stensland, W.R., Pillatzki, A.E., Gauger, P.C., Schwartz, K.J., Madson, D., Yoon, K.J., Stevenson, G.W., Burrough, E.R., Harmon, K.M., Main, R.G., Zhang, J., 2014. Isolation and characterization of porcine epidemic diarrhea viruses associated with the 2013 disease outbreak among swine in the United States. J. Clin. Microbiol. 52, 234-243.

Chen, X., Yang, X., Zheng, Y., Yang, Y., Xing, Y., Chen, Z., 2014. SARS coronavirus papain-like protease inhibits the type I interferon signaling pathway through interaction with the STING-TRAF3-TBK1 complex. Protein Cell 5, 369-381.

Cinatl, J., Jr., Michaelis, M., Scholz, M., Doerr, H.W., 2004. Role of interferons in the treatment of severe acute respiratory syndrome. Expert Opin. Biol. Ther. 4, 827-836.

Clementz, M.A., Chen, Z., Banach, B.S., Wang, Y., Sun, L., Ratia, K., Baez-Santos, Y.M., Wang, J., Takayama, J., Ghosh, A.K., Li, K., Mesecar, A.D., Baker, S.C., 2010. Deubiquitinating and interferon antagonism activities of coronavirus papain-like proteases. J. Virol. 84, 4619-4629.

Cohen, G.B., Rangan, V.S., Chen, B.K., Smith, S., Baltimore, D., 2000. The human thioesterase II protein binds to a site on HIV-1 Nef critical for CD4 down-regulation. J. Biol. Chem. 275, 23097-23105.

Colomer-Lluch, M., Serra-Moreno, R., 2017. BCA2/RABRING7 interferes with HIV-1 proviral transcription by enhancing the sumoylation of IkappaBalpha. J. Virol. 91, e02098-16.

Cong, Y., Li, X., Bai, Y., Lv, X., Herrler, G., Enjuanes, L., Zhou, X., Qu, B., Meng, F., Cong, C., Ren, X., Li, G., 2015. Porcine aminopeptidase N mediated polarized infection by porcine epidemic diarrhea virus in target cells. Virology 478, 1-8.

Connor, R.F., Roper, R.L., 2007. Unique SARS-CoV protein nsp1: bioinformatics, biochemistry and potential effects on virulence. Trends Microbiol. 15, 51-53.

Cruz, J.L., Becares, M., Sola, I., Oliveros, J.C., Enjuanes, L., Zuniga, S., 2013. Alphacoronavirus protein 7 modulates host innate immune response. J. Virol. 87, 9754-9767.

Cruz, J.L., Sola, I., Becares, M., Alberca, B., Plana, J., Enjuanes, L., Zuniga, S., 2011. Coronavirus gene 7 counteracts host defenses and modulates virus virulence. PLoS Pathog. 7, e1002090.

de Los Santos, T., de Avila Botton, S., Weiblen, R., Grubman, M.J., 2006. The leader proteinase of foot-and-mouth disease virus inhibits the induction of beta interferon mRNA and blocks the host innate immune response. J. Virol. 80, 1906-1914.

Deal, E.M., Lahl, K., Narvaez, C.F., Butcher, E.C., Greenberg, H.B., 2013. Plasmacytoid dendritic cells promote rotavirus-induced human and murine B cell responses. J. Clin. Invest. 123, 2464-2474.

Debouck, P., Pensaert, M., 1980. Experimental infection of pigs with a new porcine enteric coronavirus, CV 777. Am. J. Vet. Res. 41, 219-223.

Dedeurwaerder, A., Olyslaegers, D.A., Desmarets, L.M., Roukaerts, I.D., Theuns, S., Nauwynck, H.J., 2014. ORF7-encoded accessory protein 7a of feline infectious peritonitis virus as a counteragent against IFN-alpha-induced antiviral response. J. Gen. Virol. 95, 393-402.

Delmas, B., Gelfi, J., L'Haridon, R., Vogel, L.K., Sjostrom, H., Noren, O., Laude, H., 1992. Aminopeptidase N is a major receptor for the entero-pathogenic coronavirus TGEV. Nature 357, 417-420.

Desmyter, J., Melnick, J.L., Rawls, W.E., 1968. Defectiveness of interferon production and of rubella virus interference in a line of African green monkey kidney cells (Vero). J. Virol. 2, 955-961.

Desterro, J.M., Rodriguez, M.S., Hay, R.T., 1998. SUMO-1 modification of IkappaBalpha inhibits NF-kappaB activation. Mol. Cell 2, 233-239.

Diebold, S.S., Kaisho, T., Hemmi, H., Akira, S., Reis e Sousa, C., 2004. Innate antiviral responses by means of TLR7-mediated recognition of single-stranded RNA. Science 303, 1529-1531.

Ding, L., Huang, Y., Du, Q., Dong, F., Zhao, X., Zhang, W., Xu, X., Tong, D., 2014a. TGEV nucleocapsid protein induces cell cycle arrest and apoptosis through activation of p53 signaling. Biochem. Biophys. Res. Commun. 445, 497-503.

Ding, Z., Fang, L., Jing, H., Zeng, S., Wang, D., Liu, L., Zhang, H., Luo, R., Chen, H., Xiao, S., 2014. Porcine epidemic diarrhea virus nucleocapsid protein antagonizes beta interferon production by sequestering the interaction between IRF3 and TBK1. J. Virol. 88, 8936-8945.

Dixit, E., Boulant, S., Zhang, Y., Lee, A.S., Odendall, C., Shum, B., Hacohen, N., Chen, Z.J., Whelan, S.P., Fransen, M., Nibert, M.L., Superti-Furga, G., Kagan, J.C., 2010. Peroxisomes are signaling platforms for antiviral innate immunity. Cell 141, 668-681.

Dong, N., Fang, L., Zeng, S., Sun, Q., Chen, H., Xiao, S., 2015. Porcine Deltacoronavirus in Mainland China. Emerg. Infect. Dis. 21, 2254-2255.

Doucas, V., Tini, M., Egan, D.A., Evans, R.M., 1999. Modulation of CREB binding protein function by the promyelocytic (PML) oncoprotein suggests a role for nuclear bodies in hormone signaling. Proc. Natl. Acad. Sci. U. S. A. 96, 2627-2632.

Dragan, A.I., Hargreaves, V.V., Makeyeva, E.N., Privalov, P.L., 2007. Mechanisms of activation of interferon regulator factor 3: the role of C-terminal domain phosphorylation in IRF-3 dimerization and DNA binding. Nucleic acids Res. 35, 3525-3534.

Duarte, M., Gelfi, J., Lambert, P., Rasschaert, D., Laude, H., 1993. Genome organization of porcine epidemic diarrhoea virus. Adv. Exp. Med. Biol. 342, 55-60.

Duvigneau, J.C., Hartl, R.T., Groiss, S., Gemeiner, M., 2005. Quantitative simultaneous multiplex real-time PCR for the detection of porcine cytokines. J. Immunol. Methods 306, 16-27.

Ehrhardt, C., Kardinal, C., Wurzer, W.J., Wolff, T., von Eichel-Streiber, C., Pleschka, S., Planz, O., Ludwig, S., 2004. Rac1 and PAK1 are upstream of IKK-epsilon and TBK-1 in the viral activation of interferon regulatory factor-3. FEBS Lett. 567, 230-238.

Elinav, E., Strowig, T., Kau, A.L., Henao-Mejia, J., Thaiss, C.A., Booth, C.J., Peaper, D.R., Bertin, J., Eisenbarth, S.C., Gordon, J.I., Flavell, R.A., 2011. NLRP6 inflammasome regulates colonic microbial ecology and risk for colitis. Cell 145, 745-757.

Escalante, C.R., Shen, L., Thanos, D., Aggarwal, A.K., 2002. Structure of NF-kappaB p50/p65 heterodimer bound to the PRDII DNA element from the interferon-beta promoter. Structure 10, 383-391.

Everett, R.D., Freemont, P., Saitoh, H., Dasso, M., Orr, A., Kathoria, M., Parkinson, J., 1998. The disruption of ND10 during herpes simplex virus infection correlates with the

Vmw110- and proteasome-dependent loss of several PML isoforms. J. Virol. 72, 6581-6591.
Fang, X., Gao, J., Zheng, H., Li, B., Kong, L., Zhang, Y., Wang, W., Zeng, Y., Ye, L., 2007. The membrane protein of SARS-CoV suppresses NF-kappaB activation. J. Med. Virol. 79, 1431-1439.
Ferrari, R., Gou, D., Jawdekar, G., Johnson, S.A., Nava, M., Su, T., Yousef, A.F., Zemke, N.R., Pellegrini, M., Kurdistani, S.K., Berk, A.J., 2014. Adenovirus small E1A employs the lysine acetylases p300/CBP and tumor suppressor Rb to repress select host genes and promote productive virus infection. Cell Host Microbe 16, 663-676.
Ferreira, A.R., Magalhaes, A.C., Camoes, F., Gouveia, A., Vieira, M., Kagan, J.C., Ribeiro, D., 2016. Hepatitis C virus NS3-4A inhibits the peroxisomal MAVS-dependent antiviral signalling response. J. Cell. Mol. Med. 20, 750-757.
Finkbeiner, S.R., Zeng, X.L., Utama, B., Atmar, R.L., Shroyer, N.F., Estes, M.K., 2012. Stem cell-derived human intestinal organoids as an infection model for rotaviruses. MBio 3, e00159-00112.
Fitzgerald, K.A., McWhirter, S.M., Faia, K.L., Rowe, D.C., Latz, E., Golenbock, D.T., Coyle, A.J., Liao, S.M., Maniatis, T., 2003. IKKepsilon and TBK1 are essential components of the IRF3 signaling pathway. Nat. Immunol. 4, 491-496.
Forrest, J.C., Dermody, T.S., 2003. Reovirus receptors and pathogenesis. J. Virol. 77, 9109-9115.
Frenz, T., Graalmann, L., Detje, C.N., Doring, M., Grabski, E., Scheu, S., Kalinke, U., 2014. Independent of plasmacytoid dendritic cell (pDC) infection, pDC triggered by virus-infected cells mount enhanced type I IFN responses of different composition as opposed to pDC stimulated with free virus. J. Immunol. 193, 2496-2503.
Fu, Y., Quan, R., Zhang, H., Hou, J., Tang, J., Feng, W.H., 2012. Porcine reproductive and respiratory syndrome virus induces interleukin-15 through the NF-kappaB signaling pathway. J. Virol. 86, 7625-7636.
Gallagher, T.M., Buchmeier, M.J., 2001. Coronavirus spike proteins in viral entry and pathogenesis. Virology 279, 371-374.
Gao, Q., Zhao, S., Qin, T., Yin, Y., Yang, Q., 2015. Effects of porcine epidemic diarrhea virus on porcine monocyte-derived dendritic cells and intestinal dendritic cells. Vet. Microbiol. 179, 131-141.
Gao, S., Song, L., Li, J., Zhang, Z., Peng, H., Jiang, W., Wang, Q., Kang, T., Chen, S., Huang, W., 2012. Influenza A virus-encoded NS1 virulence factor protein inhibits innate immune response by targeting IKK. Cell Microbiol. 14, 1849-1866.
Garcia, M.A., Gallego, P., Campagna, M., Gonzalez-Santamaria, J., Martinez, G., Marcos-Villar, L., Vidal, A., Esteban, M., Rivas, C., 2009. Activation of NF-kB pathway by virus infection requires Rb expression. PLoS One 4, e6422.
Ghosh, S., May, M.J., Kopp, E.B., 1998. NF-kappa B and Rel proteins: evolutionarily conserved mediators of immune responses. Annu. Rev. Immunol. 16, 225-260.
Gibbert, K., Schlaak, J.F., Yang, D., Dittmer, U., 2013. IFN-alpha subtypes: distinct biological activities in anti-viral therapy. Br. J. Pharmacol. 168, 1048-1058.
Go, Y.Y., Li, Y., Chen, Z., Han, M., Yoo, D., Fang, Y., Balasuriya, U.B., 2014. Equine arteritis virus does not induce interferon production in equine endothelial cells: identification of nonstructural protein 1 as a main interferon antagonist. Biomed. Res. Int. 2014, 420658.

Goodman, R.H., Smolik, S., 2000. CBP/p300 in cell growth, transformation, and development. Genes Dev. 14, 1553-1577.
Gralinski, L.E., Baric, R.S., 2015. Molecular pathology of emerging coronavirus infections. J. Pathol. 235, 185-195.
Granja, A.G., Nogal, M.L., Hurtado, C., Del Aguila, C., Carrascosa, A.L., Salas, M.L., Fresno, M., Revilla, Y., 2006. The viral protein A238L inhibits TNF-alpha expression through a CBP/p300 transcriptional coactivators pathway. J. Immunol. 176, 451-462.
Gudmundsdottir, I., Risatti, G.R., 2009. Infection of porcine alveolar macrophages with recombinant chimeric porcine reproductive and respiratory syndrome virus: effects on cellular gene transcription and virus growth. Virus Res. 145, 145-150.
Guo, D., Zhu, Q., Zhang, H., Sun. D., 2014. Proteomic analysis of membrane proteins of vero cells: exploration of potential proteins responsible for virus entry. DNA Cell Biol., 33, 20-28.
Guo, L., Luo, X., Li, R., Xu, Y., Zhang, J., Ge, J., Bu, Z., Feng, L., Wang, Y., 2016. Porcine Epidemic Diarrhea Virus Infection Inhibits Interferon Signaling by Targeted Degradation of STAT1. J. Virol. 90, 8281-8292.
Guzylack-Piriou, L., Piersma, S., McCullough, K., Summerfield, A., 2006. Role of natural interferon-producing cells and T lymphocytes in porcine monocyte-derived dendritic cell maturation. Immunology 118, 78-87.
Han, M., Du, Y., Song, C., Yoo, D., 2013. Degradation of CREB-binding protein and modulation of type I interferon induction by the zinc finger motif of the porcine reproductive and respiratory syndrome virus nsp1alpha subunit. Virus Res. 172, 54-65.
Han, M., Yoo, D., 2014. Modulation of innate immune signaling by nonstructural protein 1 (nsp1) in the family Arteriviridae. Virus Res. 194, 100-109.
Hayden, M.S., Ghosh, S., 2012. NF-kappaB, the first quarter-century: remarkable progress and outstanding questions. Genes Dev. 26, 203-234.
Heil, F., Hemmi, H., Hochrein, H., Ampenberger, F., Kirschning, C., Akira, S., Lipford, G., Wagner, H., Bauer, S., 2004. Species-specific recognition of single-stranded RNA via toll-like receptor 7 and 8. Science 303, 1526-1529.
Hermant, P., Michiels, T., 2014. Interferon-lambda in the context of viral infections: production, response and therapeutic implications. J. Innate Immun. 6, 563-574.
Hernandez, P.P., Mahlakoiv, T., Yang, I., Schwierzeck, V., Nguyen, N., Guendel, F., Gronke, K., Ryffel, B., Holscher, C., Dumoutier, L., Renauld, J.C., Suerbaum, S., Staeheli, P., Diefenbach, A., 2015. Interferon-lambda and interleukin 22 act synergistically for the induction of interferon-stimulated genes and control of rotavirus infection. Nat. Immunol. 16, 698-707.
Hoffmann, H.H., Schneider, W.M., Rice, C.M., 2015. Interferons and viruses: an evolutionary arms race of molecular interactions. Trends Immunol. 36, 124-138.
Hofmann, M., Wyler, R., 1988. Propagation of the virus of porcine epidemic diarrhea in cell culture. J. Clin. Microbiol. 26, 2235-2239.
Honda, K., Takaoka, A., Taniguchi, T., 2006. Type I inteferon gene induction by the interferon regulatory factor family of transcription factors. Immunity 25, 349-360.
Honda, K., Taniguchi, T., 2006. IRFs: master regulators of signalling by Toll-like receptors and cytosolic pattern-recognition receptors. Nat. Rev. Immunol. 6, 644-658.

Hsieh, C.S., Macatonia, S.E., Tripp, C.S., Wolf, S.F., O'Garra, A., Murphy, K.M., 1993. Development of TH1 CD4+ T cells through IL-12 produced by Listeria-induced macrophages. Science 260, 547-549.

Huan, C.C., Wang, Y., Ni, B., Wang, R., Huang, L., Ren, X.F., Tong, G.Z., Ding, C., Fan, H.J., Mao, X., 2015. Porcine epidemic diarrhea virus uses cell-surface heparan sulfate as an attachment factor. Arch. Virol. 160, 1621-1628.

Huang, C., Lokugamage, K.G., Rozovics, J.M., Narayanan, K., Semler, B.L., Makino, S., 2011a. Alphacoronavirus transmissible gastroenteritis virus nsp1 protein suppresses protein translation in mammalian cells and in cell-free HeLa cell extracts but not in rabbit reticulocyte lysate. J. Virol. 85, 638-643.

Huang, C., Lokugamage, K.G., Rozovics, J.M., Narayanan, K., Semler, B.L., Makino, S., 2011b. SARS coronavirus nsp1 protein induces template-dependent endonucleolytic cleavage of mRNAs: viral mRNAs are resistant to nsp1-induced RNA cleavage. PLoS Pathog. 7, e1002433.

Huang, C., Zhang, Q., Guo, X.K., Yu, Z.B., Xu, A.T., Tang, J., Feng, W.H., 2014. Porcine reproductive and respiratory syndrome virus nonstructural protein 4 antagonizes beta interferon expression by targeting the NF-kappaB essential modulator. J. Virol. 88, 10934-10945.

Huang, J., Smirnov, S.V., Lewis-Antes, A., Balan, M., Li, W., Tang, S., Silke, G.V., Putz, M.M., Smith, G.L., Kotenko, S.V., 2007. Inhibition of type I and type III interferons by a secreted glycoprotein from Yaba-like disease virus. Proc. Natl. Acad. Sci. U. S. A. 104, 9822-9827.

Huang, Y., Ding, L., Li, Z., Dai, M., Zhao, X., Li, W., Du, Q., Xu, X., Tong, D., 2013. Transmissible gastroenteritis virus infection induces cell apoptosis via activation of p53 signalling. J. Gen. Virol. 94, 1807-1817.

Imanaka, T., Aihara, K., Suzuki, Y., Yokota, S., Osumi, T., 2000. The 70-kDa peroxisomal membrane protein (PMP70), an ATP-binding cassette transporter. Cell. Biochem. Biophys. 32, 131-138.

Ishikawa, H., Barber, G.N., 2008. STING is an endoplasmic reticulum adaptor that facilitates innate immune signaling. Nature 455, 674-678.

Jain, P., Lavorgna, A., Sehgal, M., Gao, L., Ginwala, R., Sagar, D., Harhaj, E.W., Khan, Z.K., 2015. Myocyte enhancer factor (MEF)-2 plays essential roles in T-cell transformation associated with HTLV-1 infection by stabilizing complex between Tax and CREB. Retrovirology 12, 23.

Jansson, A.M., 2013. Structure of alphacoronavirus transmissible gastroenteritis virus nsp1 has implications for coronavirus nsp1 function and evolution. J. Virol. 87, 2949-2955.

Jengarn, J., Wongthida, P., Wanasen, N., Frantz, P.N., Wanitchang, A., Jongkaewwattana, A., 2015. Genetic manipulation of porcine epidemic diarrhoea virus recovered from a full-length infectious cDNA clone. J. Gen. Virol. 96, 2206-2218.

Jennings, S., Martinez-Sobrido, L., Garcia-Sastre, A., Weber, F., Kochs, G., 2005. Thogoto virus ML protein suppresses IRF3 function. Virology 331, 63-72.

Jensen, K., Shiels, C., Freemont, P.S., 2001. PML protein isoforms and the RBCC/TRIM motif. Oncogene 20, 7223-7233.

Jordan, L.T., Derbyshire, J.B., 1994. Antiviral activity of interferon against transmissible gastroenteritis virus in cell culture and ligated intestinal segments in neonatal pigs. Vet. Microbiol. 38, 263-276.

Jordan, L.T., Derbyshire, J.B., 1995. Antiviral action of interferon-alpha against porcine transmissible gastroenteritis virus. Vet. Microbiol. 45, 59-70.
Jung, K., Annamalai, T., Lu, Z., Saif, L.J., 2015a. Comparative pathogenesis of US porcine epidemic diarrhea virus (PEDV) strain PC21A in conventional 9-day-old nursing piglets vs. 26-day-old weaned pigs. Vet. Microbiol. 178, 31-40.
Jung, K., Eyerly, B., Annamalai, T., Lu, Z., Saif, L.J., 2015b. Structural alteration of tight and adherens junctions in villous and crypt epithelium of the small and large intestine of conventional nursing piglets infected with porcine epidemic diarrhea virus. Vet. Microbiol. 177, 373-378.
Jung, K., Hu, H., Eyerly, B., Lu, Z., Chepngeno, J., Saif, L.J., 2015c. Pathogenicity of 2 porcine deltacoronavirus strains in gnotobiotic pigs. Emerg. Infect. Dis. 21, 650-654.
Jung, K., Hu, H., Saif, L.J., 2016. Porcine deltacoronavirus induces apoptosis in swine testicular and LLC porcine kidney cell lines in vitro but not in infected intestinal enterocytes in vivo. Vet. Microbiol. 182, 57-63.
Jung, K., Saif, L.J., 2015. Porcine epidemic diarrhea virus infection: Etiology, epidemiology, pathogenesis and immunoprophylaxis. Vet. J. 204, 134-143.
Jung, K., Wang, Q., Scheuer, K.A., Lu, Z., Zhang, Y., Saif, L.J., 2014. Pathology of US porcine epidemic diarrhea virus strain PC21A in gnotobiotic pigs. Emerg. Infect. Dis. 20, 662-665.
Junwei, G., Baoxian, L., Lijie, T., Yijing, L., 2006. Cloning and sequence analysis of the N gene of porcine epidemic diarrhea virus LJB/03. Virus Genes 33, 215-219.
Kamitani, W., Huang, C., Narayanan, K., Lokugamage, K.G., Makino, S., 2009. A two-pronged strategy to suppress host protein synthesis by SARS coronavirus Nsp1 protein. Nat. Struct. Mol. Biol. 16, 1134-1140.
Kamitani, W., Narayanan, K., Huang, C., Lokugamage, K., Ikegami, T., Ito, N., Kubo, H., Makino, S., 2006. Severe acute respiratory syndrome coronavirus nsp1 protein suppresses host gene expression by promoting host mRNA degradation. Proc. Natl. Acad. Sci. U. S. A. 103, 12885-12890.
Kannan, H., Fan, S., Patel, D., Bossis, I., Zhang, Y.J., 2009. The hepatitis E virus open reading frame 3 product interacts with microtubules and interferes with their dynamics. J. Virol. 83, 6375-6382.
Kariko, K., Ni, H., Capodici, J., Lamphier, M., Weissman, D., 2004. mRNA is an endogenous ligand for Toll-like receptor 3. J. Biol. Chem. 279, 12542-12550.
Kato, H., Takeuchi, O., Mikamo-Satoh, E., Hirai, R., Kawai, T., Matsushita, K., Hiiragi, A., Dermody, T.S., Fujita, T., Akira, S., 2008. Length-dependent recognition of double-stranded ribonucleic acids by retinoic acid-inducible gene-I and melanoma differentiation-associated gene 5. J. Exp. Med. 205, 1601-1610.
Kawai, T., Akira, S., 2010. The role of pattern-recognition receptors in innate immunity: update on Toll-like receptors. Nat. Immunol. 11, 373-384.
Kawai, T., Akira, S., 2011. Toll-like receptors and their crosstalk with other innate receptors in infection and immunity. Immunity 34, 637-650.
Kim, H.S., Kwang, J., Yoon, I.J., Joo, H.S., Frey, M.L., 1993. Enhanced replication of porcine reproductive and respiratory syndrome (PRRS) virus in a homogeneous subpopulation of MA-104 cell line. Arch. Virol. 133, 477-483.
Kim, L., Hayes, J., Lewis, P., Parwani, A.V., Chang, K.O., Saif, L.J., 2000. Molecular characterization and pathogenesis of transmissible gastroenteritis coronavirus (TGEV)

and porcine respiratory coronavirus (PRCV) field isolates co-circulating in a swine herd. Arch. Virol. 145, 1133-1147.
Kim, O., Sun, Y., Lai, F.W., Song, C., Yoo, D., 2010. Modulation of type I interferon induction by porcine reproductive and respiratory syndrome virus and degradation of CREB-binding protein by non-structural protein 1 in MARC-145 and HeLa cells. Virology 402, 315-326.
Kim, S.J., Han, Y.W., Rahman, M.M., Kim, S.B., Uyangaa, E., Lee, B.M., Kim, J.H., Roh, Y.S., Kang, S.H., Kim, K., Lee, J.H., Kim, B., Park, K.I., Eo, S.K., 2010. Live attenuated Salmonella enterica serovar Typhimurium expressing swine interferon-alpha has antiviral activity and alleviates clinical signs induced by infection with transmissible gastroenteritis virus in piglets. Vaccine 28, 5031-5037.
Kim, Y., Lee, C., 2014. Porcine epidemic diarrhea virus induces caspase-independent apoptosis through activation of mitochondrial apoptosis-inducing factor. Virology 460-461, 180-193.
Kim, Y., Lee, C., 2015. Extracellular signal-regulated kinase (ERK) activation is required for porcine epidemic diarrhea virus replication. Virology 484, 181-193.
Kindler, E., Thiel, V., 2014. To sense or not to sense viral RNA--essentials of coronavirus innate immune evasion. Curr. Opin. Microbiol. 20, 69-75.
Kint, J., Fernandez-Gutierrez, M., Maier, H.J., Britton, P., Langereis, M.A., Koumans, J., Wiegertjes, G.F., Forlenza, M., 2015. Activation of the chicken type I interferon response by infectious bronchitis coronavirus. J. Virol. 89, 1156-1167.
Kocherhans, R., Bridgen, A., Ackermann, M., Tobler, K., 2001. Completion of the porcine epidemic diarrhoea coronavirus (PEDV) genome sequence. Virus Genes 23, 137-144.
Koh, H.W., Kim, M.S., Lee, J.S., Kim, H., Park, S.J., 2015. Changes in the Swine Gut Microbiota in Response to Porcine Epidemic Diarrhea Infection. Microbes Environ. 30, 284-287.
Kotenko, S.V., Gallagher, G., Baurin, V.V., Lewis-Antes, A., Shen, M., Shah, N.K., Langer, J.A., Sheikh, F., Dickensheets, H., Donnelly, R.P., 2003. IFN-lambdas mediate antiviral protection through a distinct class II cytokine receptor complex. Nat. Immunol. 4, 69-77.
Kruse, T.A., Bolund, L., Grzeschik, K.H., Ropers, H.H., Olsen, J., Sjostrom, H., Noren, O., 1988. Assignment of the human aminopeptidase N (peptidase E) gene to chromosome 15q13-qter. FEBS Lett. 239, 305-308.
Kusanagi, K., Kuwahara, H., Katoh, T., Nunoya, T., Ishikawa, Y., Samejima, T., Tajima, M., 1992. Isolation and serial propagation of porcine epidemic diarrhea virus in cell cultures and partial characterization of the isolate. J. Vet. Med. Sci. 54, 313-318.
La Bonnardiere, C., Laude, H., 1981. High interferon titer in newborn pig intestine during experimentally induced viral enteritis. Infect. Immun. 32, 28-31.
La Bonnardiere, C., Laude, H., 1983. Interferon induction in rotavirus and coronavirus infections: a review of recent results. Ann. Rech. Vet. 14, 507-511.
LaMorte, V.J., Dyck, J.A., Ochs, R.L., Evans, R.M., 1998. Localization of nascent RNA and CREB binding protein with the PML-containing nuclear body. Proc. Natl. Acad. Sci. U. S. A. 95, 4991-4996.
Lappas, M., Permezel, M., Georgiou, H.M., Rice, G.E., 2002. Nuclear factor kappa B regulation of proinflammatory cytokines in human gestational tissues in vitro. Biol. Reprod. 67, 668-673.

Lau, J.F., Parisien, J.P., Horvath, C.M., 2000. Interferon regulatory factor subcellular localization is determined by a bipartite nuclear localization signal in the DNA-binding domain and interaction with cytoplasmic retention factors. Proc. Natl. Acad. Sci. U. S. A. 97, 7278-7283.

Lau, S.K., Lau, C.C., Chan, K.H., Li, C.P., Chen, H., Jin, D.Y., Chan, J.F., Woo, P.C., Yuen, K.Y., 2013. Delayed induction of proinflammatory cytokines and suppression of innate antiviral response by the novel Middle East respiratory syndrome coronavirus: implications for pathogenesis and treatment. J. Gen. Virol. 94, 2679-2690.

Laude, H., Charley, B., Gelfi, J., 1984. Replication of transmissible gastroenteritis coronavirus (TGEV) in swine alveolar macrophages. J. Gen. Virol. 65, 327-332.

Laude, H., Gelfi, J., Lavenant, L., Charley, B., 1992. Single amino acid changes in the viral glycoprotein M affect induction of alpha interferon by the coronavirus transmissible gastroenteritis virus. J. Virol. 66, 743-749.

Laude, H., Van Reeth, K., Pensaert, M., 1993. Porcine respiratory coronavirus: molecular features and virus-host interactions. Vet. Res. 24, 125-150.

Lawrence, P.K., Bumgardner, E., Bey, R.F., Stine, D., Bumgarner, R.E., 2014. Genome sequences of porcine epidemic diarrhea virus: in vivo and in vitro phenotypes. Genome Announc. 2(3).

Lazarow, P.B., 2011. Viruses exploiting peroxisomes. Curr. Opin. Microbiol. 14, 458-469.

Lazear, H.M., Nice, T.J., Diamond, M.S., 2015. Interferon-lambda: Immune Functions at Barrier Surfaces and Beyond. Immunity 43, 15-28.

Le Negrate, G., 2012. Viral interference with innate immunity by preventing NF-kappaB activity. Cell Microbiol. 14, 168-181.

Lee, B.M., Han, Y.W., Kim, S.B., Rahman, M.M., Uyangaa, E., Kim, J.H., Roh, Y.S., Kim, B., Han, S.B., Hong, J.T., Kim, K., Eo, S.K., 2011. Enhanced protection against infection with transmissible gastroenteritis virus in piglets by oral co-administration of live attenuated Salmonella enterica serovar Typhimurium expressing swine interferon-alpha and interleukin-18. Comp. Immunol. Microbiol. Infect. Dis. 34, 369-380.

Lee, H.M., Lee, B.J., Tae, J.H., Kweon, C.H., Lee, Y.S., Park, J.H., 2000. Detection of porcine epidemic diarrhea virus by immunohistochemistry with recombinant antibody produced in phages. J. Vet. Med. Sci. 62, 333-337.

Lee, S., Lee, C., 2014. Complete Genome Characterization of Korean Porcine Deltacoronavirus Strain KOR/KNU14-04/2014. Genome Announc. 2(6).

Lee, S., Lee, C., 2015. Functional characterization and proteomic analysis of the nucleocapsid protein of porcine deltacoronavirus. Virus. Res. 208, 136-145.

Lee, S.M., Schommer, S.K., Kleiboeker, S.B., 2004. Porcine reproductive and respiratory syndrome virus field isolates differ in in vitro interferon phenotypes. Vet. Immunol. Immunopathol. 102, 217-231.

Li, B.X., Ge, J.W., Li, Y.J., 2007. Porcine aminopeptidase N is a functional receptor for the PEDV coronavirus. Virology 365, 166-172.

Li, C., Li, Z., Zou, Y., Wicht, O., van Kuppeveld, F.J., Rottier, P.J., Bosch, B.J., 2013. Manipulation of the porcine epidemic diarrhea virus genome using targeted RNA recombination. PloS One 8, e69997.

Li, J., Liu, Y., Zhang, X., 2010. Murine coronavirus induces type I interferon in oligodendrocytes through recognition by RIG-I and MDA5. J. Virol. 84, 6472-6482.

Li, L., Fu, F., Xue, M., Chen, W., Liu, J., Shi, H., Chen, J., Bu, Z., Feng, L., Liu, P., 2017a. IFN-lambda preferably inhibits PEDV infection of porcine intestinal epithelial cells compared with IFN-alpha. Antiviral Res. 140, 76-82.

Li, W., Li, H., Liu, Y., Pan, Y., Deng, F., Song, Y., Tang, X., He, Q., 2012. New variants of porcine epidemic diarrhea virus, China, 2011. Emerg. Infect. Dis. 18, 1350-1353.

Li, W., Luo, R., He, Q., van Kuppeveld, FJM., Rottier, PJM., Bosch, BJ., 2017b. Aminopeptidase N is not required for porcine epidemic diarrhea virus cell entry. Virus Res. 235, 6-13.

Li, Y., Chang, H., Yang, X., Zhao, Y., Chen, L., Wang, X., Liu, H., Wang, C., Zhao, J., 2015. Antiviral Activity of Porcine Interferon Regulatory Factor 1 against Swine Viruses in Cell Culture. Viruses 7, 5908-5918.

Liao, Q.J., Ye, L.B., Timani, K.A., Zeng, Y.C., She, Y.L., Ye, L., Wu, Z.H., 2005. Activation of NF-kappaB by the full-length nucleocapsid protein of the SARS coronavirus. Acta Biochim. Biophys. Sin. (Shanghai) 37, 607-612.

Lin, C.M., Gao, X., Oka, T., Vlasova, A.N., Esseili, M.A., Wang, Q., Saif, L.J., 2015. Antigenic relationships among porcine epidemic diarrhea virus and transmissible gastroenteritis virus strains. J. Virol. 89, 3332-3342.

Lin, R., Heylbroeck, C., Pitha, P.M., Hiscott, J., 1998. Virus-dependent phosphorylation of the IRF-3 transcription factor regulates nuclear translocation, transactivation potential, and proteasome-mediated degradation. Mol. Cell. Biol. 18, 2986-2996.

Liu, C., Tang, J., Ma, Y., Liang, X., Yang, Y., Peng, G., Qi, Q., Jiang, S., Li, J., Du, L., Li, F., 2015a. Receptor usage and cell entry of porcine epidemic diarrhea coronavirus. J. Virol. 89, 6121-6125.

Liu, L.X., Heveker, N., Fackler, O.T., Arold, S., Le Gall, S., Janvier, K., Peterlin, B.M., Dumas, C., Schwartz, O., Benichou, S., Benarous, R., 2000. Mutation of a conserved residue (D123) required for oligomerization of human immunodeficiency virus type 1 Nef protein abolishes interaction with human thioesterase and results in impairment of Nef biological functions. J. Virol. 74, 5310-5319.

Liu, L.X., Margottin, F., Le Gall, S., Schwartz, O., Selig, L., Benarous, R., Benichou, S., 1997. Binding of HIV-1 Nef to a novel thioesterase enzyme correlates with Nef-mediated CD4 down-regulation. J. Biol. Chem. 272, 13779-13785.

Liu, Q., Zhang, Z., Zheng, Z., Zheng, C., Liu, Y., Hu, Q., Ke, X., Wang, H., 2016. Human Bocavirus NS1 and NS1-70 Proteins Inhibit TNF-alpha-Mediated Activation of NF-kappaB by targeting p65. Sci. Rep. 6, 28481.

Liu, S., Zhao, L., Zhai, Z., Zhao, W., Ding, J., Dai, R., Sun, T., Meng, H., 2015b. Porcine Epidemic Diarrhea Virus Infection Induced the Unbalance of Gut Microbiota in Piglets. Curr. Microbiol. 71, 643-649.

Livak, K.J., Schmittgen, T.D., 2001. Analysis of relative gene expression data using real-time quantitative PCR and the 2(-Delta Delta C(T)) Method. Methods 25, 402-408.

Lokugamage, K.G., Narayanan, K., Huang, C., Makino, S., 2012. Severe acute respiratory syndrome coronavirus protein nsp1 is a novel eukaryotic translation inhibitor that represses multiple steps of translation initiation. J. Virol. 86, 13598-13608.

Lokugamage, K.G., Narayanan, K., Nakagawa, K., Terasaki, K., Ramirez, S.I., Tseng, C.T., Makino, S., 2015. Middle east respiratory syndrome coronavirus nsp1 inhibits host gene expression by selectively targeting mRNAs transcribed in the nucleus while sparing mrnas of cytoplasmic origin. J. Virol. 89, 10970-10981.

Long, J., Wang, G., Matsuura, I., He, D., Liu, F., 2004. Activation of Smad transcriptional activity by protein inhibitor of activated STAT3 (PIAS3). Proc. Natl. Acad. Sci. U. S. A. 101, 99-104.

Lopez, S., Arias, C.F., 2006. Early steps in rotavirus cell entry. Curr. Top. Microbiol. Immunol. 309, 39-66.

Loving, C.L., Brockmeier, S.L., Ma, W., Richt, J.A., Sacco, R.E., 2006. Innate cytokine responses in porcine macrophage populations: evidence for differential recognition of double-stranded RNA. J. Immunol. 177, 8432-8439.

Ma, Y., Zhang, Y., Liang, X., Lou, F., Oglesbee, M., Krakowka, S., Li, J., 2015. Origin, evolution, and virulence of porcine deltacoronaviruses in the United States. MBio 6, e00064.

Mahlakoiv, T., Hernandez, P., Gronke, K., Diefenbach, A., Staeheli, P., 2015. Leukocyte-derived IFN-alpha/beta and epithelial IFN-lambda constitute a compartmentalized mucosal defense system that restricts enteric virus infections. PLoS Pathog. 11, e1004782.

Mahy BW, Kangro HO. 1996. Virology Methods Manual. Harcourt Brace, New York, NY.

Marthaler, D., Jiang, Y., Otterson, T., Goyal, S., Rossow, K., Collins, J., 2013. Complete Genome Sequence of Porcine Epidemic Diarrhea Virus Strain USA/Colorado/2013 from the United States. Genome Announc. 1, e00555-13.

Marthaler, D., Raymond, L., Jiang, Y., Collins, J., Rossow, K., Rovira, A., 2014. Rapid detection, complete genome sequencing, and phylogenetic analysis of porcine deltacoronavirus. Emerg. Infect. Dis. 20, 1347-1350.

McCluskey, B.J., Haley, C., Rovira, A., Main, R., Zhang, Y., Barder, S., 2016. Retrospective testing and case series study of porcine delta coronavirus in U.S. swine herds. Prev. Vet. Med. 123, 185-191.

Melroe, G.T., Silva, L., Schaffer, P.A., Knipe, D.M., 2007. Recruitment of activated IRF-3 and CBP/p300 to herpes simplex virus ICP0 nuclear foci: Potential role in blocking IFN-beta induction. Virology 360, 305-321.

Merika, M., Williams, A.J., Chen, G., Collins, T., Thanos, D., 1998. Recruitment of CBP/p300 by the IFN beta enhanceosome is required for synergistic activation of transcription. Mol. Cell 1, 277-287.

Mina-Osorio, P., 2008. The moonlighting enzyme CD13: old and new functions to target. Trends Mol. Med. 14, 361-371.

Mole, B., 2013. Deadly pig virus slips through US borders. Nature 499, 388.

Mordstein, M., Kochs, G., Dumoutier, L., Renauld, J.C., Paludan, S.R., Klucher, K., Staeheli, P., 2008. Interferon-lambda contributes to innate immunity of mice against influenza A virus but not against hepatotropic viruses. PLoS Pathog. 4, e1000151.

Mordstein, M., Neugebauer, E., Ditt, V., Jessen, B., Rieger, T., Falcone, V., Sorgeloos, F., Ehl, S., Mayer, D., Kochs, G., Schwemmle, M., Gunther, S., Drosten, C., Michiels, T., Staeheli, P., 2010. Lambda interferon renders epithelial cells of the respiratory and gastrointestinal tracts resistant to viral infections. J. Virol. 84, 5670-5677.

Nam, E., Lee, C., 2010. Contribution of the porcine aminopeptidase N (CD13) receptor density to porcine epidemic diarrhea virus infection. Vet. Microbiol. 144, 41-50.

Napetschnig, J., Wu, H., 2013. Molecular basis of NF-kappaB signaling. Annu. Rev. Biophys. 42, 443-468.

Narayanan, K., Huang, C., Lokugamage, K., Kamitani, W., Ikegami, T., Tseng, C.T., Makino, S., 2008. Severe acute respiratory syndrome coronavirus nsp1 suppresses host gene expression, including that of type I interferon, in infected cells. J. Virol. 82, 4471-4479.

Narayanan, K., Ramirez, S.I., Lokugamage, K.G., Makino, S., 2015. Coronavirus nonstructural protein 1: common and distinct functions in the regulation of host and viral gene expression. Virus Res. 202, 89-100.

Nice, T.J., Baldridge, M.T., McCune, B.T., Norman, J.M., Lazear, H.M., Artyomov, M., Diamond, M.S., Virgin, H.W., 2015. Interferon-lambda cures persistent murine norovirus infection in the absence of adaptive immunity. Science 347, 269-273.

Odendall, C., Dixit, E., Stavru, F., Bierne, H., Franz, K.M., Durbin, A.F., Boulant, S., Gehrke, L., Cossart, P., Kagan, J.C., 2014. Diverse intracellular pathogens activate type III interferon expression from peroxisomes. Nat. Immunol. 15, 717-726.

Oh, J.S., Song, D.S., Park, B.K., 2003. Identification of a putative cellular receptor 150 kDa polypeptide for porcine epidemic diarrhea virus in porcine enterocytes. J. Vet. Sci. 4, 269-275.

Okahira, S., Nishikawa, F., Nishikawa, S., Akazawa, T., Seya, T., Matsumoto, M., 2005. Interferon-beta induction through toll-like receptor 3 depends on double-stranded RNA structure. DNA Cell Biol. 24, 614-623.

Oldenburg, M., Kruger, A., Ferstl, R., Kaufmann, A., Nees, G., Sigmund, A., Bathke, B., Lauterbach, H., Suter, M., Dreher, S., Koedel, U., Akira, S., Kawai, T., Buer, J., Wagner, H., Bauer, S., Hochrein, H., Kirschning, C.J., 2012. TLR13 recognizes bacterial 23S rRNA devoid of erythromycin resistance-forming modification. Science 337, 1111-1115.

Onoguchi, K., Yoneyama, M., Takemura, A., Akira, S., Taniguchi, T., Namiki, H., Fujita, T., 2007. Viral infections activate types I and III interferon genes through a common mechanism. J. Biol. Chem. 282, 7576-7581.

Overend, C., Mitchell, R., He, D., Rompato, G., Grubman, M.J., Garmendia, A.E., 2007. Recombinant swine beta interferon protects swine alveolar macrophages and MARC-145 cells from infection with porcine reproductive and respiratory syndrome virus. J. Gen. Virol. 88, 925-931.

Palma-Ocampo, H.K., Flores-Alonso, J.C., Vallejo-Ruiz, V., Reyes-Leyva, J., Flores-Mendoza, L., Herrera-Camacho, I., Rosas-Murrieta, N.H., Santos-Lopez, G., 2015. Interferon lambda inhibits dengue virus replication in epithelial cells. Virol. J. 12, 150.

Panne, D., Maniatis, T., Harrison, S.C., 2007. An atomic model of the interferon-beta enhanceosome. Cell 129, 1111-1123.

Park, H., Serti, E., Eke, O., Muchmore, B., Prokunina-Olsson, L., Capone, S., Folgori, A., Rehermann, B., 2012. IL-29 is the dominant type III interferon produced by hepatocytes during acute hepatitis C virus infection. Hepatology 56, 2060-2070.

Park, J.E., Cruz, D.J., Shin, H.J., 2011. Receptor-bound porcine epidemic diarrhea virus spike protein cleaved by trypsin induces membrane fusion. Arch. Virol. 156, 1749-1756.

Park, J.E., Shin, H.J., 2014. Porcine epidemic diarrhea virus infects and replicates in porcine alveolar macrophages. Virus Res. 191, 143-152.

Park, S.J., Moon, H.J., Luo, Y., Kim, H.K., Kim, E.M., Yang, J.S., Song, D.S., Kang, B.K., Lee, C.S., Park, B.K., 2008. Cloning and further sequence analysis of the ORF3 gene of wild- and attenuated-type porcine epidemic diarrhea viruses. Virus Genes 36, 95-104.

Patel, D., Nan, Y., Shen, M., Ritthipichai, K., Zhu, X., Zhang, Y.J., 2010. Porcine reproductive and respiratory syndrome virus inhibits type I interferon signaling by blocking STAT1/STAT2 nuclear translocation. J. Virol. 84, 11045-11055.

Pei, J., Sekellick, M.J., Marcus, P.I., Choi, I.S., Collisson, E.W., 2001. Chicken interferon type I inhibits infectious bronchitis virus replication and associated respiratory illness. J. Interferon Cytokine Res. 21, 1071-1077.

Perantoni, A., Berman, J.J., 1979. Properties of Wilms' tumor line (TuWi) and pig kidney line (LLC-PK1) typical of normal kidney tubular epithelium. In Vitro 15, 446-454.

Pestka, S., Krause, C.D., Walter, M.R., 2004. Interferons, interferon-like cytokines, and their receptors. Immunol. Rev. 202, 8-32.

Peterson, L.W., Artis, D., 2014. Intestinal epithelial cells: regulators of barrier function and immune homeostasis. Nat. Rev. Immunol. 14, 141-153.

Pott, J., Mahlakoiv, T., Mordstein, M., Duerr, C.U., Michiels, T., Stockinger, S., Staeheli, P., Hornef, M.W., 2011. IFN-lambda determines the intestinal epithelial antiviral host defense. Proc. Natl. Acad. Sci. U. S. A. 108, 7944-7949.

Prokunina-Olsson, L., Muchmore, B., Tang, W., Pfeiffer, R.M., Park, H., Dickensheets, H., Hergott, D., Porter-Gill, P., Mumy, A., Kohaar, I., Chen, S., Brand, N., Tarway, M., Liu, L., Sheikh, F., Astemborski, J., Bonkovsky, H.L., Edlin, B.R., Howell, C.D., Morgan, T.R., Thomas, D.L., Rehermann, B., Donnelly, R.P., O'Brien, T.R., 2013. A variant upstream of IFNL3 (IL28B) creating a new interferon gene IFNL4 is associated with impaired clearance of hepatitis C virus. Nat. Genet. 45, 164-171.

Puranaveja, S., Poolperm, P., Lertwatcharasarakul, P., Kesdaengsakonwut, S., Boonsoongnern, A., Urairong, K., Kitikoon, P., Choojai, P., Kedkovid, R., Teankum, K., Thanawongnuwech, R., 2009. Chinese-like strain of porcine epidemic diarrhea virus, Thailand. Emerg. Infect. Dis. 15, 1112-1115.

Rajsbaum, R., Garcia-Sastre, A., 2013. Viral evasion mechanisms of early antiviral responses involving regulation of ubiquitin pathways. Trends Microbiol. 21, 421-429.

Randall, R.E., Goodbourn, S., 2008. Interferons and viruses: an interplay between induction, signalling, antiviral responses and virus countermeasures. J. Gen. Virol. 89, 1-47.

Reis, L.F., Ruffner, H., Stark, G., Aguet, M., Weissmann, C., 1994. Mice devoid of interferon regulatory factor 1 (IRF-1) show normal expression of type I interferon genes. EMBO J. 13, 4798-4806.

Riemann, D., Kehlen, A., Langner, J., 1999. CD13--not just a marker in leukemia typing. Immunol. Today 20, 83-88.

Riffault, S., Carrat, C., van Reeth, K., Pensaert, M., Charley, B., 2001. Interferon-alpha-producing cells are localized in gut-associated lymphoid tissues in transmissible gastroenteritis virus (TGEV) infected piglets. Vet. Res. 32, 71-79.

Riffault, S., Grosclaude, J., Vayssier, M., Laude, H., Charley, B., 1997. Reconstituted coronavirus TGEV virosomes lose the virus ability to induce porcine interferon-alpha production. Vet. Res. 28, 105-114.

Rossen, J.W., Bekker, C.P., Voorhout, W.F., Strous, G.J., van der Ende, A., Rottier, P.J., 1994. Entry and release of transmissible gastroenteritis coronavirus are restricted to apical surfaces of polarized epithelial cells. J. Virol. 68, 7966-7973.

Roth-Cross, J.K., Bender, S.J., Weiss, S.R., 2008. Murine coronavirus mouse hepatitis virus is recognized by MDA5 and induces type I interferon in brain macrophages/microglia. J. Virol. 82, 9829-9838.

Royaee, A.R., Husmann, R.J., Dawson, H.D., Calzada-Nova, G., Schnitzlein, W.M., Zuckermann, F.A., Lunney, J.K., 2004. Deciphering the involvement of innate immune factors in the development of the host response to PRRSV vaccination. Vet. Immunol. Immunopathol. 102, 199-216.

Saenz Robles, M.T., Shivalila, C., Wano, J., Sorrells, S., Roos, A., Pipas, J.M., 2013. Two independent regions of simian virus 40 T antigen increase CBP/p300 levels, alter patterns of cellular histone acetylation, and immortalize primary cells. J. Virol. 87, 13499-13509.

Sang, Y., Rowland, R.R., Blecha, F., 2010. Molecular characterization and antiviral analyses of porcine type III interferons. J. Interferon Cytokine Res. 30, 801-807.

Sato, S., Li, K., Kameyama, T., Hayashi, T., Ishida, Y., Murakami, S., Watanabe, T., Iijima, S., Sakurai, Y., Watashi, K., Tsutsumi, S., Sato, Y., Akita, H., Wakita, T., Rice, C.M., Harashima, H., Kohara, M., Tanaka, Y., Takaoka, A., 2015. The RNA sensor RIG-I dually functions as an innate sensor and direct antiviral factor for hepatitis B virus. Immunity 42, 123-132.

Schierack, P., Nordhoff, M., Pollmann, M., Weyrauch, K.D., Amasheh, S., Lodemann, U., Jores, J., Tachu, B., Kleta, S., Blikslager, A., Tedin, K., Wieler, L.H., 2006. Characterization of a porcine intestinal epithelial cell line for in vitro studies of microbial pathogenesis in swine. Histochem. Cell Biol. 125, 293-305.

Schlee, M., Roth, A., Hornung, V., Hagmann, C.A., Wimmenauer, V., Barchet, W., Coch, C., Janke, M., Mihailovic, A., Wardle, G., Juranek, S., Kato, H., Kawai, T., Poeck, H., Fitzgerald, K.A., Takeuchi, O., Akira, S., Tuschl, T., Latz, E., Ludwig, J., Hartmann, G., 2009. Recognition of 5' triphosphate by RIG-I helicase requires short blunt double-stranded RNA as contained in panhandle of negative-strand virus. Immunity 31, 25-34.

Schmidt, A., Schwerd, T., Hamm, W., Hellmuth, J.C., Cui, S., Wenzel, M., Hoffmann, F.S., Michallet, M.C., Besch, R., Hopfner, K.P., Endres, S., Rothenfusser, S., 2009. 5'-triphosphate RNA requires base-paired structures to activate antiviral signaling via RIG-I. Proc. Natl. Acad. Sci. U. S. A. 106, 12067-12072.

Schneider, W.M., Chevillotte, M.D., Rice, C.M., 2014. Interferon-stimulated genes: a complex web of host defenses. Annu. Rev. Immunol. 32, 513-545.

Schoggins, J.W., Rice, C.M., 2011. Interferon-stimulated genes and their antiviral effector functions. Curr. Opin. Virol. 1, 519-525.

Schwarz, B., Routledge, E., Siddell, S.G., 1990. Murine coronavirus nonstructural protein ns2 is not essential for virus replication in transformed cells. J. Virol. 64, 4784-4791.

Sen, A., Rott, L., Phan, N., Mukherjee, G., Greenberg, H.B., 2014. Rotavirus NSP1 protein inhibits interferon-mediated STAT1 activation. J. Virol. 88, 41-53.

Seth, R.B., Sun, L., Ea, C.K., Chen, Z.J., 2005. Identification and characterization of MAVS, a mitochondrial antiviral signaling protein that activates NF-kappaB and IRF3. Cell 122, 669-682.

Sharma, S., tenOever, B.R., Grandvaux, N., Zhou, G.P., Lin, R., Hiscott, J., 2003. Triggering the interferon antiviral response through an IKK-related pathway. Science 300, 1148-1151.

Shen, H., Zhang, C., Guo, P., Liu, Z., Sun, M., Sun, J., Li, L., Dong, J., Zhang, J., 2016. Short communication: antiviral activity of porcine IFN-lambda3 against porcine epidemic diarrhea virus in vitro. Virus genes. 52, 877-882.

Sheppard, P., Kindsvogel, W., Xu, W., Henderson, K., Schlutsmeyer, S., Whitmore, T.E., Kuestner, R., Garrigues, U., Birks, C., Roraback, J., Ostrander, C., Dong, D., Shin, J., Presnell, S., Fox, B., Haldeman, B., Cooper, E., Taft, D., Gilbert, T., Grant, F.J., Tackett,

M., Krivan, W., McKnight, G., Clegg, C., Foster, D., Klucher, K.M., 2003. IL-28, IL-29 and their class II cytokine receptor IL-28R. Nat Immunol 4(1), 63-68.

Shi, C.S., Qi, H.Y., Boularan, C., Huang, N.N., Abu-Asab, M., Shelhamer, J.H., Kehrl, J.H., 2014. SARS-coronavirus open reading frame-9b suppresses innate immunity by targeting mitochondria and the MAVS/TRAF3/TRAF6 signalosome. J. Immunol. 193, 3080-3089.

Shi, D., Lv, M., Chen, J., Shi, H., Zhang, S., Zhang, X., Feng, L., 2014b. Molecular characterizations of subcellular localization signals in the nucleocapsid protein of porcine epidemic diarrhea virus. Viruses 6, 1253-1273.

Shirato, K., Maejima, M., Matsuyama, S., Ujike, M., Miyazaki, A., Takeyama, N., Ikeda, H., Taguchi. F., 2011a. Mutation in the cytoplasmic retrieval signal of porcine epidemic diarrhea virus spike (S) protein is responsible for enhanced fusion activity. Virus Res., 161, 188-193.

Shirato, K., Matsuyama, S., Ujike, M., Taguchi, F., 2011b. Role of proteases in the release of porcine epidemic diarrhea virus from infected cells. J. Virol., 85, 7872-7880.

Siegal, F.P., Kadowaki, N., Shodell, M., Fitzgerald-Bocarsly, P.A., Shah, K., Ho, S., Antonenko, S., Liu, Y.J., 1999. The nature of the principal type 1 interferon-producing cells in human blood. Science 284, 1835-1837.

Sinha, A., Gauger, P., Zhang, J., Yoon, K.J., Harmon, K., 2015. PCR-based retrospective evaluation of diagnostic samples for emergence of porcine deltacoronavirus in US swine. Vet. Microbiol. 179, 296-298.

Siu, K.L., Chan, C.P., Kok, K.H., Chiu-Yat Woo, P., Jin, D.Y., 2014. Suppression of innate antiviral response by severe acute respiratory syndrome coronavirus M protein is mediated through the first transmembrane domain. Cell. Mol. Immunol. 11, 141-149.

Siu, K.L., Kok, K.H., Ng, M.H., Poon, V.K., Yuen, K.Y., Zheng, B.J., Jin, D.Y., 2009. Severe acute respiratory syndrome coronavirus M protein inhibits type I interferon production by impeding the formation of TRAF3.TANK.TBK1/IKKepsilon complex. J. Biol. Chem. 284, 16202-16209.

Snijder, E.J., Bredenbeek, P.J., Dobbe, J.C., Thiel, V., Ziebuhr, J., Poon, L.L., Guan, Y., Rozanov, M., Spaan, W.J., Gorbalenya, A.E., 2003. Unique and conserved features of genome and proteome of SARS-coronavirus, an early split-off from the coronavirus group 2 lineage. J. Mol. Biol. 331, 991-1004.

Snijder, E.J., van der Meer, Y., Zevenhoven-Dobbe, J., Onderwater, J.J., van der Meulen, J., Koerten, H.K., Mommaas, A.M., 2006. Ultrastructure and origin of membrane vesicles associated with the severe acute respiratory syndrome coronavirus replication complex. J. Virol. 80, 5927-5940.

Sommereyns, C., Paul, S., Staeheli, P., Michiels, T., 2008. IFN-lambda (IFN-lambda) is expressed in a tissue-dependent fashion and primarily acts on epithelial cells in vivo. PLoS Pathog. 4, e1000017.

Song, C., Krell, P., Yoo, D., 2010. Nonstructural protein 1alpha subunit-based inhibition of NF-kappaB activation and suppression of interferon-beta production by porcine reproductive and respiratory syndrome virus. Virology 407, 268-280.

Song, D., Park, B., 2012. Porcine epidemic diarrhoea virus: a comprehensive review of molecular epidemiology, diagnosis, and vaccines. Virus Genes 44, 167-175.

Spiegel, M., Pichlmair, A., Martinez-Sobrido, L., Cros, J., Garcia-Sastre, A., Haller, O., Weber, F., 2005. Inhibition of Beta interferon induction by severe acute respiratory syndrome

coronavirus suggests a two-step model for activation of interferon regulatory factor 3. J. Virol. 79, 2079-2086.
Splichal, I., Rehakova, Z., Sinkora, M., Sinkora, J., Trebichavsky, I., Laude, H., Charley, B., 1997. In vivo study of interferon-alpha-secreting cells in pig foetal lymphohaematopoietic organs following in utero TGEV coronavirus injection. Res. Immunol. 148, 247-256.
St-Germain, J.R., Chen, J., Li, Q., 2008. Involvement of PML nuclear bodies in CBP degradation through the ubiquitin-proteasome pathway. Epigenetics 3, 342-349.
Stark, G.R., Darnell, J.E., Jr., 2012. The JAK-STAT pathway at twenty. Immunity 36, 503-514.
Stevenson, G.W., Hoang, H., Schwartz, K.J., Burrough, E.R., Sun, D., Madson, D., Cooper, V.L., Pillatzki, A., Gauger, P., Schmitt, B.J., Koster, L.G., Killian, M.L., Yoon, K.J., 2013. Emergence of Porcine epidemic diarrhea virus in the United States: clinical signs, lesions, and viral genomic sequences. J. Vet. Diagn. Invest. 25, 649-654.
Subramaniam, S., Kwon, B., Beura, L.K., Kuszynski, C.A., Pattnaik, A.K., Osorio, F.A., 2010. Porcine reproductive and respiratory syndrome virus non-structural protein 1 suppresses tumor necrosis factor-alpha promoter activation by inhibiting NF-kappaB and Sp1. Virology 406, 270-279.
Sueyoshi, M., Tsuda, T., Yamazaki, K., Yoshida, K., Nakazawa, M., Sato, K., Minami, T., Iwashita, K., Watanabe, M., Suzuki, Y., et al., 1995. An immunohistochemical investigation of porcine epidemic diarrhoea. J. Comp. Pathol. 113, 59-67.
Summerfield, A., Guzylack-Piriou, L., Schaub, A., Carrasco, C.P., Tache, V., Charley, B., McCullough, K.C., 2003. Porcine peripheral blood dendritic cells and natural interferon-producing cells. Immunology 110, 440-449.
Sun, D., Shi, H., Guo, D., Chen, J., Shi, D., Zhu, Q., Zhang, X., Feng, L., 2015. Analysis of protein expression changes of the Vero E6 cells infected with classic PEDV strain CV777 by using quantitative proteomic technique. J. Virol. Methods 218, 27-39.
Sun, L., Wu, J., Du, F., Chen, X., Chen, Z.J., 2013. Cyclic GMP-AMP synthase is a cytosolic DNA sensor that activates the type I interferon pathway. Science 339, 786-791.
Sun, M., Ma, J., Wang, Y., Wang, M., Song, W., Zhang, W., Lu, C., Yao, H., 2015. Genomic and epidemiological characteristics provide new insights into the phylogeographical and spatiotemporal spread of porcine epidemic diarrhea virus in Asia. J. Clin. Microbiol. 53, 1484-1492.
Sun, R.Q., Cai, R.J., Chen, Y.Q., Liang, P.S., Chen, D.K., Song, C.X., 2012a. Outbreak of porcine epidemic diarrhea in suckling piglets, China. Emerg. Infect. Dis. 18, 161-163.
Sun, Y., Han, M., Kim, C., Calvert, J.G., Yoo, D., 2012b. Interplay between interferon-mediated innate immunity and porcine reproductive and respiratory syndrome virus. Viruses 4, 424-446.
Swamy, M., Abeler-Dorner, L., Chettle, J., Mahlakoiv, T., Goubau, D., Chakravarty, P., Ramsay, G., Reis e Sousa, C., Staeheli, P., Blacklaws, B.A., Heeney, J.L., Hayday, A.C., 2015. Intestinal intraepithelial lymphocyte activation promotes innate antiviral resistance. Nat. Commun. 6, 7090.
Szubin, R., Chang, W.L., Greasby, T., Beckett, L., Baumgarth, N., 2008. Rigid interferon-alpha subtype responses of human plasmacytoid dendritic cells. J. Interferon Cytokine Res. 28, 749-763.
Taguchi, F., Matsuyama, S., 2002. Soluble receptor potentiates receptor-independent infection by murine coronavirus. J. Virol. 76, 950-958.

Tanaka, T., Kamitani, W., DeDiego, M.L., Enjuanes, L., Matsuura, Y., 2012. Severe acute respiratory syndrome coronavirus nsp1 facilitates efficient propagation in cells through a specific translational shutoff of host mRNA. J. Virol. 86, 11128-11137.

Tanner, L.B., Chng, C., Guan, X.L., Lei, Z., Rozen, S.G., Wenk, M.R., 2014. Lipidomics identifies a requirement for peroxisomal function during influenza virus replication. J. Lipid Res. 55, 1357-1365.

Thomas, J.M., Pos, Z., Reinboth, J., Wang, R.Y., Wang, E., Frank, G.M., Lusso, P., Trinchieri, G., Alter, H.J., Marincola, F.M., Thomas, E., 2014. Differential responses of plasmacytoid dendritic cells to influenza virus and distinct viral pathogens. J. Virol. 88, 10758-10766.

Thomson, S.J., Goh, F.G., Banks, H., Krausgruber, T., Kotenko, S.V., Foxwell, B.M., Udalova, I.A., 2009. The role of transposable elements in the regulation of IFN-lambda1 gene expression. Proc. Natl. Acad. Sci. U. S. A. 106, 11564-11569.

Tohya, Y., Narayanan, K., Kamitani, W., Huang, C., Lokugamage, K., Makino, S., 2009. Suppression of host gene expression by nsp1 proteins of group 2 bat coronaviruses. J. Virol. 83, 5282-5288.

Totura, A.L., Baric, R.S., 2012. SARS coronavirus pathogenesis: host innate immune responses and viral antagonism of interferon. Curr. Opin. Virol. 2, 264-275.

Valente, G., Ozmen, L., Novelli, F., Geuna, M., Palestro, G., Forni, G., Garotta, G., 1992. Distribution of interferon-gamma receptor in human tissues. Eur. J. Immunol. 22, 2403-2412.

Verstrepen, L., Bekaert, T., Chau, T.L., Tavernier, J., Chariot, A., Beyaert, R., 2008. TLR-4, IL-1R and TNF-R signaling to NF-kappaB: variations on a common theme. Cell Mol. Life Sci. 65, 2964-2978.

Vogt, C., Preuss, E., Mayer, D., Weber, F., Schwemmle, M., Kochs, G., 2008. The interferon antagonist ML protein of thogoto virus targets general transcription factor IIB. J. Virol. 82, 11446-11453.

Vollmer, J., Weeratna, R., Payette, P., Jurk, M., Schetter, C., Laucht, M., Wader, T., Tluk, S., Liu, M., Davis, H.L., Krieg, A.M., 2004. Characterization of three CpG oligodeoxynucleotide classes with distinct immunostimulatory activities. Eur. J. Immunol. 34, 251-262.

Wang, D., Fang, L., Liu, L., Zhong, H., Chen, Q., Luo, R., Liu, X., Zhang, Z., Chen, H., Xiao, S., 2011. Foot-and-mouth disease virus (FMDV) leader proteinase negatively regulates the porcine interferon-lambda1 pathway. Mol. Immunol. 49, 407-412.

Wang, D., Fang, L., Shi, Y., Zhang, H., Gao, L., Peng, G., Chen, H., Li, K., Xiao, S., 2015a. Porcine Epidemic Diarrhea Virus 3C-Like Protease Regulates Its Interferon Antagonism by Cleaving NEMO. J. Virol. 90, 2090-2101.

Wang, K., Lu, W., Chen, J., Xie, S., Shi, H., Hsu, H., Yu, W., Xu, K., Bian, C., Fischer, W.B., Schwarz, W., Feng, L., Sun, B., 2012. PEDV ORF3 encodes an ion channel protein and regulates virus production. FEBS Lett. 586, 384-391.

Wang, L., Byrum, B., Zhang, Y., 2014. Detection and genetic characterization of deltacoronavirus in pigs, Ohio, USA, 2014. Emerg. Infect. Dis. 20, 1227-1230.

Wang, P., Zhu, S., Yang, L., Cui, S., Pan, W., Jackson, R., Zheng, Y., Rongvaux, A., Sun, Q., Yang, G., Gao, S., Lin, R., You, F., Flavell, R., Fikrig, E., 2015b. Nlrp6 regulates intestinal antiviral innate immunity. Science. 350, 826-830.

Wang, Y., Shi, H., Rigolet, P., Wu, N., Zhu, L., Xi, X.G., Vabret, A., Wang, X., Wang, T., 2010. Nsp1 proteins of group I and SARS coronaviruses share structural and functional similarities. Infect. Genet. Evol. 10, 919-924.

Watanabe, H., Shiratori, T., Shoji, H., Miyatake, S., Okazaki, Y., Ikuta, K., Sato, T., Saito, T., 1997. A novel acyl-CoA thioesterase enhances its enzymatic activity by direct binding with HIV Nef. Biochem. Biophys. Res. Commun. 238, 234-239.

Wathelet, M.G., Orr, M., Frieman, M.B., Baric, R.S., 2007. Severe acute respiratory syndrome coronavirus evades antiviral signaling: role of nsp1 and rational design of an attenuated strain. J. Virol. 81, 11620-11633.

Wicht, O., Li, W., Willems, L., Meuleman, T.J., Wubbolts, R.W., van Kuppeveld, F.J., Rottier, P.J., Bosch, B.J., 2014. Proteolytic activation of the porcine epidemic diarrhea coronavirus spike fusion protein by trypsin in cell culture. J. Virol. 88, 7952-7961.

Wolff, T., O'Neill, R.E., Palese, P., 1996. Interaction cloning of NS1-I, a human protein that binds to the nonstructural NS1 proteins of influenza A and B viruses. J. Virol. 70, 5363-5372.

Woo, P.C., Huang, Y., Lau, S.K., Yuen, K.Y., 2010. Coronavirus genomics and bioinformatics analysis. Viruses 2, 1804-1820.

Woo, P.C., Lau, S.K., Lam, C.S., Lau, C.C., Tsang, A.K., Lau, J.H., Bai, R., Teng, J.L., Tsang, C.C., Wang, M., Zheng, B.J., Chan, K.H., Yuen, K.Y., 2012. Discovery of seven novel Mammalian and avian coronaviruses in the genus deltacoronavirus supports bat coronaviruses as the gene source of alphacoronavirus and betacoronavirus and avian coronaviruses as the gene source of gammacoronavirus and deltacoronavirus. J. Virol. 86, 3995-4008.

Wood, E.N., 1977. An apparently new syndrome of porcine epidemic diarrhoea. Vet. Rec. 100, 243-244.

Wu, J., Sun, L., Chen, X., Du, F., Shi, H., Chen, C., Chen, Z.J., 2013. Cyclic GMP-AMP is an endogenous second messenger in innate immune signaling by cytosolic DNA. Science 339, 826-830.

Wurm, T., Wright, D.G., Polakowski, N., Mesnard, J.M., Lemasson, I., 2012. The HTLV-1-encoded protein HBZ directly inhibits the acetyl transferase activity of p300/CBP. Nucleic Acids Res. 40, 5910-5925.

Xing, J., Ni, L., Wang, S., Wang, K., Lin, R., Zheng, C., 2013a. Herpes simplex virus 1-encoded tegument protein VP16 abrogates the production of beta interferon (IFN) by inhibiting NF-kappaB activation and blocking IFN regulatory factor 3 to recruit its coactivator CBP. J. Virol. 87, 9788-9801.

Xing, Y., Chen, J., Tu, J., Zhang, B., Chen, X., Shi, H., Baker, S.C., Feng, L., Chen, Z., 2013b. The papain-like protease of porcine epidemic diarrhea virus negatively regulates type I interferon pathway by acting as a viral deubiquitinase. J. Gen. Virol. 94, 1554-1567.

Xu, X., Zhang, H., Zhang, Q., Dong, J., Liang, Y., Huang, Y., Liu, H.J., Tong, D., 2013a. Porcine epidemic diarrhea virus E protein causes endoplasmic reticulum stress and up-regulates interleukin-8 expression. Virol. J. 10, 26.

Xu, X., Zhang, H., Zhang, Q., Huang, Y., Dong, J., Liang, Y., Liu, H.J., Tong, D., 2013b. Porcine epidemic diarrhea virus N protein prolongs S-phase cell cycle, induces endoplasmic reticulum stress, and up-regulates interleukin-8 expression. Vet. Microbiol. 164, 212-221.

Xu, X.G., Zhang, H.L., Zhang, Q., Dong, J., Huang, Y., Tong, D.W., 2015. Porcine epidemic diarrhea virus M protein blocks cell cycle progression at S-phase and its subcellular localization in the porcine intestinal epithelial cells. Acta Virol. 59, 265-275.

Yang, X., Huo, J.Y., Chen, L., Zheng, F.M., Chang, H.T., Zhao, J., Wang, X.W., Wang, C.Q., 2013. Genetic variation analysis of reemerging porcine epidemic diarrhea virus prevailing in central China from 2010 to 2011. Virus Genes 46, 337-344.

Ye, S., Li, Z., Chen, F., Li, W., Guo, X., Hu, H., He, Q., 2015. Porcine epidemic diarrhea virus ORF3 gene prolongs S-phase, facilitates formation of vesicles and promotes the proliferation of attenuated PEDV. Virus Genes 51, 385-392.

You, J., Hou, S., Malik-Soni, N., Xu, Z., Kumar, A., Rachubinski, R.A., Frappier, L., Hobman, T.C., 2015. Flavivirus Infection Impairs Peroxisome Biogenesis and Early Antiviral Signaling. J. Virol. 89, 12349-12361.

Yuan, L., Chen, Z., Song, S., Wang, S., Tian, C., Xing, G., Chen, X., Xiao, Z.X., He, F., Zhang, L., 2015. p53 degradation by a coronavirus papain-like protease suppresses type I interferon signaling. J. Biol. Chem. 290, 3172-3182.

Zeng, S., Zhang, H., Ding, Z., Luo, R., An, K., Liu, L., Bi, J., Chen, H., Xiao, S., Fang, L., 2015. Proteome analysis of porcine epidemic diarrhea virus (PEDV)-infected Vero cells. Proteomics 15, 1819-1828.

Zhang, J., Yamada, O., Kawagishi, K., Araki, H., Yamaoka, S., Hattori, T., Shimotohno, K., 2008. Human T-cell leukemia virus type 1 Tax modulates interferon-alpha signal transduction through competitive usage of the coactivator CBP/p300. Virology 379, 306-313.

Zhang, Q., Ke, H., Blikslager, A., Fujita, T., Yoo, D., 2017a. Type III Interferon Restriction by Porcine Epidemic Diarrhea Virus and the Role of Viral Protein nsp1 in IRF1 Signaling. J. Virol.

Zhang, Q., Ma, J., Yoo, D., 2017b. Inhibition of NF-κB activity by the porcine epidemic diarrhea virus nonstructural protein 1 for innate immune evasion. Virology 510, 111-126.

Zhang, Q., Shi, K., Yoo, D., 2016. Suppression of type I interferon production by porcine epidemic diarrhea virus and degradation of CREB-binding protein by nsp1. Virology 489, 252-268.

Zhang, Q., Yoo, D., 2016. Immune evasion of porcine enteric coronaviruses and viral modulation of antiviral innate signaling. Virus Res. 226, 128-141.

Zhao, L., Jha, B.K., Wu, A., Elliott, R., Ziebuhr, J., Gorbalenya, A.E., Silverman, R.H., Weiss, S.R., 2012. Antagonism of the interferon-induced OAS-RNase L pathway by murine coronavirus ns2 protein is required for virus replication and liver pathology. Cell Host Microbe 11, 607-616.

Zhao, S., Gao, J., Zhu, L., Yang, Q., 2014. Transmissible gastroenteritis virus and porcine epidemic diarrhoea virus infection induces dramatic changes in the tight junctions and microfilaments of polarized IPEC-J2 cells. Virus Res. 192, 34-45.

Zhou, H., Perlman, S., 2007. Mouse hepatitis virus does not induce Beta interferon synthesis and does not inhibit its induction by double-stranded RNA. J. Virol. 81, 568-574.

Zhou, J., Chu, H., Li, C., Wong, B.H., Cheng, Z.S., Poon, V.K., Sun, T., Lau, C.C., Wong, K.K., Chan, J.Y., Chan, J.F., To, K.K., Chan, K.H., Zheng, B.J., Yuen, K.Y., 2014. Active replication of Middle East respiratory syndrome coronavirus and aberrant induction of inflammatory cytokines and chemokines in human macrophages: implications for pathogenesis. J. Infect. Dis. 209, 1331-1342.

Zhu, L., Yang, X., Mou, C., Yang, Q., 2017. Transmissible gastroenteritis virus does not suppress IFN-beta induction but is sensitive to IFN in IPEC-J2 cells. Vet. Microbiol. 199, 128-134.

Ziebuhr, J., 2005. The coronavirus replicase. Curr. Top. Microbiol. Immunol. 287, 57-94.

Ziebuhr, J., Schelle, B., Karl, N., Minskaia, E., Bayer, S., Siddell, S.G., Gorbalenya, A.E., Thiel, V., 2007. Human coronavirus 229E papain-like proteases have overlapping specificities but distinct functions in viral replication. J. Virol. 81, 3922-3932.

Zielecki, F., Weber, M., Eickmann, M., Spiegelberg, L., Zaki, A.M., Matrosovich, M., Becker, S., Weber, F., 2013. Human cell tropism and innate immune system interactions of human respiratory coronavirus EMC compared to those of severe acute respiratory syndrome coronavirus. J. Virol. 87, 5300-5304.

Zust, R., Cervantes-Barragan, L., Kuri, T., Blakqori, G., Weber, F., Ludewig, B., Thiel, V., 2007. Coronavirus non-structural protein 1 is a major pathogenicity factor: implications for the rational design of coronavirus vaccines. PLoS Pathog. 3, e109.